Modelling of the Fifth Case Study Glaciation and Erosion Scenarios

NWMO-TR-2015-14

October 2015

John Avis and Nicola Calder

Geofirma Engineering Ltd.

NUCLEAR WASTE MANAGEMENT ORGANIZATION

SOCIÉTÉ DE GESTION DES DÉCHETS NUCLÉAIRES

Nuclear Waste Management Organization
22 St. Clair Avenue East, 6th Floor
Toronto, Ontario
M4T 2S3
Canada

Tel: 416-934-9814
Web: www.nwmo.ca

Modelling of the Fifth Case Study Glaciation and Erosion Scenarios

NWMO-TR-2015-14

October 2015

John Avis and Nicola Calder
Geofirma Engineering Ltd.

Document History

Title:	Modelling of the Fifth Case Study Glaciation and Erosion Scenarios		
Report Number:	NWMO-TR-2015-14		
Revision:	R000	Date:	October 2015
Geofirma Engineering Ltd.			
Authored by:	John Avis and Nicola Calder		
Verified by:	Nicola Calder, Robert Walsh, and Othman Nasir		
Approved by:	John Avis		
Nuclear Waste Management Organization			
Reviewed by:	Frank Garisto, Jeremy Chen, Eric Sykes, Andre Vorauer and Erik Kremer		
Accepted by:	Paul Gierszewski		

ABSTRACT

Title: **Modelling of the Fifth Case Study Glaciation and Erosion Scenarios**
Report No.: **NWMO-TR-2015-14**
Author(s): John Avis and Nicola Calder
Company: Geofirma Engineering Ltd.
Date: October 2015

Abstract

This technical report presents the results of detailed numeric modelling of the effects of glaciation on a hypothetical deep geologic repository (DGR) for used fuels situated in a sedimentary formation. The Nuclear Waste Management Organization (NWMO) has undertaken post-closure safety assessments of hypothetical DGRs in both crystalline and sedimentary rock formations (NWMO 2012; NWMO 2013). The safety assessment for a DGR in sedimentary formations documented the behaviour of reference and sensitivity cases associated with the normal evolution of the repository system under constant climate conditions, with a qualitative discussion of the potential effects of glaciation on calculated impacts. However, a complete safety assessment requires a quantitative assessment of the impact of glaciation events. Two scenarios are considered in this report: (1) a glaciation only scenario, and (2) an erosion scenario, which accounts for erosion occurring during glaciation events.

The base glaciation scenario first describes the evolution of the groundwater flow regime in a three-dimensional domain at the sub-regional scale, extending several tens of kilometres around the repository location, for eight glacial cycles over a one million year (1 Ma) period. A performance metric is developed describing the time required for radionuclides to be transported from the repository location by advective-dispersive and diffusive processes over multiple glacial cycles with a transient groundwater flow regime. Multiple sensitivity cases are conducted to quantify the effect of variations in geosphere parameters, assumed model initial and boundary conditions, and transport process. Additional two-dimensional simulations assess the impact of possible methane presence as a gas phase within the low-permeability host formations. Subsequently, a 3D transport model is developed encompassing a limited local domain immediately surrounding the repository. Model boundary conditions are extracted directly from the 3D transient flow model results. The transport model discretization and property assignment includes all repository features such tunnels, shafts, placement rooms and engineered barrier system (EBS) components as well as excavation damaged zones (EDZ) surrounding all mined features. A defective container provides a single radionuclide source (the long-lived and radiotoxic isotope ^{129}Iodine, or I-129) and a water-supply well is the point of biosphere impact. Performance metrics are activity transport rates through geologic formations between the repository and the water supply aquifer and uptake at the water supply well. Simulations are conducted for several source and well location combinations and for a limited number of geosphere and numeric parameter sensitivity cases, including a disruptive event case describing shaft-seal failure.

The erosion scenario extends the base glaciation scenario to incorporate removal of surface geologic material during each glacial cycle. A total of 100m of overburden and bedrock are removed over the 1 Ma performance period in two different manners: 1) uniform erosion (UE), where an equal amount of material is removed over the entire surface of the domain, and 2) valley erosion (VE), where glaciers incise a 100m deep and 15 km wide valley located directly over the repository. Results from the sub-regional scale groundwater flow and the local scale transport models were compared to the glaciation only case.

In all cases, the transport behaviour of the low-permeability sedimentary geosphere proved extremely robust, with virtually no changes in performance metrics for glaciation or erosion cases when compared to constant climate cases with steady-state groundwater flow.

TABLE OF CONTENTS

Page

LIST OF TABLES

LIST OF FIGURES

1. INTRODUCTION

The NWMO has undertaken post-closure safety assessments of hypothetical geologic repositories for used fuels hosted in crystalline and sedimentary rock formations (NWMO 2012; NWMO 2013). Initial reports documented the behaviour of reference and sensitivity cases associated with the normal evolution of the repository system under constant climate conditions. Since glaciation is considered as part of the normal evolution scenario, the initial reports also include a qualitative discussion of the potential effects of glaciation on calculated impacts. However, a complete safety assessment requires a quantitative assessment of the impact of glaciation events during the normal evolution scenario. This technical report presents detailed results for the effects of glaciation on a repository in a sedimentary formation. Two glaciations scenarios are considered: (1) a base glaciation scenario, and (2) an erosion scenario, which extends the base glaciation scenario to account for erosion occurring during glaciation events.

The Fifth Case Study (5CS) Glaciation scenario is derived from the nn9930 glaciation model used for paleohydrogelogy simulations in in NWMO (2013) and originally described in Peltier (2011). Glacial climate data provided for this scenario consists of ice sheet thickness and permafrost depth at locations surrounding the repository as a function of time for a single glacial cycle occurring over a period of 120 ka. This cycle is repeated eight times to provide an approximately 1 Ma scenario.

This report describes the evolution of the groundwater flow regime during multiple glacial cycles and the transport of a single radionuclide from a hypothetical repository to the surface. Sensitivity cases are conducted to evaluate different parameterizations for geosphere hydrogeologic and geomechanical properties.

A nested modelling approach is used wherein flow-only simulations are performed at the Sub-Regional scale of several tens of kilometres surrounding the hypothetical repository location. Head and loading boundary conditions are extracted from the Sub-Regional model and used as input for the smaller Site-Scale transport simulations restricted to a domain of several kilometres outside the repository footprint. The Site-Scale models include a representation of the repository within the model grid.

This report is structured as follows:

- Code and Theory – describes the theory behind glacial loading and unloading, and the modelling codes and approaches used to implement the theory.

- Geoscience Data Preparation – describes the approaches used to generate surfaces used for geologic formation discretization, to extract glaciation data at the repository location and to determine the direction of glacial advances and retreats.

- Glaciation Scenario – describes the Glaciation Sub-Regional Flow model construction and flow model results for reference and sensitivity cases. The Site-Scale transport model is described and results for reference and sensitivity case transport scenarios. Two-dimensional simulations were also conducted using a two-phase flow model to consider the impact of gas present in the geologic formations on the groundwater flow regime during a glaciation event.

- Erosion Scenario – extends the Glaciation scenario to include uniform and localized erosion. The Erosion Sub-Regional Flow Model is described and results are compared to those of the Glaciation Sub-Regional Flow Model. Modifications to the Site-Scale transport model are described and transport results for four reference case scenarios are presented and compared to corresponding Glaciation Scenario Site-Scale model results.

- Conclusions – summarizes the results of the modelling and the possible impacts of glaciation and erosion as compared to the steady-state normal evolution results. Provides an assessment of the modelling approaches.

2. CODE AND THEORY

2.1 Modelling Codes and Software Used

All single-phase flow and transport simulations are performed with the FRAC3DVS-OPG V1.30 code. FRAC3DVS-OPG is a 3D control volume finite-element / finite-difference code (Therrien et al., 2010) for groundwater flow and solute transport. It includes the ability to represent discrete fractures (not used here), variable density flow and glaciation using a 1D hydro-mechanical model, assuming uniaxial strain. FRAC3DVS-OPG was used for all paleohyrogeology and radionuclide transport simulations presented in NWMO (2013).

Two-phase flow simulations, conducted for the 2D Glaciation Sub-Regional scale flow modelling described in Section 4.3, were performed with T2GGM v3.2 (Suckling et al., 2015). T2GGM is a modified version of TOUGH2 v2.0 with an optional gas generation model. The gas generation model (GGM) capabilities were not used. TOUGH2 is a general-purpose numerical simulation program for multi-phase fluid and heat flow in porous and fractured media developed by Lawrence Berkeley National Laboratory (Pruess et al. 1999). The EOS3 equation of state module used in T2GGM simulates the transport of a single separate gas phase in water (note that T2GGM allows for specification of alternative gases to air (in this case methane), the EOS3 default). Thermophysical properties of water are represented by steam-table equations, while the gas is treated as ideal gas. Dissolution of gas in water is modeled with Henry's law. The phase relationship between gas and liquid is based on a local thermodynamic equilibrium assumption. EOS3 models the transport of dissolved gas in water by diffusion and advection. Dispersive processes are not modelled. T2GGM also includes a 1D hydro-mechanical model.

mView version 4.21, developed by Geofirma Engineering, is used for all model pre- and post-processing. paCalc version 1.7, also developed by Geofirma Engineering, is used as an execution framework for generating Mean Life Expectancy (MLE) time series.

2.2 Theory: 1D Hydro-Mechanical Loading and Unloading

External stresses arising from transient ice-sheet mechanical loading and elevated sub-glacial hydraulic head can potentially influence groundwater system dynamics and solute migration. The presence of gas in formations is expected to reduce the magnitude of hydro-mechanical coupling. Fully coupled 3D hydro-mechanical (HM) models, such as TOUGH-FLAC (Rutqvist and Tsang, 2003) are demanding to use at the repository scale, in terms of computational and human effort, and may require some approximation in accounting for markedly increased fluid compressibility in a gas-water system. An approximate 1D solution to the coupled hydro-mechanical processes, relying on the simplifying assumptions of horizontally bedded formations and vertical uniaxial strain, is reasonable for a relatively homogeneous and extensive vertical load, such as occurs during continental glaciations or laterally extensive erosion/deposition events. The 1D assumption may not be not valid where vertical loads vary significantly across the model domain, such as would occur at the toe of a glacier during the early stages of a glacial advance when the ice margin is within the model domain. In these cases, horizontal stresses may cause additional hydro-mechanical effects. The interval during which the ice margin crosses the domain is typically short relative to the entire glaciation period, and the 1D HM model is reasonably accurate for the majority of the simulation time. The 1D approach is described for single phase flow in Wang (2000) and Neuzil (2003), and two-phase flow in Walsh et al. (2012), and is implemented in both FRAC3DVS-OPG (single phase only) and T2GGM (two-phase).

One-dimensional HM coupling, assuming uniaxial vertical strain, is analogous to the addition or subtraction of water from storage in single-phase codes. In the FRAC3DVS-OPG single-phase code, 1D hydro-mechanical coupling is included as an additional term in the governing equation (the second term on the right hand side):

$$\nabla(K\nabla h) = S_{s-1D}\frac{\partial h}{\partial t} + \zeta S_{s-1D}\frac{1}{\rho g}\frac{\partial \sigma_{zz}}{\partial t} \pm Q \quad \textbf{(2-1)}$$

Where parameters are:

S_{S-1D} 1D (uniaxial) specific storage (m^{-1});
ζ 1D loading efficiency (-);
σ_{zz} vertical load (Pa);
K hydraulic conductivity tensor (m/s);
h hydraulic head (m);
t time (s);
ρ density of water (kg/m^3);
g gravitational acceleration (m/s^2); and
Q sink or source term.

In the two-phase code T2GGM, the change in porosity as a function of the pressure is analogous to the storage term in single-phase flow mass balance equations, and is included within the mass accumulation term (Equation 2-2) of the governing mass balance equation (Equation 2-3). Porosity (ϕ) is not a constant material property, but is transient and updated at the end of each time-step.

$$M^\kappa = \phi \sum_\psi S_\psi \rho_\psi X_\psi^\kappa \quad \textbf{(2-2)}$$

$$\frac{d}{dt}\int_{V_n} M^\kappa dV_n = \int_{\Gamma_n} F^\kappa \cdot n d\Gamma_n + \int_{V_n} q^\kappa dV_n \quad \textbf{(2-3)}$$

Where parameters are:

M^κ mass accumulation term (kg/m^3) of component κ (air or water);
ϕ porosity (-);
S_ψ saturation (-) of phase ψ (liquid or gas);
ρ_ψ density (kg/m^3) of phase ψ;
X_ψ^κ mass fraction of component κ in phase ψ (kg/kg);
V_n subdomain volume (m^3);
Γ_n closed surface bounding volume V_n (m^2);
n is a normal vector on suface element Γ_n pointing inward into V_n;
F^κ mass flux of component κ ($kg/(m^2s)$); and
q^κ sink or source term of component κ (kg/s).

Hydro-mechanical coupling is implemented as a change in porosity due to a change in the vertical load. The total change in porosity at the end of each time step, including storage and hydro-mechanical components, is described as follows:

$$\phi_t = \phi_{t-1} + \phi_{t-1} C_{pore} dp + S_{S-1D} \zeta d\sigma_{zz} \quad \textbf{(2-4)}$$

Where parameters are:

ϕ_t	porosity at time t;
ϕ_{t-1}	porosity at time t-1;
C_{pore}	pore compressibility (Pa^{-1});
p	pressure (Pa),
S_{S-1D}.	1D (uniaxial) specific storage (Pa^{-1}),
ζ	one-dimensional loading efficiency (-), and
$d\sigma_{zz}$	change in vertical load during time step t-1 (Pa).

The input parameters common to the FRAC3DVS-OPG and T2GGM hydro-mechanical terms are the one-dimensional loading efficiency (ζ), and the vertical loading rate ($d\sigma_{zz}$).

The one-dimensional loading efficiency is defined for each material type. This parameter is used to determine what percentage of the applied vertical stress is borne by the pore-fluids. The equation used to calculate one-dimensional loading efficiency (ζ) is (Neuzil 2003):

$$\zeta = \frac{\beta(1+\nu)}{3(1-\nu) - 2\alpha\beta(1-2\nu)} \quad \textbf{(2-5)}$$

Where parameters are:

β	Skempton's coefficient (-);
α	Biot-Willis coefficient (-); and
ν	Poisson’s Ratio (-).

The one-dimensional specific storage is also defined for each material type, according to Equations 2-6 through 2-10.

$$S_{S-1D} = \left(\frac{1}{K} - \frac{1}{K_S}\right)(1-\lambda) + \phi\left(\frac{1}{K_f} - \frac{1}{K_\phi}\right) \quad \textbf{(2-6)}$$

$$\frac{1}{K_S} = \frac{1-\alpha}{K} \quad \textbf{(2-7)}$$

$$\lambda = \frac{2\alpha(1-2\nu)}{3(1-\nu)} \quad \textbf{(2-8)}$$

$$\frac{1}{K_f} = \frac{S_w}{K_w} + \frac{S_g}{K_g} \quad \textbf{(2-9)}$$

$$\frac{1}{K_\phi} = -\frac{1}{\phi}\left[\left(\frac{1}{K} - \frac{1}{K_S}\right)\left(\frac{1}{\beta} - 1\right) - \frac{\phi}{K_f}\right] \quad \textbf{(2-10)}$$

Where parameters are:

- K drained bulk modulus (Pa), ($1/K = \phi C_{pore}$);
- $\mathrm{K_s}$ unjacketed bulk modulus, often denoted solid phase bulk modulus (Pa);
- $\mathrm{K_f}$ effective fluid bulk modulus (Pa);
- $\mathrm{S_w}$ water saturation (-);
- $\mathrm{S_g}$ gas saturation (-);
- $\mathrm{K_w}$ water bulk modulus, calculated by TOUGH2 (Pa);
- $\mathrm{K_g}$ gas bulk modulus, calculated by TOUGH2 (Pa); and
- $\mathrm{K_\phi}$ unjacketed pore compressibility (Pa).

Within FRAC3DVS-OPG, S_{S-1D} is an input parameter for each material type. For T2GGM, the storage term is not used directly, but inferred from the pore compressibility term (change in porosity with pressure). As implemented in TOUGH2, the pore compressibility term assumes incompressible grains ($\alpha = 1$), equivalent to a storage coefficient defined as follows:

$$S_{S-1D} = \frac{1}{K} + \frac{\phi}{K_f} \quad \textbf{(2-11)}$$

In order for the pressure effects of externally applied loads and changes in pore pressure to be expressed in a consistent fashion, it is necessary to use this simplified form of the storage coefficient equation (Equation 2-11) in the T2GGM hydro-mechanical coupling term. The value of the T2GGM input parameter C_{pore} ($1/K = \phi C_{pore}$) should account for uniaxial rather than triaxial mechanical constraints.

At first glance, it appears that the 1D hydro-mechanical term is a function of fluid compressibility, and thereby gas saturation; however, the term $S_{S-1D}\,\zeta$ reduces to:

$$S_{S-1D}\,\zeta = \frac{\left(\frac{1}{K} - \frac{1}{K_S}\right)(1+\nu)}{3(1-\nu)} \quad \textbf{(2-12)}$$

Thus, this formulation is a function of material parameters which we assume, in a linear poroelastic model, do not change significantly (i.e. $S_{S-1D}\,\zeta$ is a constant). In a two-phase flow model such as T2GGM, the effects of the gas phase on reducing the magnitude of hydro-mechanical coupling are realized in the effects of the change in porosity on gas pressure, compared to liquid pressure, rather than the hydro-mechanical term itself.

The vertical loading rate is provided as a time-variable input for each element or node column (FRAC3DVS uses elements, T2GGM nodes). An element or node column refers to a group of elements or nodes with a single X and Y coordinate, and different depth or Z coordinates. The method of calculating the vertical loading rate for the glaciations and erosion models in this report is described in the following section.

2.3 1D Glacial Boundary Conditions

Two boundary conditions are required to simulate glaciation using the 1D hydro-mechanical models in FRAC3DVS and T2GGM: (1) hydraulic head at ground surface, and (2) vertical loading rate. These boundaries are spatially variable to represent glacial advance and retreat.

The hydraulic head at ground surface due to glaciation is developed based on the approach described in Walsh and Avis (2010). During periods of ice cover, an assumed glacial profile traverses the site at rates that reproduce the ice thickness calculated by glacial climate data (described in Section 3.2). An analytic equation for the glacial surface profile as a function of the strength and density of the ice was developed by Oerlemans (2001):

$$i(x) = \sqrt{\frac{2\tau_0}{\rho g(1+\delta)}x} \qquad \textbf{(2-13)}$$

where:

- $i(x)$ glacial ice thickness profile, as a function of distance from terminus (m);
- x distance from glacial terminus (m);
- τ_0 yield stress (Pa);
- ρ ice density (kg m^{-3}); and
- δ isostatic depression parameter.

Oerlemans (2001) suggests values of 50 kPa to 300 kPa for yield stress and 0.33 for the isostatic depression parameter. A value of 50 kPa was specified for yield stress and ice density was assumed to be 900 kg m^{-3}.

The ice thickness profile is converted to hydraulic head by multiplying the thickness by an assumed ice-sheet density of 900 kg/m^3. Water pressures below the glacier are therefore assumed to be close to the pressure required to float the glacier. Glacial advance and retreat rates are inferred by calculating ice profile movement required to match predicted ice thicknesses. This approach and calculated boundary conditions are further described in Section 4.1.1.3.

For glacial advance and retreat only, the vertical loading rate is calculated as the derivative of the surface hydraulic head with respect to time. Inclusion of erosion requires additional stress changes caused by material removal, as further described in Section 5.1.2.3.

The effects of crustal deformation due to ice load is ignored in the current formulation.

3. GEOSCIENCE DATA PREPARATION

The 5CS study geosphere is described in detail in NWMO (2013). The hypothetical site is consistent with the Michigan Basin in Southern Ontario. Information describing the site is largely derived from regional and site-specific investigations for Ontario Power Generation's Deep Geological Repository for Low & Intermediate Level Waste (INTERA 2011, AECOM and Itasca 2011). For the purposes of the 5CS the repository was assumed to be located in the middle of the Cobourg formation at an approximate depth of 500 mBGS.

3.1 Geologic Surfaces

Formation topography is required for three dimensional grid discretization and property assignment. Digital elevation models (DEMs) of geologic formation tops were provided by the NWMO in the triangular irregular network (TIN) format used for the Regional Geologic Framework Model (GFM) (AECOM and Itasca, 2011). The TIN node points were used as known elevation points and interpolated onto regular 500 m grids encompassing the maximum potential model domain using a minimum curvature algorithm. The actual Sub-Regional model domains for both the Glaciation and Erosion scenarios are defined within this larger potential area, with the repository located near the middle of the domain. TIN points were pre-processed to reduce density and delete anomalous points prior to interpolation. Reef structures were also removed from all formations above the Guelph to ensure maximum surface smoothness. In addition to previously identified structures, the presence of some additional reefs was inferred from point elevations. Note that areas containing reef structures are well outside of the actual Sub-Regional model domains (Section 4.1 and Section 5.1). Figure 3-1 shows the Cobourg formation GFM input data and the reduction and interpolation grid extents. The original GFM domain is approximately 170 km (Easting) by 200 km (Northing), while the Sub-Regional interpolation domain is approximately 90 km by 100 km.

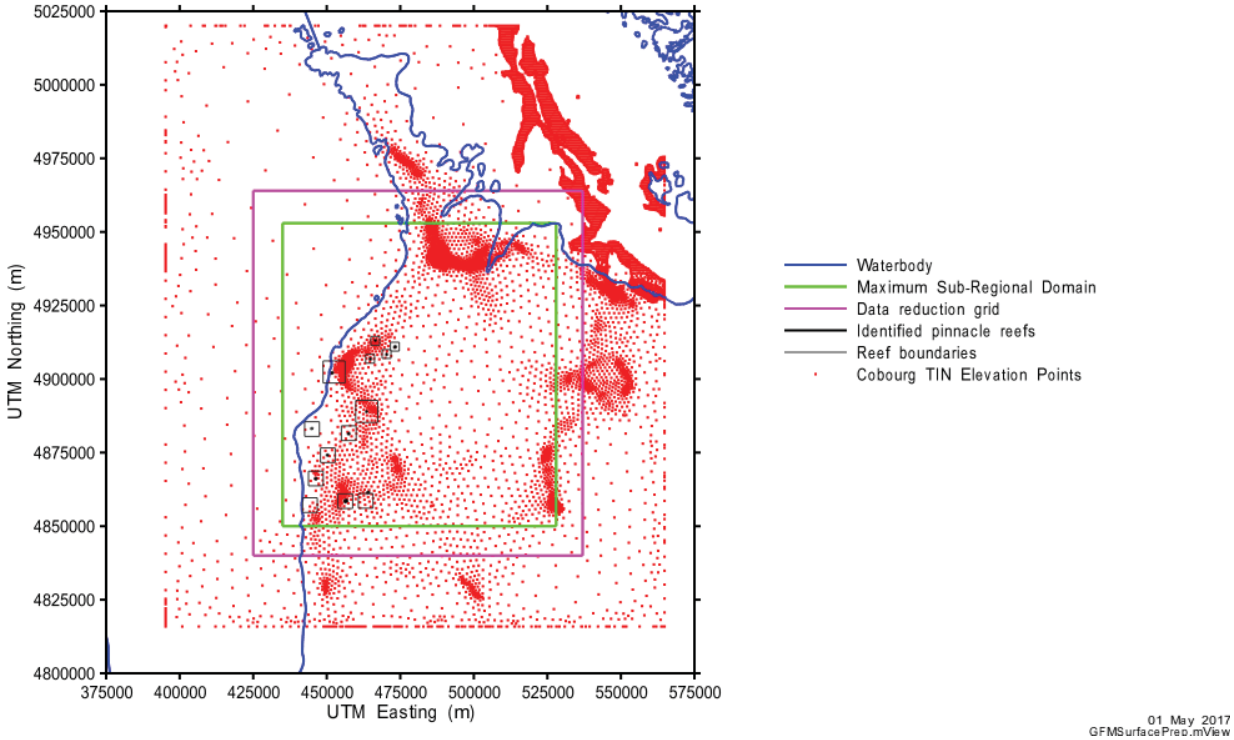

Figure 3-1: Geologic Framework Model (GFM) Data for the Cobourg Formation and Pre-Processing Grid Extents

The Paleozoic sedimentary bedrock formations dip to the south-west and are overlain by Quaternary deposits. The area where a given bedrock unit is present directly below the Quaternary deposits is termed its sub-crop area. In the absence of overburden (Quaternary deposits), the bedrock would outcrop. For formations which sub-crop below the upper drift unit within the possible 5CS Sub-Regional domain, the sub-cropping region was manually delineated and only those points not associated with sub-crop zones used in the formation surface interpolation. Figure 3-2 shows the interpolated surface and input data for the Guelph formation. Sub-crop regions are clearly defined with increased GFM data density.

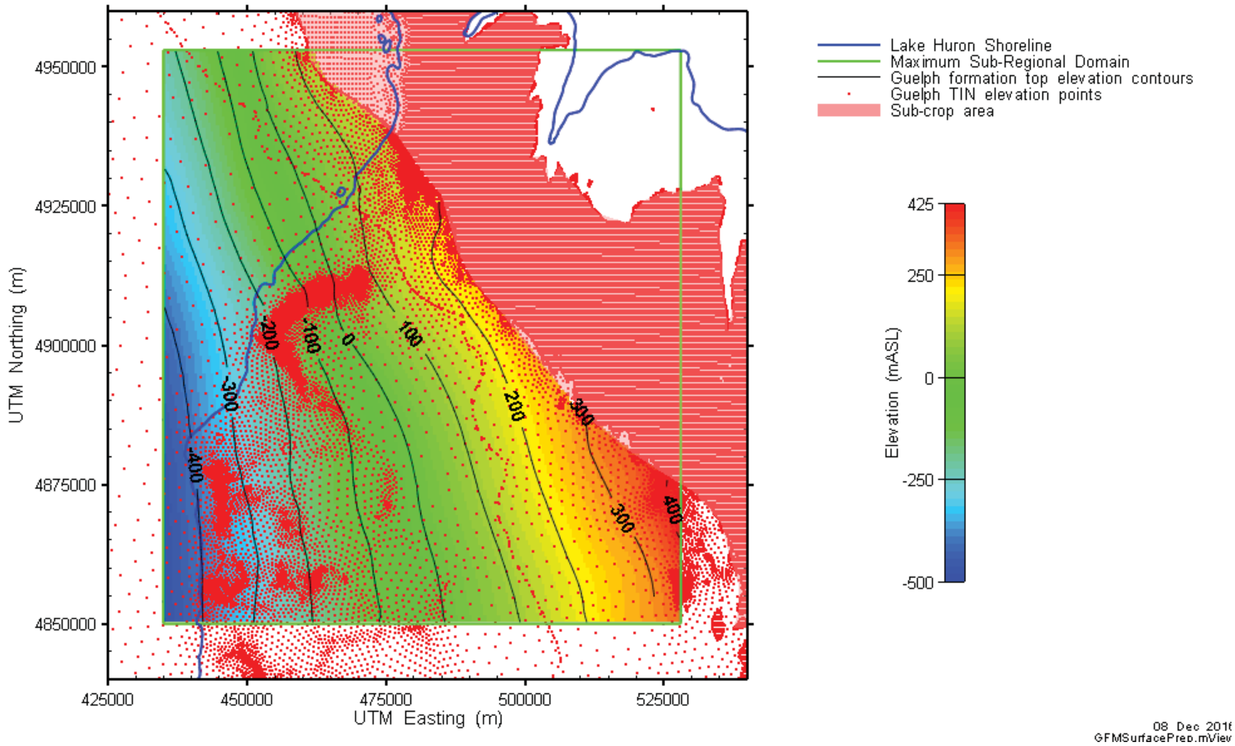

Note: High TIN point density in sub-crop region appears as red lines

Figure 3-2: Guelph Formation Interpolated Formation Top and GFM Input Data

A total of 27 surfaces were created ranging from the Pre-Cambrian to the Detroit River group. An additional surface describing top of bedrock was created from the combined sub-crop data. Ground surface was interpolated from DEM data provided on a 475 m grid spacing. Figure 3-3 shows interpolated formation tops.

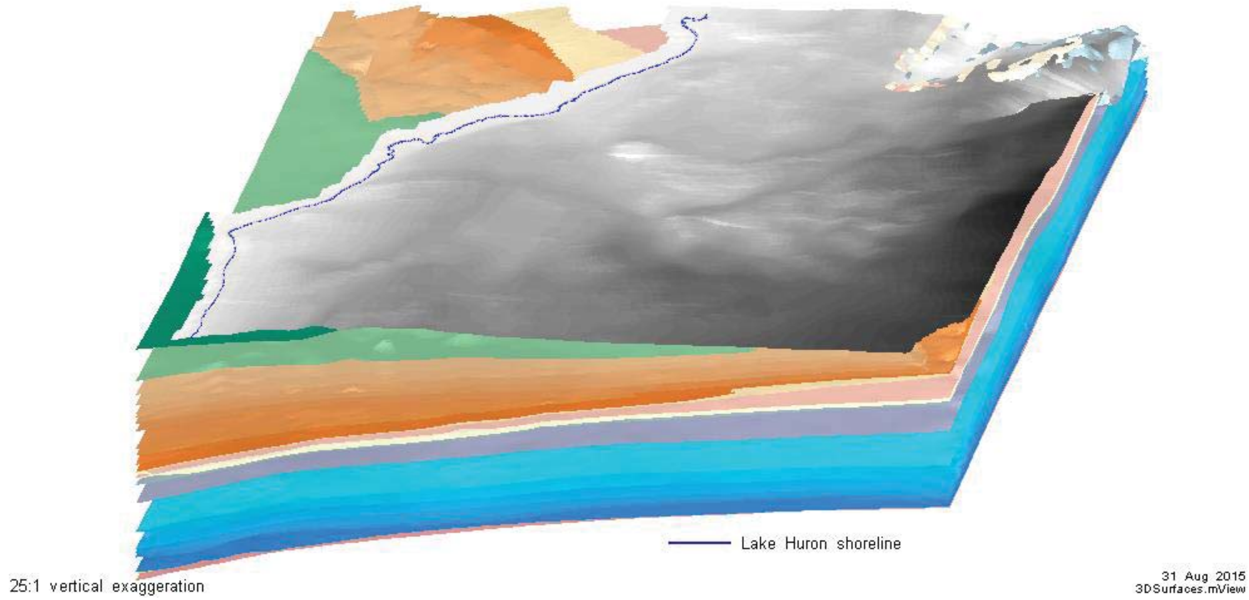

Figure 3-3: Three-Dimensional Visualization of Geologic Surfaces

3.2 Glacial Climate Data

Glacial climate data used in the 5CS simulations are derived from the Glacial Systems Model (GSM) nn9930 glaciation scenario referenced in NWMO (2013) and described in Peltier (2011). Of the eight models presented in Peltier (2011), the nn9930 scenario was one of two models with the best fit to observational constraints. The nn9930 model had warm-based glaciers while the other best fit model (nn9921) was cold based. Warm based glaciers were thought to have a greater impact on flow system behaviour due to large transients in surface hydraulic head boundary conditions as well as ice-sheet loading. Cold-based glaciers provide ice-sheet loading only.

Continent wide data are available on a 1 degree longitude and 0.5 degree latitude spacing at 500 year intervals from 120 ka before present day to present day. At the 5CS site there are two periods of glacial advance and retreat at approximate times of -60 ka and -20 ka. Figure 3-4 and Figure 3-5 show simulated ice thicknesses at the time of peak local ice thickness on a continent wide scale and 5CS local scale respectively. Data were interpolated at the site location from the surrounding GSM model grid points (see Figure 3-5). Resulting time series data for glacial thickness and permafrost depth at the 5CS site location are shown in Figure 3-6 and Figure 3-7.

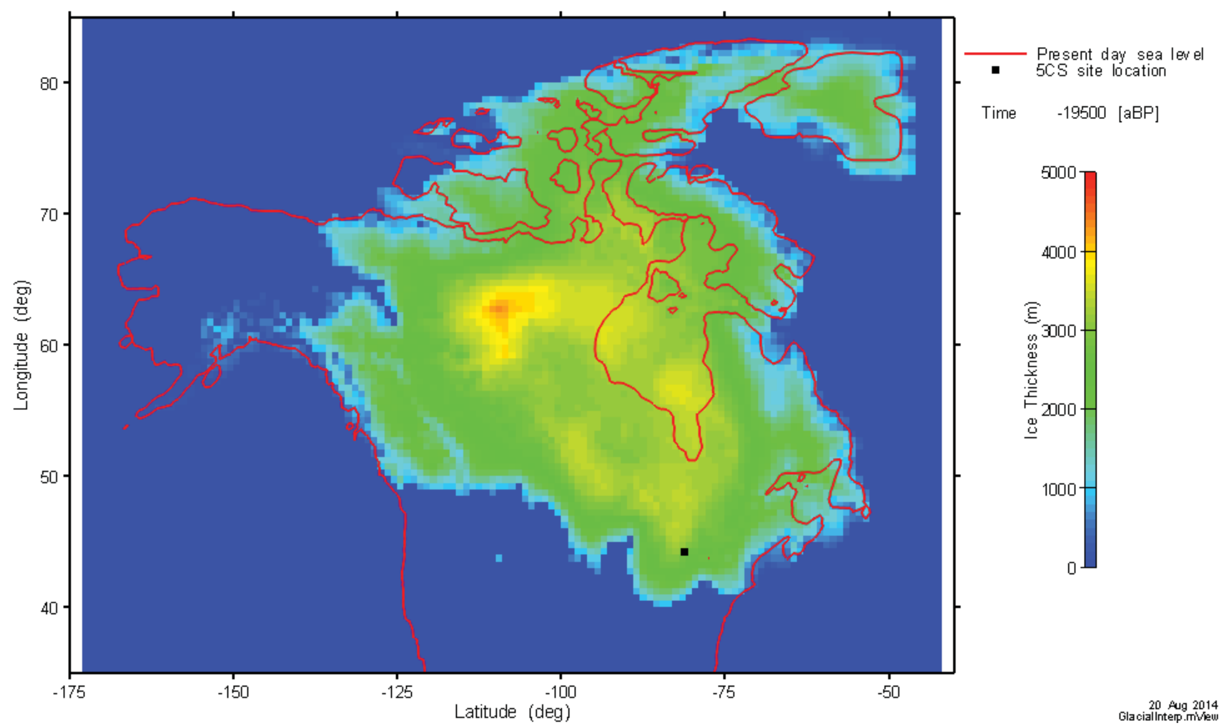

Figure 3-4: Continent Wide Ice Thickness for nn9930 Scenario at -19500 a

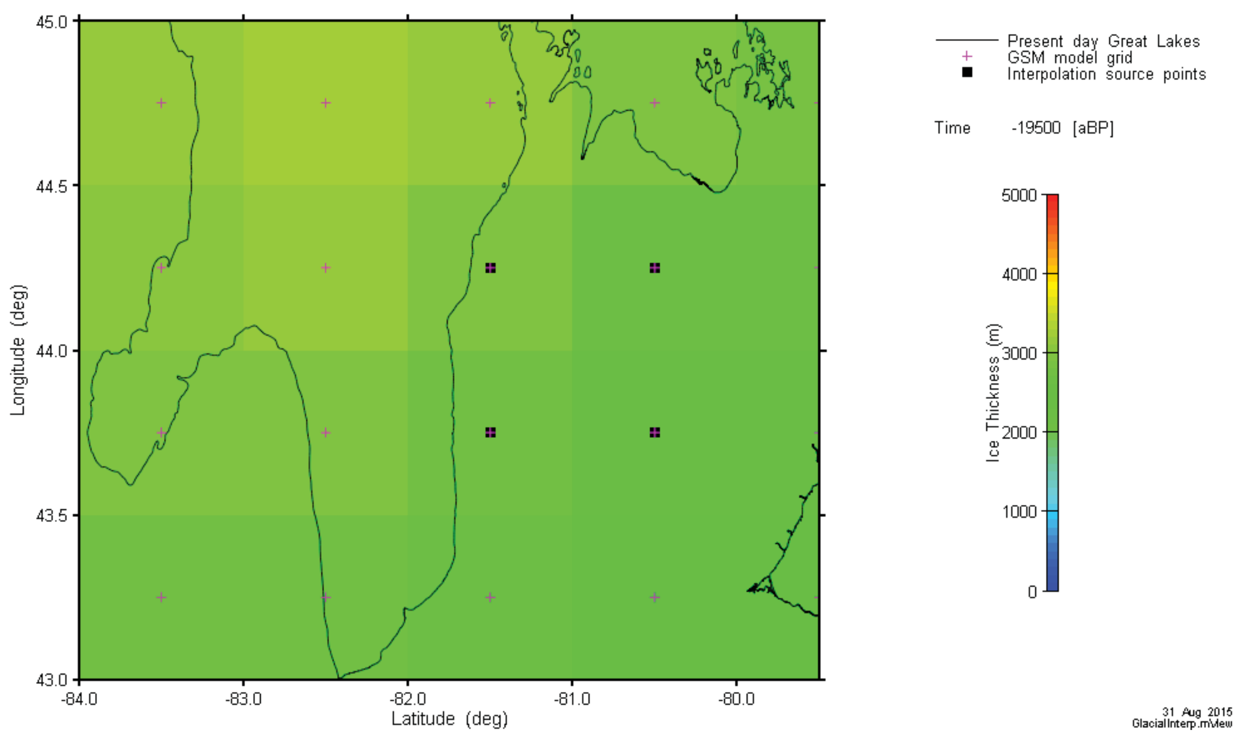

Figure 3-5: Local 5CS Ice Thickness for nn9930 Scenario at -19500 a

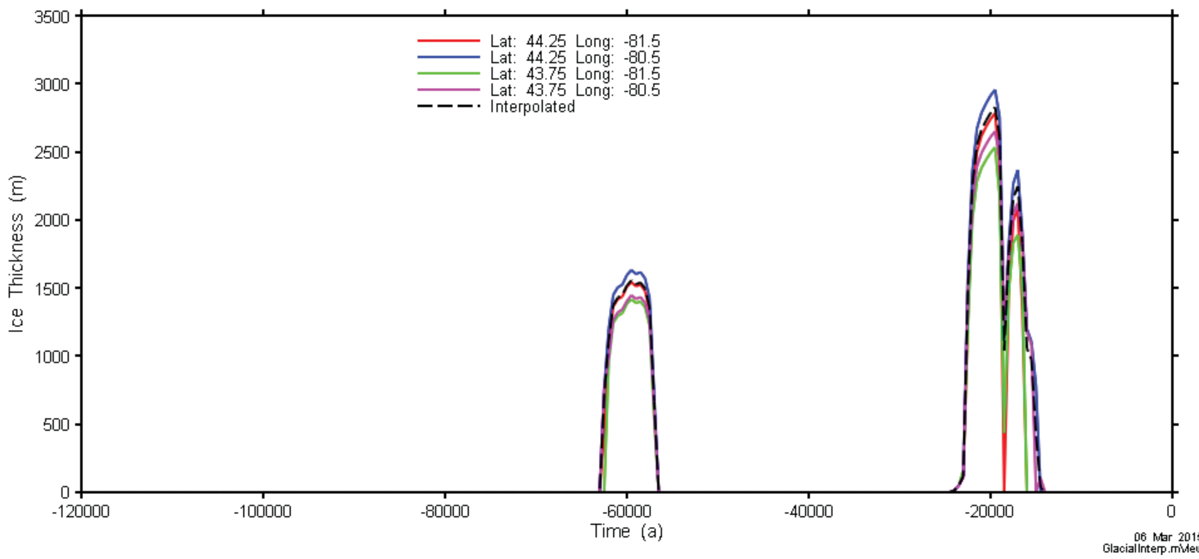

Figure 3-6: Source Data and 5CS Site Interpolated Glacial Ice Thickness

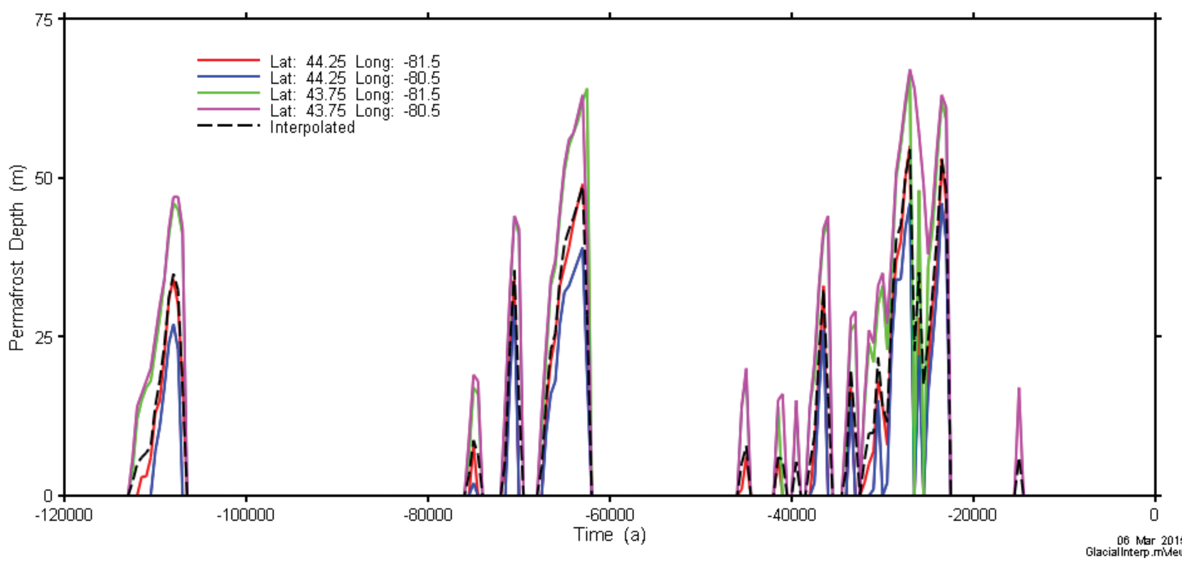

Figure 3-7: Source Data and 5CS Site Interpolated Permafrost Depth

The data indicate that there is no or little overlap between periods of permafrost and ice cover. As a consequence, all glaciation events are assumed to correspond to warm based glaciers where both hydraulic head and stress loading boundary conditions are applied at ground surface during periods of ice cover.

The GSM simulation describes a glacial cycle of 120 ka duration. This cycle assumed to restart at the present day and then repeat eight times to cover a 960 ka performance period for simulations.

4. GLACIATION SCENARIO

The implementation and results of the base Glaciation Scenario are described in the following subsections:

- Glaciation Sub-Regional Flow Model – model definition (discretization, property assignment, boundary conditions) and results of variable density and glacial climate flow modelling at the Sub-Regional scale. Sensitivity cases assess the impact of geosphere properties, boundary and initial conditions, and simulated processes on advective velocities in the vicinity of the repository.

- Site-Scale Transport Model– model definition, including repository and engineered barrier system (EBS) description, and results for combined glacial climate groundwater flow and radionuclide transport modelling for reference cases and limited sensitivity cases.

- Sub-Regional Two-Phase Flow Model – based on the Glaciation Sub-Regional Flow model, 2D simulations were conducted to consider the impact of gas in the Ordovician units on the groundwater flow regime during glacial climate cycles.

4.1 Glaciation Sub-Regional Scale Flow Modelling

The Glaciation Sub-Regional scale flow modelling provides boundary conditions for Site-Scale transport modelling and assesses the impact of variable density groundwater and other defined sensitivity cases. The repository location is indicated in figures in this section for reference only. There are no discretization adjustments or property assignments reflecting the presence of a repository in the Glaciation Sub-Regional Flow Model.

4.1.1 Model Description

4.1.1.1 Model Domain and Discretization

The Glaciation Sub-Regional flow model domain shown in Figure 4-1 was determined from the repository location and an assumed North-South direction of glacial advance and retreat (NWMO, personal communication). A domain of 25 km by 50 km is adequate to capture regional groundwater flow processes in the vicinity of the repository without excessive boundary effects. The origin was set at 47600E, 485860N in the UTM coordinate system, the lower-left corner of the Sub-Regional model domain. The domain was centred on the repository in the X direction but shifted 10 km southwards to ensure that flow from glacial advances was captured. The Northern grid limit includes an area of Guelph formation sub-crop to the North-East of the repository. The model was discretized with 500 m square elements in the plan section.

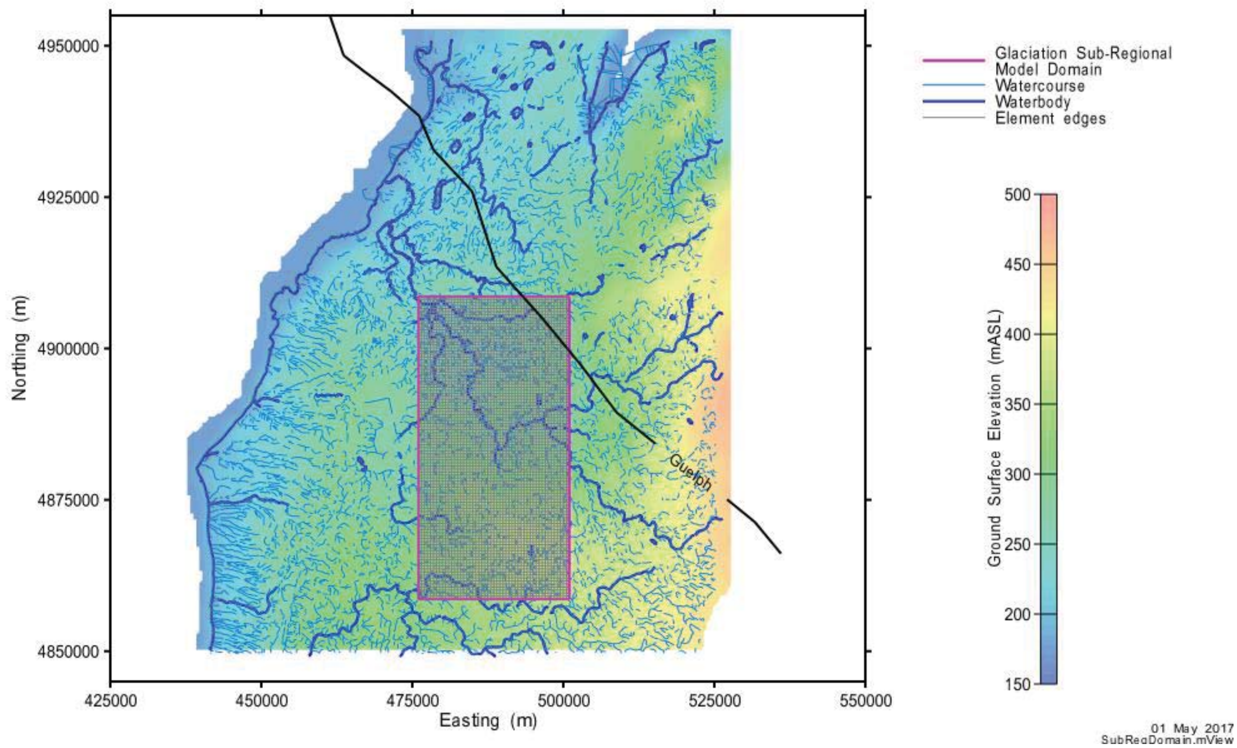

Figure 4-1: Glaciation Sub-Regional Model Domain

Vertical discretization was based on the geologic surfaces described in Section 3.1 and illustrated in Figure 4-2 and Figure 4-3. Not all formation tops are indicated in the figure; however, all were used in the discretization. Upper layers were modified so that a minimum of 50 m thickness weathered bedrock/overburden zone could be assigned. A minimum grid layer thickness of 0.1 m was enforced in the northern end of the grid where sub-cropping layers were merged into the drift/weathered bedrock zone.

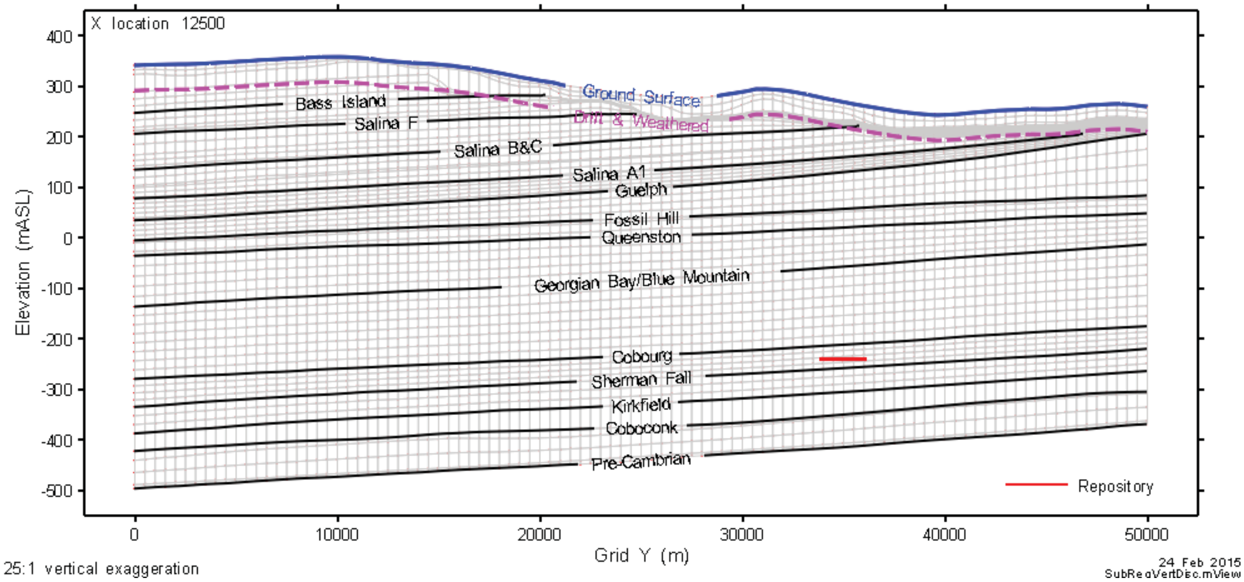

Figure 4-2: Glaciation Sub-Regional Model Discretization on Vertical Slice Through X = 12500 m

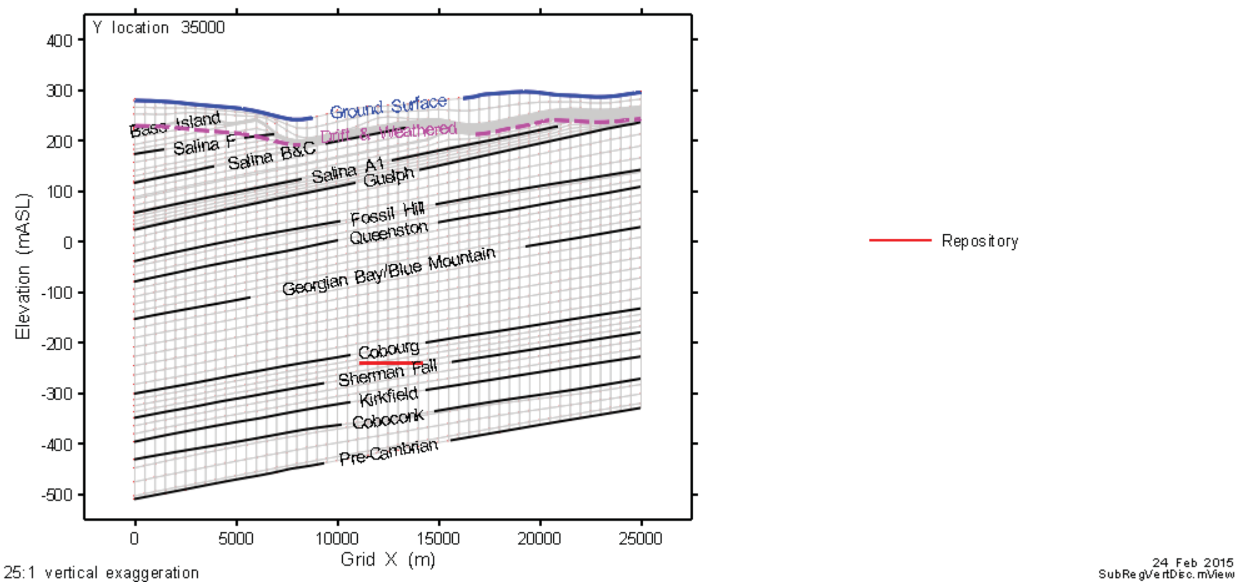

Figure 4-3: Glaciation Sub-Regional Model Discretization on Vertical Slice Through Y = 35000 m

The resulting model domain consists of 51 nodes in the X direction, 101 in the Y direction and 59 node layers, for a total of 303,909 nodes and 290,000 elements.

4.1.1.2 Property Assignment

Properties were assigned based on element position relative to geologic surfaces (Figure 4-4). Figure 4-5 details pinch outs (A1 Evaporite, A2 Evaporite and B Anhydrite) and sub-crops. Guelph formation properties are assigned across the full thickness of the Niagaran group, which also includes other, thinner formations, such as the Goat Island, Gasport and Lions Head formations. Reference case values for flow and hydro-mechanical model parameters are tabulated in Appendix A.

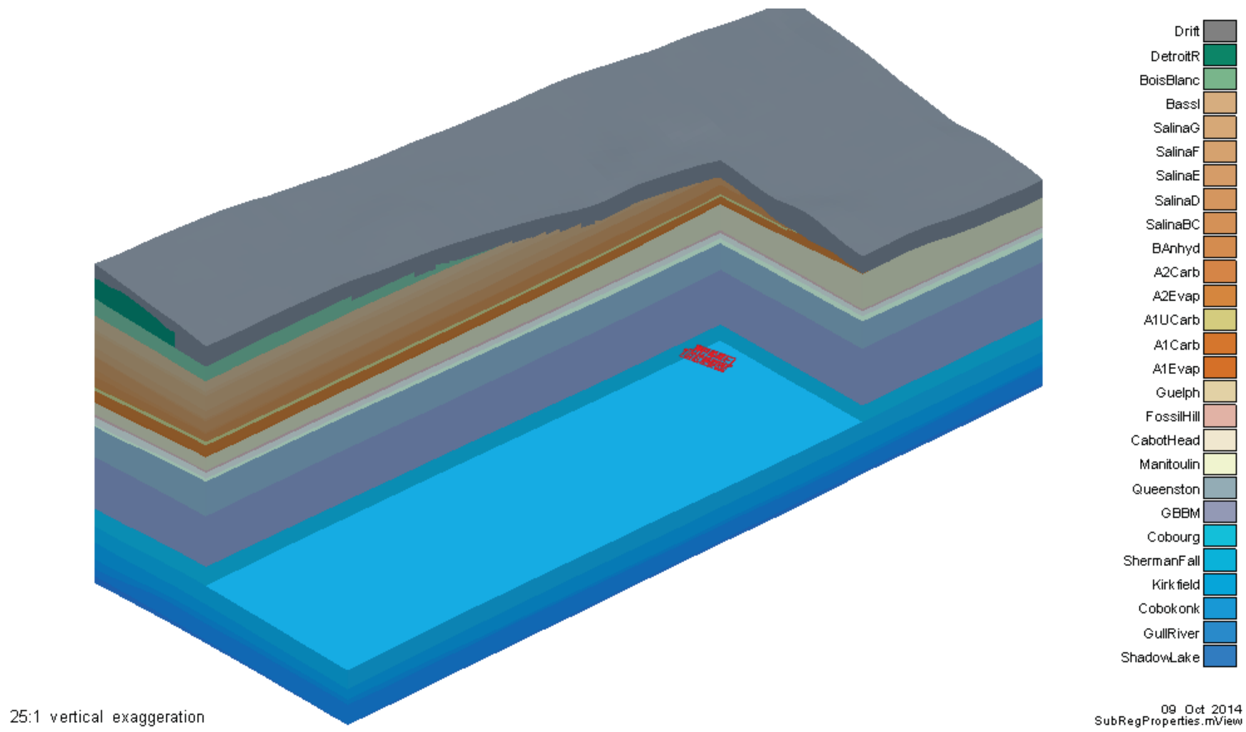

Note: Repository shown for location reference only

Figure 4-4: Glaciation Sub-Regional Model Property Assignment

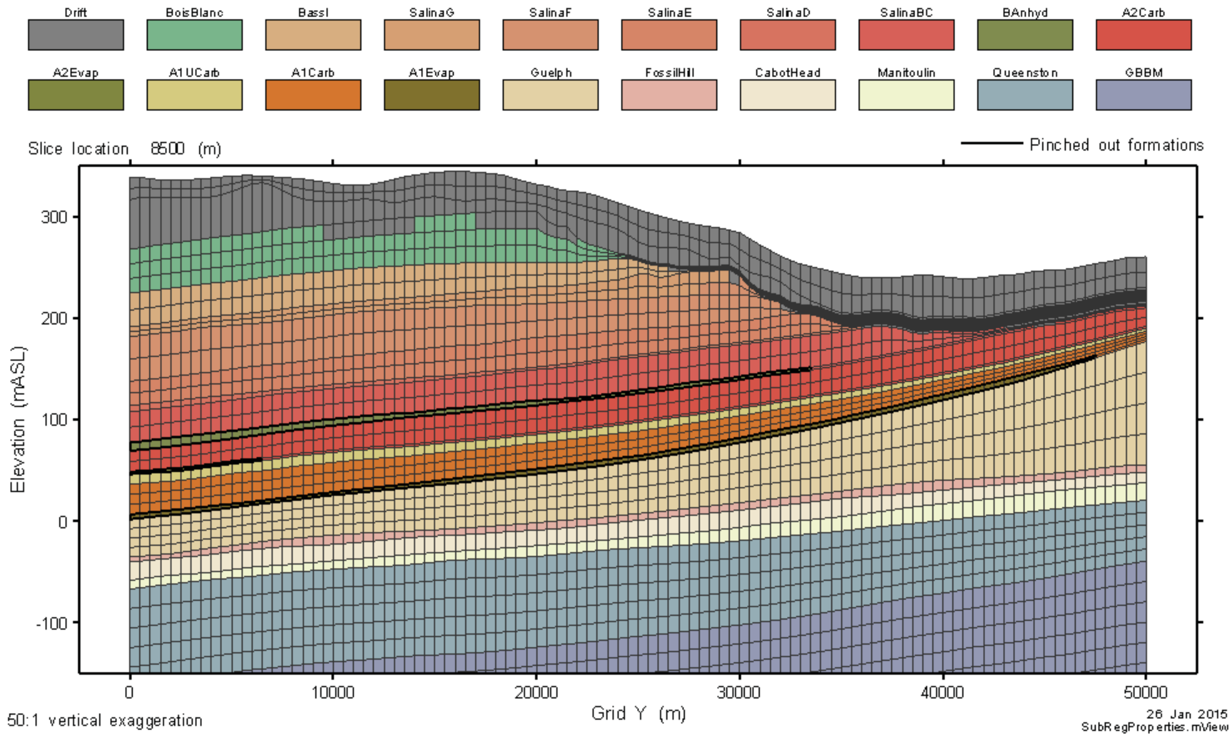

Figure 4-5: Glaciation Sub-Regional Model Property Assignment on Vertical Slice Through X = 8500 m

Many of the figures in this report are presented with substantial vertical exaggerations to allow formations to be clearly represented. It is worth noting that the model domain is much more extensive laterally than vertically. In a true perspective figure with no vertical exaggeration, Figure 4-4 appears as shown in Figure 4-6.

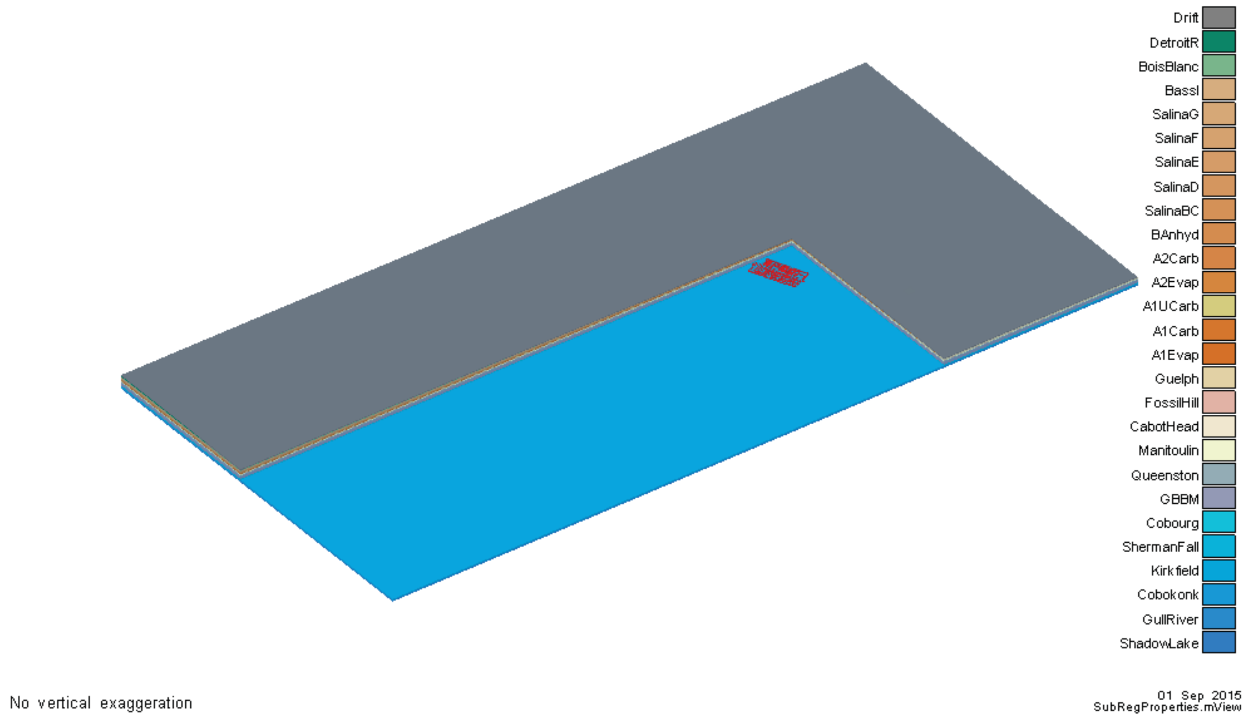

Note: Repository shown for location reference only

Figure 4-6: Glaciation Sub-Regional Model Property Assignment (no vertical exaggeration)

4.1.1.3 Boundary Conditions

Two sets of surface boundary conditions are used: 1) constant head at ground surface elevation for steady-state flow (required for model verification and comparison simulations) and preparatory variable density simulations, and 2) varying head and stress-loading rate at ground surface for glacial climate simulations. For steady-state flow and variable density simulations, zero flow boundary conditions are applied at bottom of the model and on all vertical model sides. This is not strictly accurate as it eliminates the possibility of regional flow within the model domain. However, experience has shown that the formations are of sufficiently low permeability to preclude virtually any regional flow in the aquitard units. Regional modelling results (Sykes et al., 2011) show horizontal gradients which are essentially zero within the Ordovician units. Flow directions within the more permeable Guelph are not well known on the regional scale and thus would not benefit from specification with fixed heads. For glacial climate cases time variable fixed head boundary conditions are applied at the North and South end of the model. The time varying glacial heads at surface are propagated downwards over the full vertical extent of the North and South grid nodes, as shown in Figure 4-7. This has the effect of forcing a gradient in the permeable units that would be consistent with expectations during a glacial advance/retreat, and allows flow into and out of the domain. The boundary conditions have only a very limited impact on flow in the impermeable units. Implications of this choice in boundary conditions are addressed with a sensitivity case.

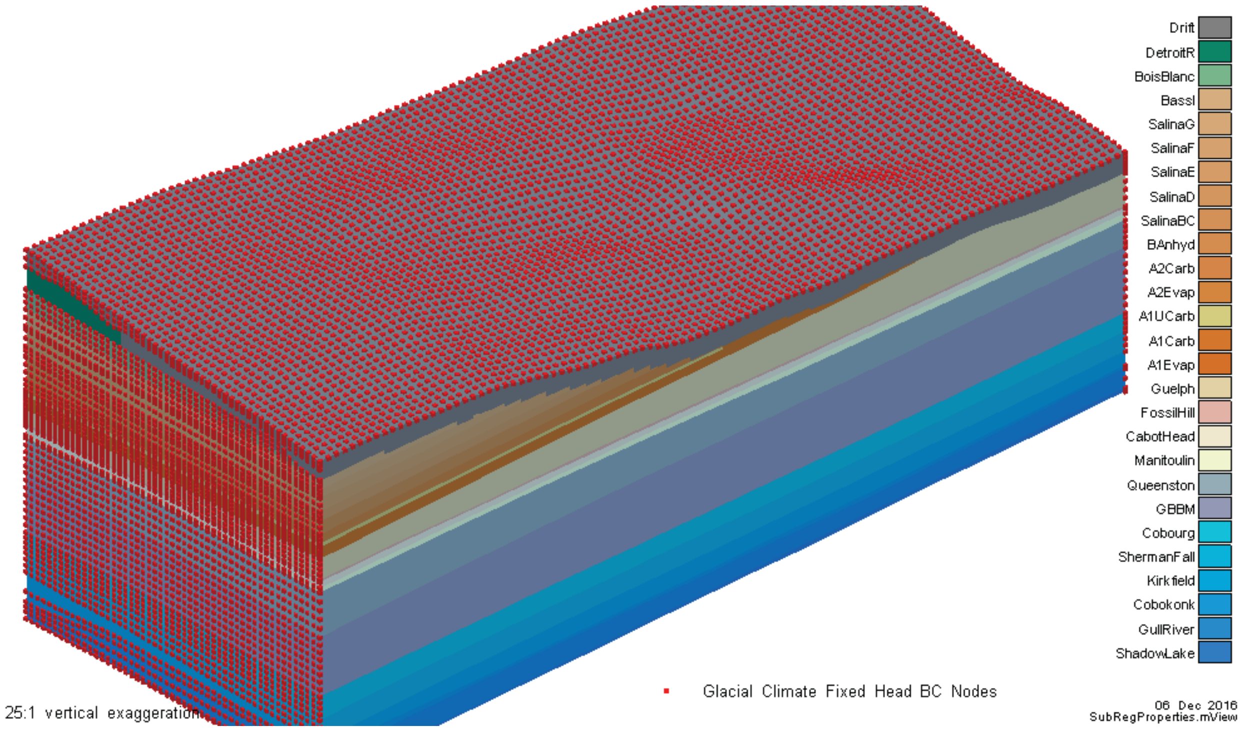

Figure 4-7: Glaciation Sub-Regional Model Fixed Head Boundary Condition Nodes

Glacial boundary conditions for the model surface and the North and South vertical boundaries are developed based on the approach described in Section 2.3, using the ice thickness calculated by the GSM model described in Section 3.2 above. Time-varying hydraulic head and loading stress rate applied at ground surface directly above the repository are shown for a single glacial cycle in Figure 4-8.

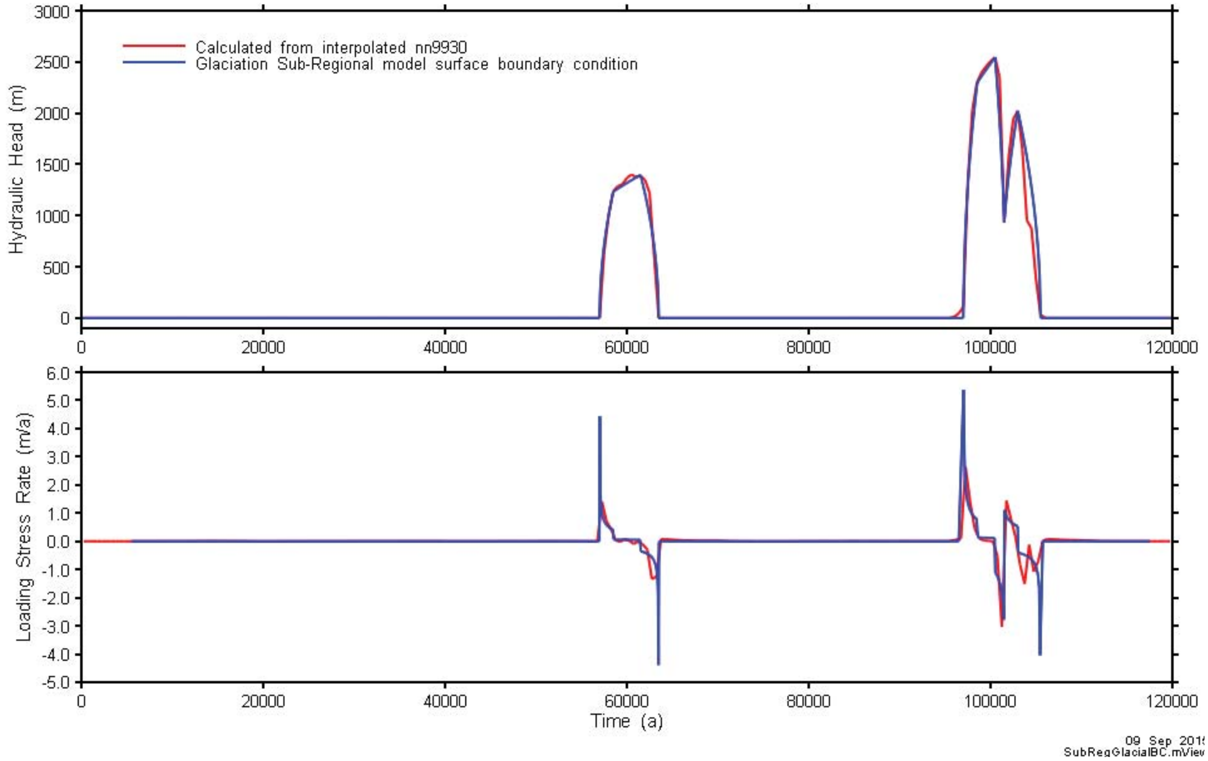

Figure 4-8: Glaciation Sub-Regional Model Glacial Surface Boundary Conditions

Figure 4-9 presents specified surface boundary conditions at four times associated with the first glacial event at 60 ka. The upper left quadrant figure is at ground surface elevation and reflects surface topography before the ice-sheet intercepts the model grid. The toe of the ice-sheet has advanced approximately 15 km across the domain in the upper right figure. The lower left figure is at Glacial Peak where the upper ice sheet surface is an attenuated reflection of the underlying topography. The ice sheet is retreating in the lower right figure.

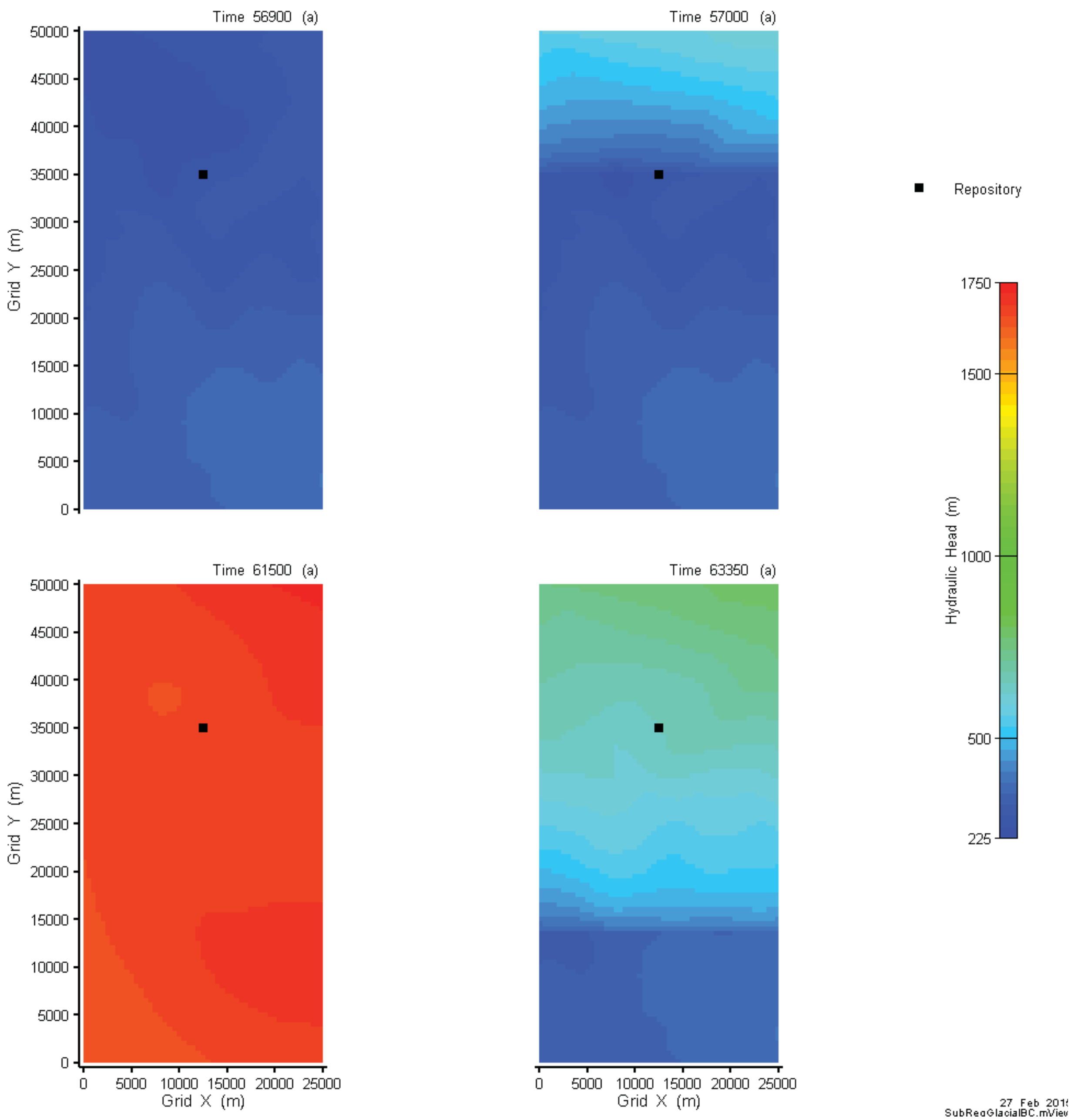

Figure 4-9: Glaciation Sub-Regional Model Surface Hydraulic Head Boundary Conditions at Selected Times (Pre-Glacial, Glacial Onset, Glacial Peak, Glacial Retreat)

Unlike Walsh and Avis (2010), where each glacial cycle was subdivided into multiple simulations connected with simulation restarts, the Glaciation Sub-Regional Flow model described here includes continuous boundary conditions for a full 960 ka simulation period.

4.1.1.4 Permafrost

Permafrost is implemented using the available FRAC3DVS-OPG facility where the hydraulic conductivity of elements is set to specified permafrost values during time periods when the specified permafrost depth exceeds the depth of the element centroid. Affected elements are those for which the element centroid is shallower than the permafrost depth. The reference case hydraulic conductivity for permafrost is specified as 5 x10^{-11} m/s (McCauley et al. 2002). Other material properties (porosity, effective diffusion for transport) are not modified. The maximum depth of permafrost is 55 metres, which limits permafrost primarily to the otherwise relatively permeable overburden/weathered bedrock zone, as shown in Figure 4-10. Reference case permeability in this zone in the absence of permafrost is 10^{-7} m/s.

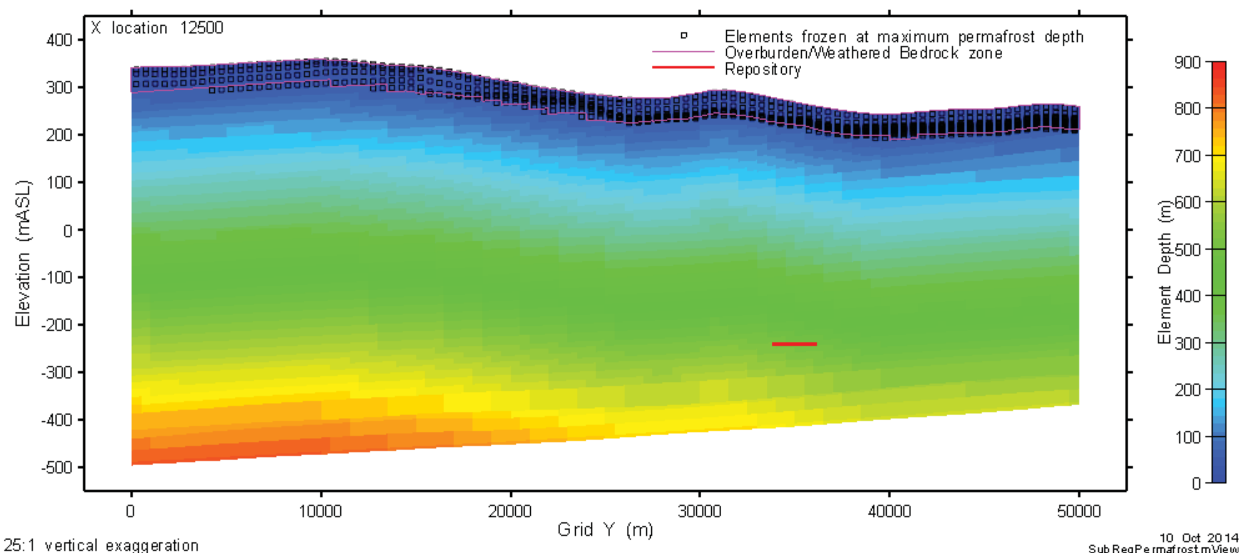

Figure 4-10: Glaciation Sub-Regional Model Maximum Permafrost Depth on Vertical Slice Through X = 12500 m

4.1.1.5 Well Operation

A single water supply well is assumed to be present and operating during all periods where neither permafrost nor ice cover occurs. The well abstraction rate is set to the reference rate of 1307 m^3/a when operating. Figure 4-11 illustrates well abstraction over the first glacial cycle. The well operates for 60,500 a, or for just over 50% of the glacial cycle. The same abstraction rates and timings are used for all eight simulated glacial cycles. Three cases with different well locations are defined: a reference and main shaft well location, as described in NWMO (2013), and a well located approximately at the centre of the facility. As shown in Figure 4-12, the coarseness of the Glaciation Sub-Regional Flow model discretization creates minor discrepancies between simulated well locations and specified well locations. Wells are implemented as line elements across the entire Guelph formation at each location, an interval of approximately 70 m, with the top of the pumping interval at a depth of approximately 140 mBGS.

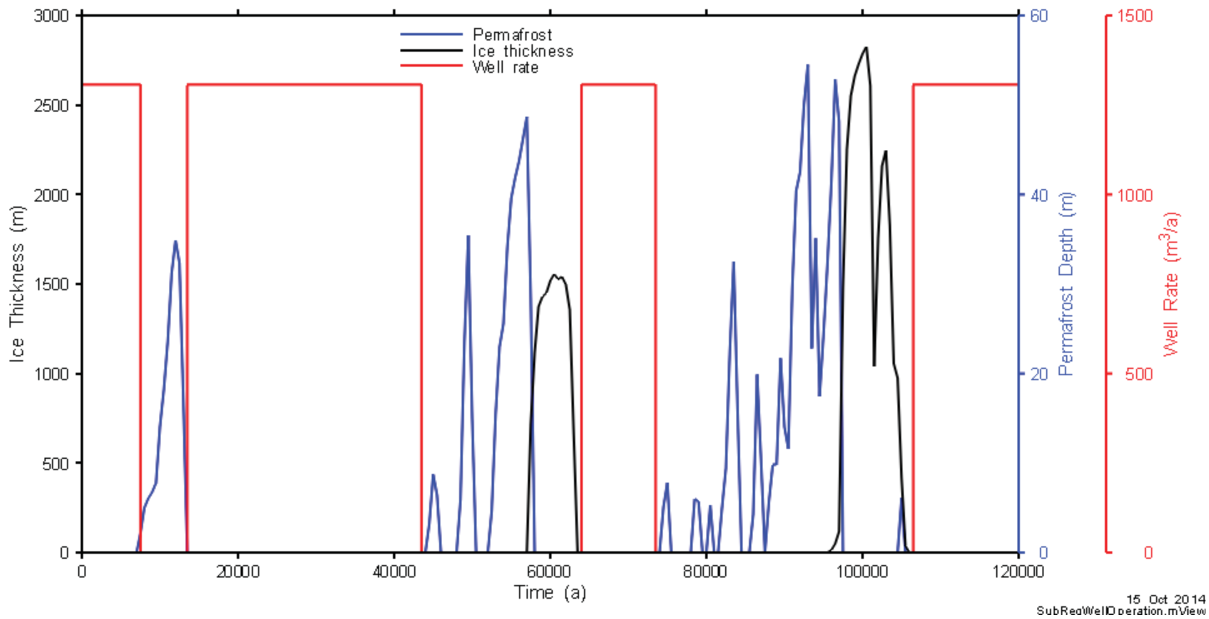

Figure 4-11: Water Supply Well Operation during a 120 ka Glacial Cycle

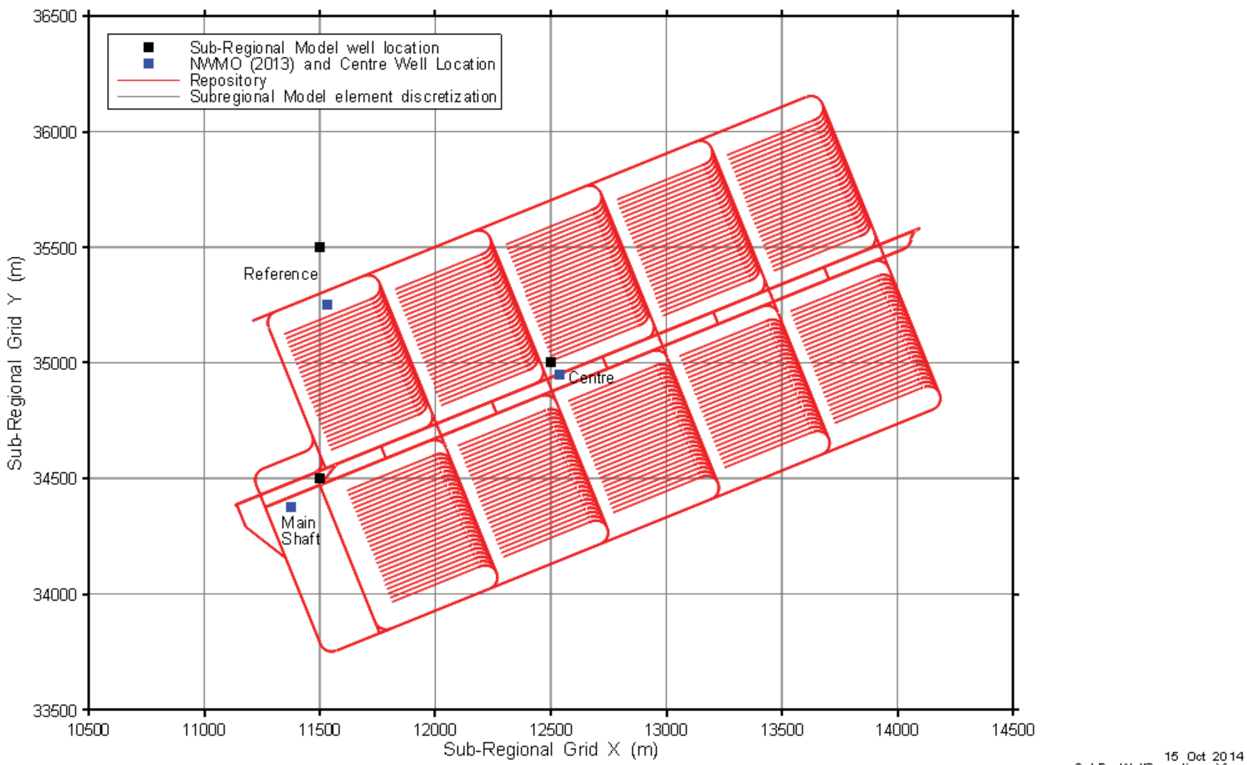

Figure 4-12: Water Supply Well Locations

4.1.2 Steady-State Flow Simulations

Constant density steady-state (constant climate) flow simulations were conducted to provide initial heads for variable density simulations and to provide a reference flow system for comparison to transient variable density and glacial climate simulations. Selected results for reference case properties with no water supply well are given in Figure 4-13 through Figure 4-16. The figures also define a 6.5 km x 5 km area surrounding the repository. This area, within the vertical limits of the Cobourg formation, defines a “repository volume” which is used to provide comparative statistics such as maximum velocity and minimum Mean Life Expectancy (MLE) for assessing sensitivity case results. Within this report, the term “Repository MLE” refers to the minimum MLE within this volume. MLE simulations determine the mean travel time to discharge for groundwater from any point within the model domain. MLE calculations include the effects of diffusion, advection, and dispersion. With FRAC3DVS-OPG, MLE simulations can only be performed for steady-state flow simulations.

As expected, the extreme low permeabilities of the deep geosphere, when coupled with very low hydraulic head gradients result in stagnant flow systems below the permeable Guelph formation. Advective velocities are less than 10^{-6} m/a while Repository MLE is greater than 200 million years. Note that advective velocity arrows shown in Figure 4-14 indicate areas where flow velocity is greater than 10^{-4} m/a (i.e., greater than 100 m transport in 1 Ma). This convention is used for all other figures presented in this report that illustrate advective velocities.

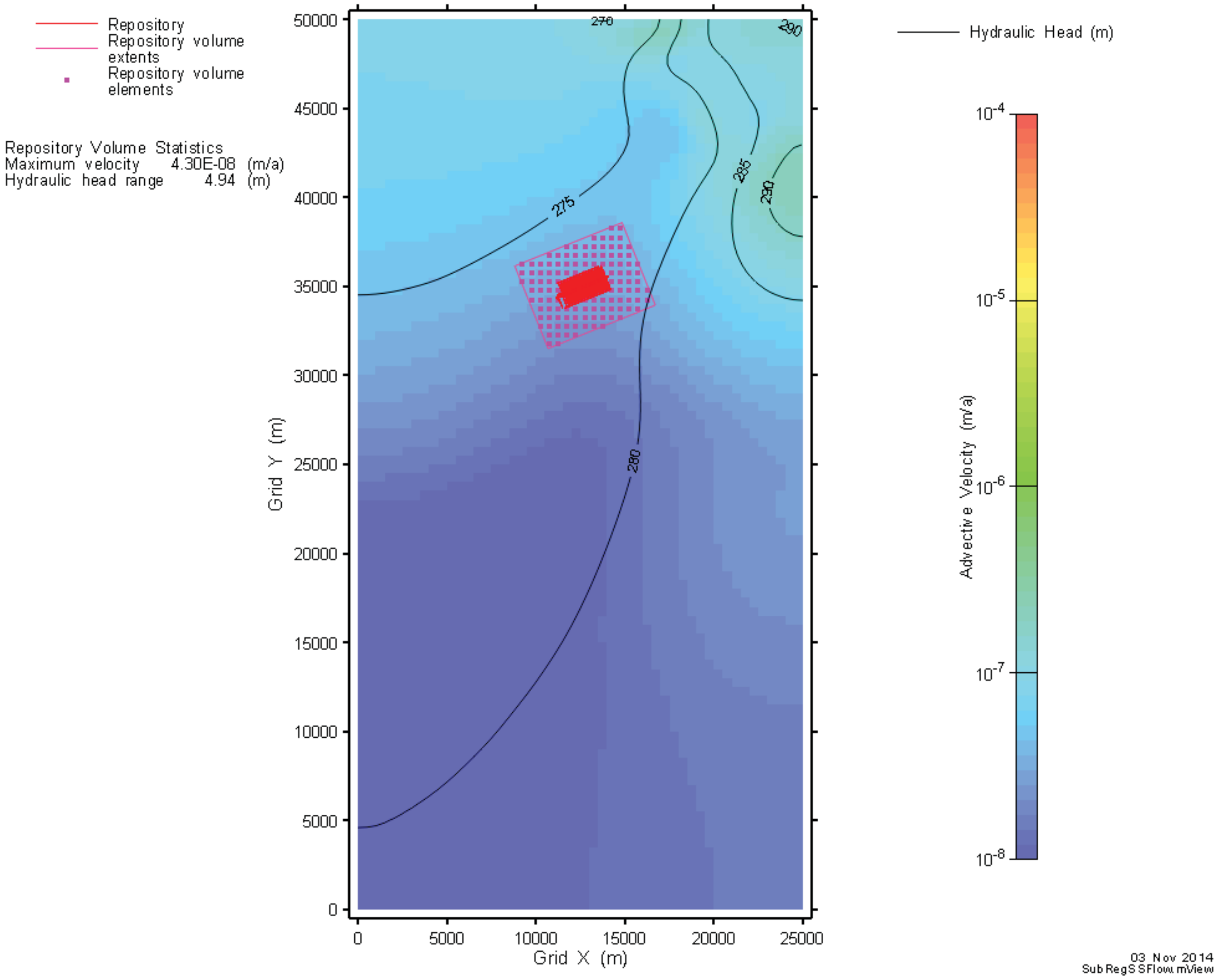

Figure 4-13: Steady State Reference Flow: Advective Velocity and Hydraulic Head Distribution on Model Layer Through Cobourg Formation

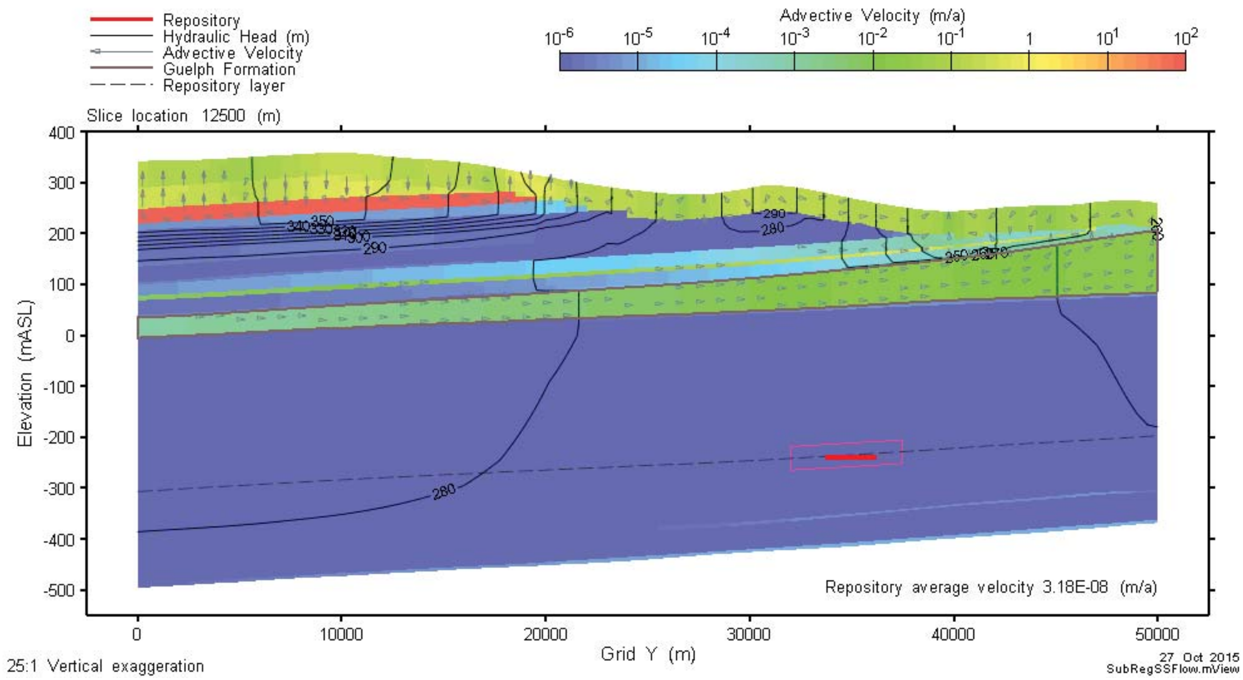

Figure 4-14: Steady State Reference Flow: Advective Velocity and Hydraulic Head Distribution on Vertical Slice Through Repository

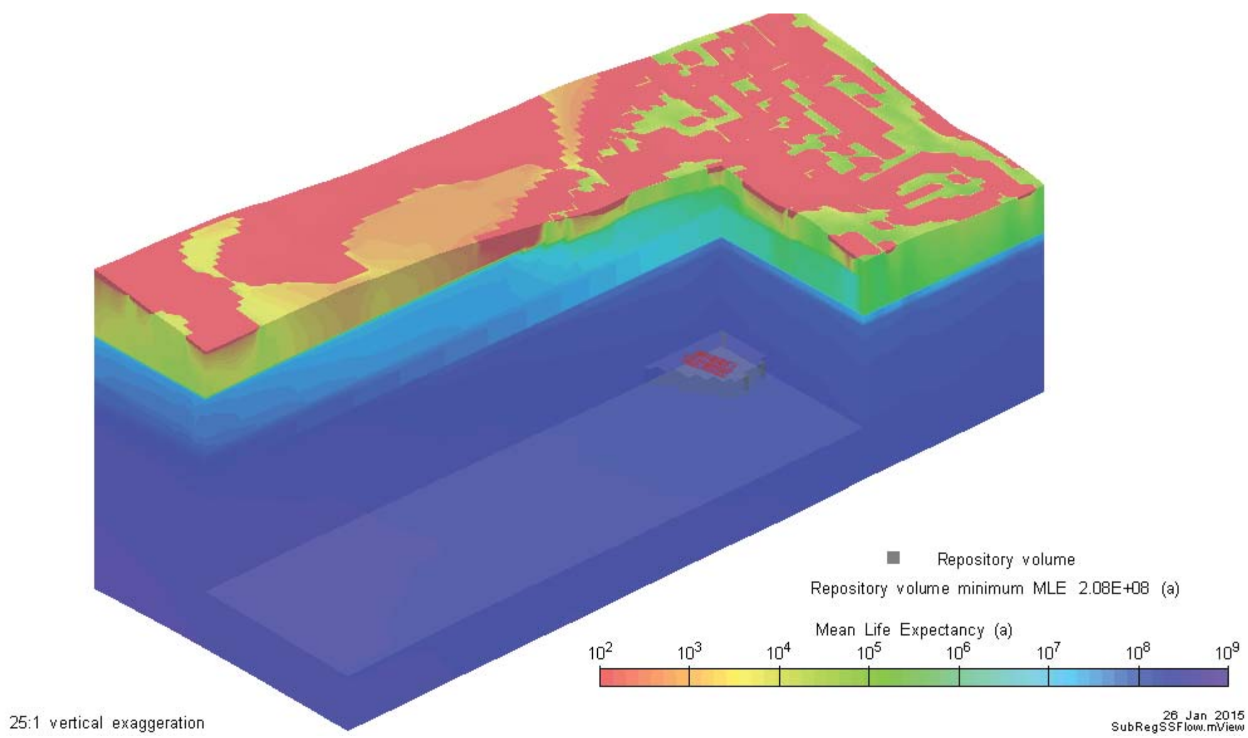

Figure 4-15: Steady State Reference Flow: Mean Life Expectancy (a)

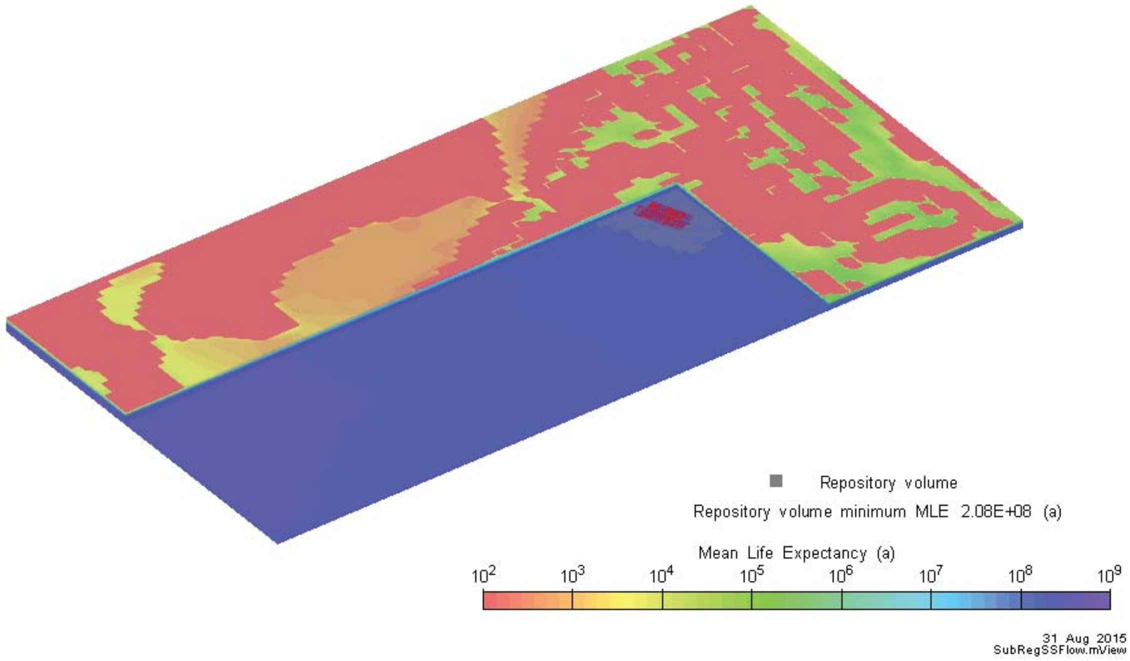

Figure 4-16: Steady State Reference Flow: Mean Life Expectancy (a) (no vertical exaggeration)

The very long MLEs are reflective of a diffusion dominated transport system. The nature of transport in the system can be seen by examining sensitivity cases showing the impact of increases in hydraulic conductivity. Two cases, KHigh and KHigh100, increase hydraulic conductivities for all geologic formations by a factor of 10 and 100 respectively. Given no other changes in boundary conditions these cases should yield corresponding increases in advective velocity. In an advective transport dominated system these increases in velocity would translate into identical decreases in MLE. As shown in Figure 4-17, there are decreases in MLE in formations above and including the Guelph. However, MLE decreases in the stagnant Ordovician (Queenston formation and below) flow system in the vicinity of the repository are only a factor of 1.25 (for K x 10) and 6.25 (for K x 100). As noted for analogous paleohydrogeological simulations presented in NWMO (2013), “this highly nonlinear relationship between MLE and hydraulic conductivities indicates the dominance of molecular diffusion in the transport mechanism.”

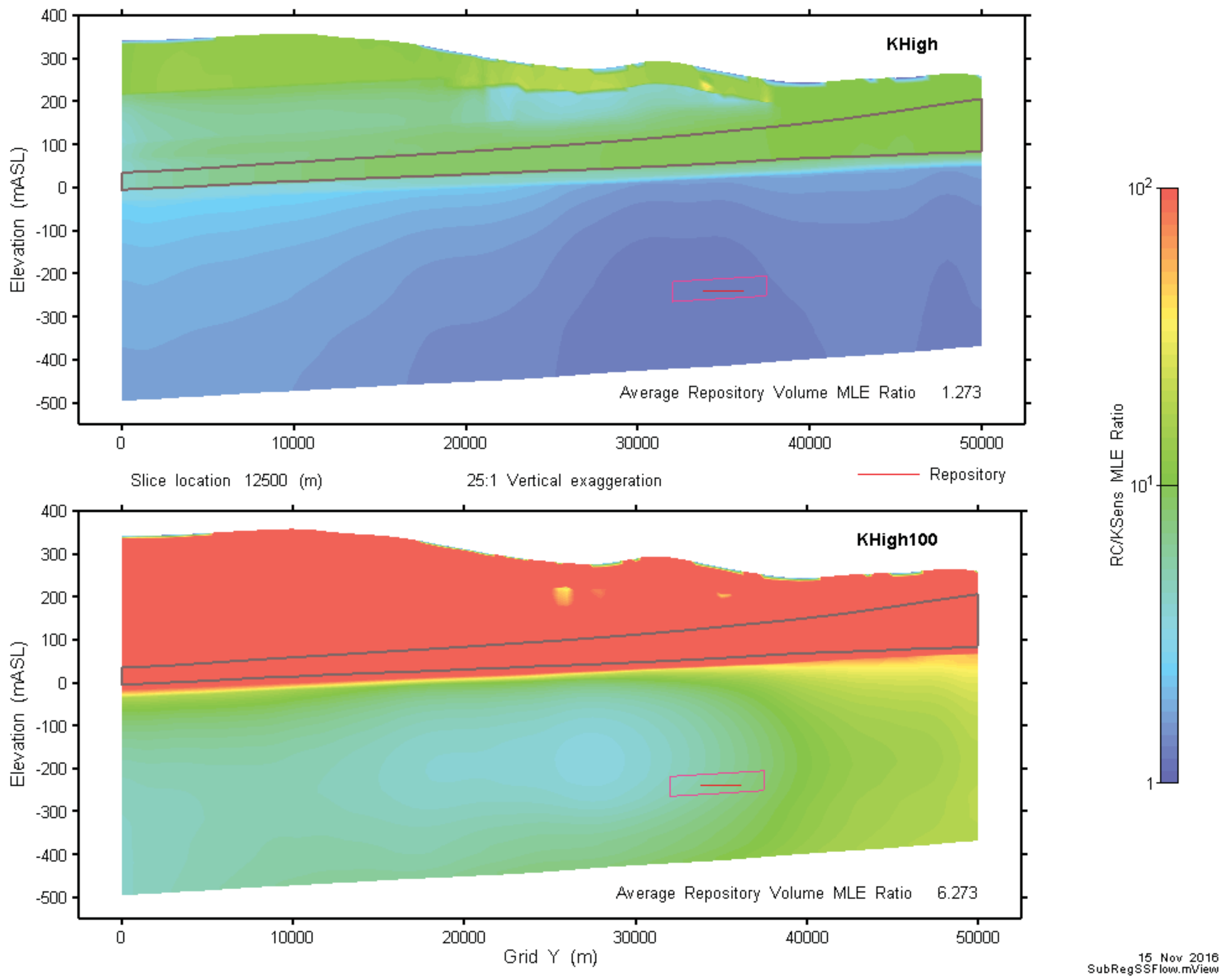

Figure 4-17: Steady State Reference Flow: Comparison of Mean Life Expectancy on Vertical Slice Through Repository – Khigh and Khigh100 Cases

Additional simulations with constant water supply well operation were performed to provide boundary conditions for Site-Scale steady state flow simulations. As shown in Figure 4-18, the presence of the well primarily affects flow in the Guelph formation in the immediate vicinity of the well.

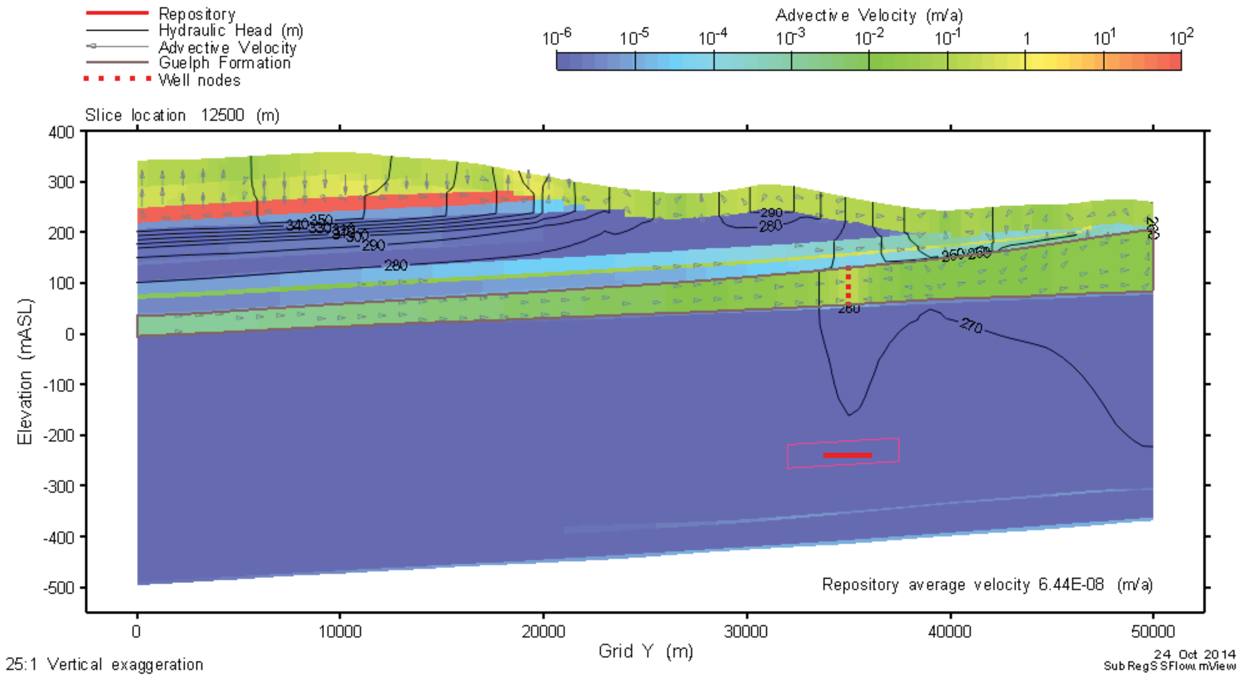

Figure 4-18: Steady State Reference Flow: Advective Velocity and Hydraulic Head Distribution on Vertical Slice Through Repository With Centre Well

Figure 4-19 and Figure 4-20 compare MLE on a vertical slice through the repository for the no-well and centre well cases respectively. The water supply well can be seen to have only minor impact on the age distribution in the deeper Middle Ordovician formations, with MLE in the vicinity of the repository decreasing from 210 Ma to 180 Ma. In this case, the 30 Ma reduction in the MLE relates mainly to the shortened distance for diffusive transport from the repository to discharge (i.e., surface or well), and relates less importantly to the small impact of slight increases in advective velocity induced by well operation.

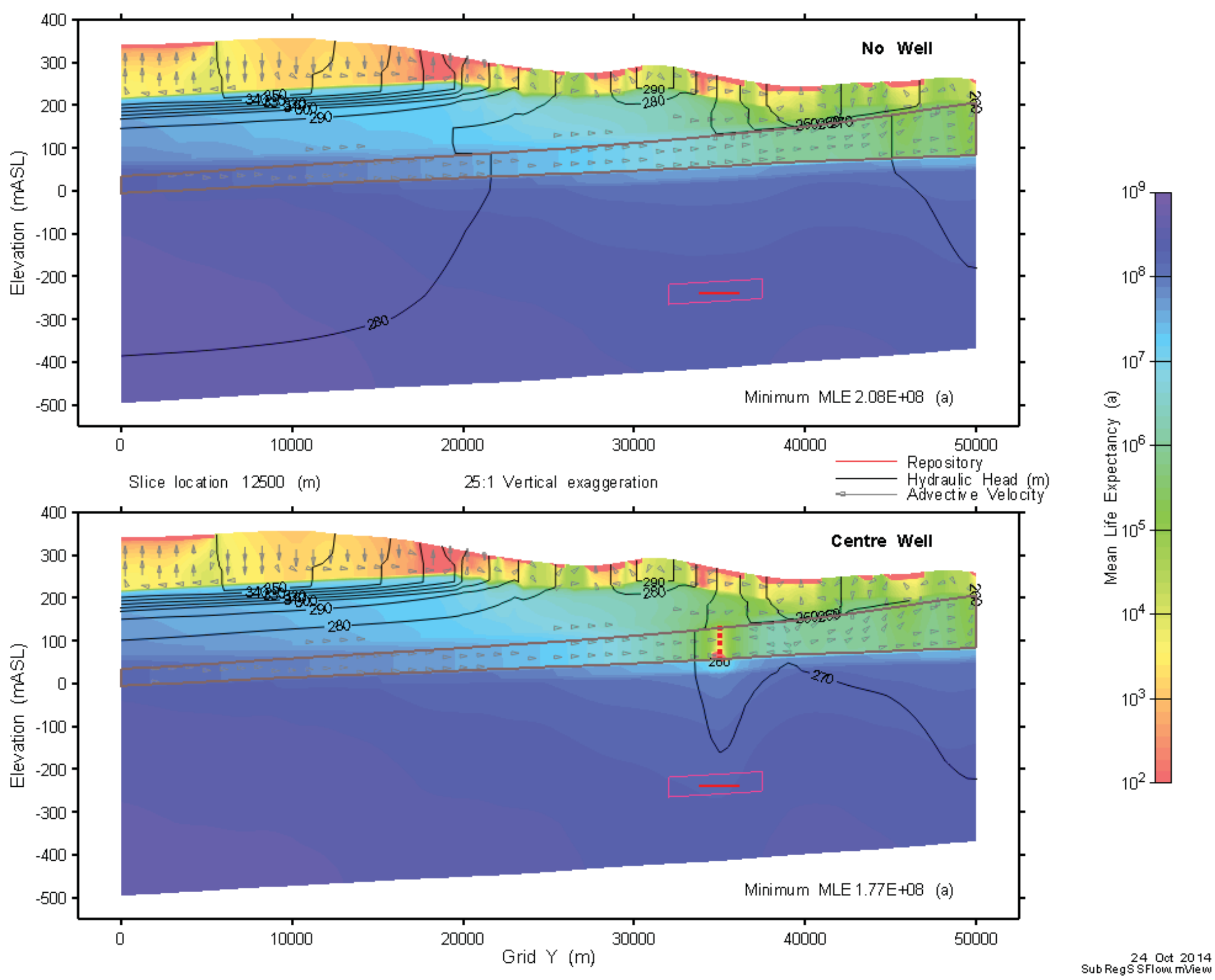

Figure 4-19: Steady State Reference Flow: Comparison of Mean Life Expectancy on Vertical Slice Through Repository – No Well and Centre Well

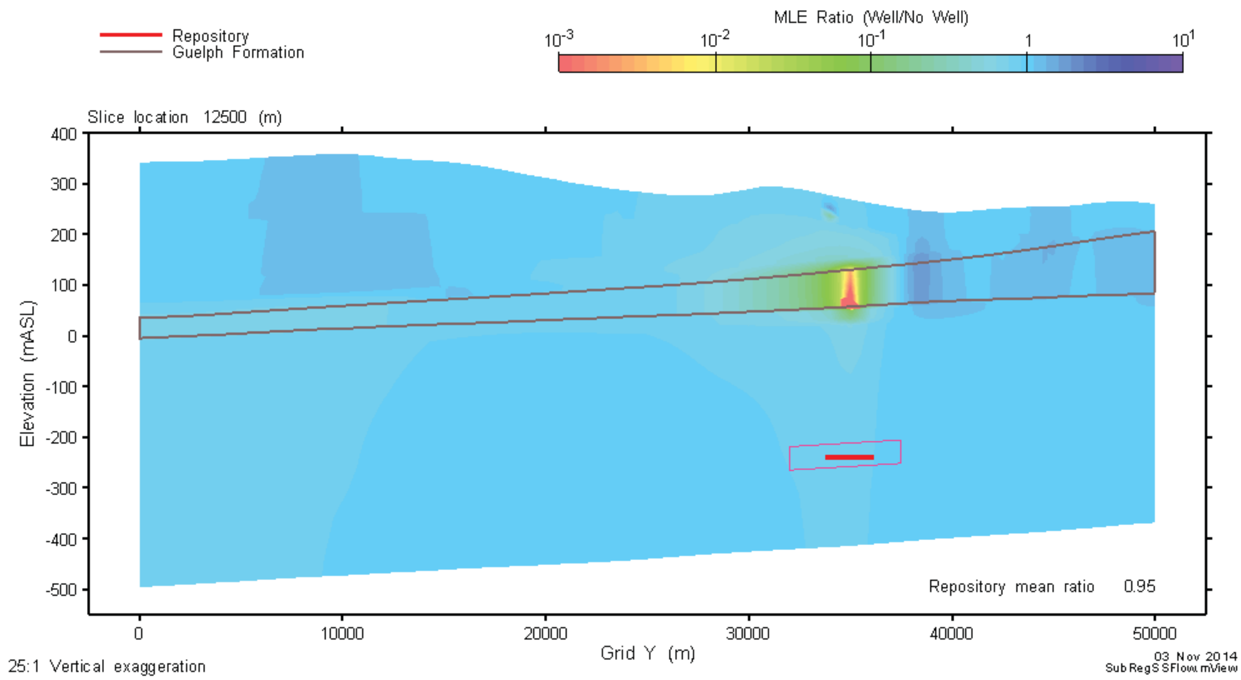

Figure 4-20: Steady State Reference Flow: Ratio Comparison of Mean Life Expectancy on Vertical Slice Through Repository – No Well and Centre Well

4.1.3 Variable Density Simulations

Variable density simulations were conducted to determine the impact of porewater salinity on transport processes. These simulations require a description of the distribution of variable density fluids in the geosphere. Initially, this profile was specified on a formation basis from measured data (INTERA, 2011) as shown in Figure 4-21 and Figure 4-22. Appendix A contains formation fluid densities used as initial conditions for the simulations.

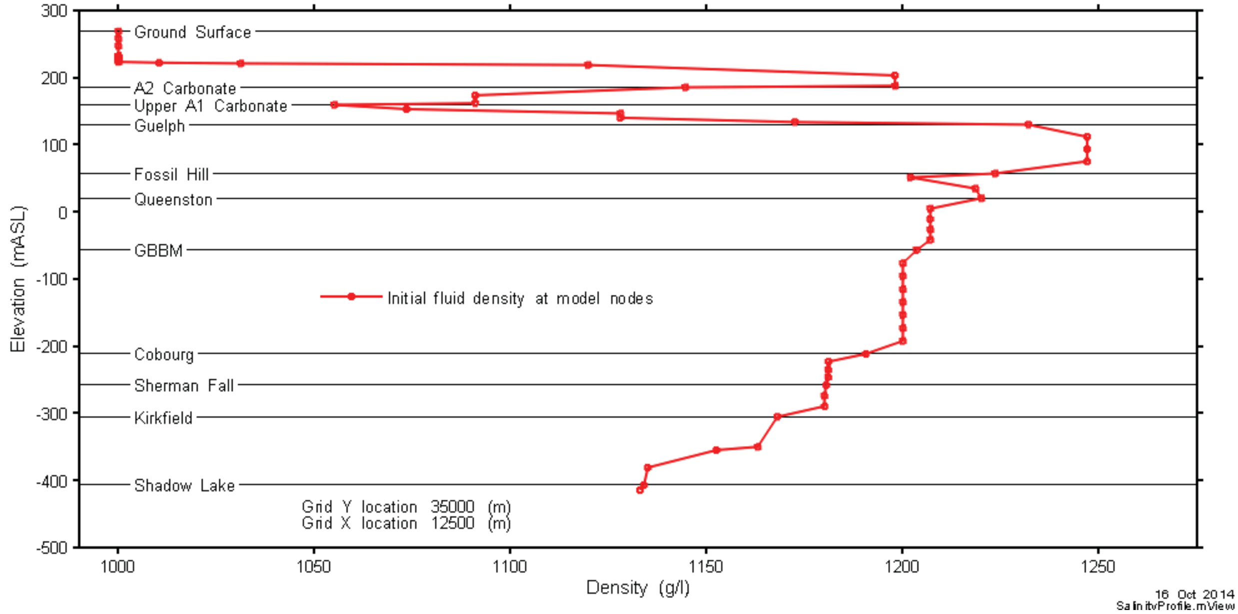

Figure 4-21: Initial Fluid Density Profile at Repository Location

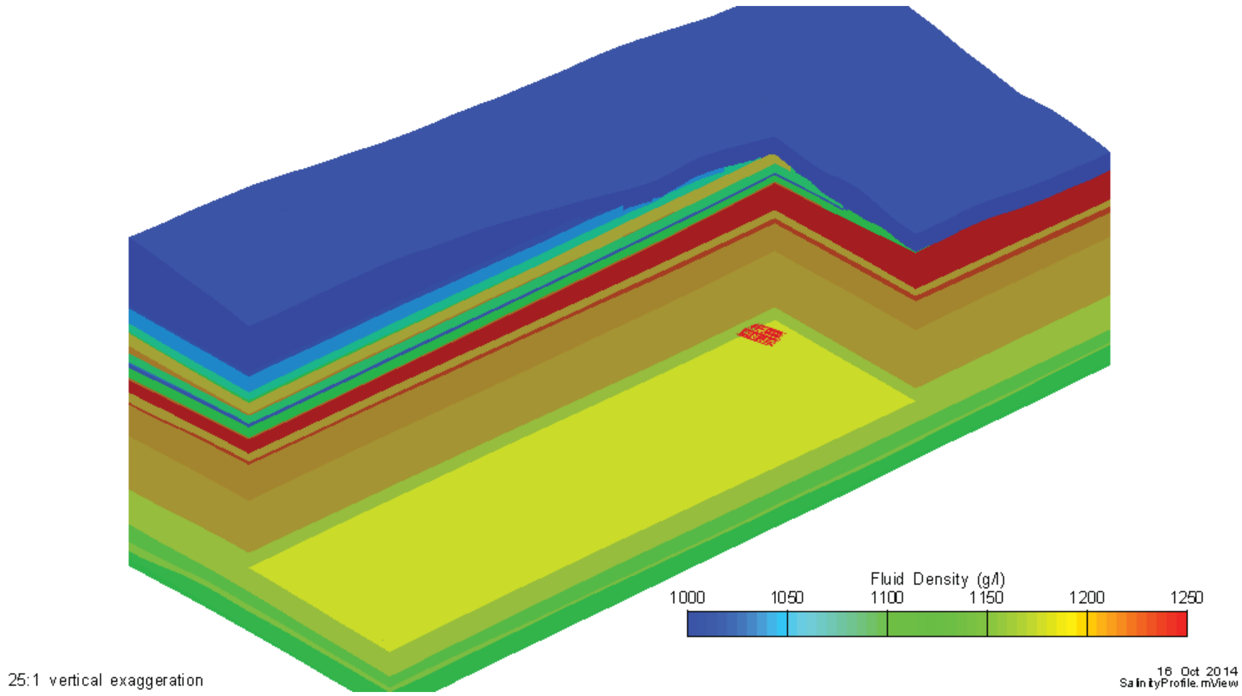

Figure 4-22: Initial Fluid Density in Model Domain

It should be noted that the salinity profile is based on measurements taken at the Bruce site (INTERA, 2011), where formation depths are much greater and where all formations to the Detroit River group are present. At the Bruce site, the permeable Guelph and Salina A-1 Upper Carbonate formations are highly saline and are not considered potable water supplies. In contrast, salinities in the shallow groundwater zone within the larger Glacial Sub-Regional Flow model domain are much reduced in areas where the Guelph formation sub-crops and where the Guelph is a potable water supply aquifer.

As described in NWMO (2013), variable density simulations require an initial spatial distribution of fluid density consistent with both measured values and characteristics of the flow system. To obtain a reasonable set of initial conditions, variable density simulations followed the general methodology described for regional density dependent flow modelling NWMO (2013):

1. Initial fluid head is determined from steady-state constant density simulations.

2. Fluid density is initialized on a formation basis as specified. The steady-state head from 1) is converted to an initial freshwater head based on the density profile.

3. Fluid flow simulations are conducted with the density profile set as fixed concentrations to determine a consistent freshwater head profile. Calculated freshwater heads from 2) are used as initial conditions. The flow system is allowed to evolve until steady-state conditions are attained.

4. The steady state freshwater head profile is used as initial freshwater head to a variable density simulation. This simulation is run forward to 1 Ma at which point “pseudo-steady-state” conditions are obtained. Freshwater head and brine concentration at 1 Ma are used as initial conditions for variable density glacial simulations.

For all steps, surface hydraulic boundary conditions are constant fixed heads at elevation on the upper surface of the model. Third-type transport, or Cauchy, boundary conditions with 0.0 concentration are applied at surface. This allows free outflow of saline discharge while ensuring that recharge is freshwater. The bottom boundary condition is a fixed concentration at a density consistent with the Shadow Lake formation.

Initial simulations indicated that the salinity in the Guelph formation would substantially dissipate throughout the entire formation during step 4). Although salinity was expected to be reduced in areas where the Guelph formation sub-crops and freshwater recharge or mixing occurs, high fluid densities should persist in deeper portions of the formation, consistent with the measured densities used in the initial profile. Consequently, fixed concentration nodes were specified in deeper portions of the Guelph, corresponding approximately to the extents of non-potable water in the formation as shown in Figure 4-23.

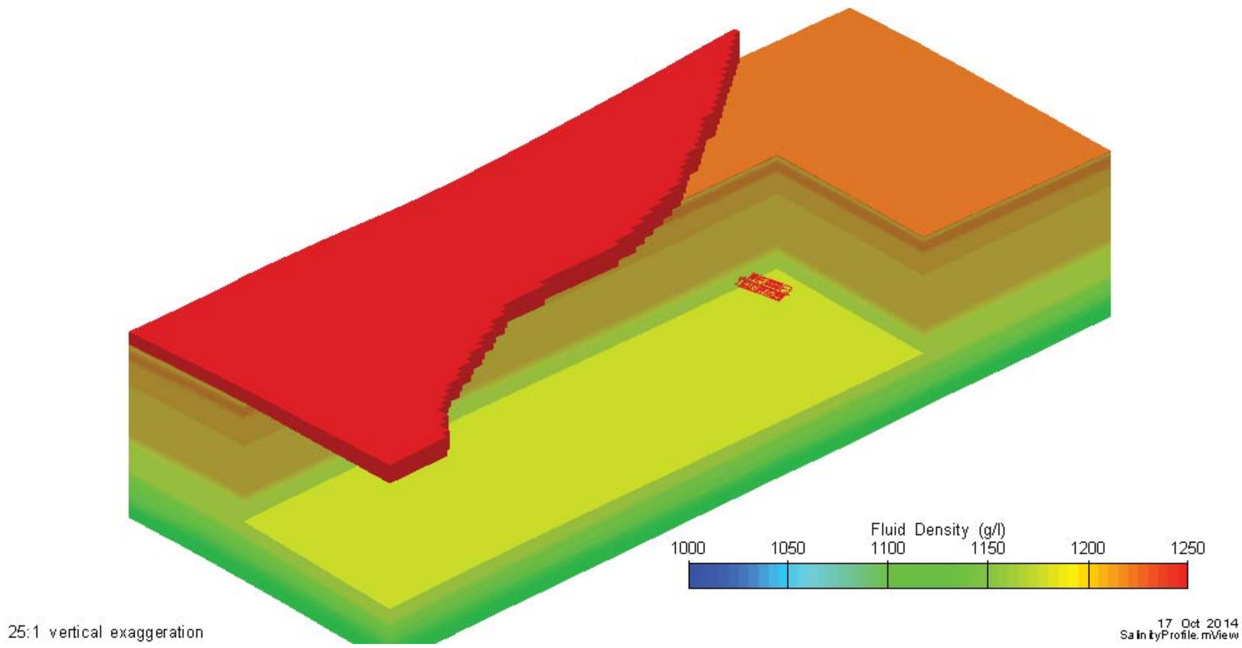

Figure 4-23: Fixed Concentration Nodes in Guelph Formation (Red Elements Above Cut-Away)

The 1 Ma results do not represent an actual steady-state condition as the brine system continues to evolve, albeit at a very slow rate, driven by diffusion processes from the saline Middle Ordovician into the fresher water above. This primarily affects the potable water zones where the Guelph is diluted by inflowing fresh water. Variations in the salinity profile (Figure 4-24) clearly show this effect.

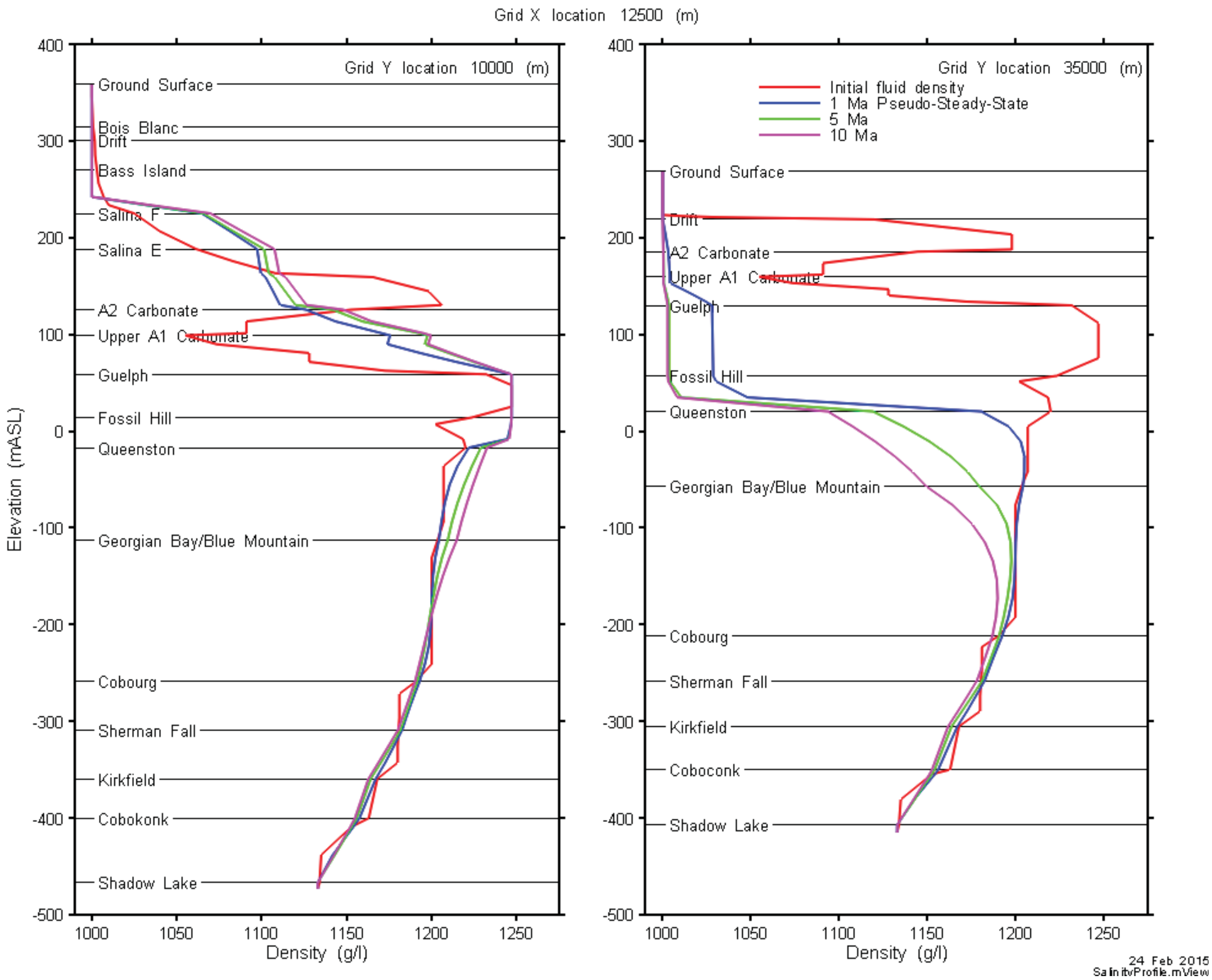

Figure 4-24: Variable Density Reference Flow: Evolution of Fluid Density Profiles at Locations Under the Fixed Concentration (Y = 10,000 m) and Freshening (Y = 35,000 m) Guelph Formation on a Slice at X = 12,500 m.

MLE simulation results are defined only for steady-state flow systems. However, FRAC3DVS-OPG has a capability where results from a transient flow system can be used to define a constant velocity field that can then be used for MLE simulations. MLE results can thus represent a “snapshot” of system behaviour and are used in this report to provide a metric for comparing model results.

“Snapshot” MLE results (Figure 4-25) at 1 Ma and 5 Ma show that freshening in the Guelph has virtually no impact on transport processes in the vicinity of the repository.

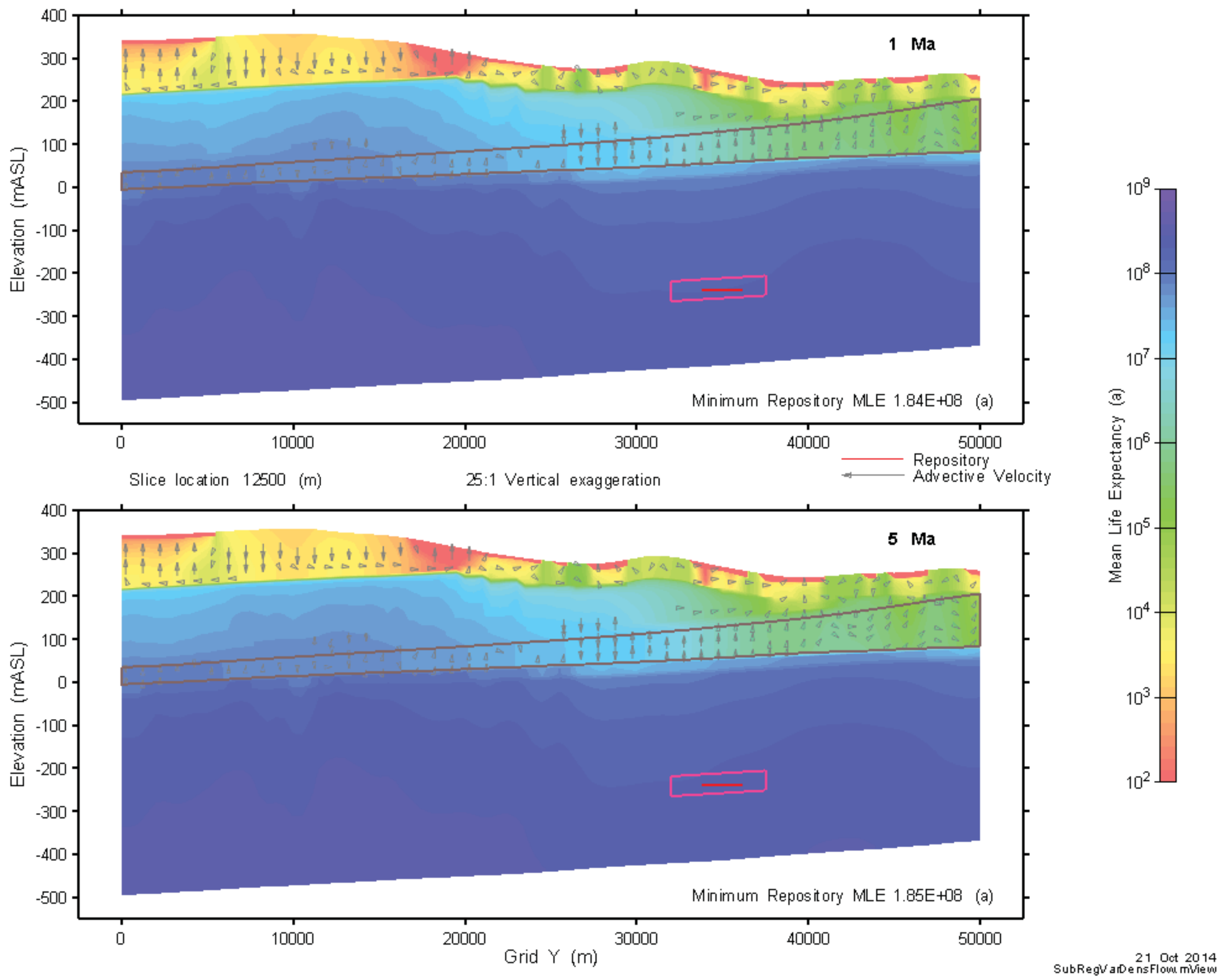

Figure 4-25: Variable Density Reference Flow: Comparison of Mean Life Expectancy on Vertical Slice Through Repository at 1 Ma and 5 Ma.

It is interesting to note that both variable density flow fields (1 Ma or 5 Ma) are quite similar to the steady-state constant density flow system described in Section 4.1.2. Within the Ordovician sediments the advective velocities of the constant density case are generally slower than for the 1 Ma variable density case while the MLEs are virtually identical (Figure 4-26). As MLEs are reflective of an advective flow regime, this is consistent with the diffusion dominated characterization of transport within the repository host rock and adjacent sedimentary units.

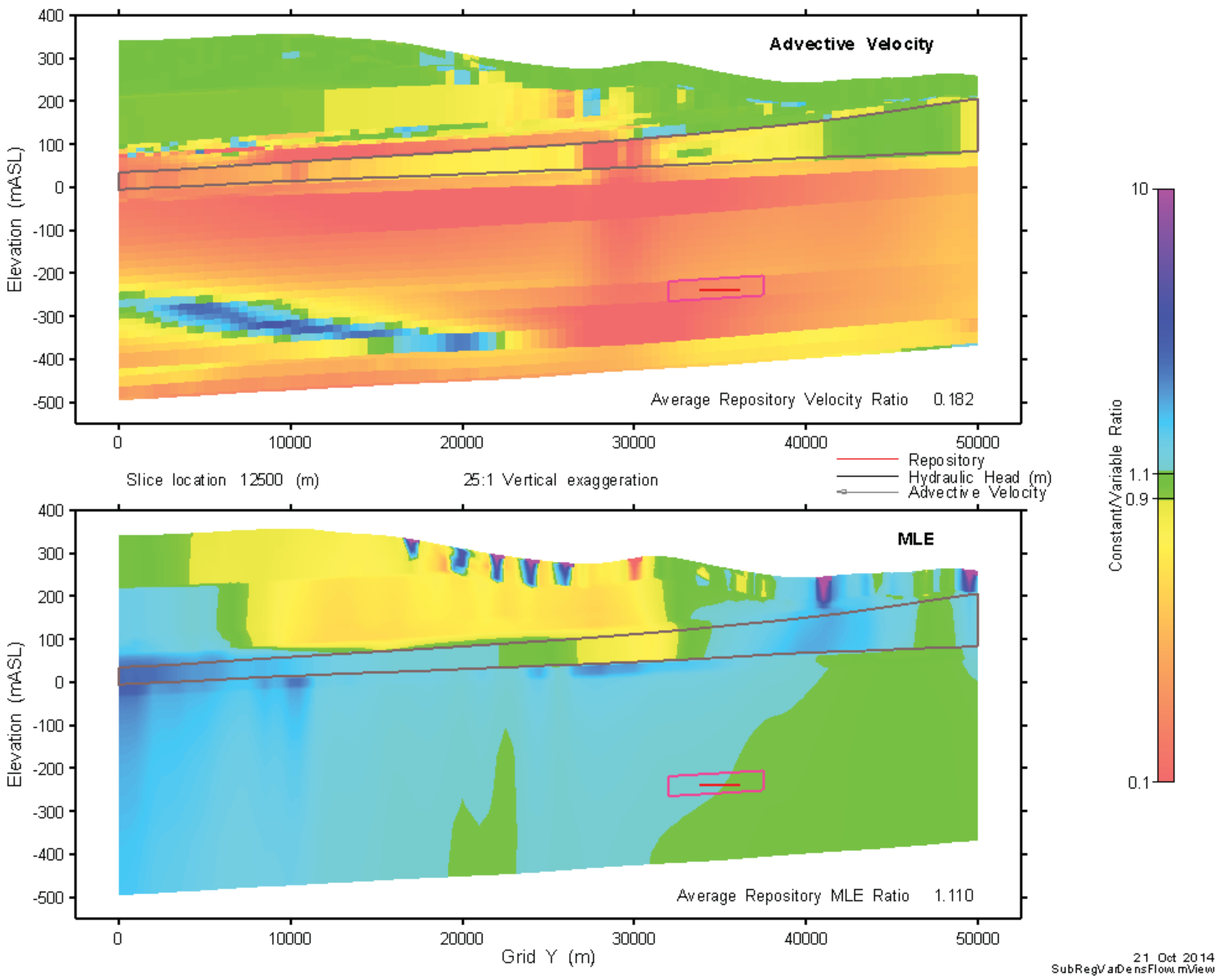

Figure 4-26: Comparison of Constant and Variable Density Reference Flow: Ratio of Constant to 1 Ma Variable Density Advective Velocity and MLE

Execution time is one area where the simulations for the two approaches are not similar. The variable density simulations are extremely time-consuming. The reference case variable density simulation required 12 days to reach 1 Ma, 65 days to reach 5 Ma, and 118 days to reach 10 Ma, even with relatively relaxed convergence criteria. Execution times are further increased when coupled with glacial cycle boundary conditions (as described in Section 4.1.5.4 below). Given the great similarity between variable density and constant density flow fields, and the prohibitive computational cost of variable density simulations, most sensitivity cases and all transport simulations were conducted with constant density flow.

4.1.4 Reference Case Glacial Climate Simulations

The glacial surface boundary conditions, glacial hydro-mechanical loading, permafrost specification and water supply well operation schedule described in Section 2 and Section 4.1.1 were applied to the constant density flow model. Model results include transient hydraulic head and advective velocity over the 960 ka simulation period. Time series results below present simulated hydraulic head at the repository centre (Figure 4-27) and maximum advective velocities in the vicinity of the repository (Figure 4-28) through a selection of formations.

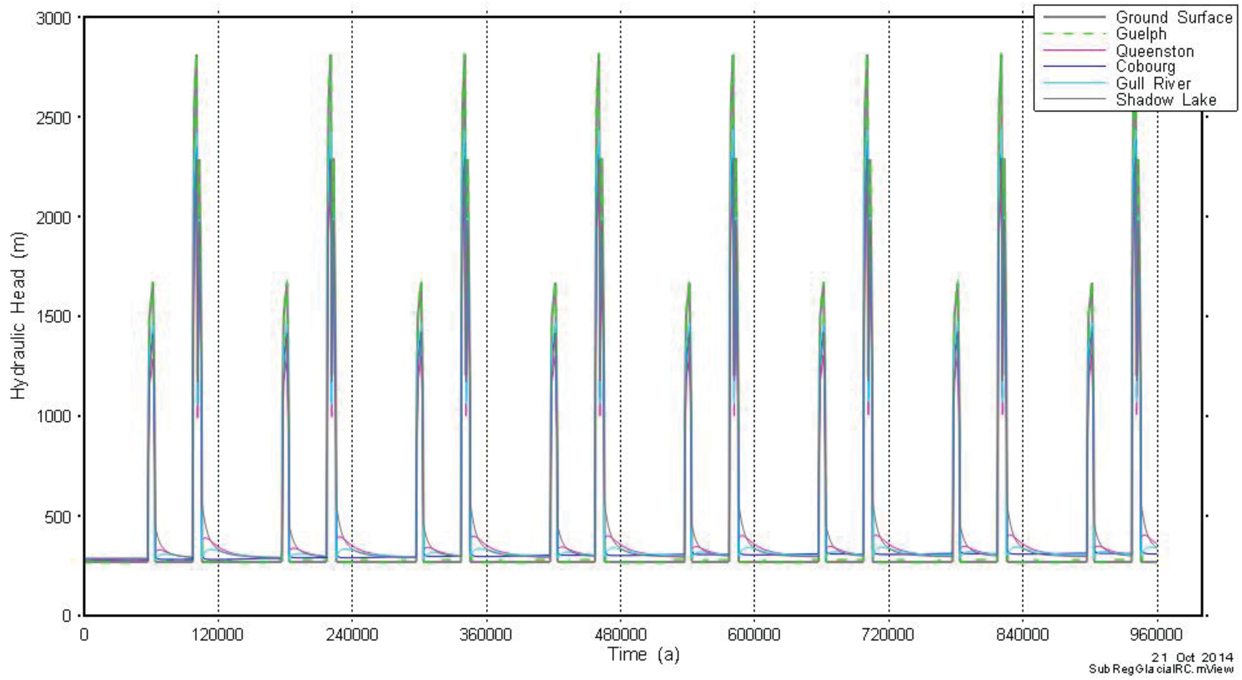

Figure 4-27: Glaciation Sub-Regional Glacial Cycle Simulations: Hydraulic Head at Repository Location (X = 12,500 m, Y = 35,000 m) and Selected Formations

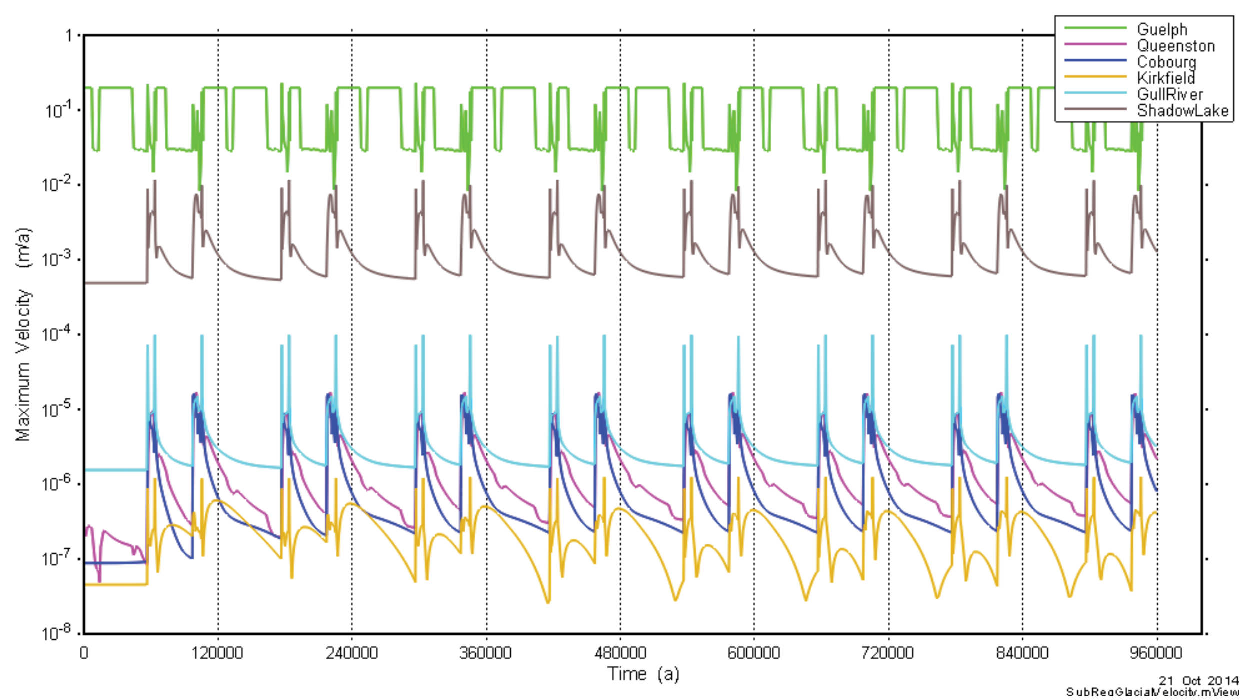

Figure 4-28: Glaciation Sub-Regional Glacial Cycle Simulations: Maximum Advective Velocity in Repository Vicinity and Selected Formations

The results clearly indicate the timing of glacial advance and retreat, and also show that there is very little cumulative impact, with heads and velocities generally repeating for each cycle. The initial cycle is slightly different as initial head conditions at t = 0 are extracted from a steady-state flow model representing present day climate.

Glacially induced upwards velocities are of most interest from a transport perspective. Figure 4-29 and Figure 4-30 show maximum vertical velocities during the first (lower X axis) and fifth (upper X axis) glacial cycle in the repository vicinity within selected Ordovician formations. The figure is also labeled with the times of five events:

1. <u>maximum well operation</u> - the end of the longest period of continual well operation (43,500 a);
2. <u>maximum permafrost</u> – the time of maximum permafrost depth (93,000 a);
3. <u>peak Cobourg velocity</u> – maximum vertical velocity in the repository formation (98,500 a);
4. <u>peak ice load</u> – the time of maximum ice thickness over the repository (100,500 a); and
5. <u>maximum retreat</u> – the time of maximum downward velocities (106,000 a).

Responses are similar for both first and fifth cycle with the exception of velocity at maximum well operation time. In the first cycle, the only influence on the flow system is the well, which affects velocities in the Queenston, but not the Cobourg or Kirkfield. In the fifth cycle, the formation is still responding to the glacial event at the end of the third cycle, with higher upwards velocities in the Queenston and Kirkfield and downward velocities in the Cobourg. Note that downward (negative) velocities that occur during glacial retreat are not shown on Figure 4-29 due to the log scale on the Y axis. The vertical direction of groundwater velocities is driven by vertical head gradients. Relative pressures are largely a function of different loading efficiencies (Sherman Fall 0.88, Cobourg 0.80), with higher values causing greater responses. At maximum glacial load, the hydraulic head in the Sherman Fall formation (below the Cobourg formation) is higher than in the Cobourg formation; at maximum retreat it is lower. It remains lower over most of the assessment period (Figure 4-31) resulting in prevailing downward advective velocities, albeit of extremely small magnitude.

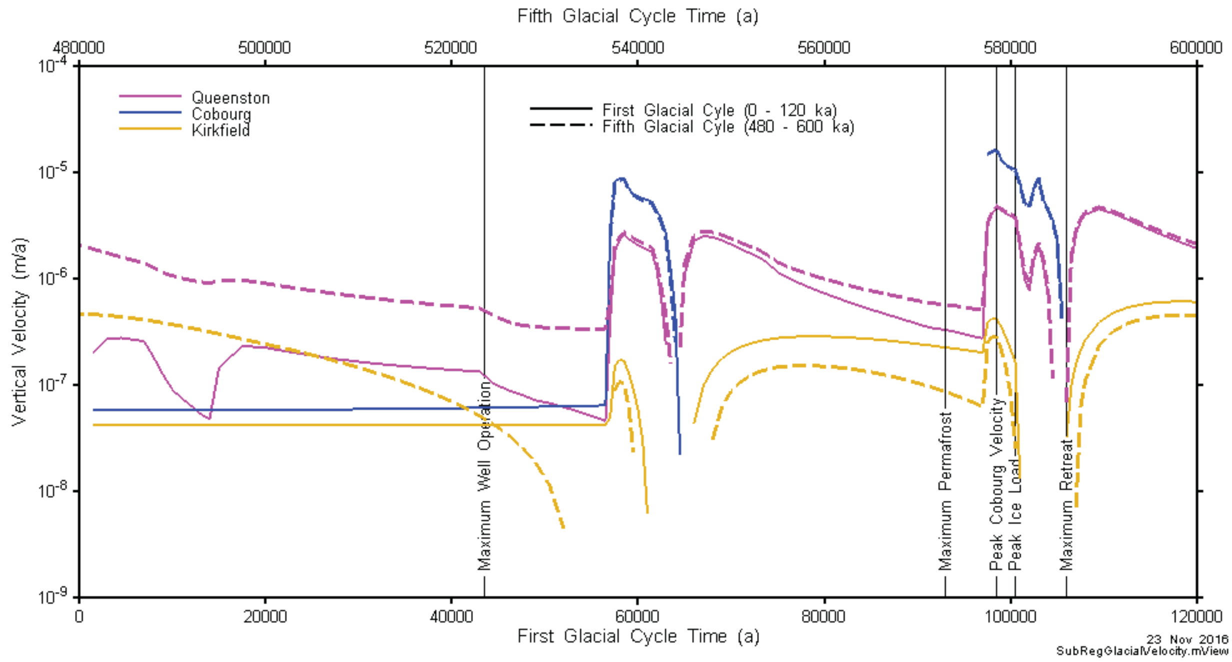

Figure 4-29: Glaciation Sub-Regional Glacial Cycle Simulations: Maximum Vertical Velocity in Repository Vicinity and Selected Formations – Logarithmic Velocity Scale

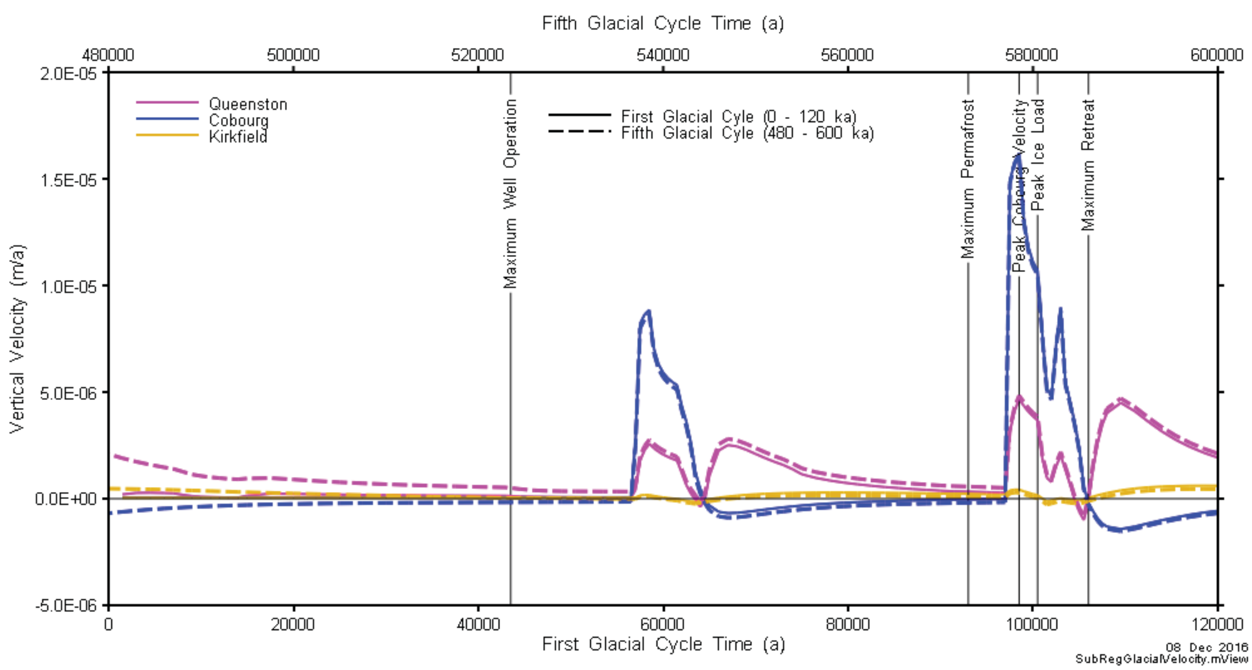

Figure 4-30: Glaciation Sub-Regional Glacial Cycle Simulations: Maximum Vertical Velocity in Repository Vicinity and Selected Formations – Linear Velocity Scale

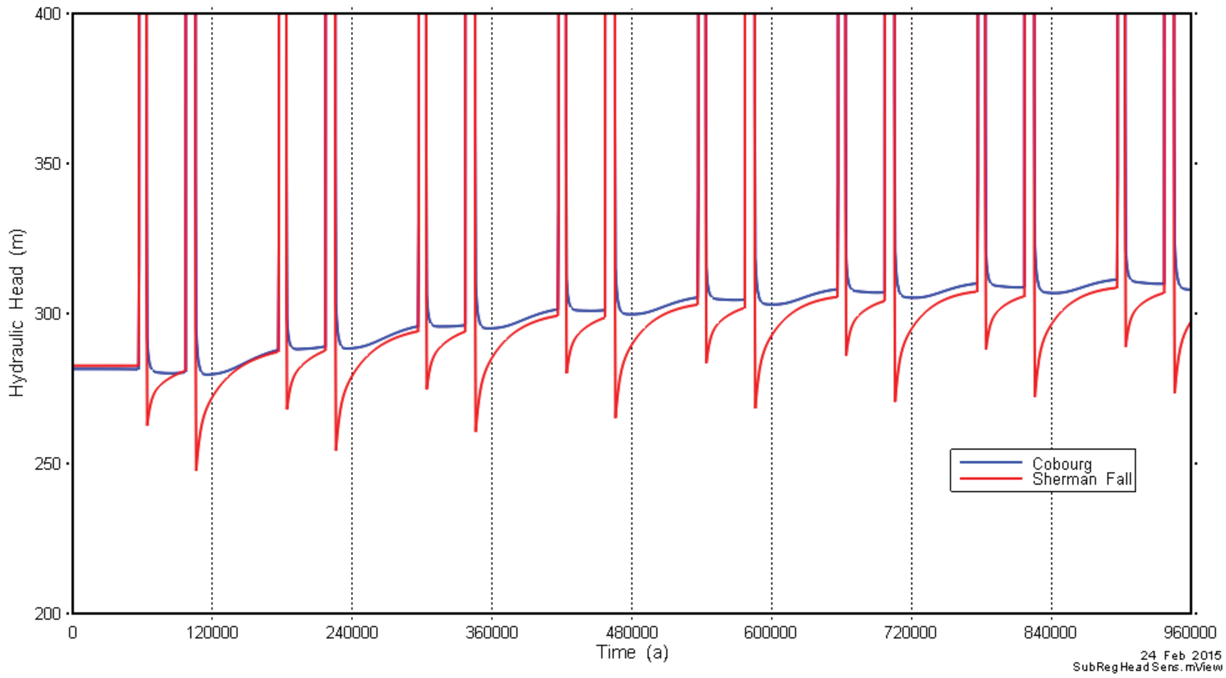

Figure 4-31: Glaciation Sub-Regional Glacial Cycle Simulations: Detail of Hydraulic Head in Cobourg and Sherman Fall Formations in Repository Vicinity

Figure 4-32 through Figure 4-38 present velocity magnitude and head contours on a vertical slice through the repository at the simulation start (t = 0) and at each of the first cycle events designated in Figure 4-29. Peak well operation in the fifth cycle is also presented (Figure 4-34). Note that the vertical slice for Figure 4-33 and Figure 4-34 (peak well operation in first and fifth cycle) is through the reference well location (see Figure 4-12) rather than the centre of the repository.

The head contours in Figure 4-32 differ from those in Figure 4-14 due to the difference in boundary conditions at the North and South ends of the model. The steady state flow results (Figure 4-14) use zero flow BC, while the glacial climate cases use time-varying fixed head BC at the North and South ends of the grid, as described in Section 4.1.1.3. This does not significantly impact velocity or MLE at the repository location.

Water well operation (Figure 4-33 and Figure 4-34) has a minimal impact with velocity vectors and head contours in the Guelph affected only within the immediate vicinity of the well. Maximum permafrost depth (Figure 4-35) substantially reduces velocities in the upper 50 m but has little impact on velocities elsewhere. Differences in head at depth are due to continuing effects of the previous glacial loading rather than the permafrost. The two events with ice-sheets over the repository (Figure 4-36 and Figure 4-37) are similar in that the head profiles are markedly changed due to hydro-mechanical loading. At the time of the retreat (Figure 4-38), residual overpressures remain in the upper Salina units to the south of the repository, although under pressurization is apparent in the Sherman Fall formation below the repository.

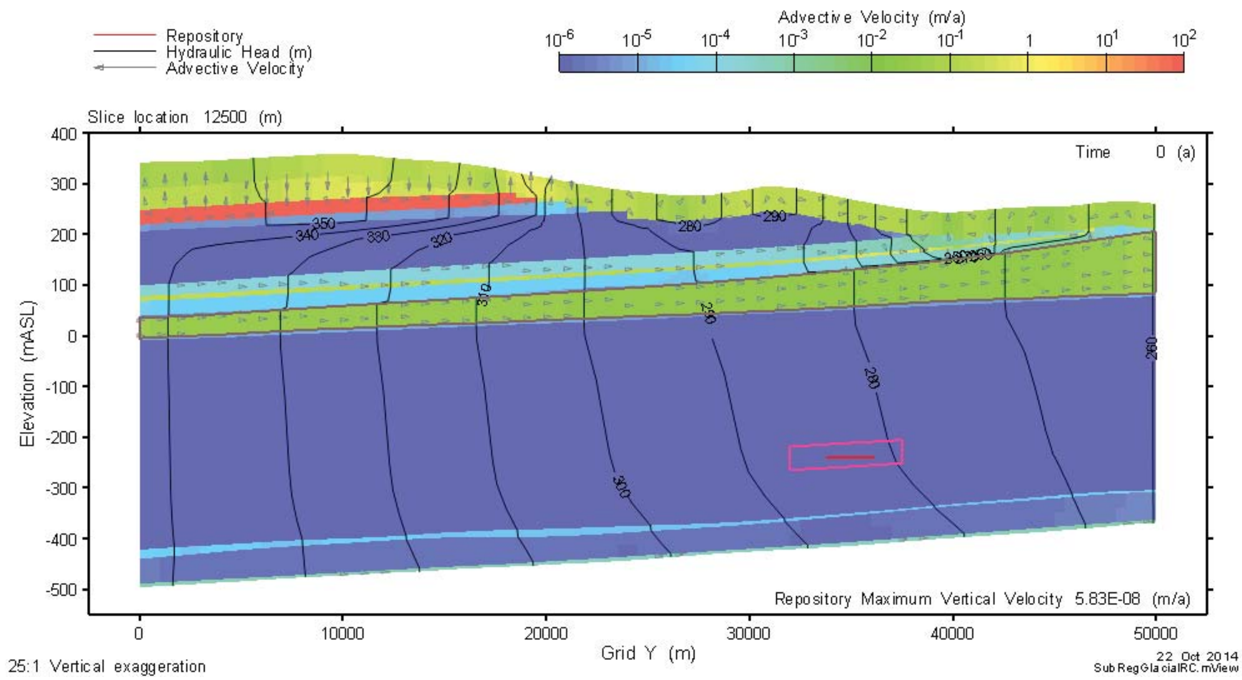

Figure 4-32: Glaciation Sub-Regional Glacial Cycle Simulations: Advective Velocity and Hydraulic Head at Simulation Start (T = 0 a)

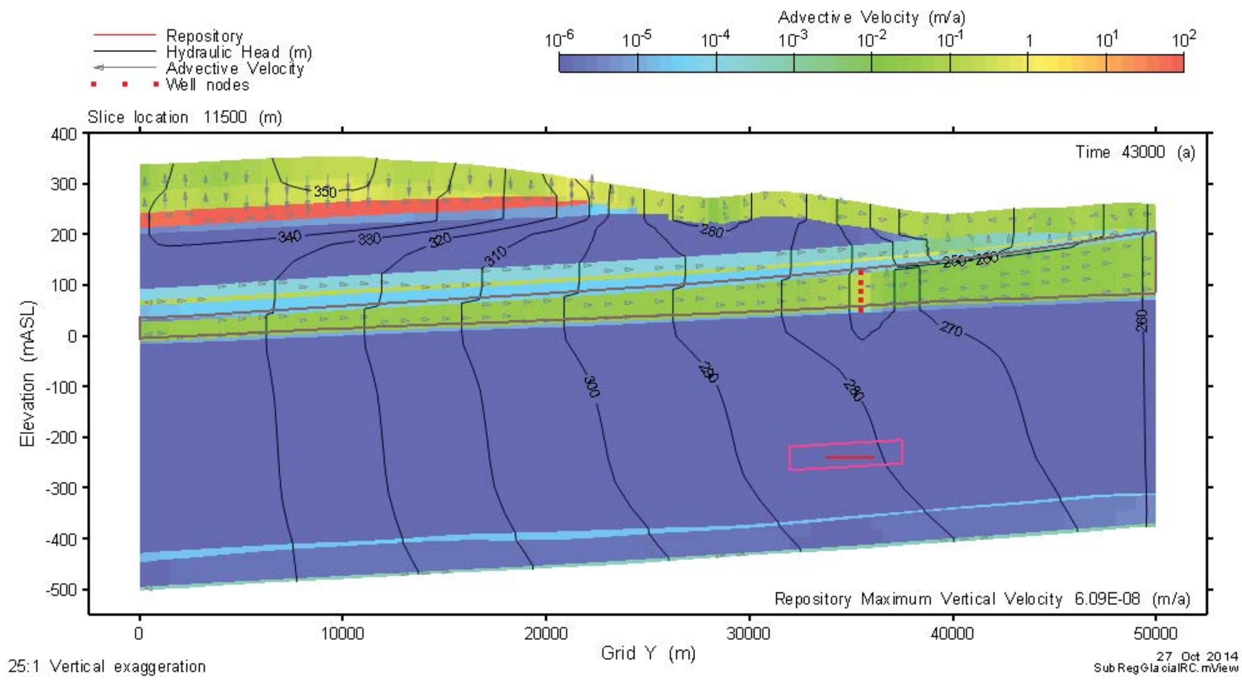

Figure 4-33: Glaciation Sub-Regional Glacial Cycle Simulations: Advective Velocity and Hydraulic Head at Time of First Cycle Peak Well Operation (T = 43,000 a)

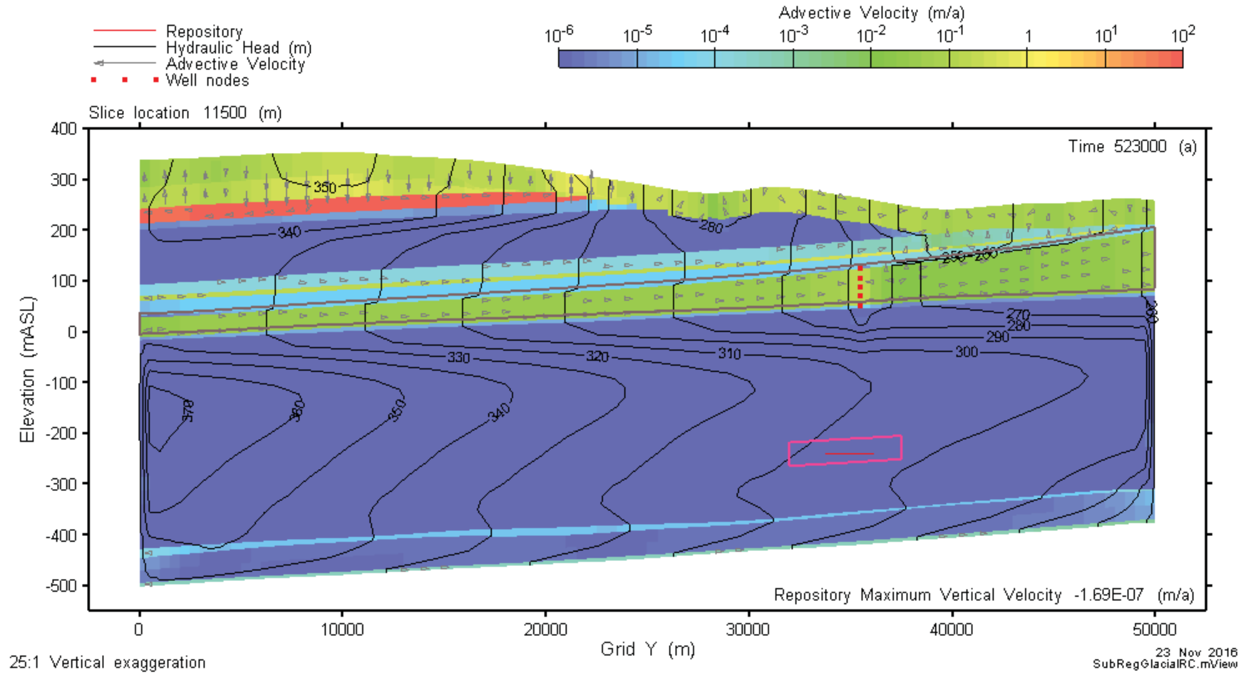

Figure 4-34: Glaciation Sub-Regional Glacial Cycle Simulations: Advective Velocity and Hydraulic Head at Time of Fifth Cycle Peak Well Operation (T = 523,000 a)

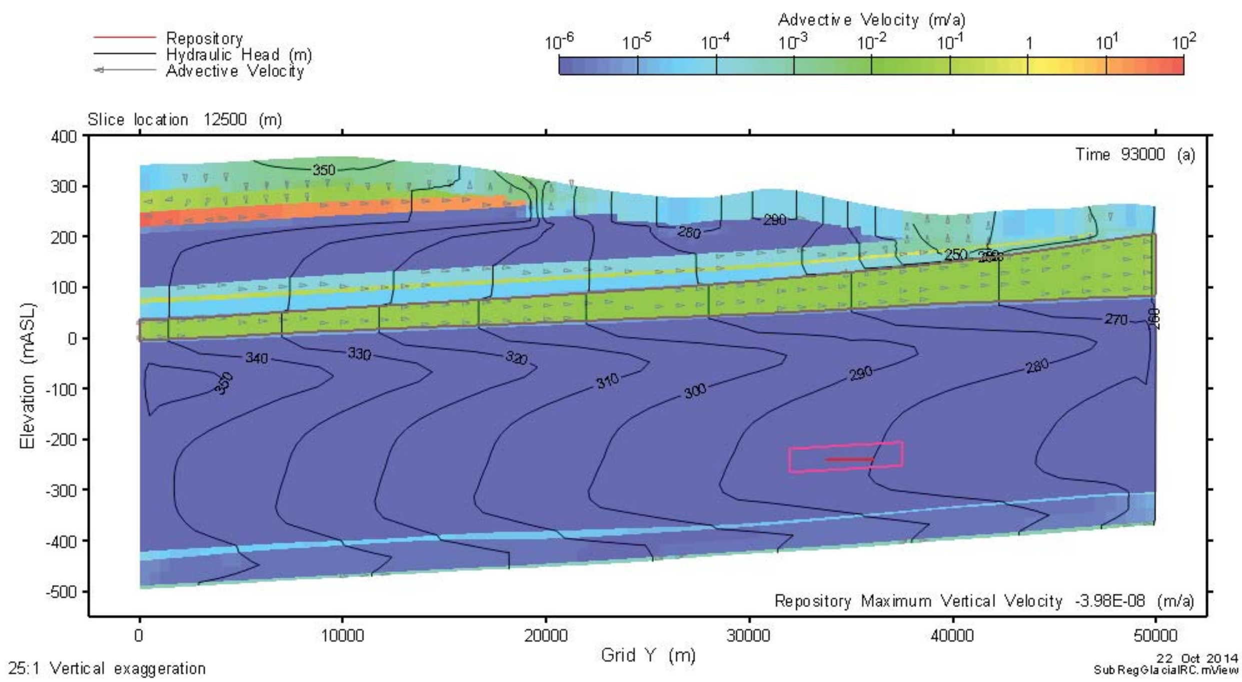

Figure 4-35: Glaciation Sub-Regional Glacial Cycle Simulations: Advective Velocity and Hydraulic Head at Time of Maximum Permafrost (T = 93,000 a)

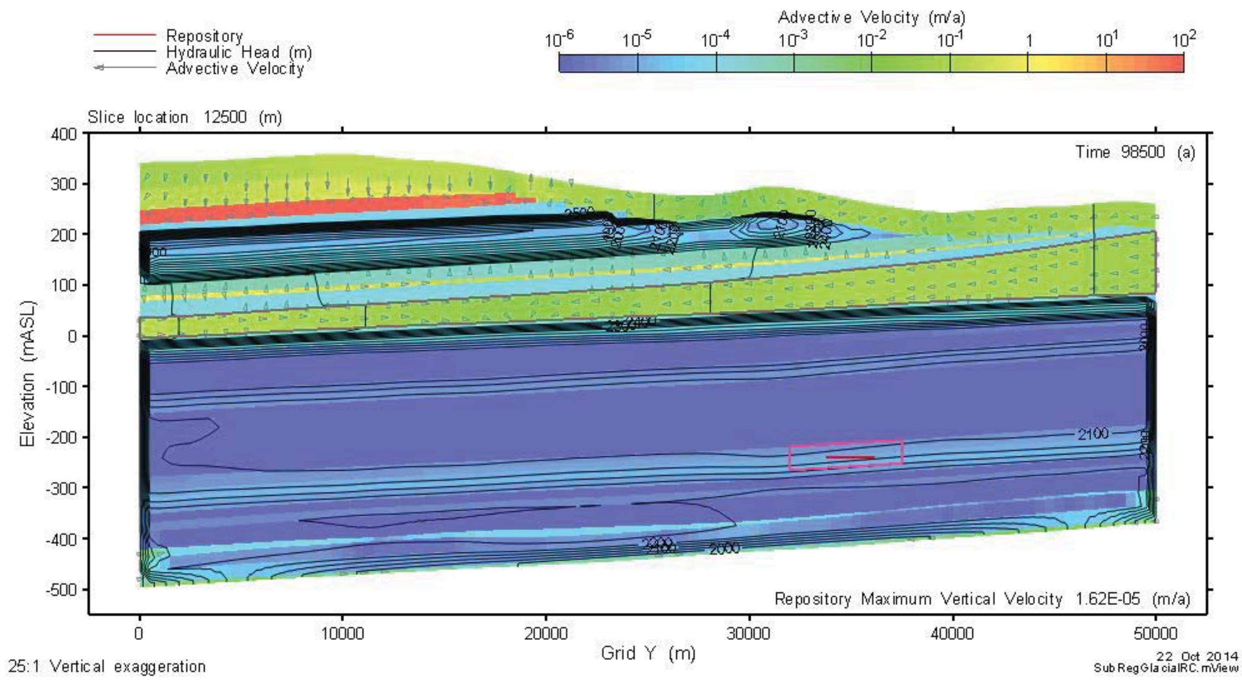

Figure 4-36: Glaciation Sub-Regional Glacial Cycle Simulations: Advective Velocity and Hydraulic Head at Time of Peak Upward Velocities in Cobourg Formation at Repository (T = 98,500 a)

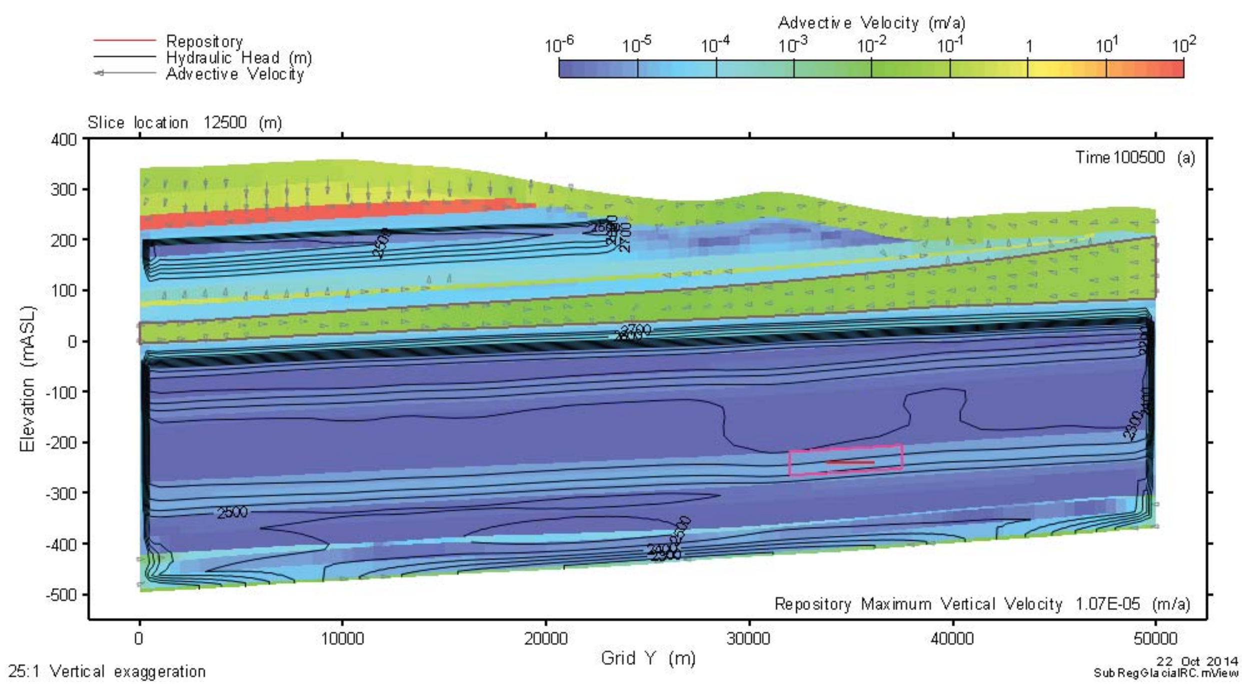

Figure 4-37: Glaciation Sub-Regional Glacial Cycle Simulations: Advective Velocity and Hydraulic Head at Time of Maximum Glacial Load at Repository (T = 100,500 a)

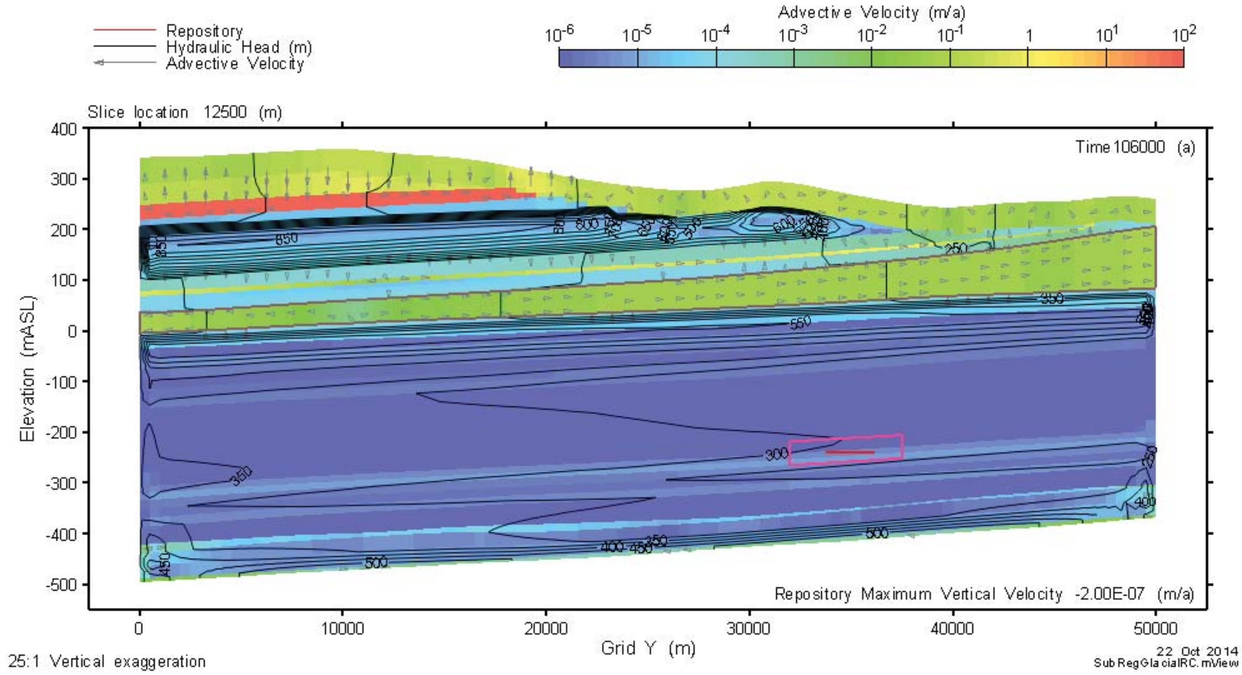

Figure 4-38: Glaciation Sub-Regional Glacial Cycle Simulations: Advective Velocity and Hydraulic Head at Time of Maximum Glacial Retreat at Repository (T = 106,000 a)

Hydraulic head profiles at the water supply well location at the selected event times (Figure 4-39 and Figure 4-40) show the wide range of heads propagated through the flow system over the cycle. The second figure provides greater resolution for the events without ice loading, including the presence of the underpressured zone in the Sherman Fall formation at the time of maximum retreat. The head profiles are useful for explaining the direction of vertical groundwater flow at various times. Advective flow will always be in the direction of positive gradient; from high head to relatively lower heads. For example, the Cobourg formation shows upwards flow at Peak Cobourg and Peak Ice load times in Figure 4-39, while velocities are downward during Maximum Retreat and Peak Well (Cycle 5) in Figure 4-40.

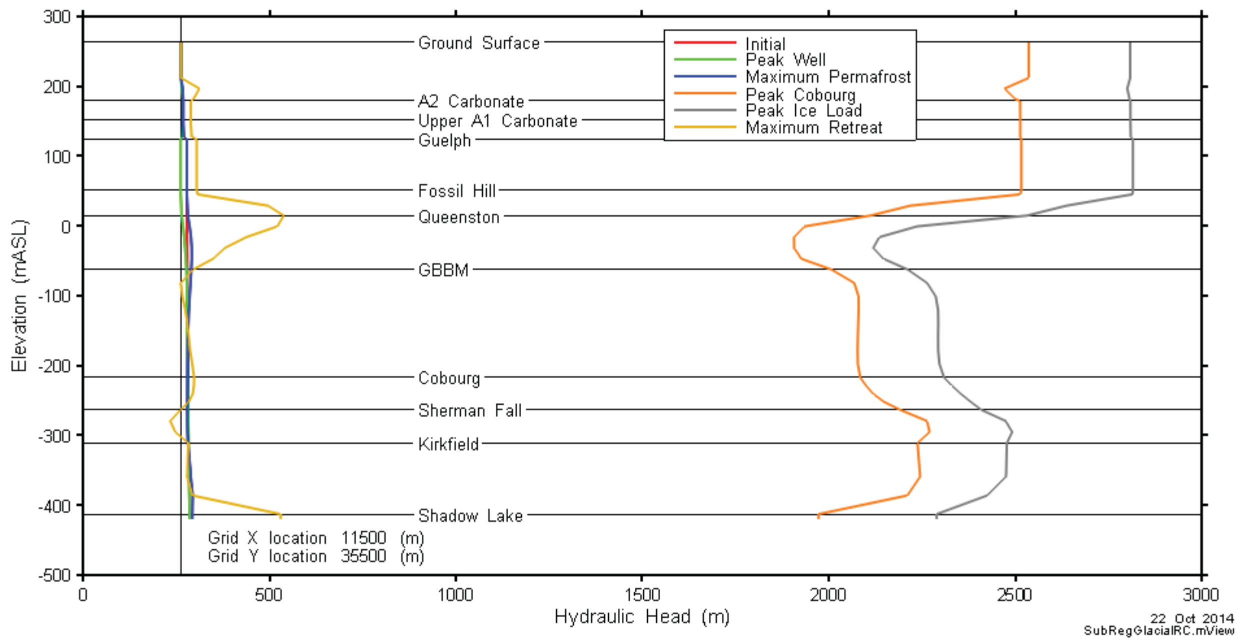

Figure 4-39: Glaciation Sub-Regional Glacial Cycle Simulations: Hydraulic Head Profiles at Water-Supply Well Location

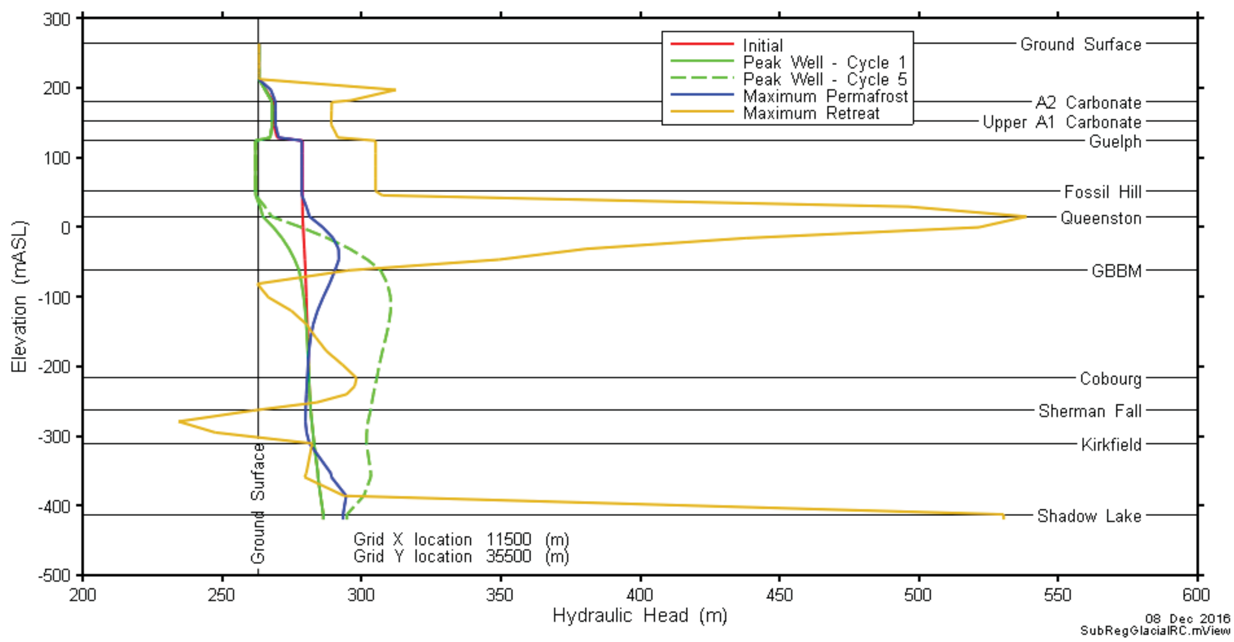

Figure 4-40: Glaciation Sub-Regional Glacial Cycle Simulations: Hydraulic Head Profiles at Water-Supply Well Location (Detail)

However, in spite of significant hydraulic stresses, the advective velocity in the Ordovician units near the repository remains very low over the duration of the glacial cycle (Figure 4-41). The snapshot MLE using the peak Cobourg velocity (Figure 4-42) still maintains an MLE of nearly 80 Ma in the vicinity of the repository. The ratios of advective velocities and “snapshot” MLE at initial and at peak Cobourg velocity (Figure 4-43) show that even though velocities have increased significantly, MLE has not decreased significantly. Even if the peak velocities were to persist, overall MLE would be reduced by only a factor of 2.5 over the constant climate MLE of 185 Ma.

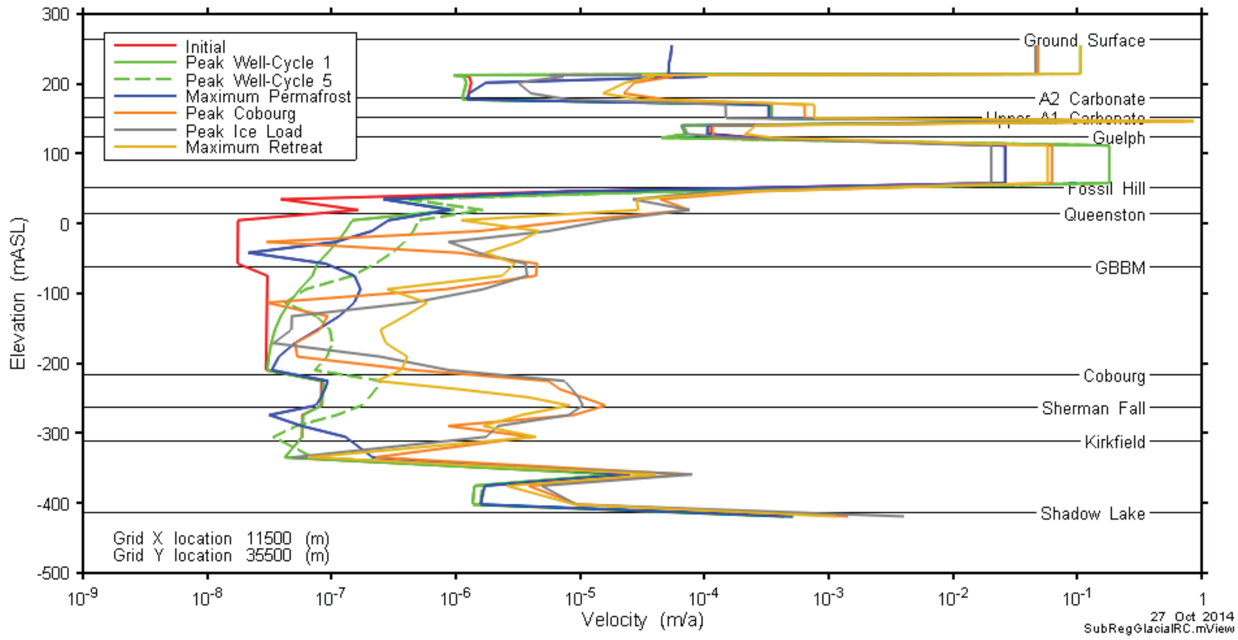

Figure 4-41: Glaciation Sub-Regional Glacial Cycle Simulations: Velocity Magnitude Profiles at Water-Supply Well Location

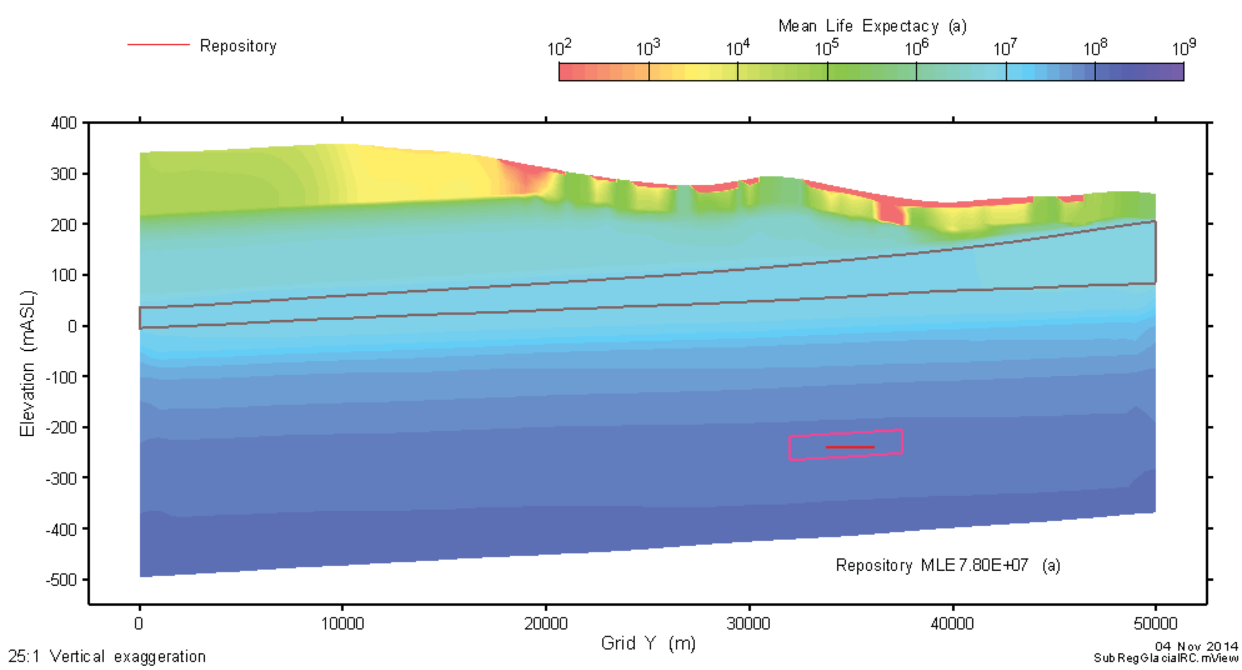

Figure 4-42: Glaciation Sub-Regional Glacial Cycle Simulations: Snapshot MLE at Peak Cobourg Velocity Magnitude

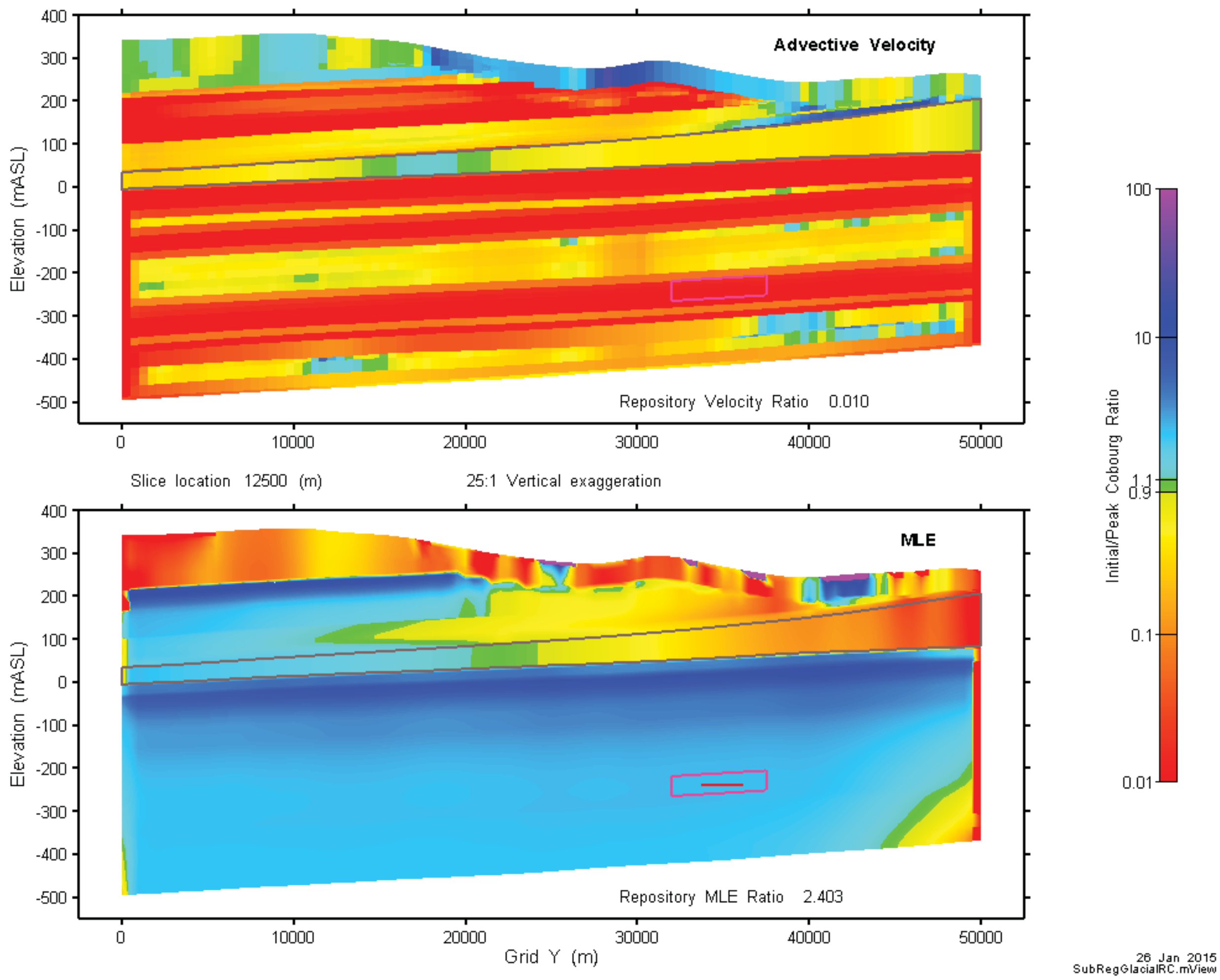

Figure 4-43: Glaciation Sub-Regional Glacial Cycle Simulations: Comparison of Initial and Peak Cobourg Velocity Snapshot MLE

All results show the resiliency of the reference case flow system and its relative insensitivity to glacial events. As mentioned previously, velocity time series show no evidence of significant cumulative impacts. This is not to say that the system returns to a common head profile at any point. The time of maximum well operation in each cycle after Cycle 1 occurs at the longest time period without a glacial stress, at which time the system will have reverted closer to a steady-state than at any other time. Figure 4-44 shows head profiles at this time within each cycle. There is a steady accumulation of glacial overpressure, although the rate of increase diminishes with each cycle.

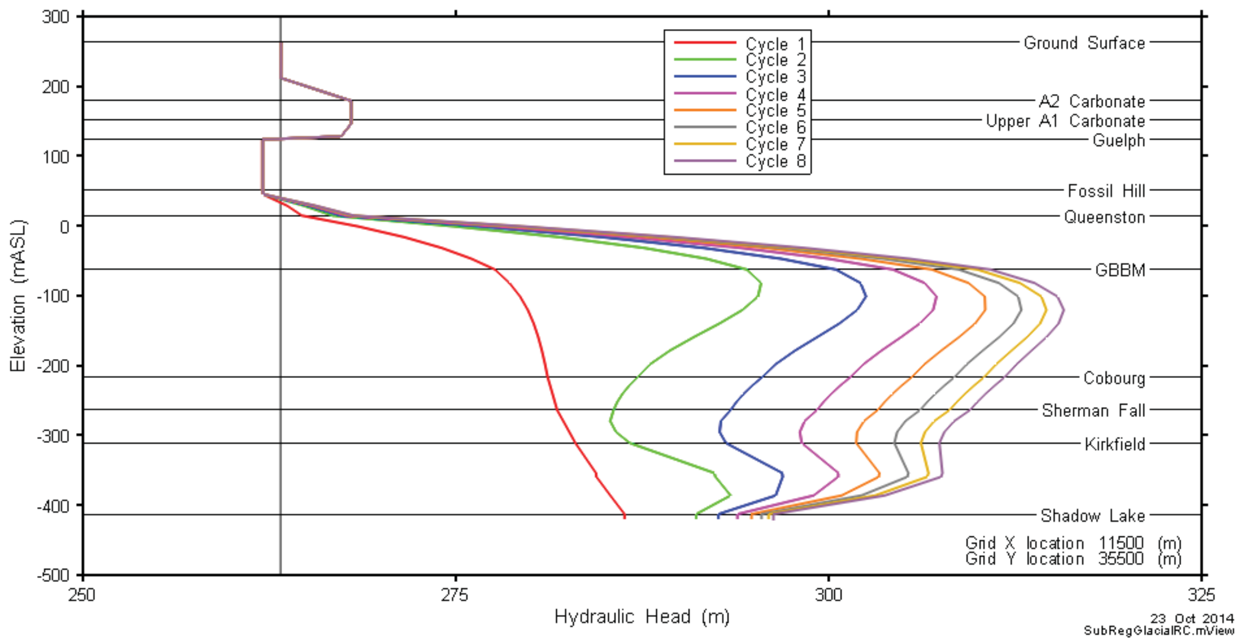

Figure 4-44: Glaciation Sub-Regional Glacial Cycle Simulations: Hydraulic Head Profiles at Water-Supply Well Location at Time of Maximum Well Impact for All Cycles

Velocity profiles at the same times (Figure 4-45) show little variation after the initial glacial cycle.

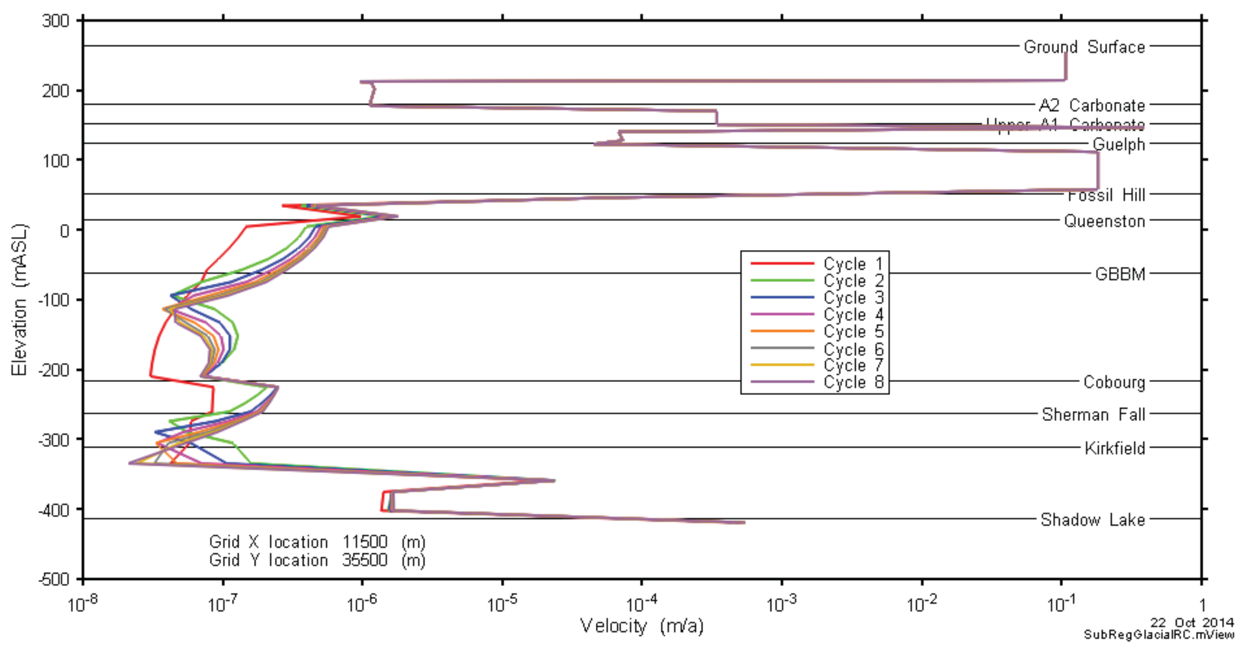

Figure 4-45: Glaciation Sub-Regional Glacial Cycle Simulations: Velocity Magnitude Profiles at Water-Supply Well Location at Time of Maximum Well Impact for All Cycles

4.1.5 Sensitivity Assessment

Sensitivity cases are specified to determine the variation in system response to changes in parameters, boundary conditions, initial conditions or modelling processes. The reference case flow model, RC, is defined as having constant density, glacial climate, reference case parameters, reference water supply well location and abstraction rates, and initial conditions from steady-state fixed head boundary conditions at model surface and North and South sides. Defined sensitivity cases are assessed in terms of velocity and head response in the repository volume and profiles of velocity and head at the time of maximum Cobourg velocity and maximum ice thickness events.

4.1.5.1 Sensitivity Cases

Table 1 provides a description of the cases evaluated.

Table 1 - Sensitivity Cases for Glaciation Sub-Regional Flow Model

Type	Case	Description
Parameter	KHigh	High range hydraulic conductivity – hydraulic conductivity values for all formations increased by factor of 10
	KHigh 100	Hydraulic conductivity values for all formations increased by factor of 100.
	KHigh 1000	Hydraulic conductivity values for all formations increased by factor of 1000
	SHigh	High range storativity – specific storage for all formations increased by factor of 10
	LEHigh	High range loading efficiency – loading efficiency for all formations increased by factor of 1.5 to a maximum of 1.0
	LELow	Low range loading efficiency – loading efficiency for all formations decreased by factor of 0.5
Boundary and Initial Condition	DPF	Discontinuous or “patchy” permafrost - permafrost coverage reduced to half the domain in a patchwork pattern
	No PF	No permafrost
	Surface BC	Time-varying fixed head boundary conditions applied at surface only. North and South model extents are zero-flow.
	NoLoad	No Loading – hydro-mechanical processes not included, only the glacially-induced increase in hydraulic head.
	Load Only	No surface hydraulic head BC associated with glaciation. Corresponds to cold based glacier.
	HUnder	Underpressured hydraulic head – underpressures consistent with DGR-4 (INTERA, 2011) applied as initial conditions for Ordovician formations
	HOver	Overpressured hydraulic head on lower boundary. Overpressures consistent with measured Cambrian DGR-4 (INTERA, 2011) applied as lower boundary condition.
Process	ConstDens - CC	Constant density, constant climate - previously described in Section 4.1.2
	VarDens-CC	Variable density, constant climate - previously described in Section 4.1.3
	VarDens-Glac	Variable density, glaciation

Note that the KHigh100 and KHigh1000 cases do not represent physically likely parameter sets, and that the No Load case ignores processes that are almost certainly occurring. These cases are presented to gather insight on overall system performance rather than to represent physically possible performance. Additional details of specific cases are provided in the following subsections.

4.1.5.1.1 Discontinuous Permafrost (DPF) Case Description

The reference case model assumes that permafrost is applied continuously over the surface of the model at time intervals and depths as shown in Figure 4-11. The DPF sensitivity case restricts permafrost to a 5 km by 5 km checkerboard pattern as shown in Figure 4-46 and Figure 4-47.

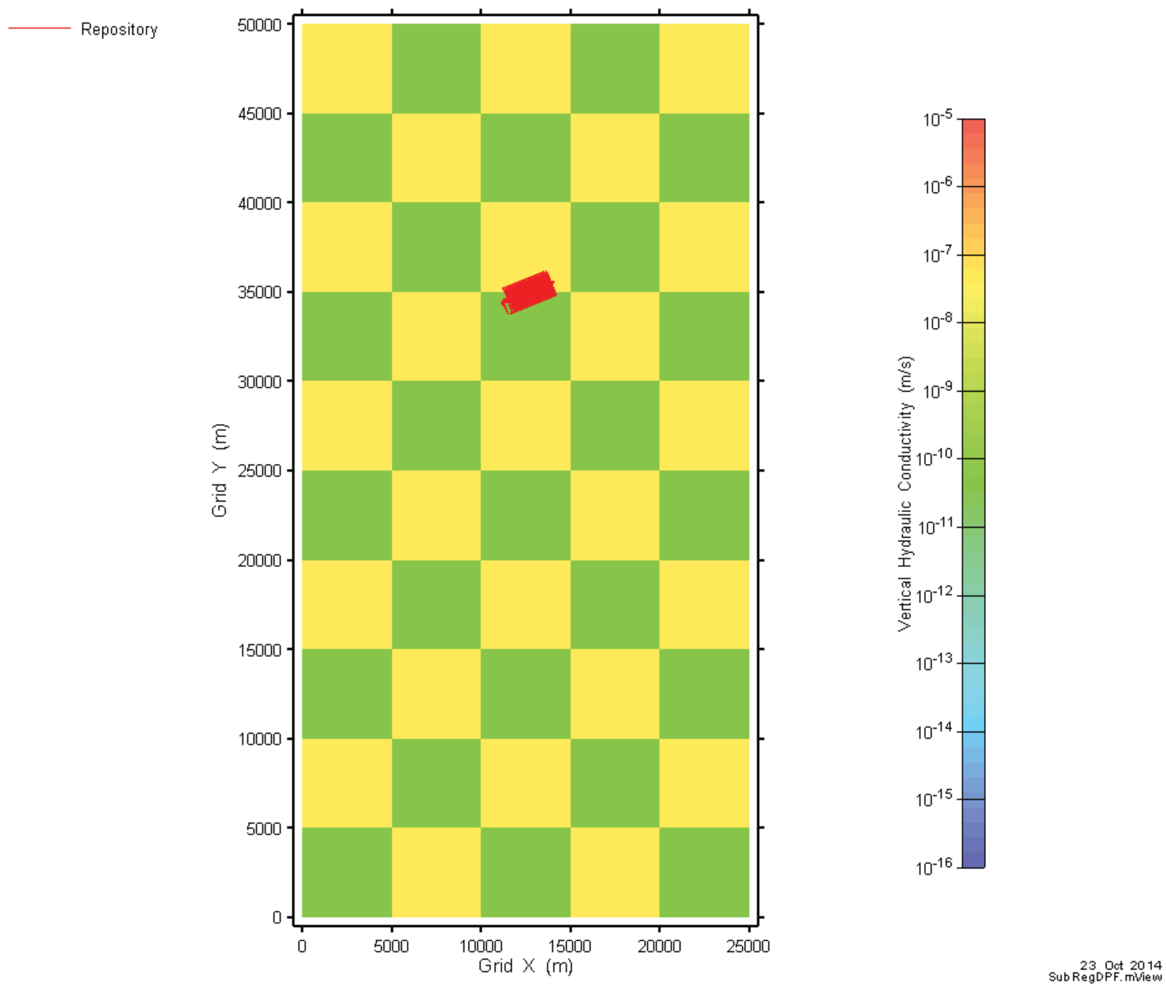

Figure 4-46: Glaciation Sub-Regional Glacial Cycle Simulations: DPF Case Specification – Hydraulic Conductivity of Top Model Layer at Time of Maximum Permafrost Depth

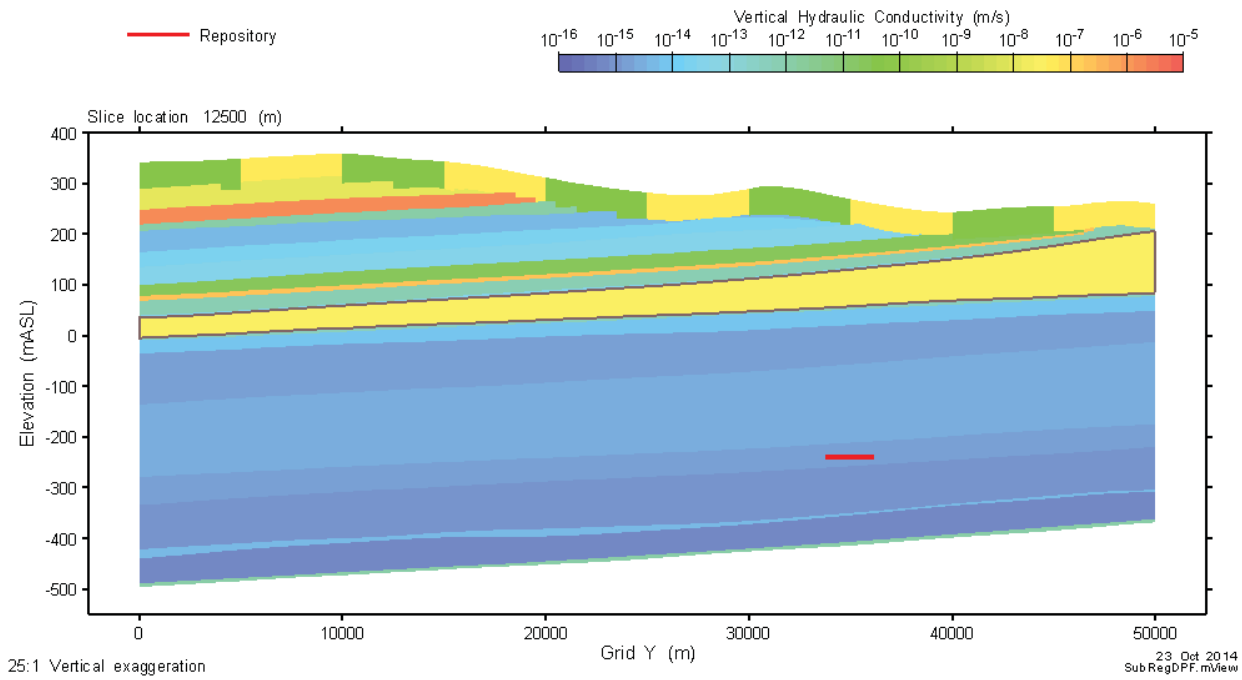

Figure 4-47: Glaciation Sub-Regional Glacial Cycle Simulations: DPF Case Specification – Hydraulic Conductivity of Vertical Slice Through Repository at Time of Maximum Permafrost Depth

4.1.5.1.2 HUnder Case Description

Anomalous formation pressures were measured at the OPG DGR Site Characterization boreholes (INTERA, 2011). Significant underpressures were found in the Ordovician shales and limestones while overpressures were measured in the permeable Cambrian sandstone underlying the site. It is possible that underpressures are present throughout the model domain. An underpressure profile, defined in terms of difference in hydraulic head from steady-state on a formation basis, approximated the measured underpressure at DGR-4, as shown in Figure 4-48.

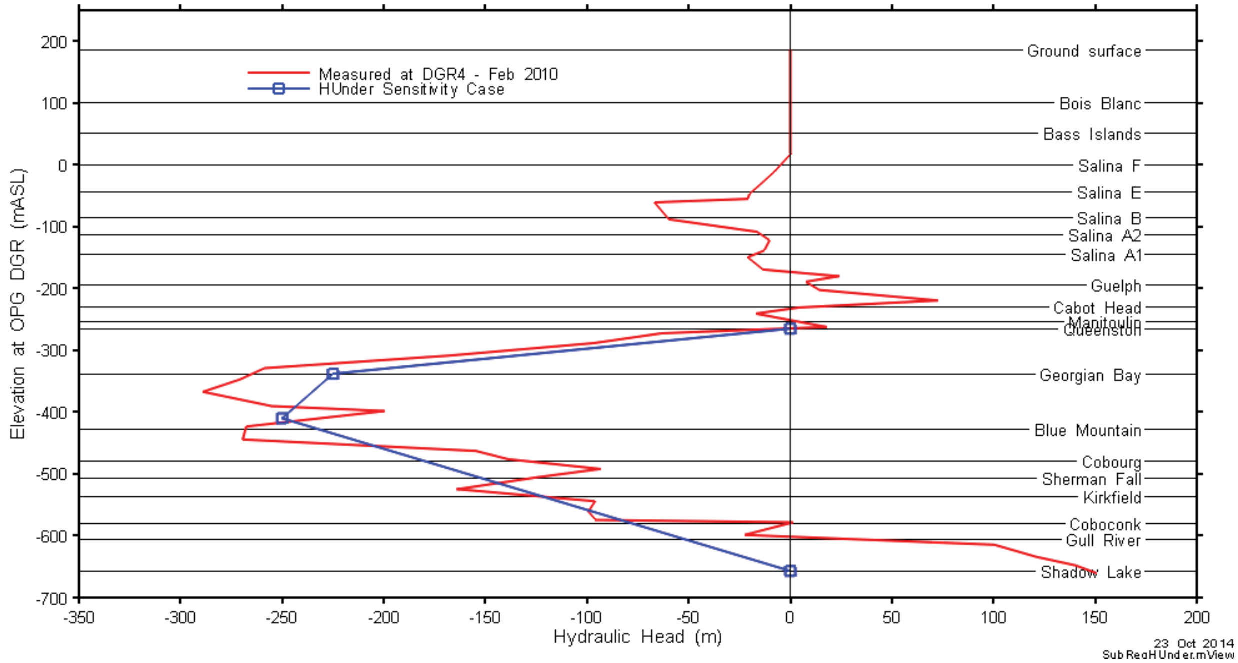

Figure 4-48: Glaciation Sub-Regional Glacial Cycle Simulations: HUnder Case Specification – Defined Underpressure Profile

The profile was used to modify the calculated steady-state hydraulic head distribution from the constant density model described in Section 4.1.2 with a resulting initial head distribution as shown in Figure 4-49.

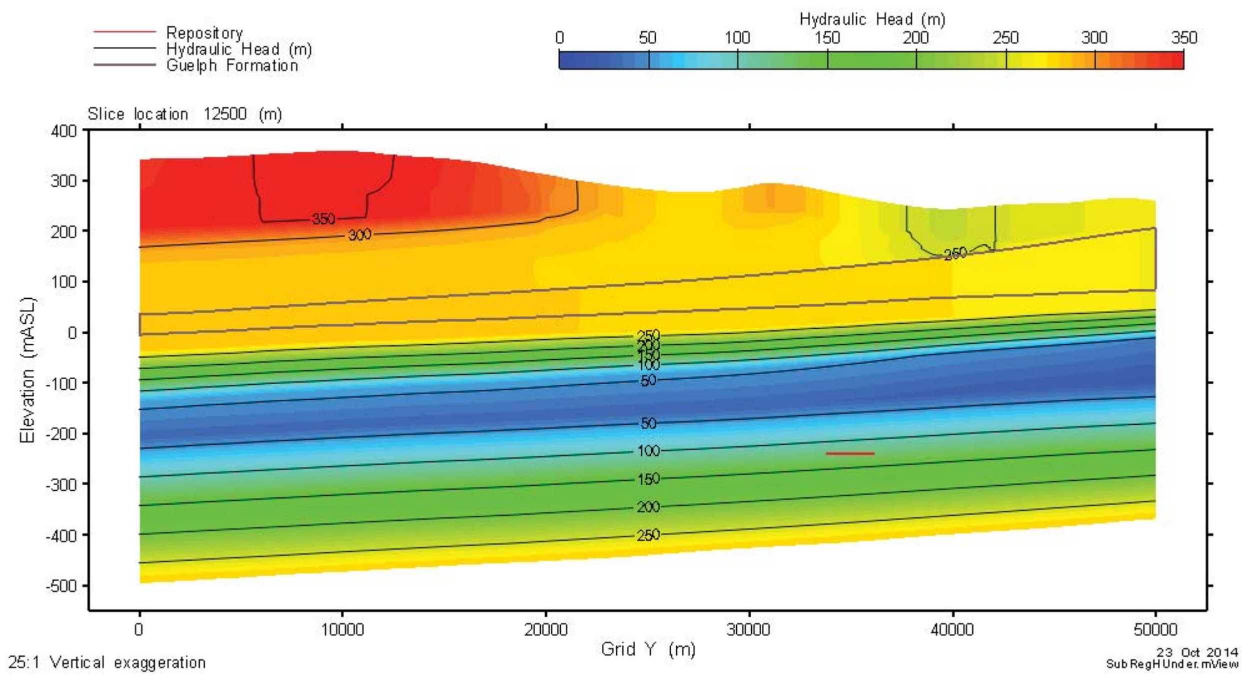

Figure 4-49: Glaciation Sub-Regional Glacial Cycle Simulations: HUnder Case Specification – Modified Hydraulic Head Distribution

This head distribution was used as initial head in a transient flow, constant climate simulation to both smooth the rather coarsely specified initial head and to examine the evolution of the underpressure. As shown in Figure 4-50, the underpressure at the repository location dissipates over a 5 Ma period. The hydraulic head distribution at 10 ka was assumed to be reflective of possible underpressure conditions and is used as the initial head for the HUnder sensitivity case. These underpressures are not compatible with the reference case glacial head boundary conditions where varying fixed heads are applied at the North and South vertical ends of the model. Consequently, only surface boundary conditions are applied for the HUnder case, with zero flow specified on all vertical sides of the model.

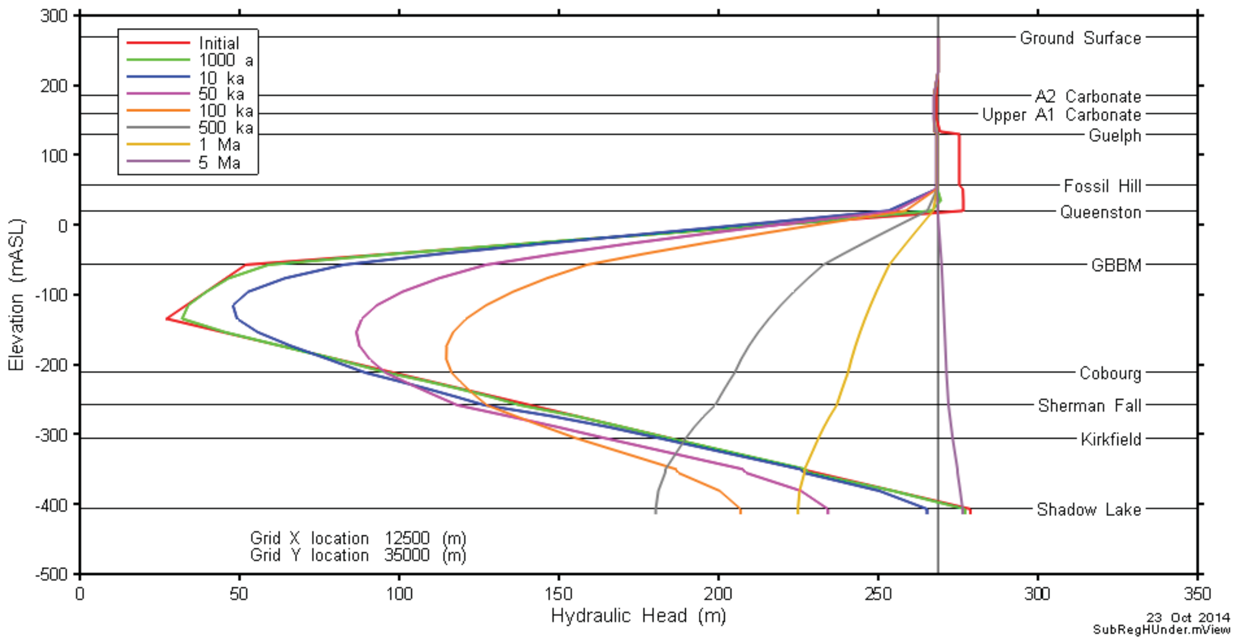

Figure 4-50: Glaciation Sub-Regional Glacial Cycle Simulations: HUnder Case Specification – Underpressure Evolution

4.1.5.1.3 HOver Case Description

The Cambrian formation is discontinuous and does not appear within the domain of the Glaciation Sub-Regional flow model, however, excess pressures present at the OPG DGR Site and shown at the top of the Shadow Lake formation in Figure 4-48 may propagate along a possible permeable weathered zone at the top of the Pre-Cambrian. The HOver case assumes 150 m of hydraulic head is imposed on the lower boundary of the reference case constant climate head profile. For a constant climate case, these boundary conditions result in the steady-state head distribution shown in Figure 4-51 and compared to the reference case profile in Figure 4-52.

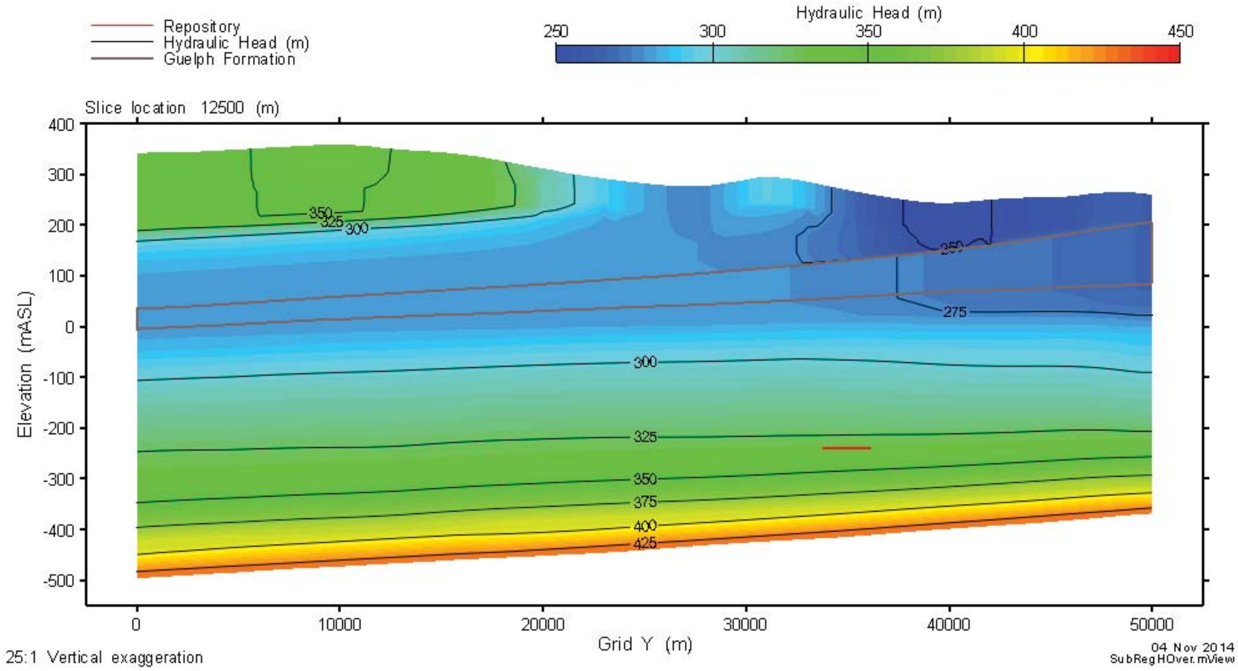

Figure 4-51: Glaciation Sub-Regional Glacial Cycle Simulations: HOver Case Specification – Constant Climate Head Distribution

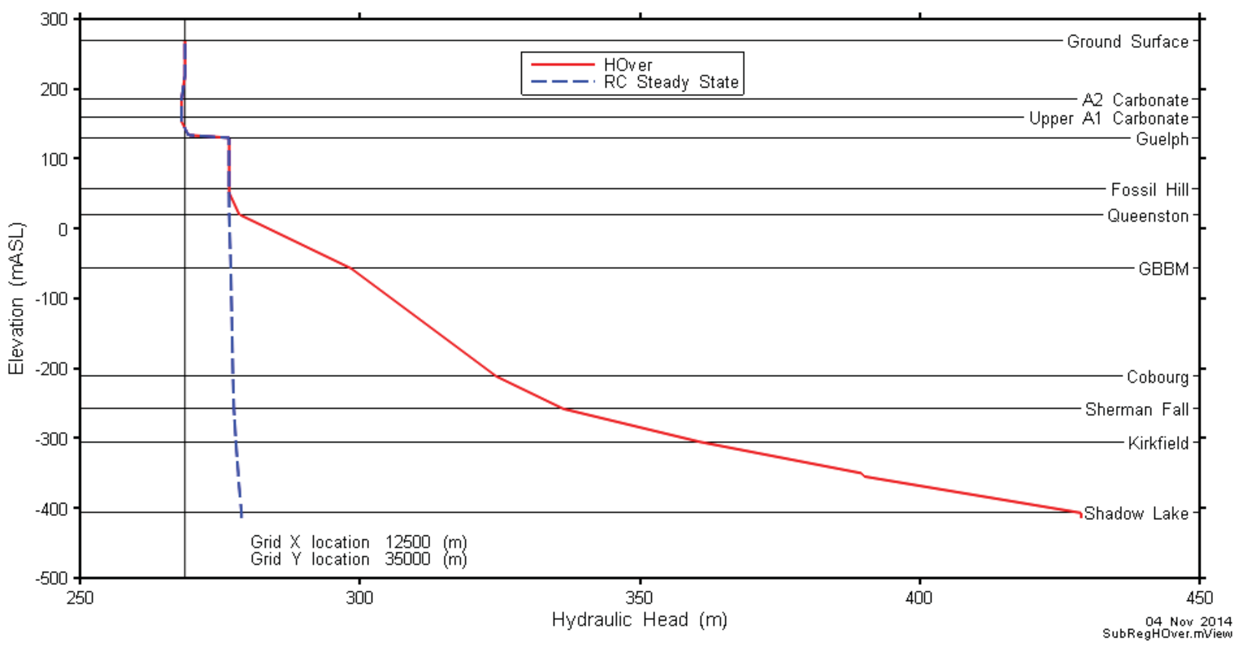

Figure 4-52: Glaciation Sub-Regional Glacial Cycle Simulations: HOver Case Specification – Head Profile Comparison to Constant Climate Reference Case

4.1.5.2 Parameter Sensitivity Case Results

Figure 4-53 through Figure 4-57 present a selection of results which, in aggregate, provide a characterization of flow system sensitivity to the selected parameter cases when compared to the RC glacial climate and RC constant climate results. Figure 4-53 indicates that the general system response remains non cumulative over the 8 glacial cycles simulated, and that any particular cycle is relatively representative of other cycle behaviours.

The increase in KHigh case velocities is expected; for a given gradient, velocity will be proportional to conductivity. This is true for overall magnitude (Figure 4-53) which clearly shows order of magnitude increases in the periods between glacial advances and retreats. Detailed vertical velocities in the fifth cycle (Figure 4-54) show that the various KHigh cases provide the biggest increase in vertical velocities although the increases are not proportional to K increase as for total velocity (approximately a factor of 4, 15 and 40 for KHigh, KHigh100 and KHigh1000 respectively). Figure 4-57 provides an explanation for this result; as hydraulic conductivities increase, vertical head gradients decrease, so velocities increase less than would be the case if the gradients were sustained. For a similar reason, vertical velocities for the LEHigh case are much reduced, being near constant and approximately a factor of two higher than the steady state constant climate case. The velocity relationships are consistent over the Ordovician formations at the time of peak Cobourg velocity (Figure 4-56).

Peak hydraulic head in the Cobourg is dependent on loading efficiency as clearly shown in Figure 4-55. The relatively flat hydraulic profile of the LEHigh case in Figure 4-57 results in a very small vertical hydraulic gradient, which corresponds to the very low velocity in the case. Somewhat counter intuitively, the LELow case also has a relatively flat gradient and a vertical velocity lower than the RC, although much higher at peak than the LEHigh case. This is explained by the fact that gradients are induced based on the difference in loading efficiency between formations. For the LEHigh case most formations have a loading efficiency of 1.0, the maximum possible. This results in all formations having a similar response to applied load, and consequently low vertical gradient between formations. For the LELow case the difference in loading efficiency between formations is reduced because of the constant 0.5 multiplier specified in the case.

SHigh case results show that overall response is relatively insensitive to storativity.

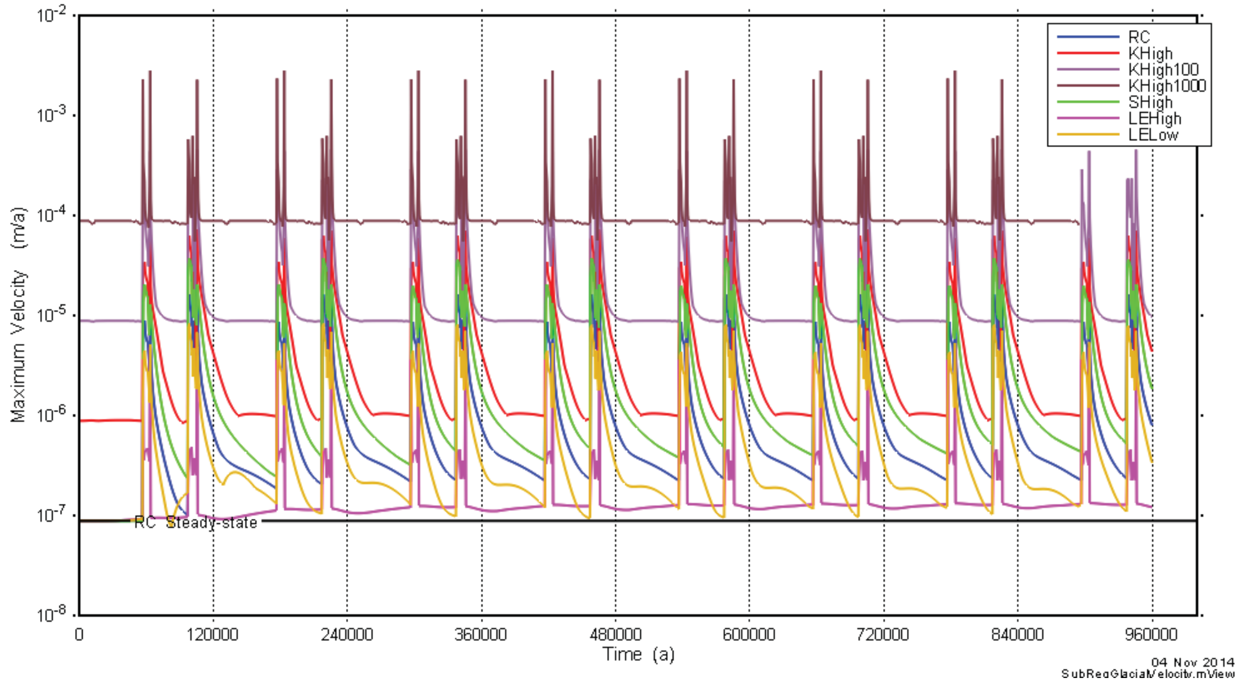

Figure 4-53: Glaciation Sub-Regional Flow – Parameter Sensitivity: Maximum Advective Velocity Magnitude in Vicinity of Repository in Cobourg Formation

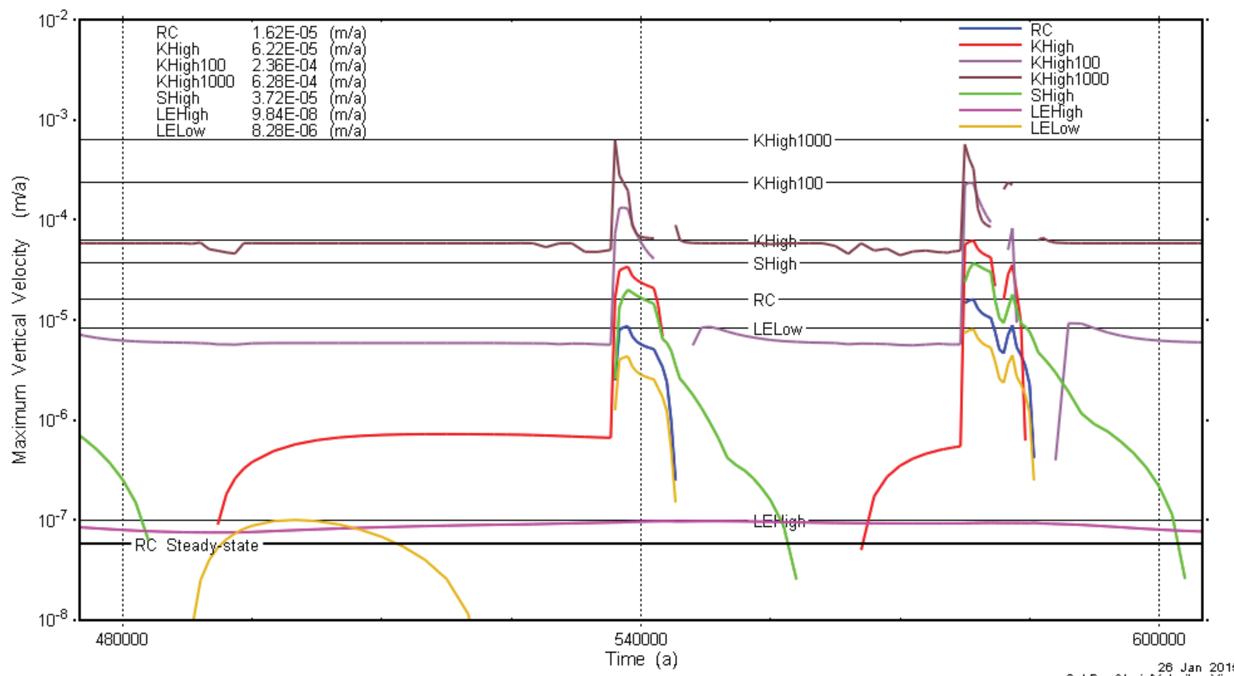

Figure 4-54: Glaciation Sub-Regional Flow – Parameter Sensitivity Detail: Maximum Vertical Advective Velocity Magnitude in Vicinity of Repository in Cobourg Formation Over Fifth Glacial Cycle

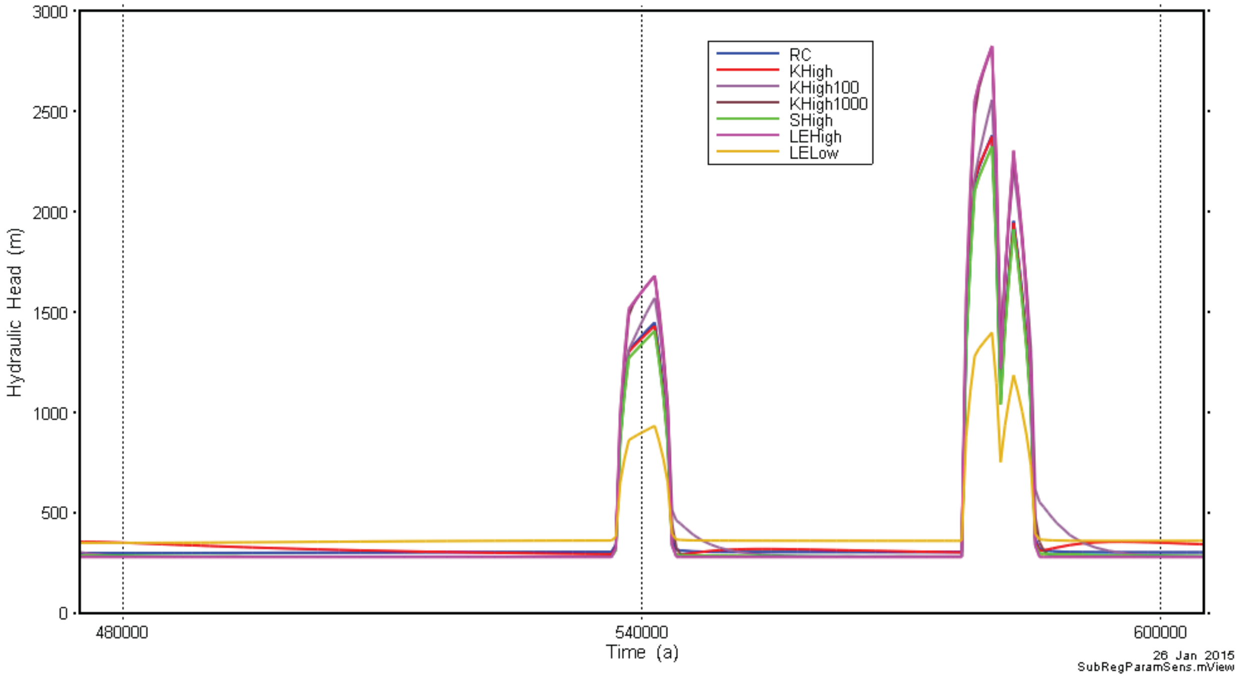

Figure 4-55: Glaciation Sub-Regional Flow – Parameter Sensitivity Detail: Hydraulic Head in Centre of Repository Over Fifth Glacial Cycle

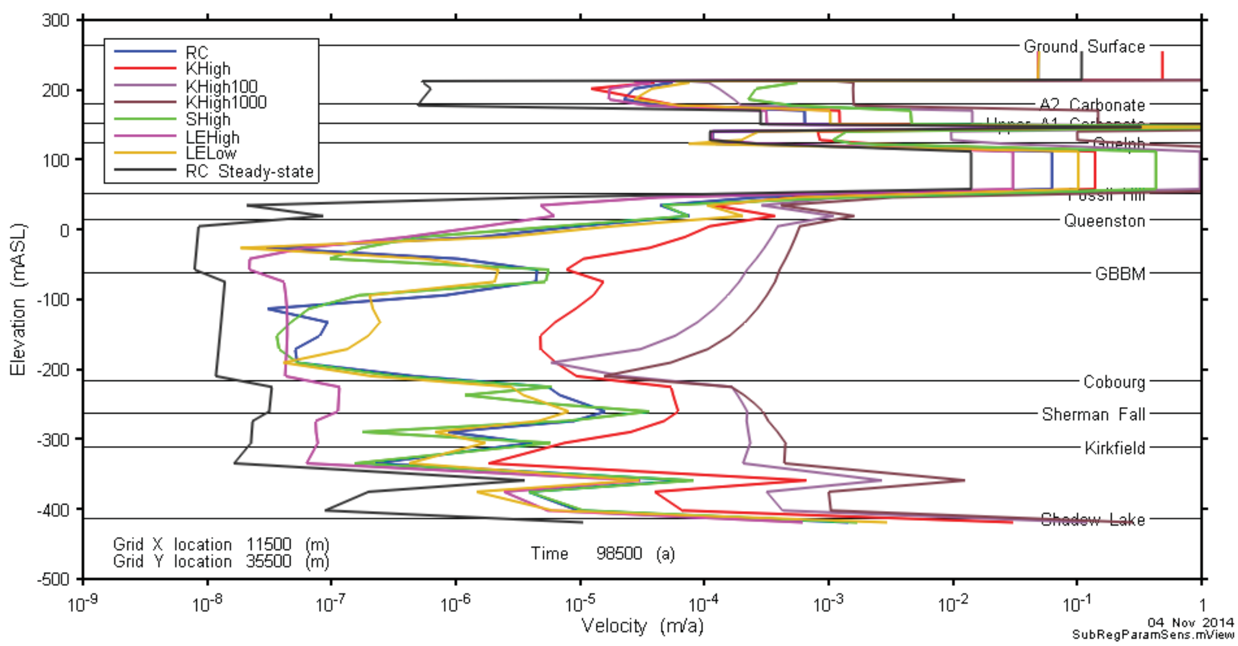

Figure 4-56: Glaciation Sub-Regional Flow – Parameter Sensitivity: Velocity Profile Through Reference Well Location at Time of Maximum Cobourg Velocity in First Glacial Cycle

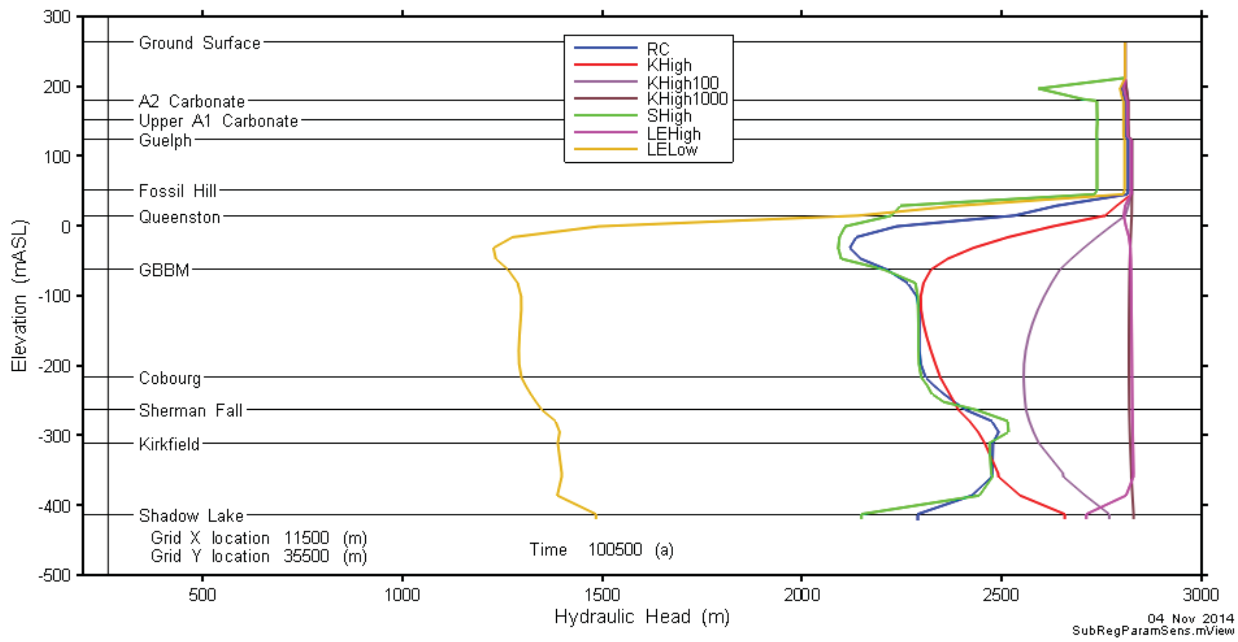

Figure 4-57: Glaciation Sub-Regional Flow – Parameter Sensitivity: Hydraulic Head Profile Through Reference Well Location at Time of Maximum Ice Thickness in First Glacial Cycle

4.1.5.3 Boundary and Initial Condition Sensitivity Case Results

Figure 4-58 through Figure 4-64 present a selection of results for the boundary and initial condition sensitivity cases. The DPF, No PF, and Surface BC cases are very similar to the RC for nearly all results, indicating that the model is not sensitive to either permafrost or the vertical fixed head boundary conditions at the North and South ends. In most figures the RC results mask those of the other cases.

The HUnder, NoLoad, and Load Only cases show some differences between cycles over the simulation duration (Figure 4-60). The underpressures that characterize the HUnder case dissipate over the time frame and Cobourg head responses converge on the RC head response. The NoLoad case shows a gradual increase in Cobourg head, the rate of which flattens towards the end of the simulation, while the Load Only case shows an opposing trend, with a steady decline in Cobourg head.

The largest impact on vertical velocities is seen with the NoLoad case which reduces maximum vertical velocities by a factor of 20 (Figure 4-59). All other cases have similar peak vertical velocities, although overall velocity magnitude is on average slightly higher for the HOver and HUnder cases (Figure 4-58).

Head profiles (Figure 4-63) clearly show differences between the Load Only and No Load cases. The response in the Silurian and Devonian formations is driven by the surface head boundary condition, while the Ordovician response is clearly due to glacial loading.

For the HUnder case, the initial underpressures in the Ordovician (Figure 4-64) dissipate at a rate similar to the constant climate HUnder case (Figure 4-50).

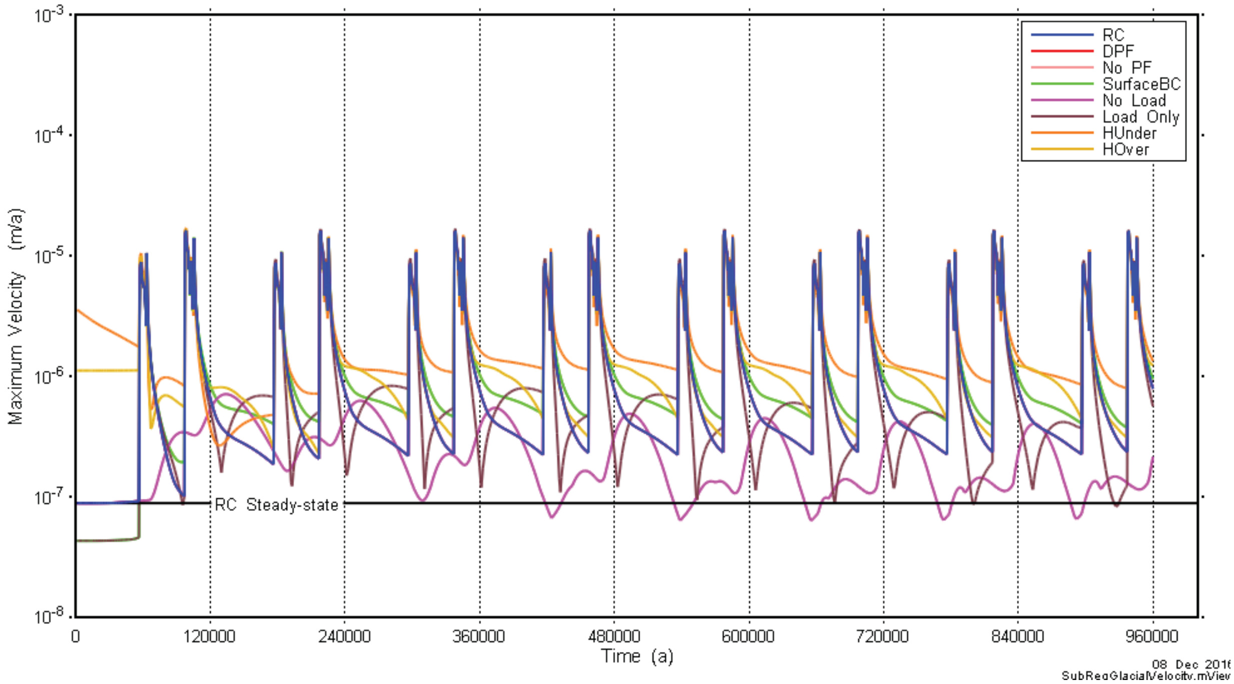

Figure 4-58: Glaciation Sub-Regional Flow – BC Sensitivity: Maximum Advective Velocity Magnitude in Vicinity of Repository in Cobourg Formation

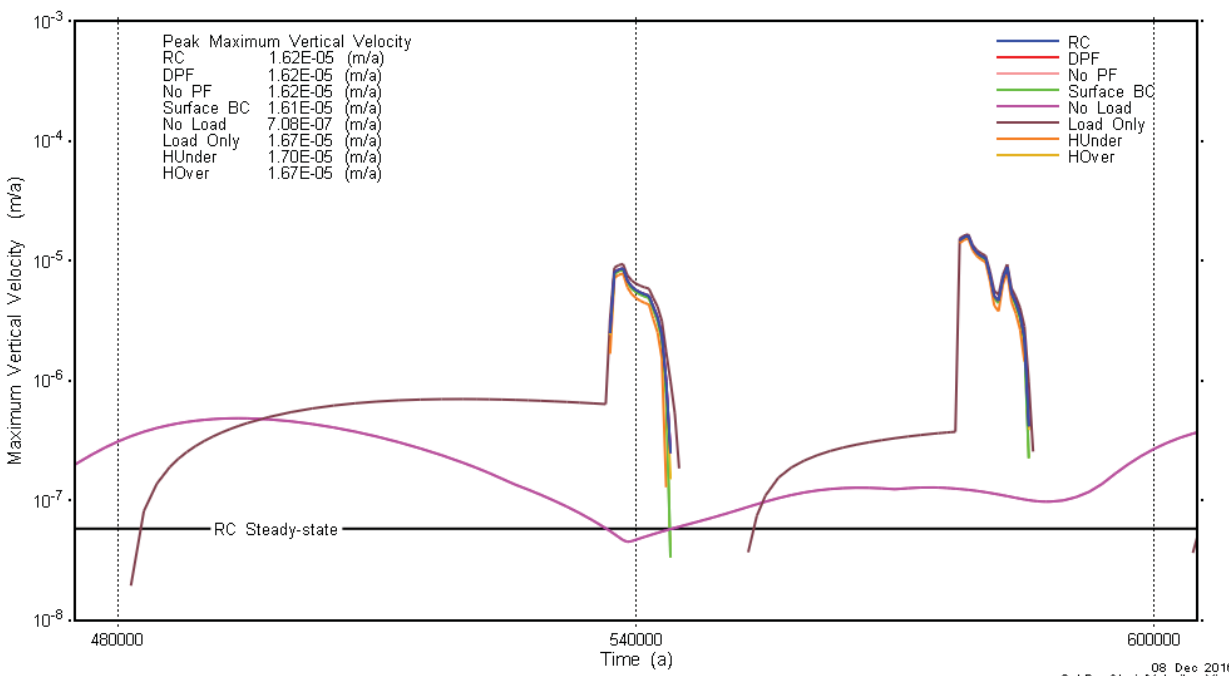

Figure 4-59: Glaciation Sub-Regional Flow – BC Sensitivity Detail: Maximum Vertical Advective Velocity Magnitude in Vicinity of Repository in Cobourg Formation Over Fifth Glacial Cycle

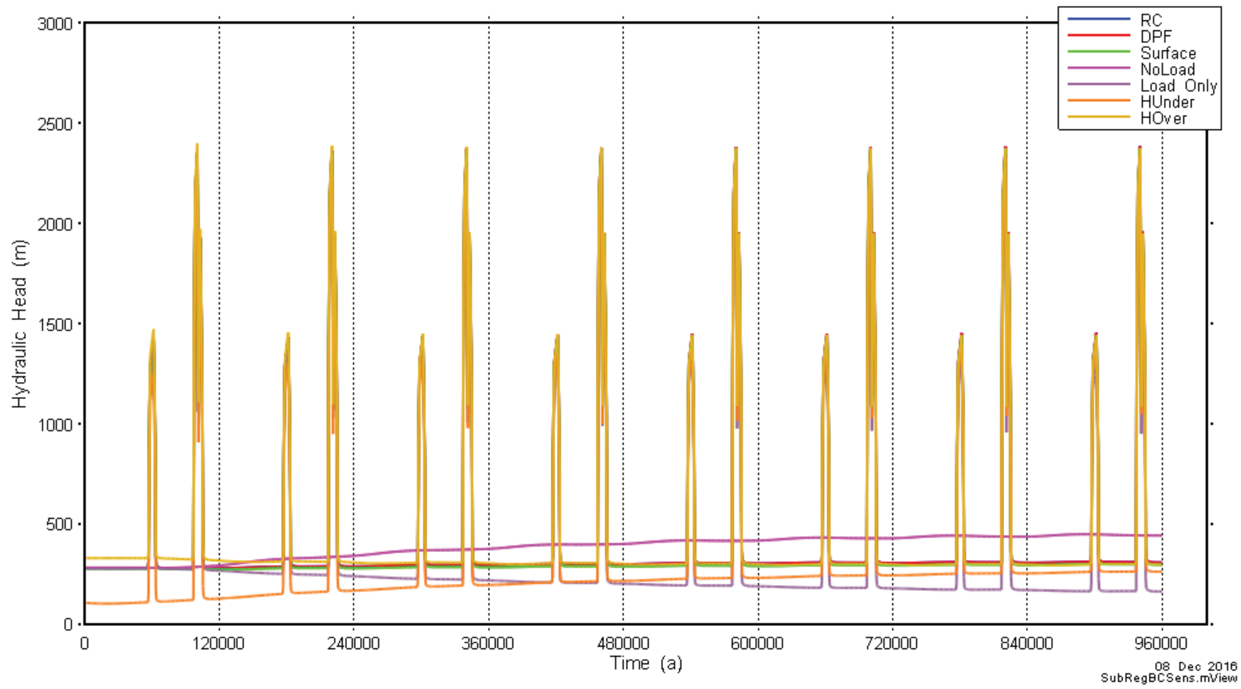

Figure 4-60: Glaciation Sub-Regional Flow – BC Sensitivity Detail: Hydraulic Head in Centre of Repository

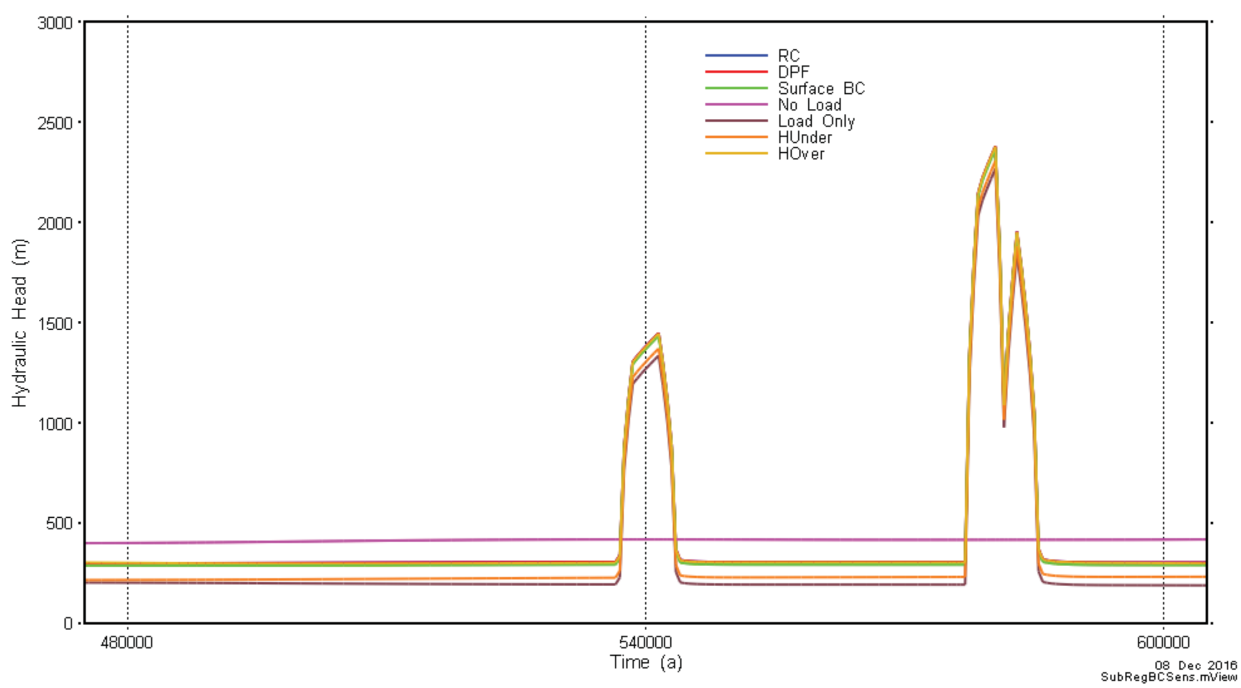

Figure 4-61: Glaciation Sub-Regional Flow – BC Sensitivity Detail: Hydraulic Head in Centre of Repository Over Fifth Glacial Cycle

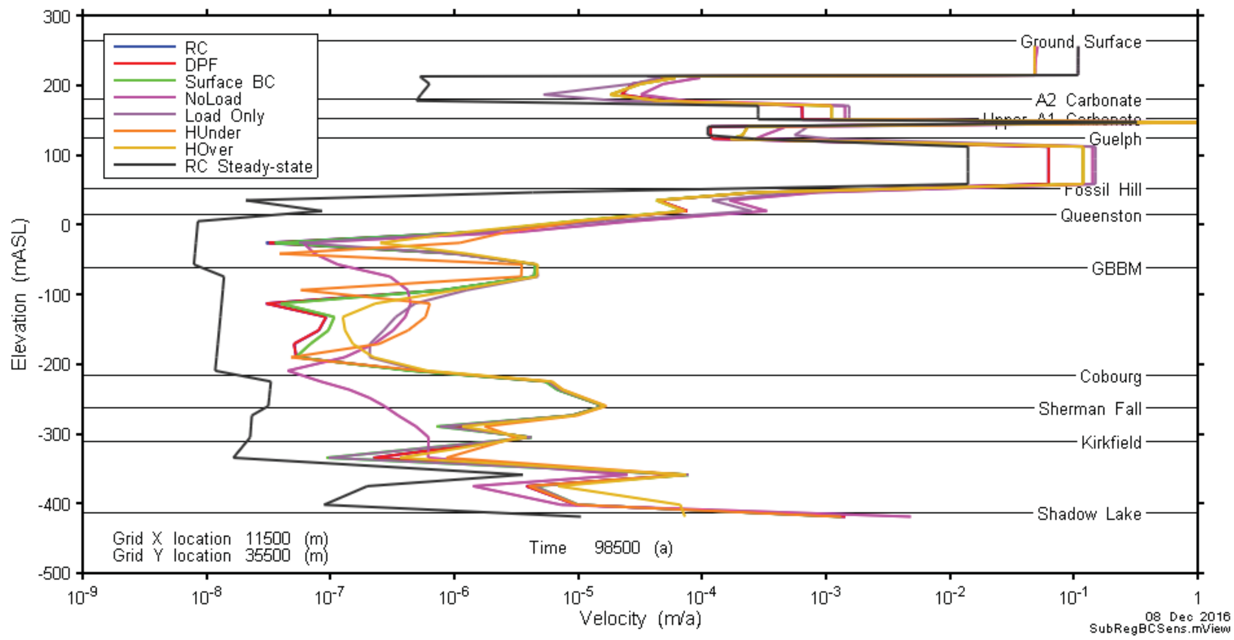

Figure 4-62: Glaciation Sub-Regional Flow – BC Sensitivity: Velocity Profile Through Reference Well Location at Time of Maximum Cobourg Velocity in First Glacial Cycle

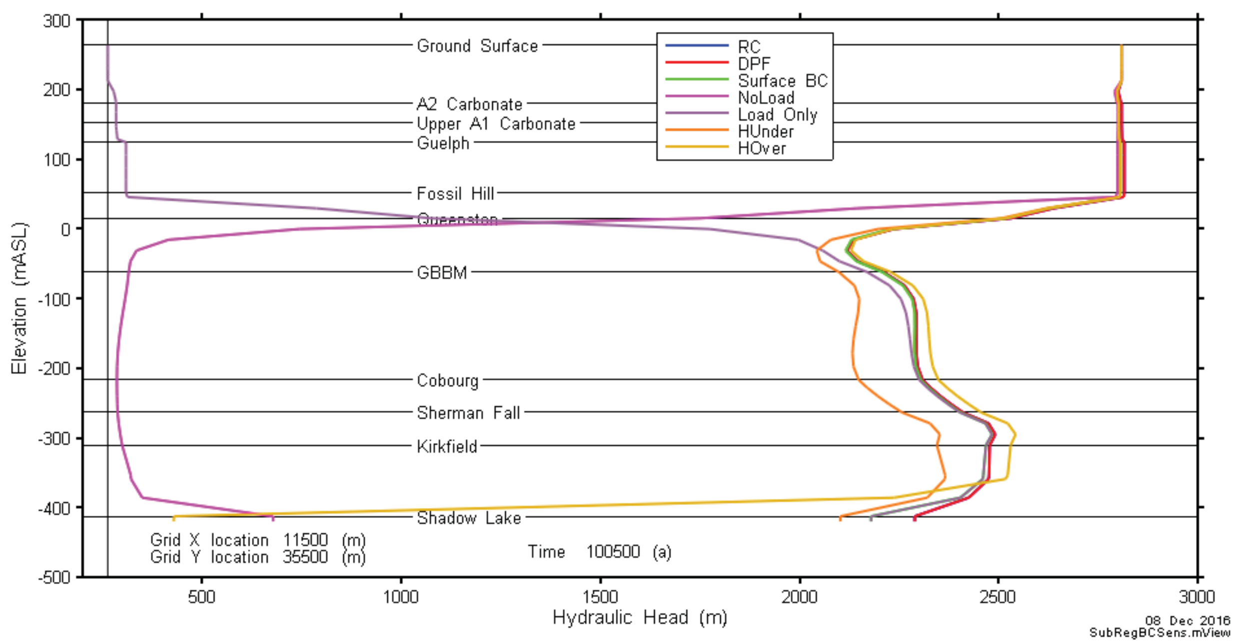

Figure 4-63: Glaciation Sub-Regional Flow – BC Sensitivity: Hydraulic Head Profile Through Reference Well Location at Time of Maximum Ice Thickness in First Glacial Cycle

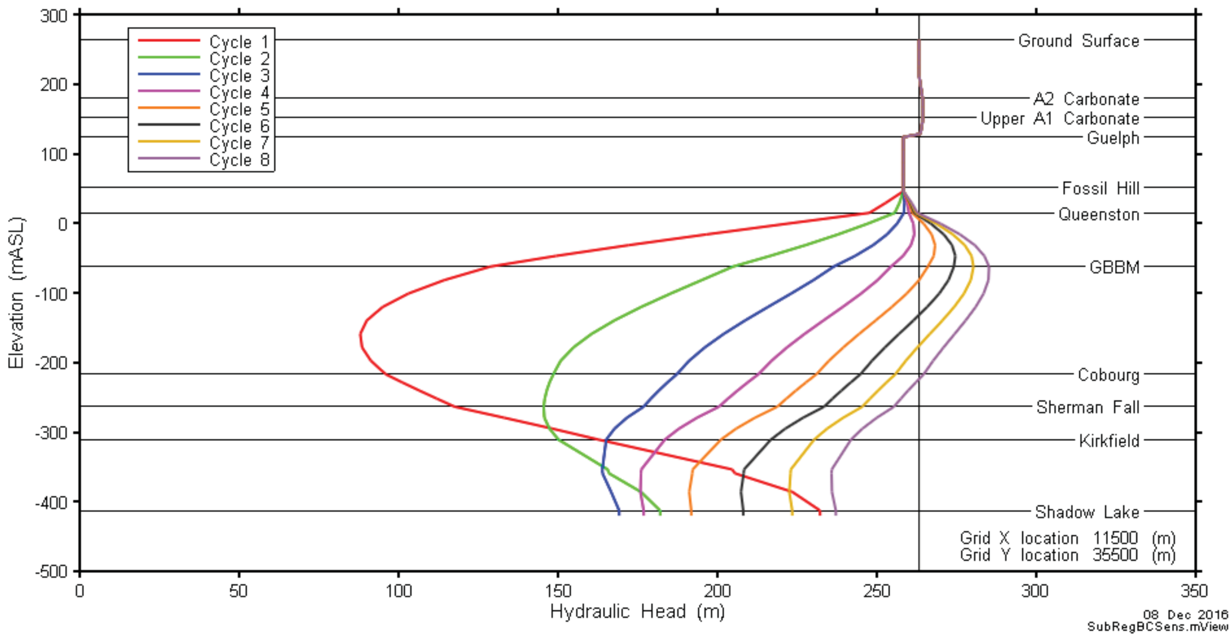

Figure 4-64: Glaciation Sub-Regional Flow – HUnder Sensitivity Case: Hydraulic Head Profile Through Reference Well Location at Time of Maximum Well Operation in Each Glacial Cycle

4.1.5.4 Process Sensitivity Case Results

Figure 4-65 through Figure 4-70 present results for the process sensitivity cases. The two glacial climate cases are very similar in all respects, having virtually identical vertical advective velocities. Differences between the variable-density and constant-density constant climate head profiles (Figure 4-70) are due to the differences in the head formulation used in the model. The variable density freshwater head includes a pressure component from the higher density saline porewater in the deeper geosphere, while the constant density constant climate (steady-state) head does not.

The most significant difference in the results is not visible in the figures: model execution time. The RC (constant density, glacial climate) simulation completed in 7.5 days, while the variable density, glacial climate sensitivity case was terminated at approximately 650 ka after 128 days of simulation. Estimated time to complete the simulation was over 200 days.

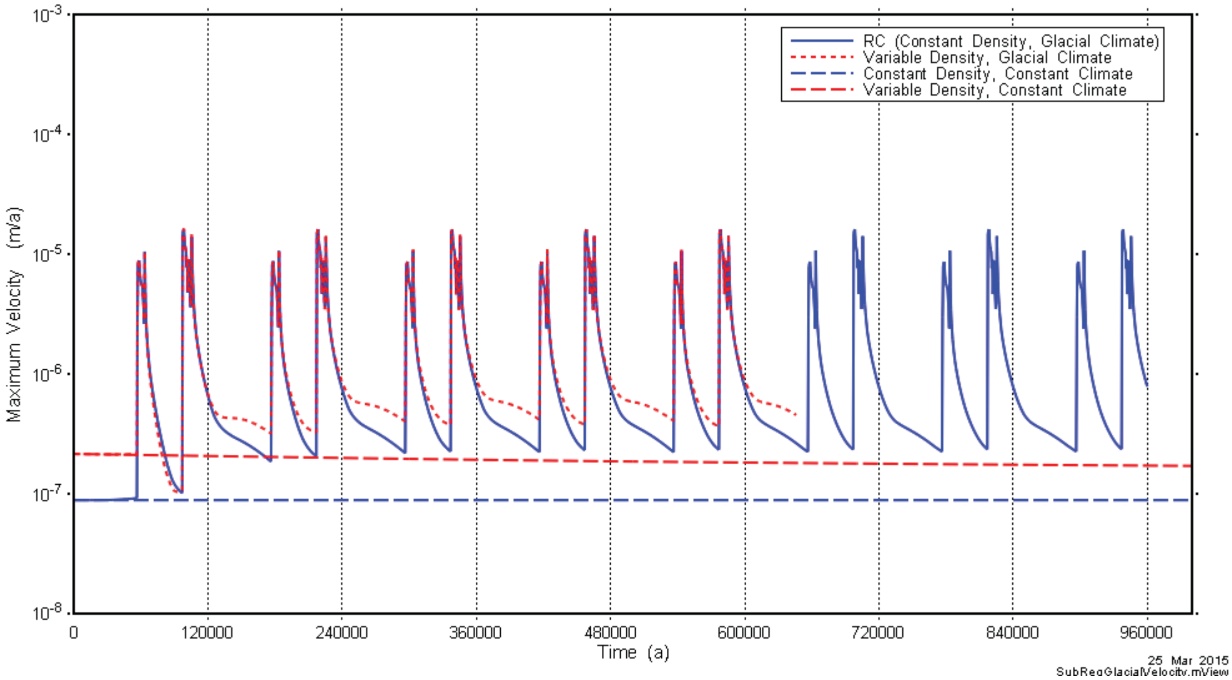

Figure 4-65: Glaciation Sub-Regional Flow – Process Sensitivity: Maximum Advective Velocity Magnitude in Vicinity of Repository in Cobourg Formation

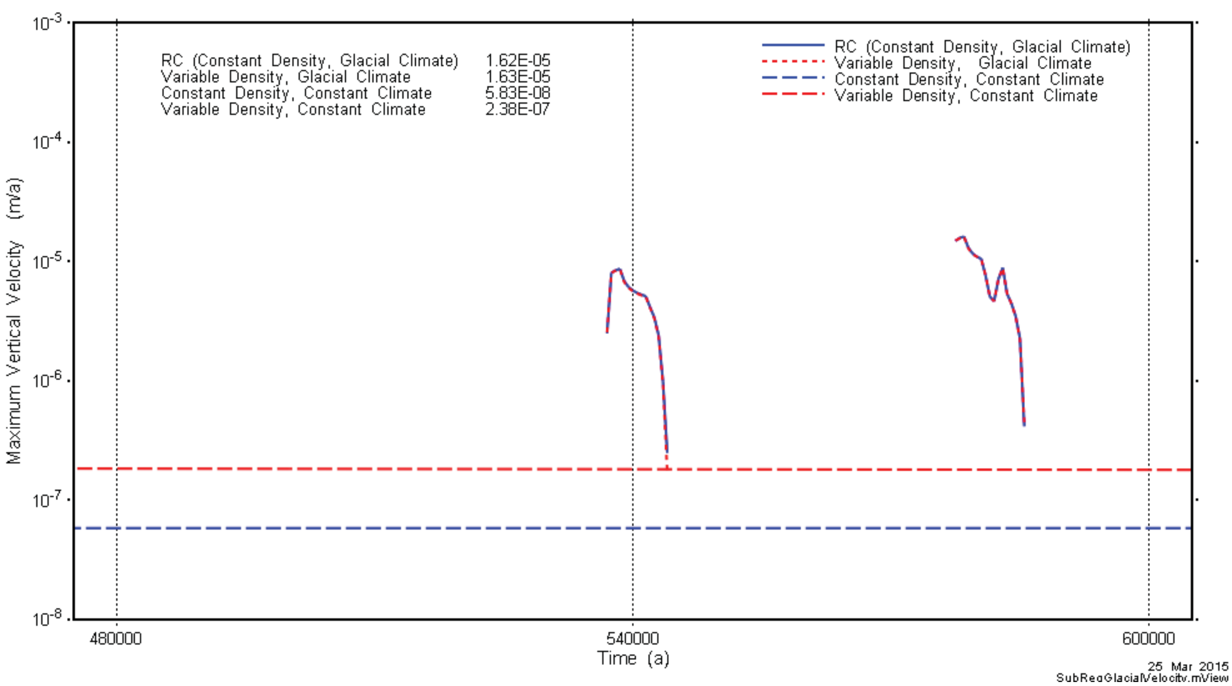

Figure 4-66: Glaciation Sub-Regional Flow – Process Sensitivity Detail: Maximum Upwards Vertical Advective Velocity Magnitude in Vicinity of Repository in Cobourg Formation Over Fifth Glacial Cycle

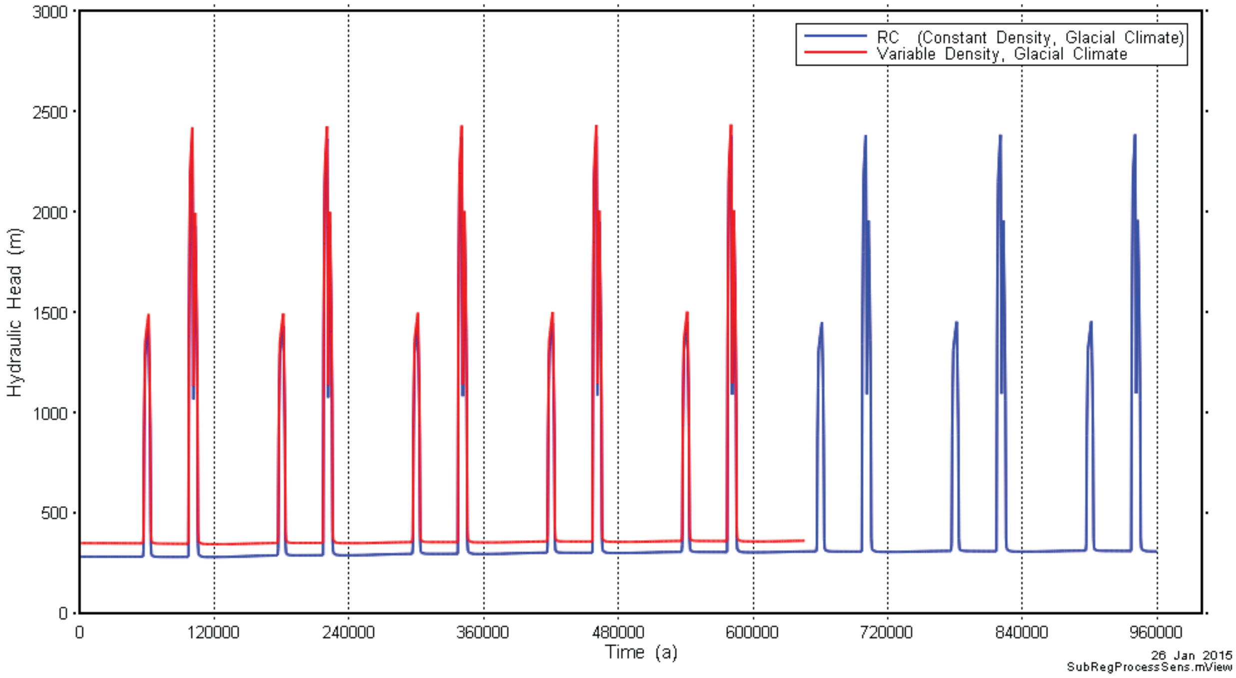

Figure 4-67: Glaciation Sub-Regional Flow – Process Sensitivity Detail: Hydraulic Head in Centre of Repository

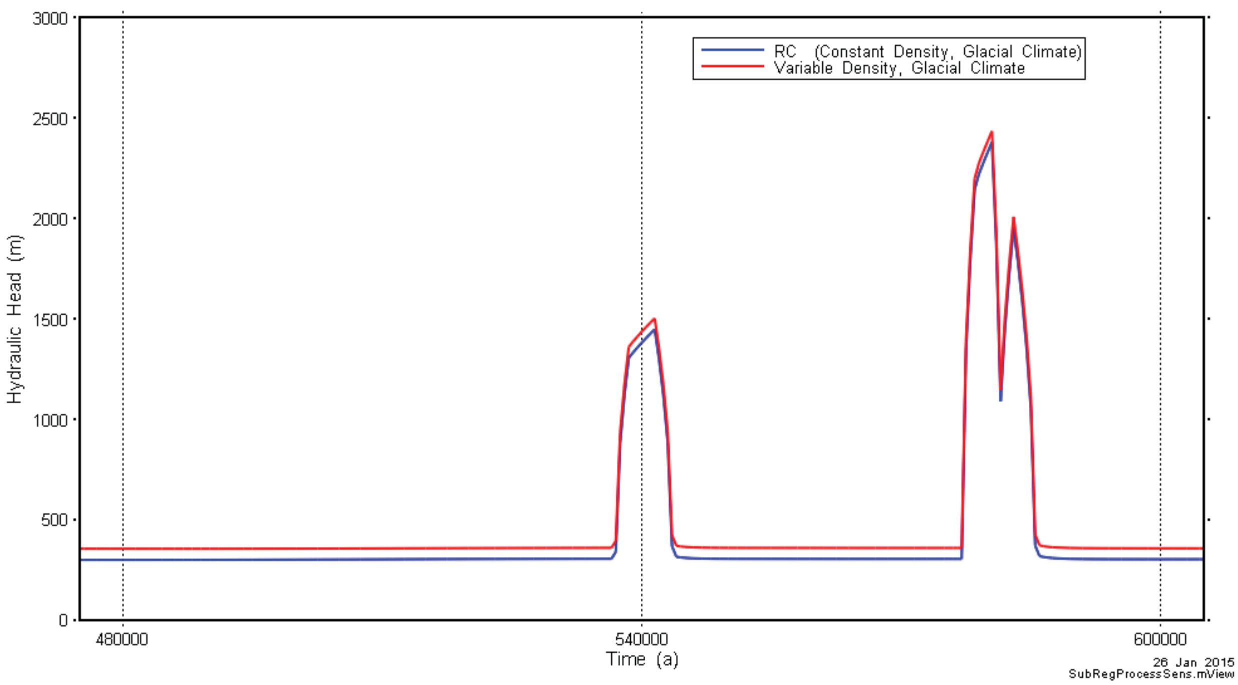

Figure 4-68: Glaciation Sub-Regional Flow – Process Sensitivity Detail: Hydraulic Head in Centre of Repository Over Fifth Glacial Cycles

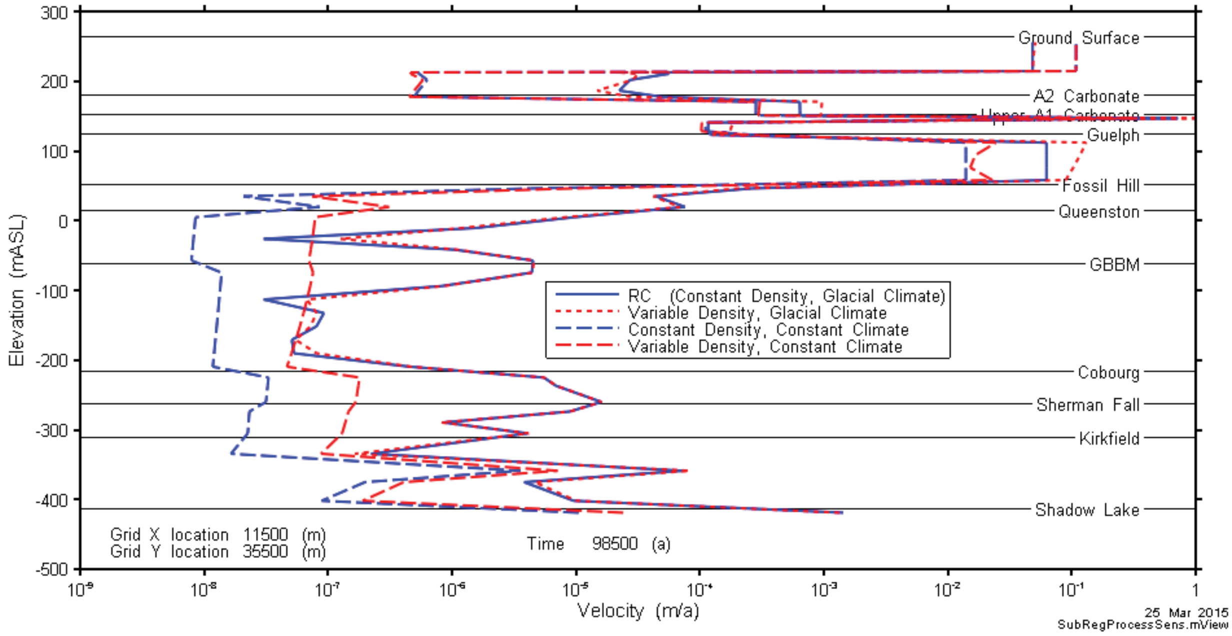

Figure 4-69: Glaciation Sub-Regional Flow – Process Sensitivity: Velocity Profile Through Reference Well Location at Time of Maximum Cobourg Velocity (Glacial Climate Cases) in First Glacial Cycle

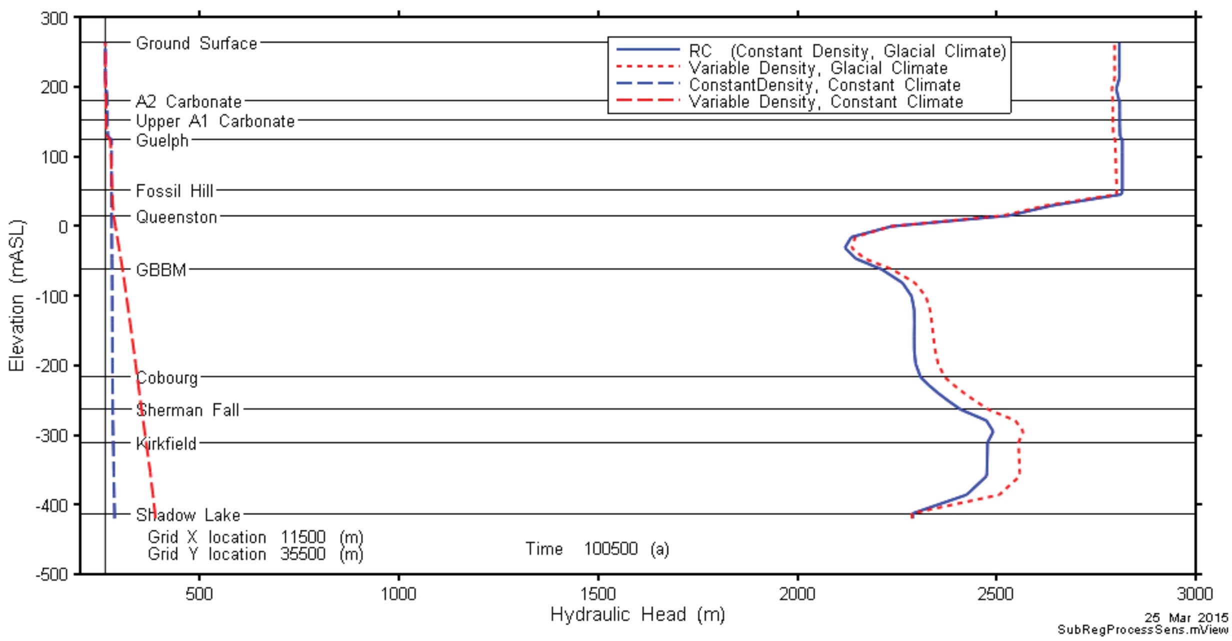

Figure 4-70: Glaciation Sub-Regional Flow – Process Sensitivity: Hydraulic Head Profile Through Reference Well Location at Time of Maximum Ice Thickness (Glacial Climate Cases) in First Glacial Cycle

4.1.6 Significance of Glacial Climate to Safety Assessment

From the perspective of post-closure safety assessment, the possible negative impact of the glacial climate conditions is to increase velocities within the Ordovician host rock to such an extent that transport is no longer diffusion dominated. Assessments of steady-state flow velocities (Figure 4-17) have shown that increases in advective velocity of two orders of magnitude within the Ordovician formations are generally insufficient to meet this threshold.

This leads to the larger question of "what is diffusion dominant?" Qualitatively, and by definition, diffusion dominant systems are those in which mechanisms not related to groundwater movement are responsible for the majority of transport. Quantitatively, attempts have been made to relate dimensionless Péclet numbers to this behaviour. Bear (1979) refers to Péclet numbers of less than 0.4 being representative of diffusion dominated transport. Huysmans and Dassargues (2004) review this approach and find no less than 10 different approaches to calculating Péclet number, with a wide variation in results. The analysis is further confused with differing diffusion nomenclature. Diffusion properties used in transport modelling in this report are calculated from effective diffusion coefficients (D_e), which are directly measured using the through diffusion method (INTERA, 2011). Typical effective diffusion coefficients for I-129 in the formations of interest range from 4.4E-13 m^2/s to 2.0E-12 m^2/s (see Appendix A, Table A-2). D_e is related to the free-water, or molecular diffusion coefficient (D_m) by:

$$D_e = D_m \tau \theta \qquad \textbf{(4-1)}$$

where:

D_m	molecular, or free water, diffusion coefficient	$[L^2/T]$
τ	tortuosity	[ ]
θ	porosity	[ ]

In other references, the effective diffusion coefficient does not include the porosity term, a coefficient we refer to as apparent, or pore-water diffusion:

$$D_{pw} = D_m \tau = \frac{D_e}{\theta} \qquad \textbf{(4-2)}$$

In equations below, we have substituted D_e/θ where appropriate.

The general form of the Péclet equation is:

$$Pe = \frac{Vx}{D} \qquad \textbf{(4-3)}$$

where :

Pe	Péclet number	[ ]
V	advective velocity	[L/T]
x	characteristic length	[L]
D	hydrodynamic dispersion (and diffusion) coefficient	$[L^2/T]$

The hydrodynamic dispersion coefficient considers both dispersion and diffusion, and is typically defined as:

$$D = \alpha V + D_e \qquad \textbf{(4-4)}$$

where:

α dispersivity coefficient [L]

Differences in the approaches to calculating the Péclet number are manifested by the choice of values for characteristic length and the processes to include in D. The earliest approach (Ogata and Banks, 1961) uses a characteristic distance from the contaminant source to the receptor. A modification of this approach (Remenda et al, 1996) replaces x with VT, where T is the time scale of interest. Note that this is in effect a variable characteristic distance as x = VT will increase with increasing V. Other approaches (Freeze and Cherry, 1979; Bear, 1979) ignore the contribution from dispersion and set D to D_{pw}. The analysis presented in Bear (1979) is discussed in the context of flow through a sand column and the characteristic length is suggested to be on the order of the particle size. Freeze and Cherry (1979) also suggest particle size as characteristic length. Sykes et al. (2011) use the Freeze and Cherry (1979) approach but select a characteristic length of unity (1 m). Sykes et al. (2011) describe the selection as conservative in comparison to Bear (1979) recommendation of particle size.

The characteristics of a specific transport scenario will guide selection of appropriate parameter values for characteristic length and diffusion coefficient. Péclet numbers can compare the relative dominance of diffusive transport across a system or between systems; however, Péclet numbers do not provide an unambiguous measure of diffusion-dominance.

Freeze and Cherry (1979) suggest the ratio of dispersive to diffusive flux as an alternative metric for evaluating importance of diffusion at low velocities. Walsh and Avis (2010) applied this approach and developed a “Figure of Merit”, or FOM, calculated as:

$$FOM = \frac{\alpha V}{D_{pw}} \qquad \textbf{(4-5)}$$

In this approach, FOM less than 0.1 are diffusion dominant; greater than 10 are advective dominated, while values between 0.1 and 10 represent a transition region. Reference case results presented in Figure 4-71 show diffusion dominated transport for non ice cover periods, with transition region transport during glacial advance and retreat.

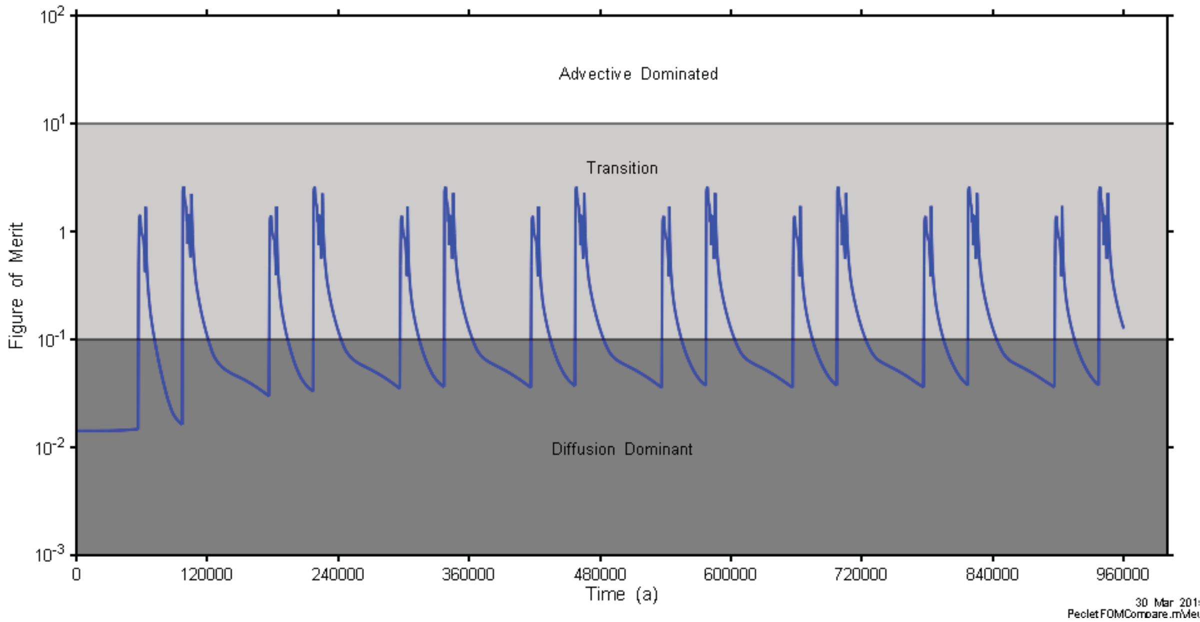

Figure 4-71: FOM Calculations for Reference Case Cobourg Velocities in the Vicinity of the Repository

Another approach to evaluating the impact of glacial climate induced increases in velocity is to ignore the process implications (diffusion or advection dominant) and instead concentrate on an easily understood measure of transport: the cumulative distance a particle would move with groundwater over the performance period. This measure, travel distance, is a simple integration of the maximum velocity, as shown in Figure 4-72. The integration conservatively ignores the direction of travel. Note that the distance to the nearest permeable formation (i.e. the distance to potential biosphere exposure) is on the order 280 m.

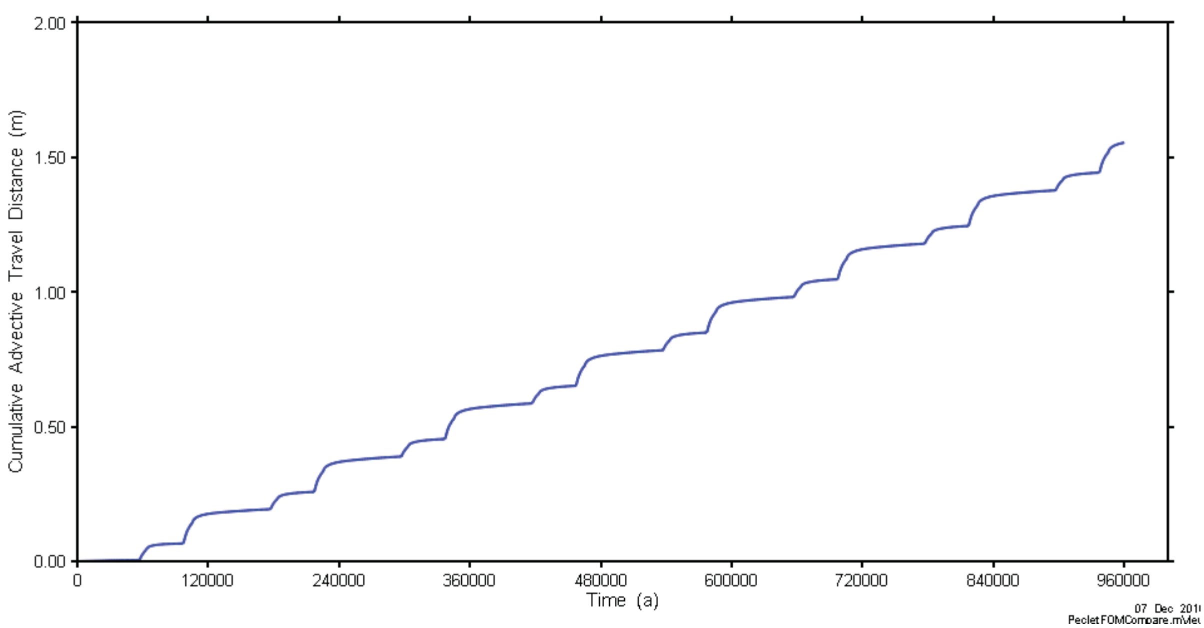

Figure 4-72: Cumulative Travel Distance for Reference Case Cobourg Velocities in the Vicinity of the Repository

A better approach may be to incorporate all transport processes in a conservative sense by creating time series of “snapshot” MLE for the repository volume. As with the previous methods, this approach will not determine advective or diffusive dominance, but focuses on a measure of transport. Calculations are performed using head fields extracted at 500 year intervals over the entire performance period. MLE are extracted for all nodes in the vicinity of the repository within the Cobourg formation (see Figure 4-15), and the minimum MLE value selected as the representative Repository MLE for the time period. This approach is computationally costly (1921 separate MLE calculations for each case) but removes all of the conjecture and uncertainty associated with Péclet comparisons while still incorporating the results of all transport processes. Furthermore, the metric is conceptually easily understood – the aggregate best estimate of time to surface (or well) discharge from the repository. Figure 4-73 presents MLE calculations for the RC and parameter sensitivity cases, while Figure 4-74 presents similar results for other sensitivity cases. The variability in the other cases is much less than for parameter sensitivity and is displayed on a more limited Y axis range.

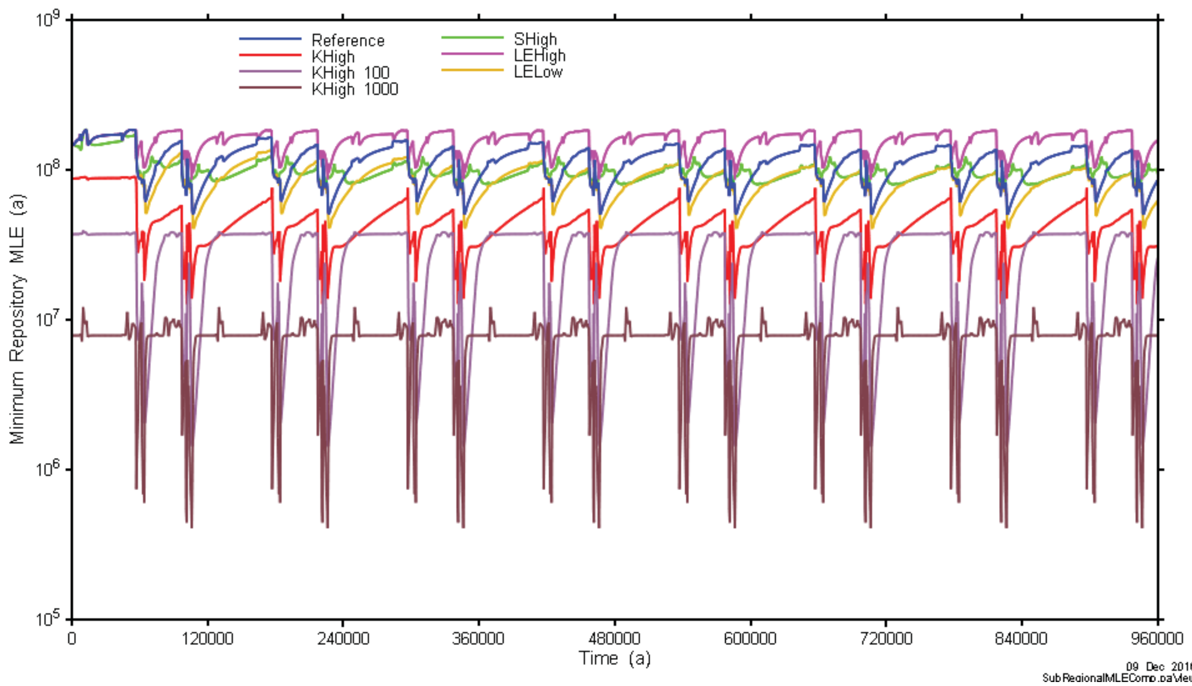

Figure 4-73: Repository MLE Time Series for Reference and Parameter Sensitivity

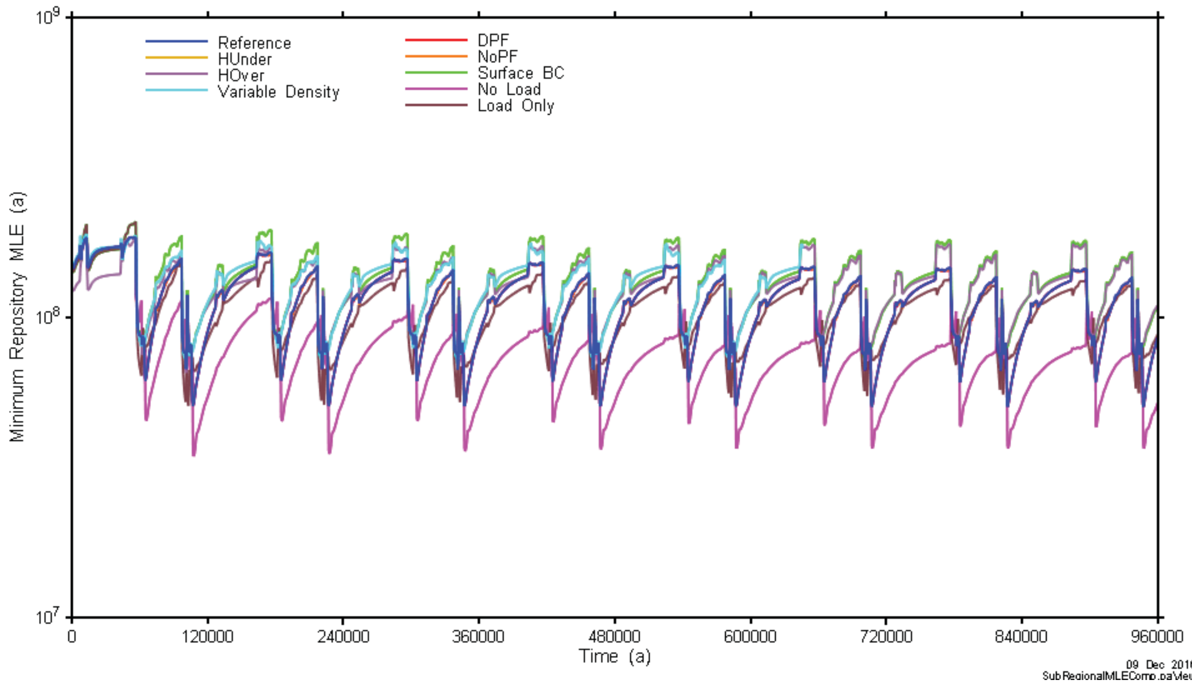

Figure 4-74: Repository MLE Time Series for Reference and Process and Boundary Condition Sensitivity

Repository MLE time series for selected cases during glacial cycle 5 (Figure 4-75) clearly show that even for the implausibly high conductivity case (KHigh100) transport is extremely slow, with snapshot MLE of over 20 Ma except for periods of glacial advance and retreat. It is also clear that the higher velocities associated with the peak glaciation events do not persist for any significant period and therefore the mean Repository MLE is likely a reasonable estimate of the actual transport times to discharge under glacial climate conditions.

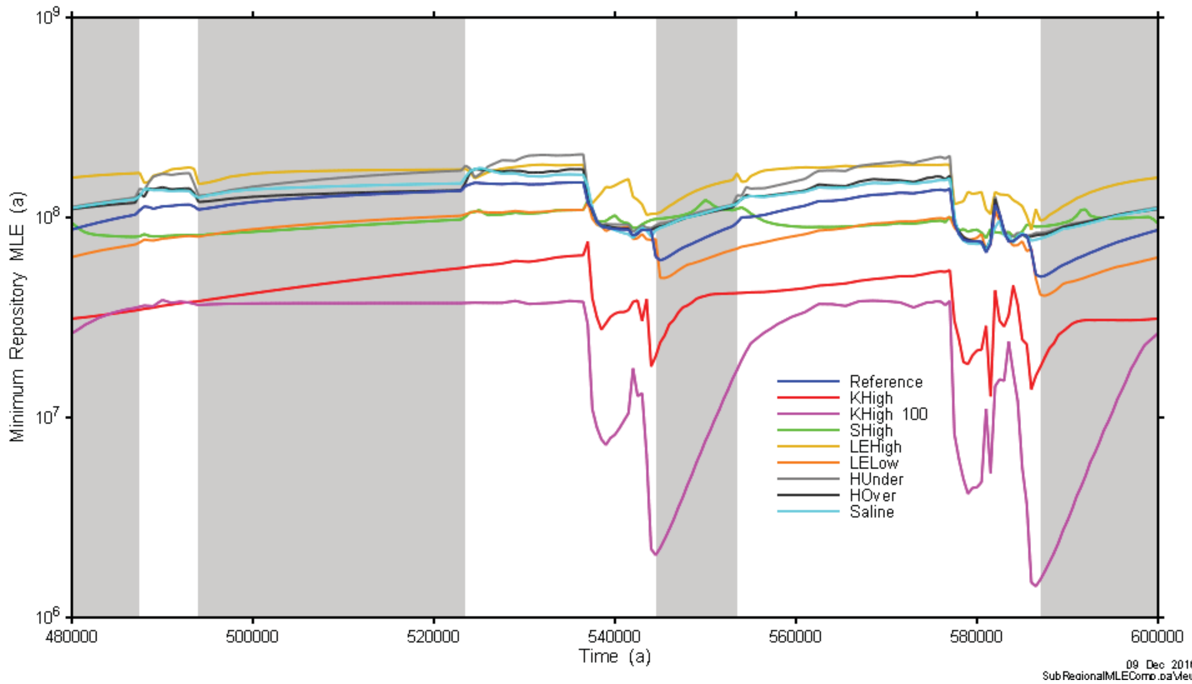

Figure 4-75: Glaciation Sub-Regional Glacial Cycle Simulations: Repository MLE for Fifth Glacial Cycle – Reference Case and Selected Sensitivity Cases

Mean, maximum, and minimum repository MLE over the full 960 ka period for all cases are listed in Table 2 and plotted in Figure 4-76.

Table 2 - Repository MLE for Reference and Sensitivity Cases

	Repository MLE (a)		
Case	Mean	Minimum	Maximum
RC	1.13E+08	5.04E+07	1.85E+08
KHigh	4.45E+07	1.28E+07	8.97E+07
KHigh 100	2.71E+07	1.43E+06	3.94E+07
KHigh1000	7.42E+06	4.08E+05	1.21E+07
SHigh	9.86E+07	7.63E+07	1.86E+08
LEHigh	1.58E+08	8.71E+07	1.85E+08
LELow	8.91E+07	4.06E+07	1.85E+08
HUnder	1.36E+08	6.90E+07	2.16E+08
Hover	1.25E+08	6.55E+07	1.83E+08
NoLoad	7.80E+07	3.45E+07	1.85E+08
LoadOnly	1.07E+08	5.09E+07	2.09E+08
NoPF	1.12E+08	5.04E+07	1.85E+08
DPF	1.12E+08	5.04E+07	1.85E+08
Surface BC	1.30E+08	6.73E+07	2.08E+08
Saline (to 640 ka)	1.31E+08	6.77E+07	1.90E+08
RC (Constant Climate)		2.08E+08	

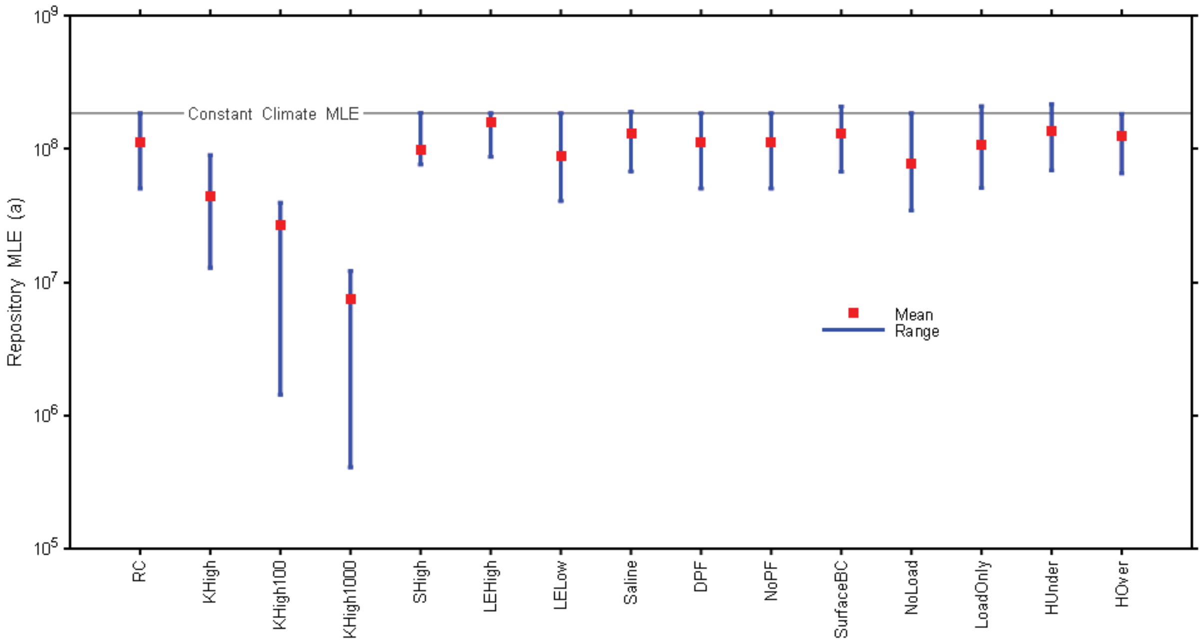

Figure 4-76: Glaciation Sub-Regional Glacial Cycle Simulations: Repository MLE for Reference Case and Sensitivity Cases

These results have additional conservatism due to a relatively high value of longitudinal dispersivity (250 m) used for numeric reasons. MLE estimates with smaller dispersivities are slightly greater. By contrast, increased diffusion coefficients will result in shorter Repository MLE. Sensitivity to decreased dispersivity (reduced from 250 to 100 m) and increased diffusion (D_e x 2) are shown in Figure 4-77. There is less uncertainty in diffusion coefficients as data are based on laboratory measurements.

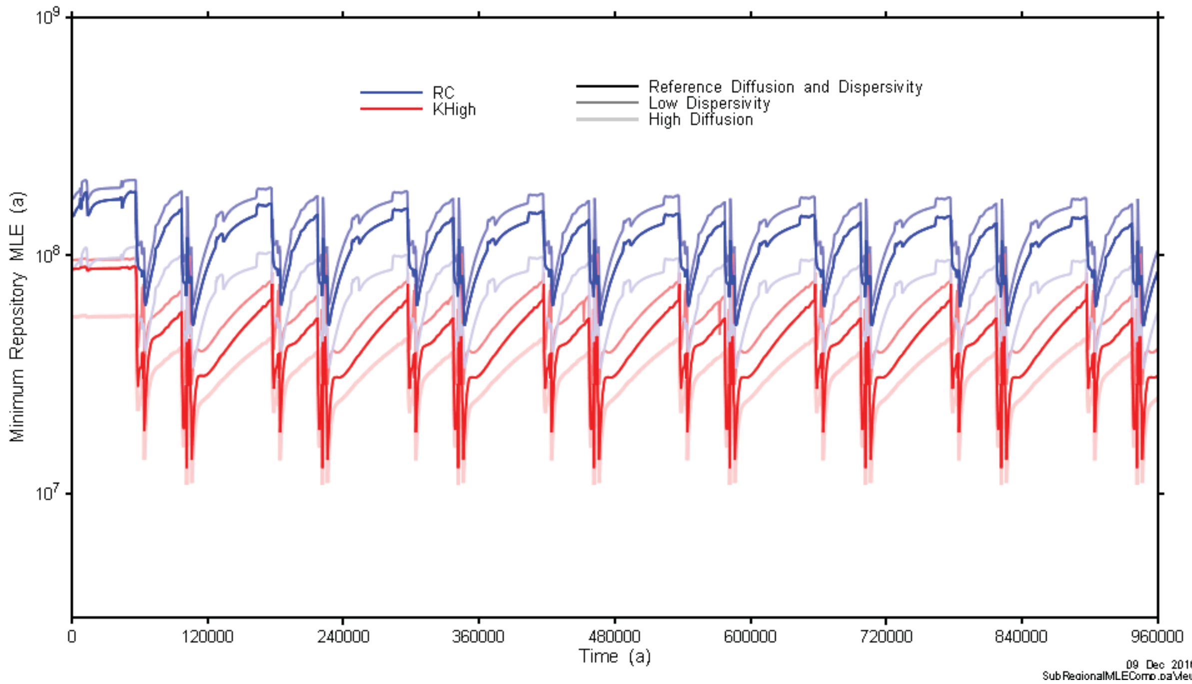

Figure 4-77: Glaciation Sub-Regional Glacial Cycle Simulations: Repository MLE Time Series Sensitivity to Dispersivity and Diffusion for Reference Case and KHigh Sensitivity Case

4.2 Site-Scale Transport Modelling

Site-Scale transport modelling simulates the transport of a single radionuclide (Iodine-129) from release locations associated with hypothetical defective containers. Release locations and source terms are consistent with those presented in NWMO (2013) for the shaft and reference case simulations, with an additional case representing release from the centre of the repository to a centrally located well. Constant climate and glacial climate boundary conditions are used. Constant climate cases are compared to NWMO (2013) releases to confirm consistent results. Glacial climate results are compared to those for constant climate for the three source term location/well location cases, as well as for selected sensitivity cases.

4.2.1 Model Description

4.2.1.1 Model Domain and Discretization

Constant climate radionuclide transport modelling presented in NWMO (2013) used a detailed model of the repository that included nearly all repository features with high fidelity to the actual design and geosphere conceptual model. However, the model was extremely large (nearly 12M nodes) with attendant large memory requirements and long execution times. Given that the current modelling incorporates time varying boundary conditions and transient flow with additional resource requirements, some effort was made to reduce the complexity of the discretization while still retaining essential repository features which dominate transport response. The main simplifications include the following: combining inner and outer repository EDZ into a single composite EDZ with equivalent transmissivity (conductivity × area); limiting EDZ to above and below rooms and tunnels only, reducing the number of elements used in seals, and using a common height for all repository room, drifts, and tunnels.

The Site-Scale model domain includes the repository foot print plus a portion of surrounding geosphere extending approximately 1 km in each direction. Vertically, the model includes all formations from the bottom of the Shadow Lake to the top of the Salina A2 Carbonate. As boundary conditions for the glacial climate transport model are extracted directly from Glaciation Sub-Regional model results, it is not necessary to extend the model all the way to ground surface. The Salina A2 was selected as the upper boundary for the model as it is sufficiently distant from the Guelph formation containing the well, and its low permeability will minimize any local boundary effects.

The model coordinate system is defined consistently with the Site-Scale model in NWMO (2013), with the origin located at the intersection of the main tunnel and first cross cut drift and cardinal directions aligned with the tunnel and cross-cut drifts. Note that this coordinate system is rotated approximately 160 degrees compared to the Glaciation Sub-Regional local and UTM coordinate systems. In this case, positive X increases approximately from East to West and positive Y from North to South. The horizontal model domain and coordinate system are presented with the Glaciation Sub-Regional model extents for context in Figure 4-78 and Figure 4-79.

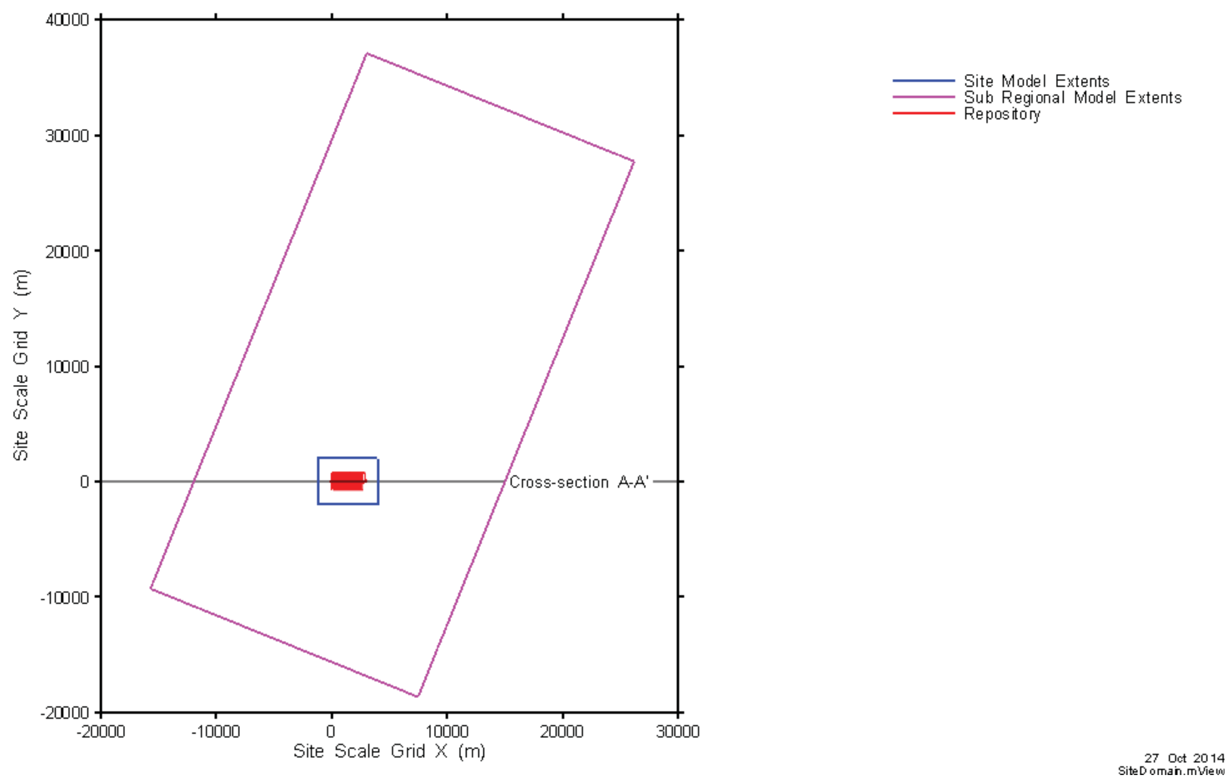

Figure 4-78: Site-Scale Model Domain – Plan View

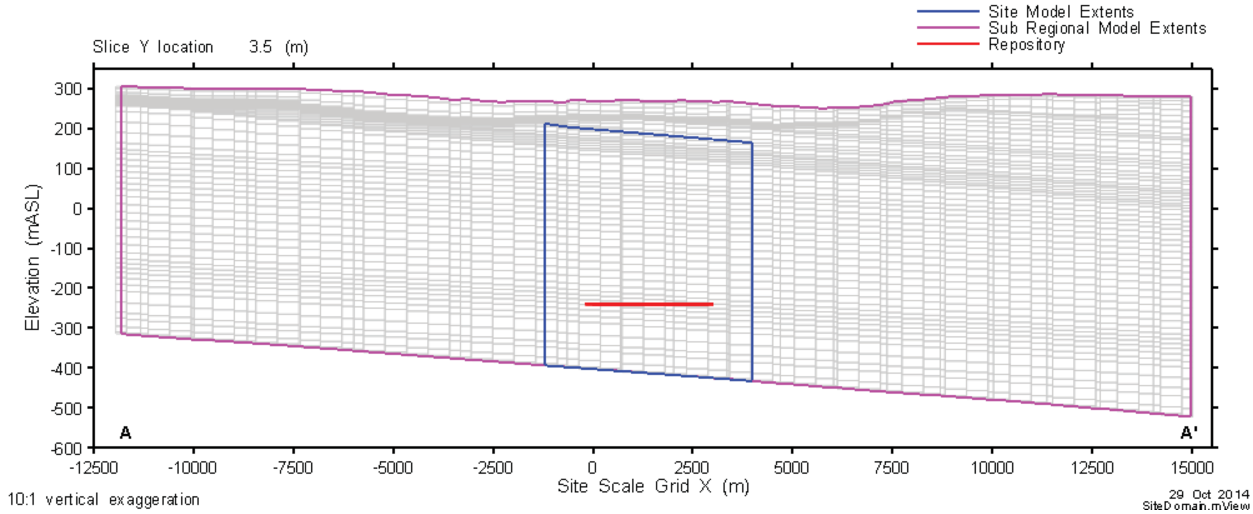

Figure 4-79: Site-Scale Model Domain – Vertical Section Through Site Y = 0

Model layers were discretized and geosphere properties assigned using the approach described in Section 4.1.1.1 and 4.1.1.2, except that model layers within the Cobourg formation were defined as flat over the portion of the X axes domain containing the repository footprint. The Site-Scale model geosphere is shown within the surrounding Glaciation Sub-Regional geosphere in Figure 4-80. Cross-section A-A’ from Figure 4-79 is also shown to assist in orienting the viewpoint.

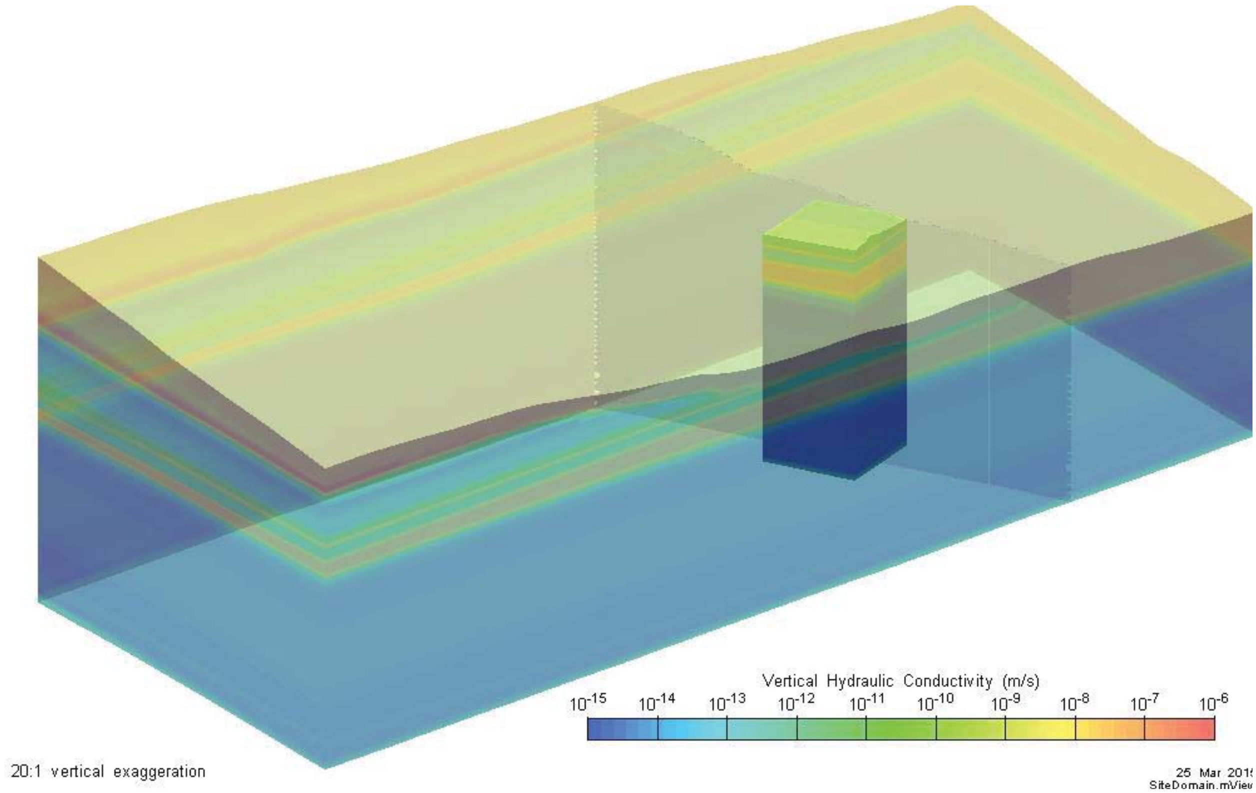

Figure 4-80: Site-Scale and Glaciation Sub-Regional Model Domains and Assigned Geosphere Hydraulic Conductivities

Vertical discretization consisted of 58 model layers, compared to 40 layers used in the Glaciation Sub-Regional model to the top of the Salina A2 Carbonate. Horizontal discretization was markedly increased to support property assignment for most repository features. Each layer was discretized with 301 nodes in the X direction and 223 in Y for a total of 3.89M nodes and 3.79M elements. Although still very large, this is significantly reduced compared to the NWMO (2013) site model, which contained 11.95M nodes for a similar size domain. The vertical domain of the current model is slightly smaller, as the NWMO (2013) model extended to ground surface with 80 layers. Model discretization is shown in Figure 4-81 through Figure 4-83.

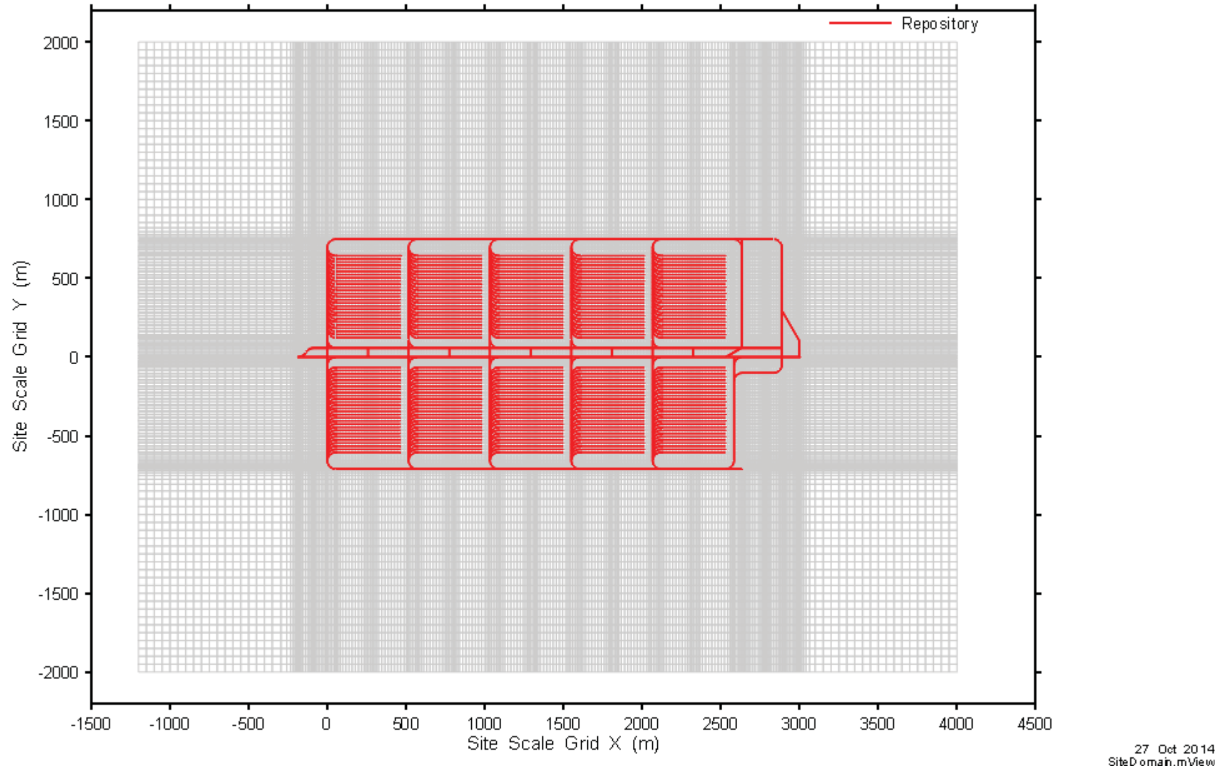

Figure 4-81: Site-Scale Model Plan Discretization

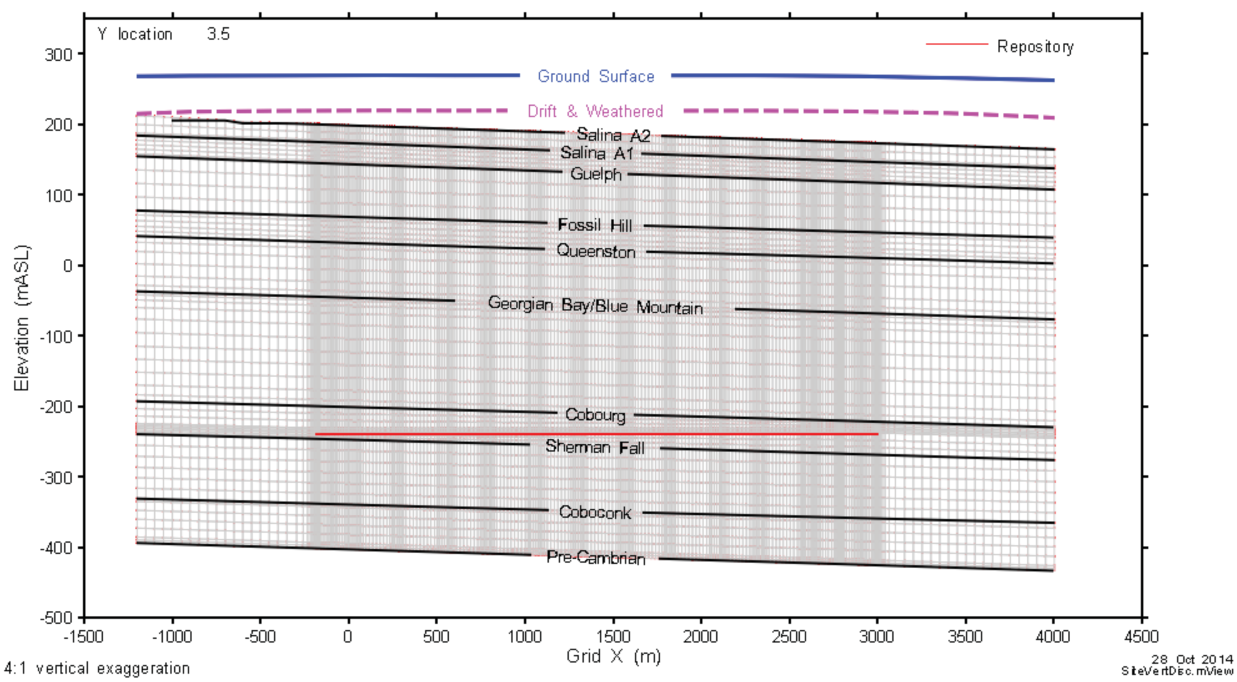

Figure 4-82: Site-Scale Model Discretization in XZ Plane Through Centre of Grid

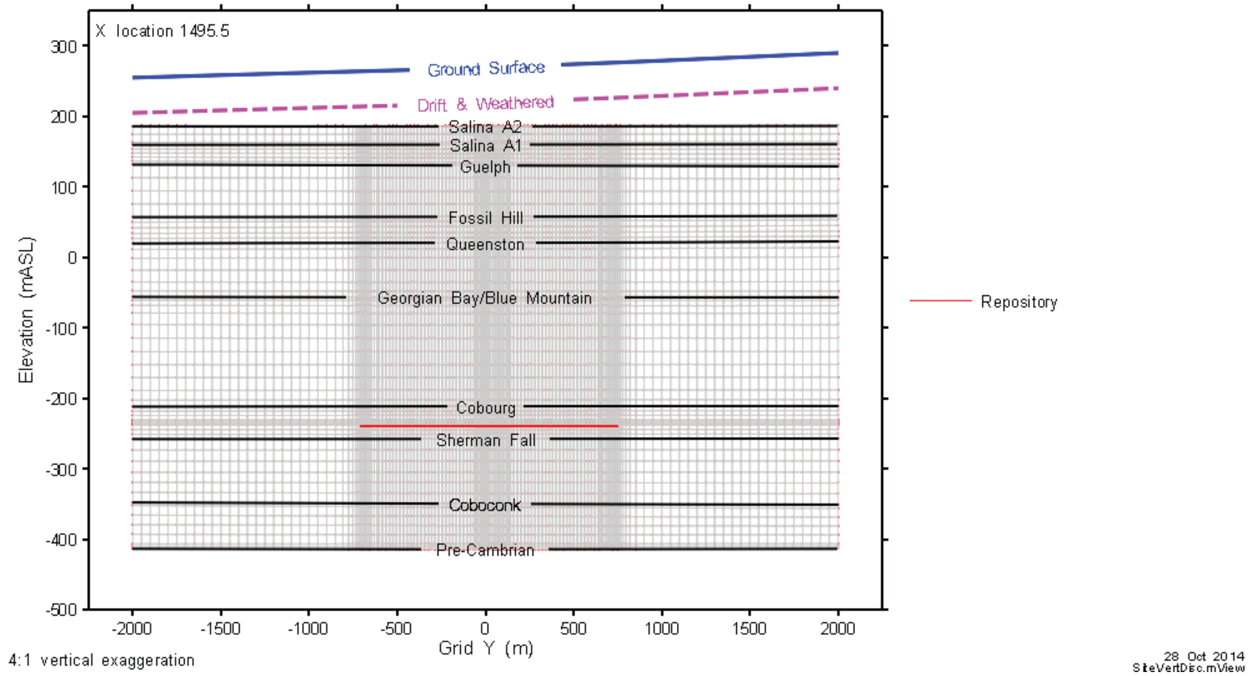

Figure 4-83: Site Model Discretization in YZ Plane Through Centre of Grid

4.2.1.2 Property Assignment

Formation properties were assigned based on element elevations using the same approach as for the Glaciation Sub-Regional model. Subsequently, repository EBS and EDZ parameters were assigned. As discussed above, the grid discretization was simplified by using a constant height of 5m for all placement rooms, tunnels and drifts. To compensate for differences from defined heights (specifically 4m for cross-cut drifts, and 2.5m for emplacement rooms), hydraulic conductivities were adjusted to maintain conductivity × area equivalency with the design. Inner and outer EDZ are combined into 1m layers above and below the repository with similar conductivity adjustments. The EDZ surrounding room and tunnel seals was handled separately to reflect the reduced inner EDZ present. Both inner and outer EDZ are implemented for the shaft and shaft seals. Values for all RC parameters are tabulated in Appendix A.

Property assignments are illustrated in Figure 4-84 through Figure 4-89. Shaft and shaft EDZ discretization was set so that the plan section areas of the rectangular discretized shafts and EDZs are identical to the circular areas of the designed shaft and shaft EDZ. Shaft sealing (Figure 4-85) consists of bentonite/sand mixture through most of the shaft extents, with concrete at the shaft base and through the entire Fossil Hill, Guelph and A1 Evaporite. The Guelph concrete seal is also assumed to replace the inner EDZ to approximate grout injected for water control during operational phases. A 40m long asphalt seal is placed in the middle of the Georgian Bay/Blue Mountain formation over an interval from 80m to 120m above the top of the Cobourg formation.

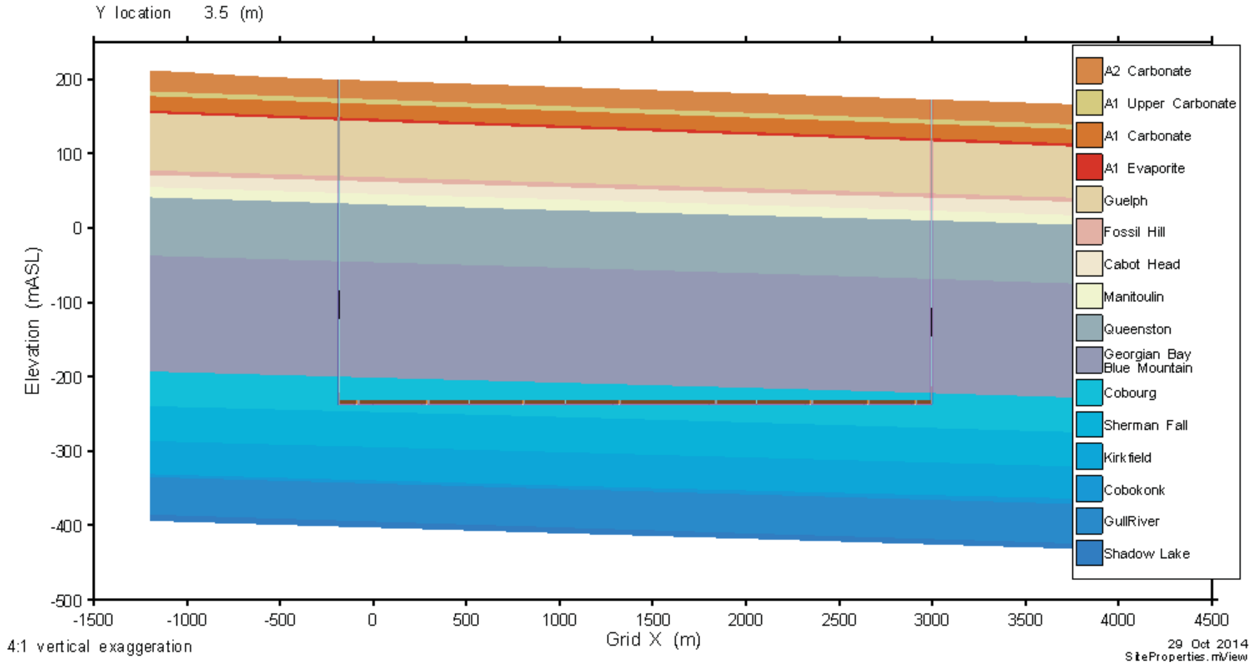

Figure 4-84: Site Model Property Assignment in XZ Plane Through Centre of Grid

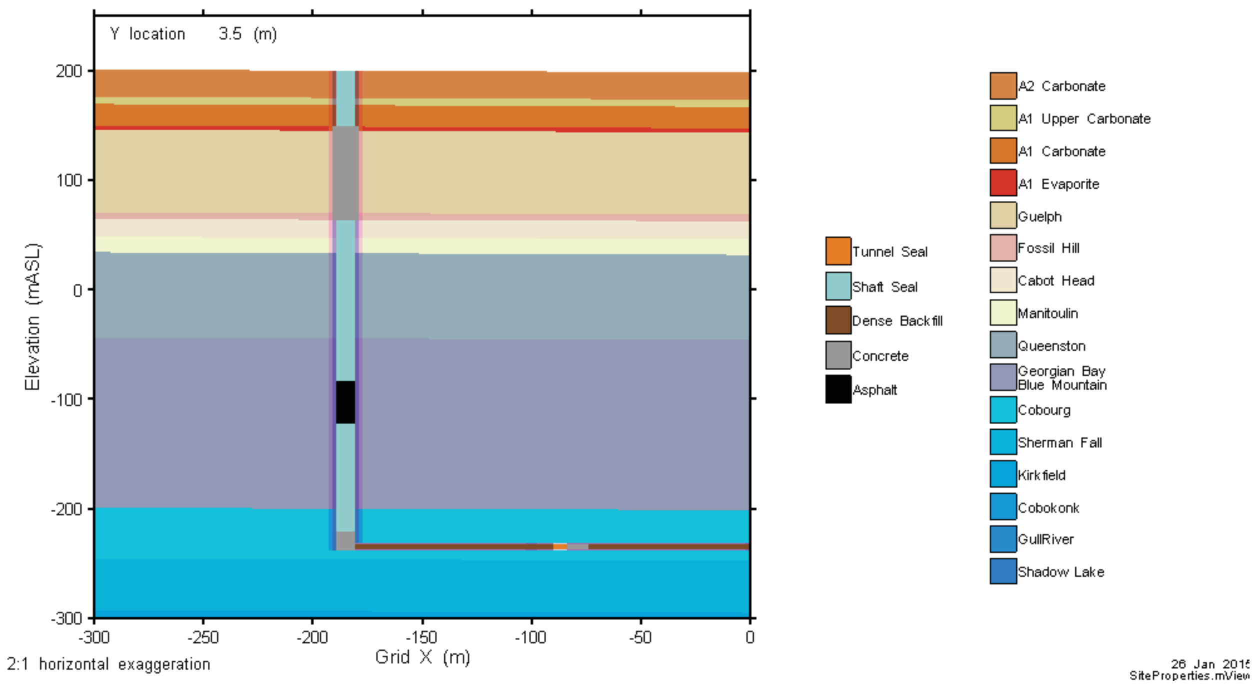

Figure 4-85: Site Model Property Assignment in XZ Plane – Main Shaft Detail

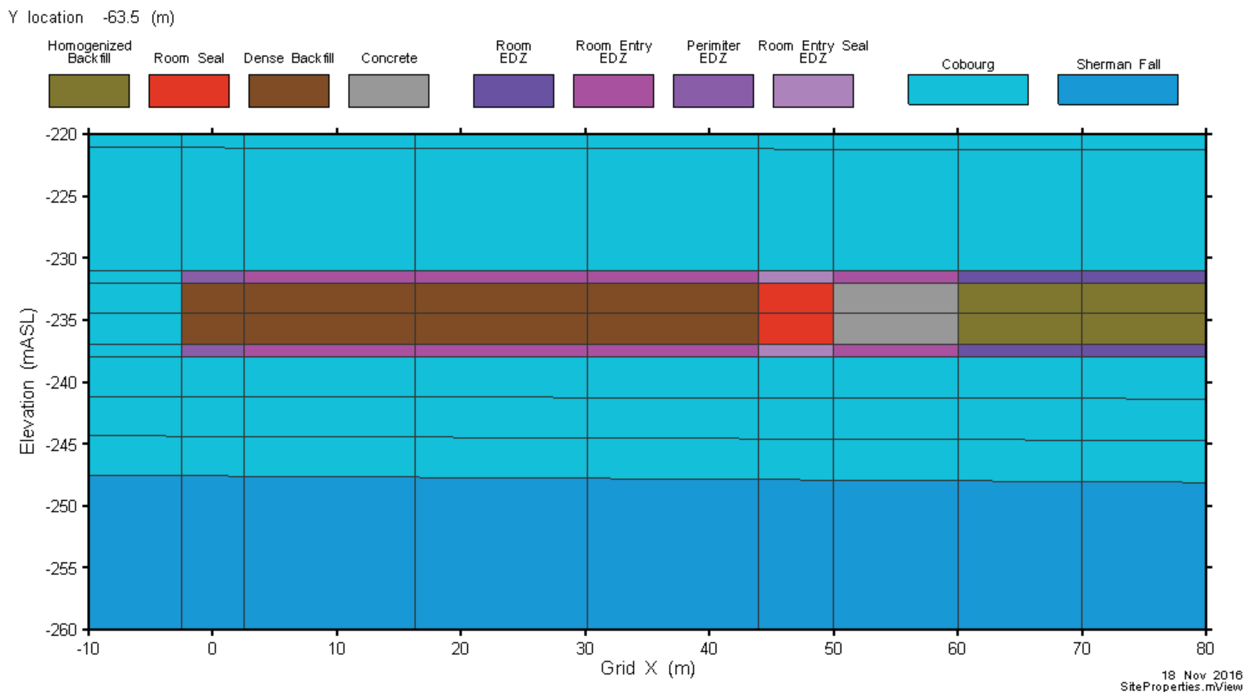

Figure 4-86: Site Model Property Assignment in XZ Plane – Room Detail

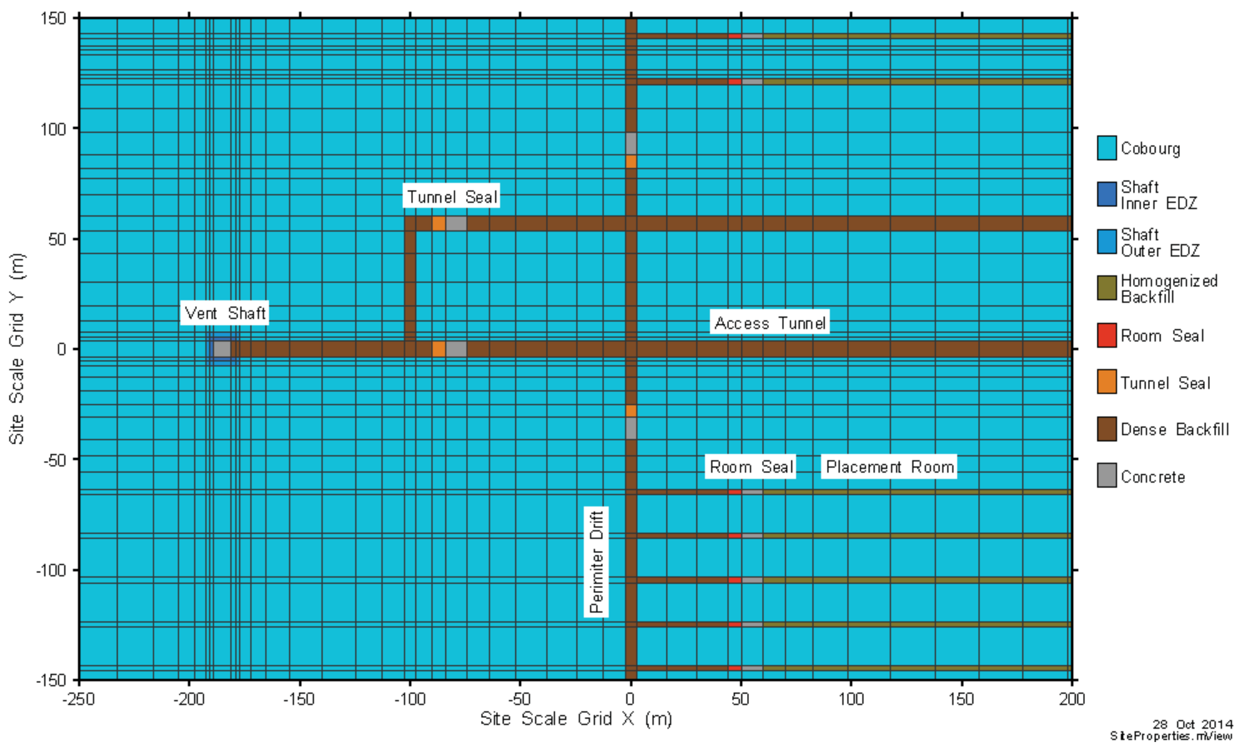

Figure 4-87: Site Model Property Assignment – Plan Detail Near Vent Shaft

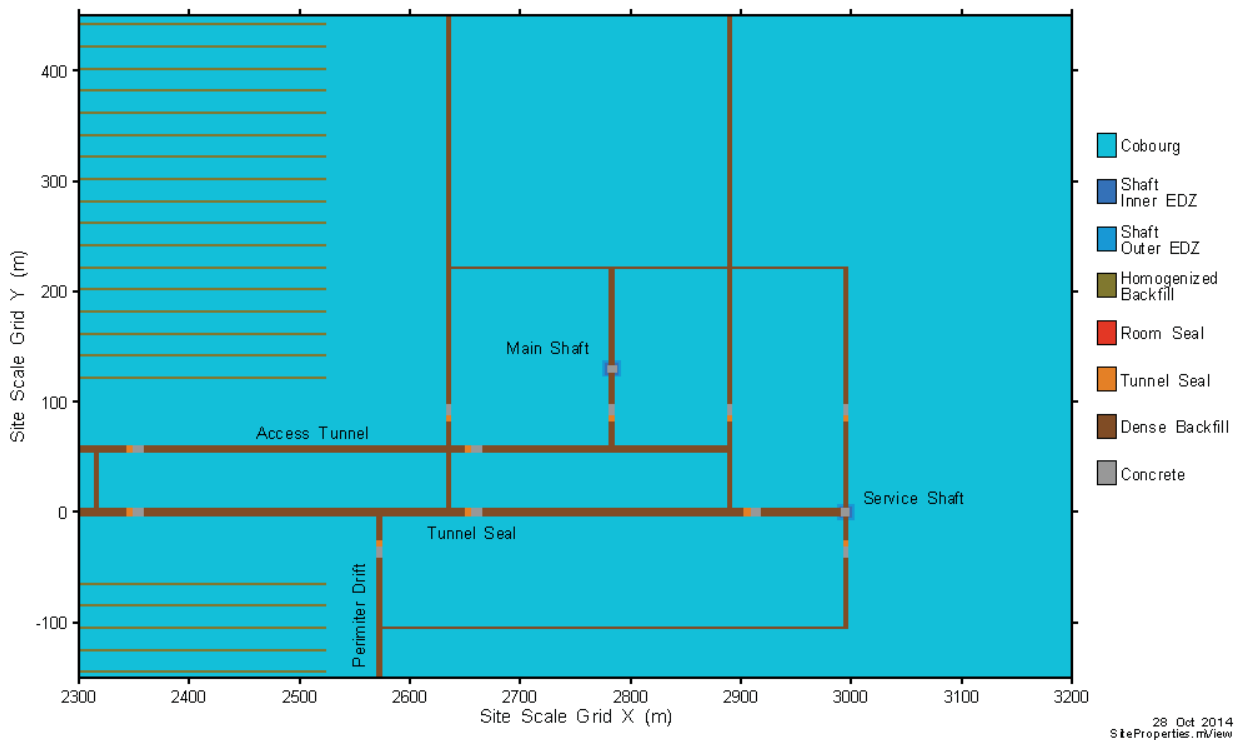

Figure 4-88: Site Model Property Assignment – Plan Detail Near Main Shaft

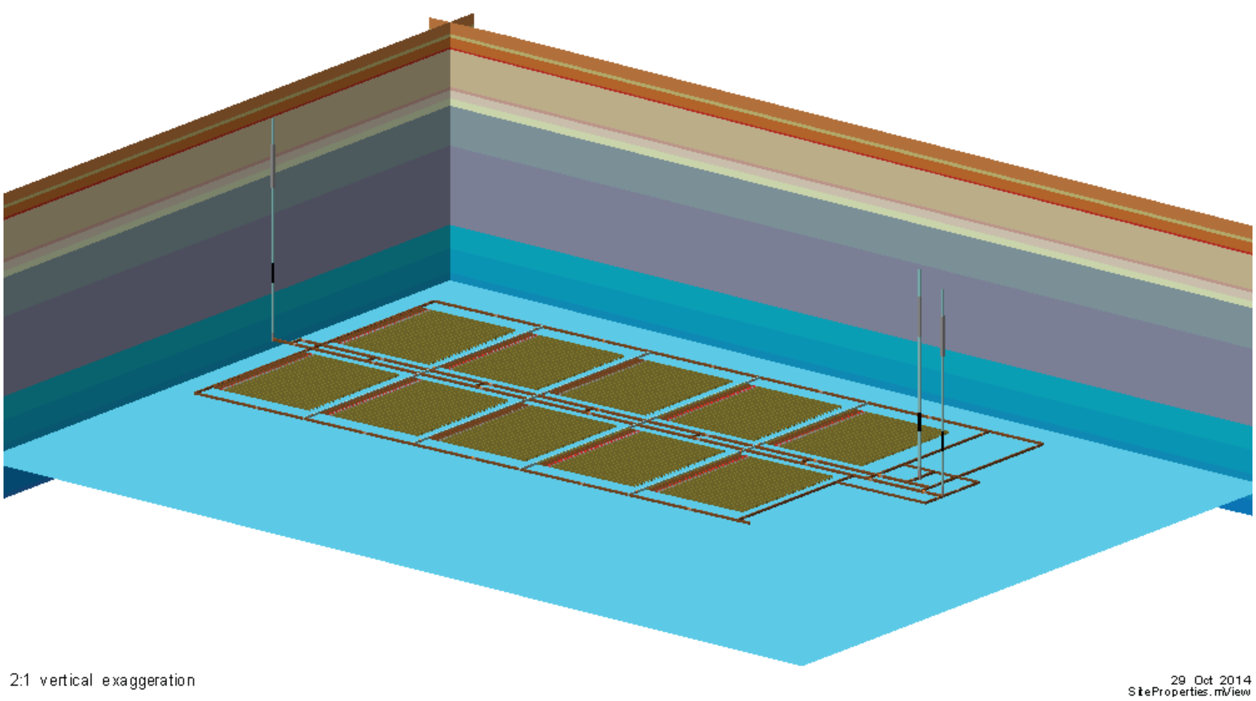

Figure 4-89: Site Model Property Assignment – 3D View of Repository and Surrounding Geosphere

4.2.1.3 Boundary Conditions

Boundary conditions were applied as fixed head on all faces of the model except for the bottom, which was defined as zero flow. Surface loading was applied at the top of the model only. Heads and loading data were extracted from Glaciation Sub-Regional model glacial climate and constant climate simulation results. Figure 4-90 illustrates head boundary conditions at first cycle times associated with maximum well operation, peak Cobourg velocity, maximum ice load and maximum retreat velocities. Capturing the changes in glacial climate boundary conditions requires a time series of hydraulic heads at each node with 109 values for each glacial cycle. Time series for the fifth glacial cycle for selected nodes indicated in Figure 4-90 (middle of top and bottom faces, at Guelph and Cobourg on South face) are shown in Figure 4-91.

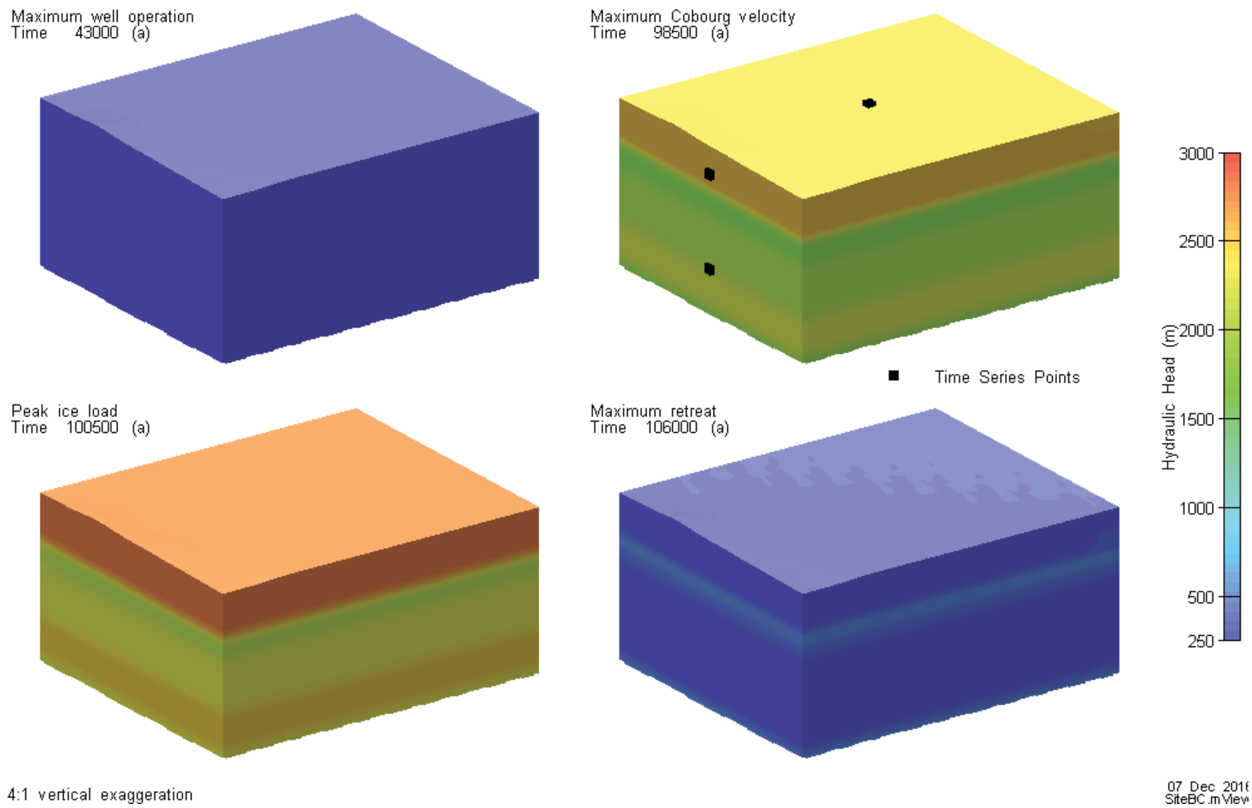

Figure 4-90: Site-Scale Model Boundary Conditions – Specified Heads At Selected Times

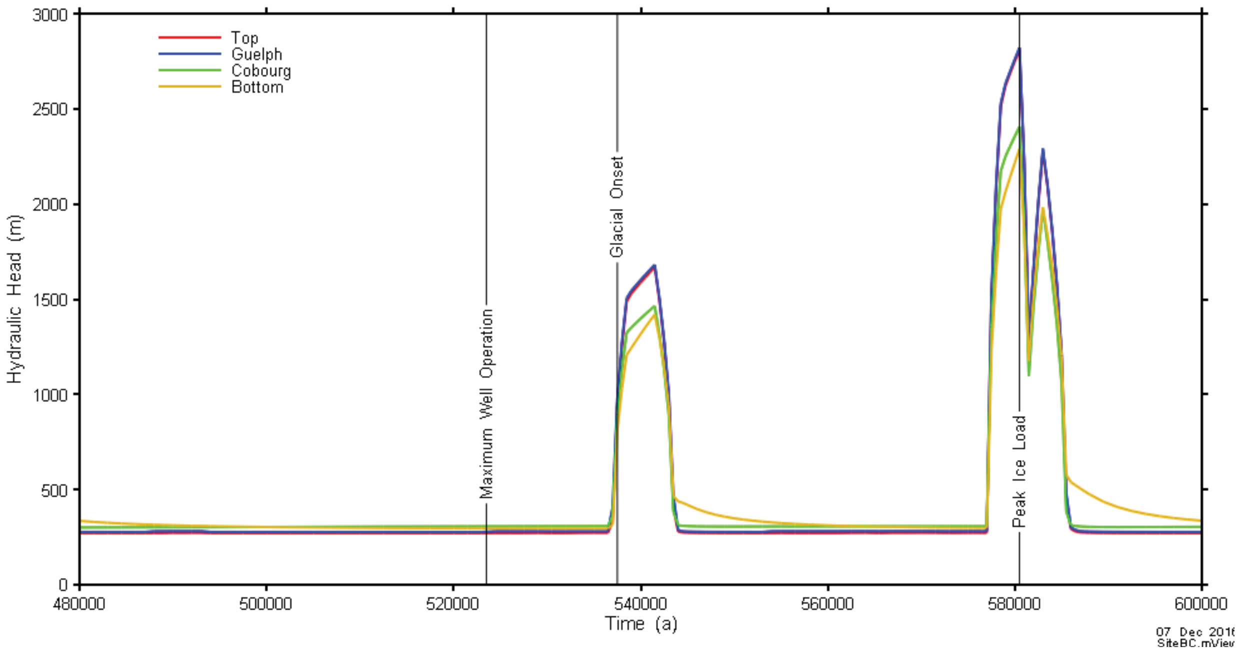

Figure 4-91: Site-Scale Model Boundary Conditions – Time Series at Selected Locations

Although the boundary condition input data is available over all eight cycles simulated with the Glaciation Sub-Regional Flow model, it was necessary for computational performance reasons to subdivide the transport simulation into a series of separate simulations. There were two primary factors: 1) including time series with 872 entries at each 126,631 nodes requires 2.6 GB of RAM for boundary condition and surface loading storage, and 2) the inefficient implementation of head boundary conditions and surface loading within FRAC3DVS-OPG causes exponential increases in execution time with increasing number of values in the boundary condition/HM loading time series. Glacial climate transport simulations were therefore divided into eight sequences, corresponding to each glacial cycle. Each cycle had boundary condition heads and surface loading data extracted from the corresponding period of the Glaciation Sub-Regional Flow glacial climate model. Final heads and radionuclide concentrations for one sequence form the initial heads and concentrations for the succeeding sequence. This provided a reasonable trade-off between increased operational and pre-/post-processing complexity and reduced memory and execution time requirements.

4.2.1.4 Permafrost

The selection of the A2 Carbonate as the upper boundary for the site-scale grid eliminates nearly all possible permafrost elements. As shown in Figure 4-82, only a small portion of the Salina A2 Carbonate sub-crops within the model domain and is shallower than the maximum permafrost depth. Figure 4-92 shows the extent of permafrost penetration in the site model grid at the time of maximum permafrost depth. Permafrost was implemented using the same approach as for the Glaciation Sub-Regional model. As mentioned in Section 4.1.1.4, other material properties were not modified. This is a limitation of the FRAC3DVS-OPG code that could have implications for transport as diffusion coefficients are significantly decreased in permafrost. Note that the effects of continuous permafrost are included, as surface boundary heads are extracted from the Glaciation Sub-Regional model.

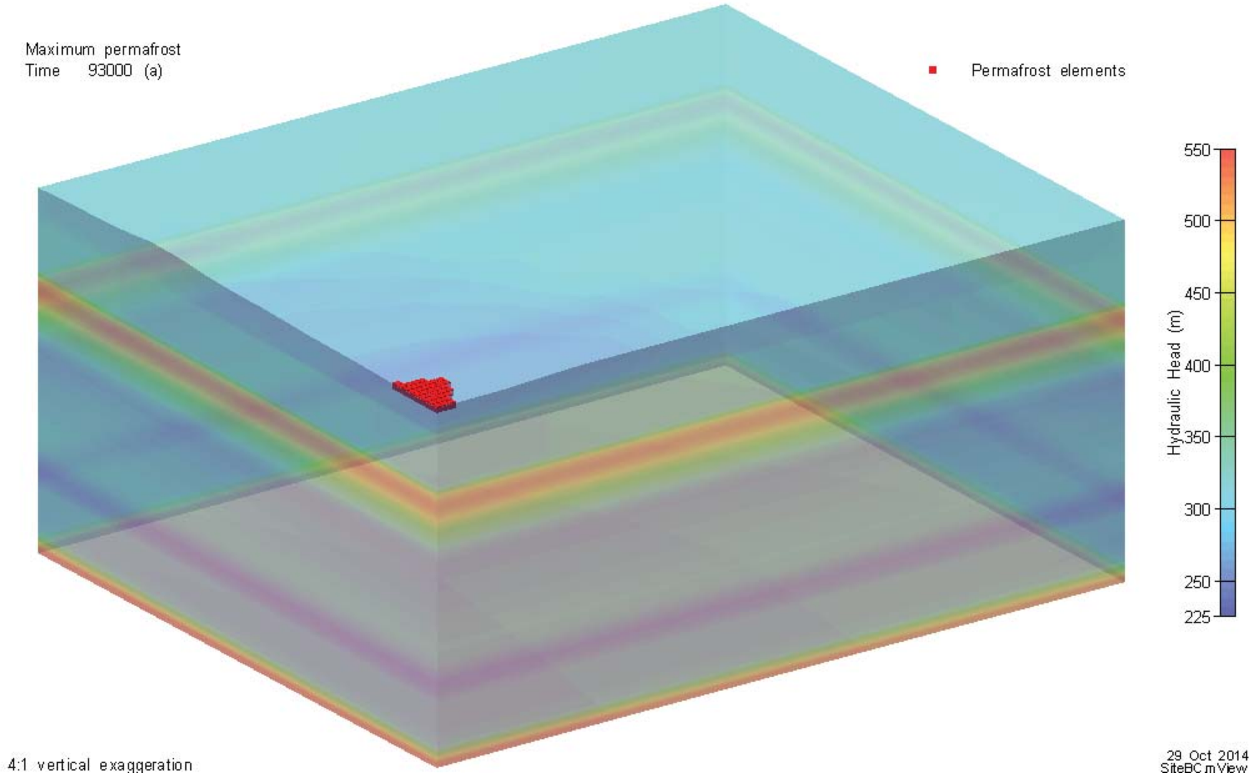

Figure 4-92: Site Model Permafrost – Specified Permafrost Elements at Time of Maximum Permafrost Depth

4.2.1.5 Well and Source Node Location

As described in Section 4.1.1.5, simulations are performed using three well locations. Previously shown in Figure 4-12, the locations are shown again relative to the site model discretization and associated source term node locations in Figure 4-93. Wells nodes are placed across the entire Guelph formation while source nodes are placed at the top corner nodes of elements in the release location. Note that the centre source does not correspond to a placement room, but is a synthetic case used as an example to show impact of enhanced diffusion in EBS components.

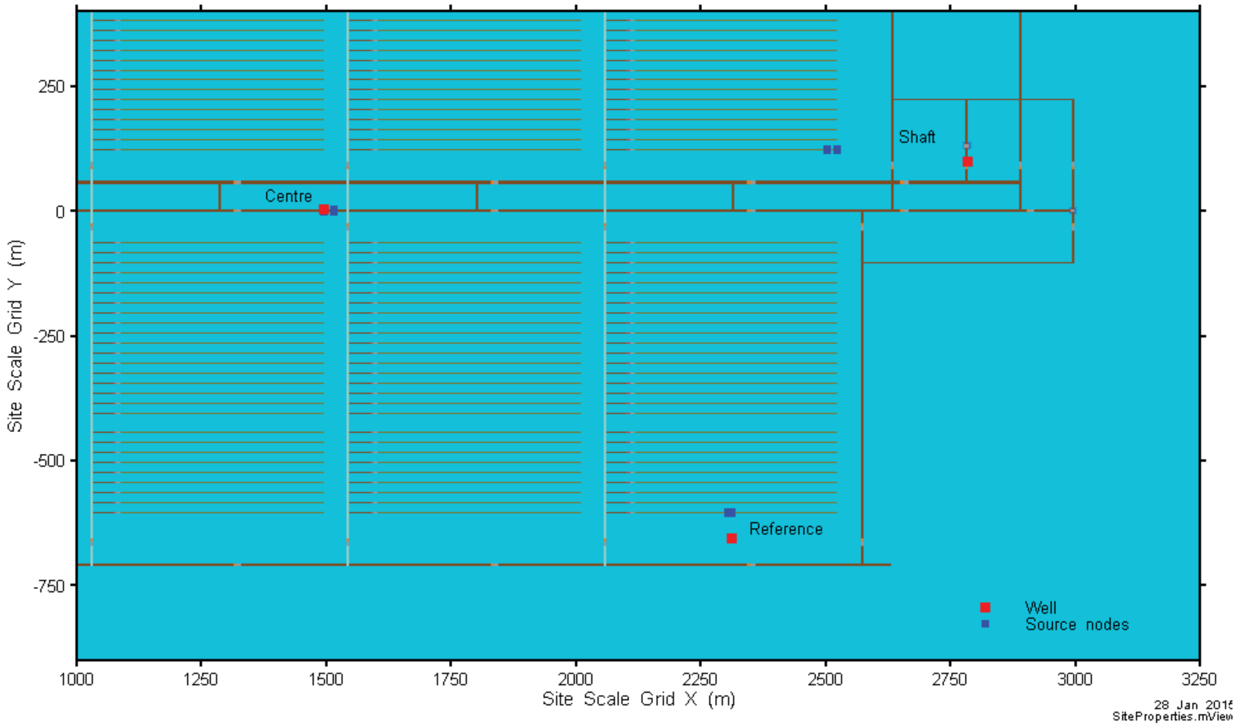

Figure 4-93: Site Model – Well and Source Term Nodes

4.2.1.6 Source Term

The Iodine-129 source term is identical to that used in NWMO (2013) and describes a pinhole release from a single defective container, starting at 10,000 a. The single container release is scaled by a factor of three to simulate three co-located failed containers (Figure 4-94).

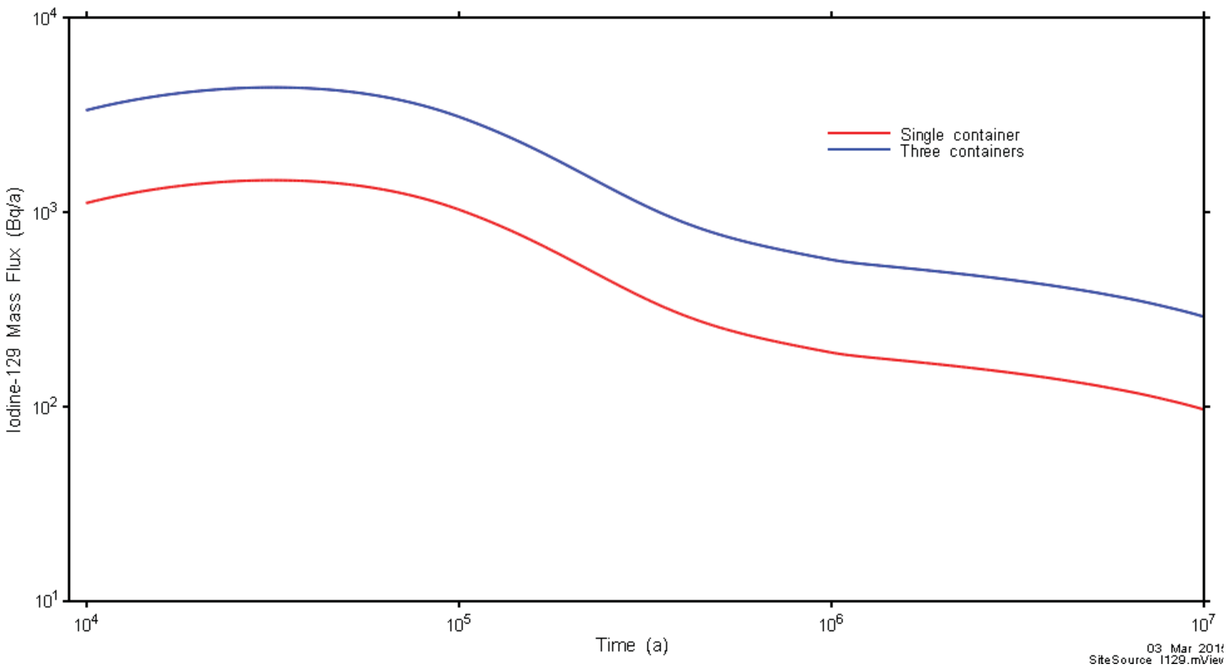

Figure 4-94: Site Model – Iodine-129 Source Term

4.2.2 Modelling Cases

Reference case simulations were undertaken for each of the three well/source term combinations. As discussed in Section 4.1.6, the sensitivity cases performed with the Glaciation Sub-Regional Flow model indicated virtually no impact on transport related processes. Consequently, only one of the prior geosphere sensitivity case (KHigh) was carried forward to transport simulations. Additional transport parameter sensitivity cases were added to assess the impact of dispersivity (High Dispersivity - RC Dispersivity x 10) and diffusion (High Diffusion – RC Diffusion x 2). A shaft fail (SF) case was defined based on the RC geosphere with increased inner and outer shaft EDZ multipliers (1000 and 100 respectively): all shaft sealing materials were replaced with a single material with hydraulic conductivity of 10^{-9} m/s, and the shaft well/source location was used.

All cases were simulated for both constant climate and glacial climate boundary conditions.

4.2.3 Steady State Flow (Constant Climate) Transport Simulations

4.2.3.1 Flow System Verification

Correct implementation of boundary conditions and formation property assignment was verified by comparing simulated hydraulic heads and advective velocities from the Site-Scale model to the corresponding Glaciation Sub-Regional model. Figure 4-95 shows a good match between simulated heads with some minor discrepancy near the well, due to slight differences in pumping well location (see Figure 4-12). The ratio of advective velocities (Figure 4-96) is generally close to one, except in the vicinity of the repository where the higher conductivity of the EBS and EDZ results in higher velocities

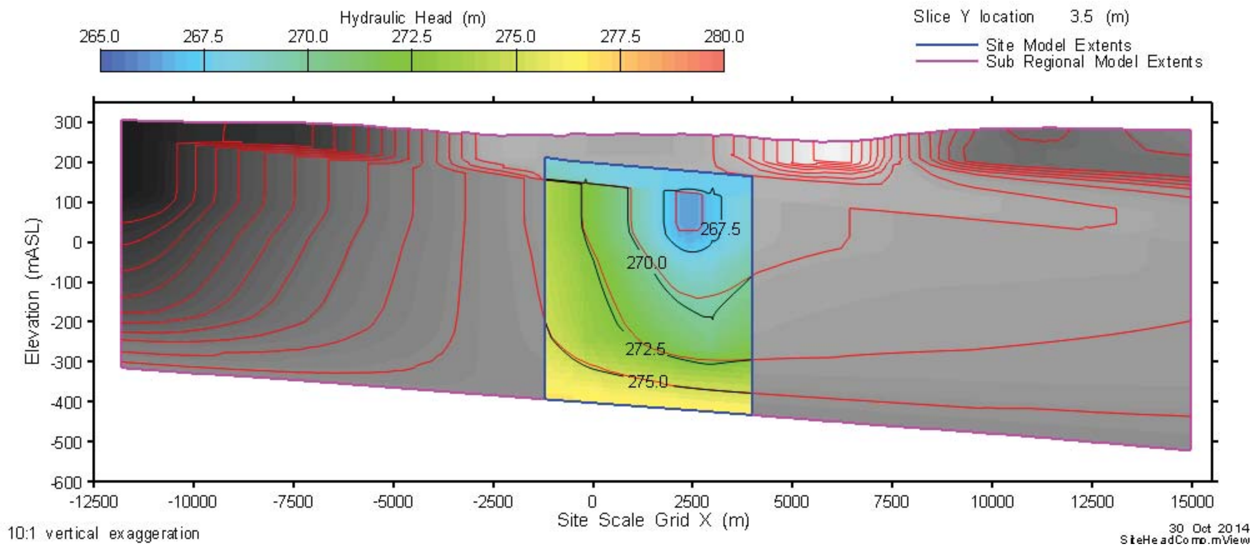

Figure 4-95: Site-Scale Model: Reference Well – Comparison of Heads to Glaciation Sub-Regional Model

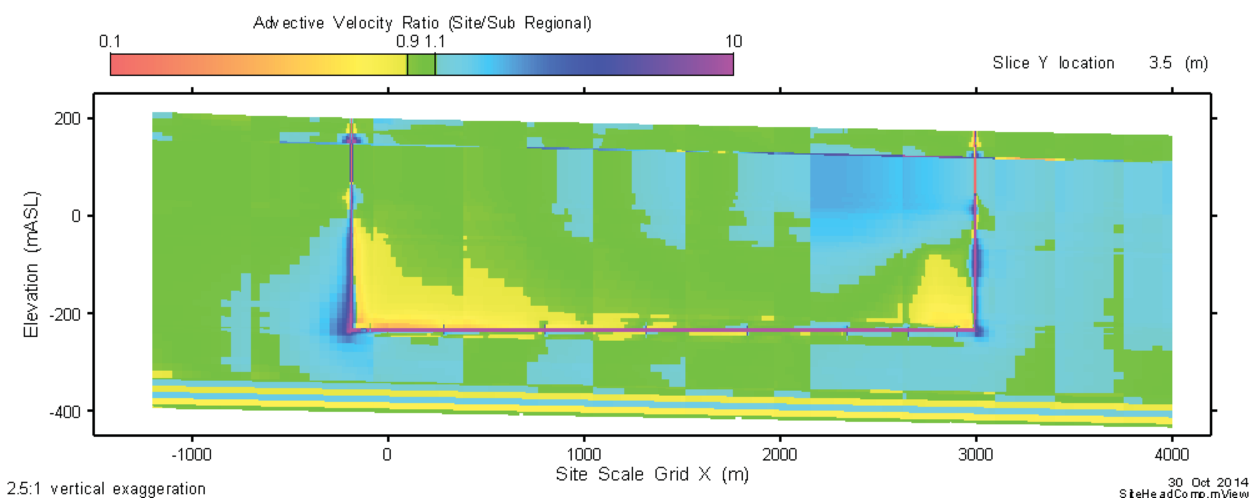

Figure 4-96: Site-Scale Model: Reference Well – Comparison of Advective Velocity to Glaciation Sub-Regional Model

4.2.3.2 Transport Results

Transport model results for all well/source cases at 500 ka and 1 Ma are shown in Figure 4-97 through Figure 4-106. The contour plots are on a logarithmic scale. The outer concentration contour, 1 Bq/m^3, corresponds to an effective I-129 drinking water dose of about 0.1 μSv/a based on a water consumption rate of 0.84 m^3/a per person.

Results are consistent for each case with transport being dominated by diffusion through the repository EBS. Mass flux results (Figure 4-105) show significantly higher mass flux at 1 Ma for the shaft well, although still extremely low in absolute terms. Mass flux into the wells is nearly coincident with the corresponding Guelph formation flux, indicating almost complete capture of the plume by the wells (Figure 4-106).

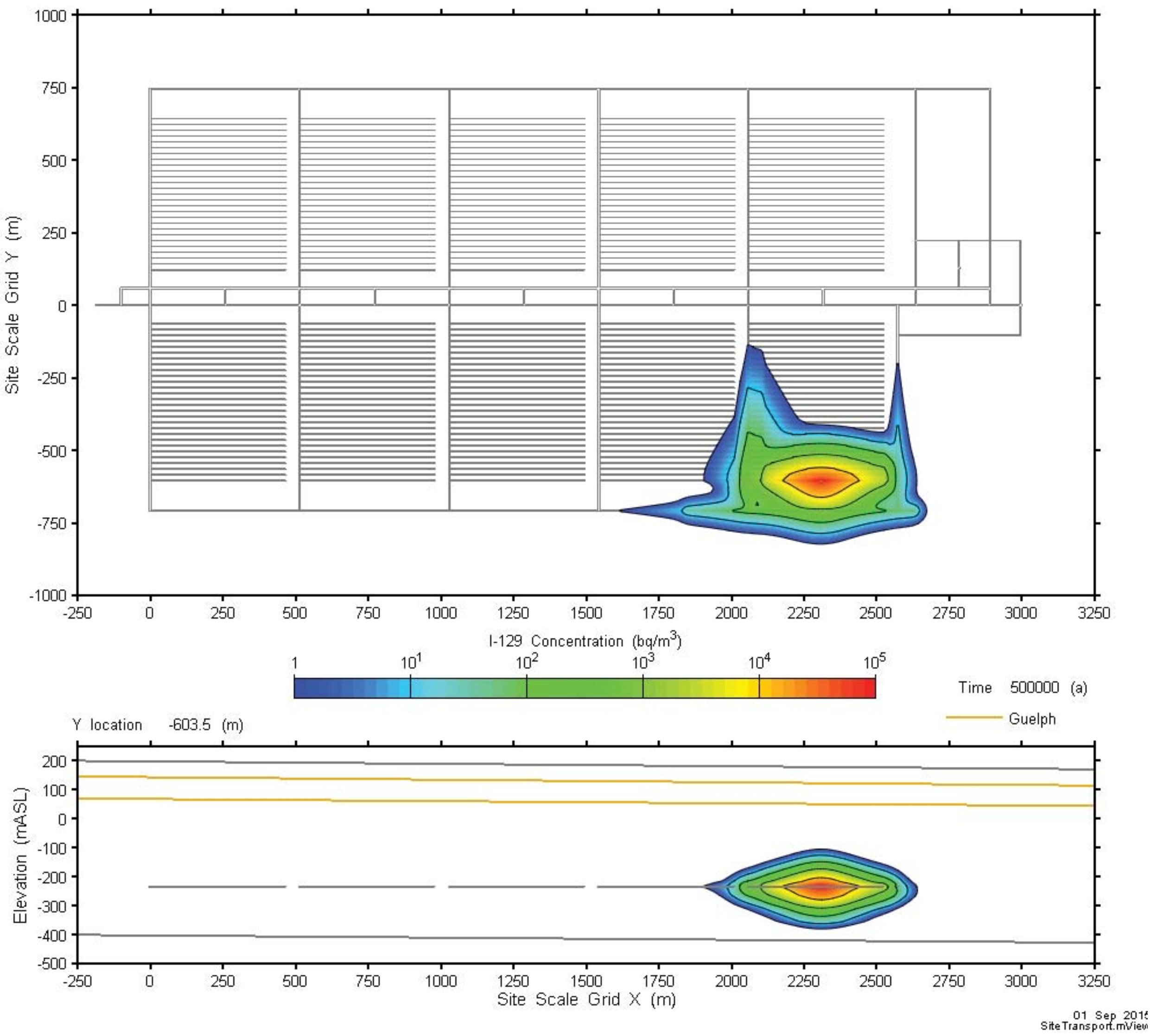

Figure 4-97: Site-Scale Model: Reference Well – I-129 Transport at 500 ka

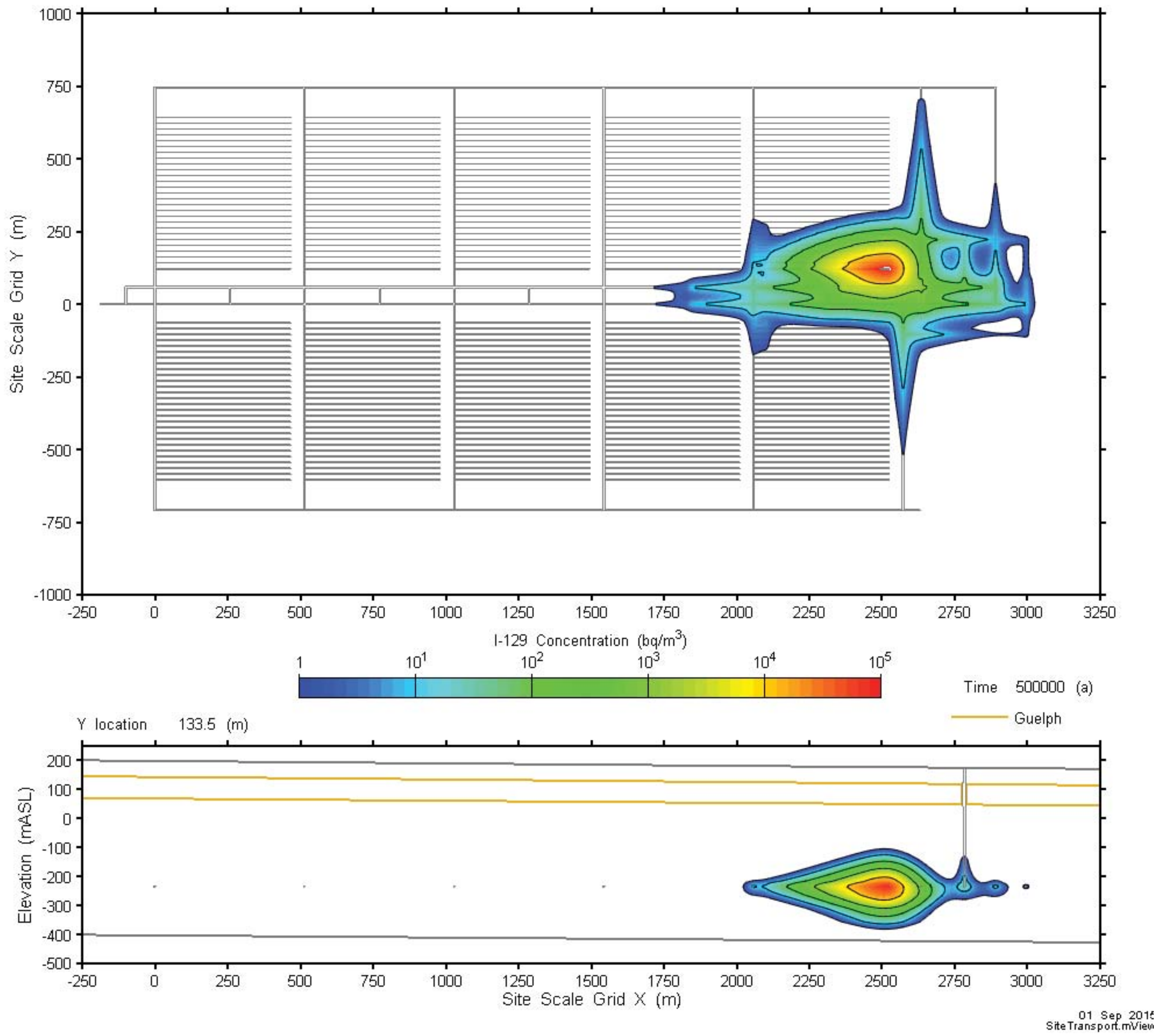

Figure 4-98: Site-Scale Model: Shaft Well – I-129 Transport at 500 ka

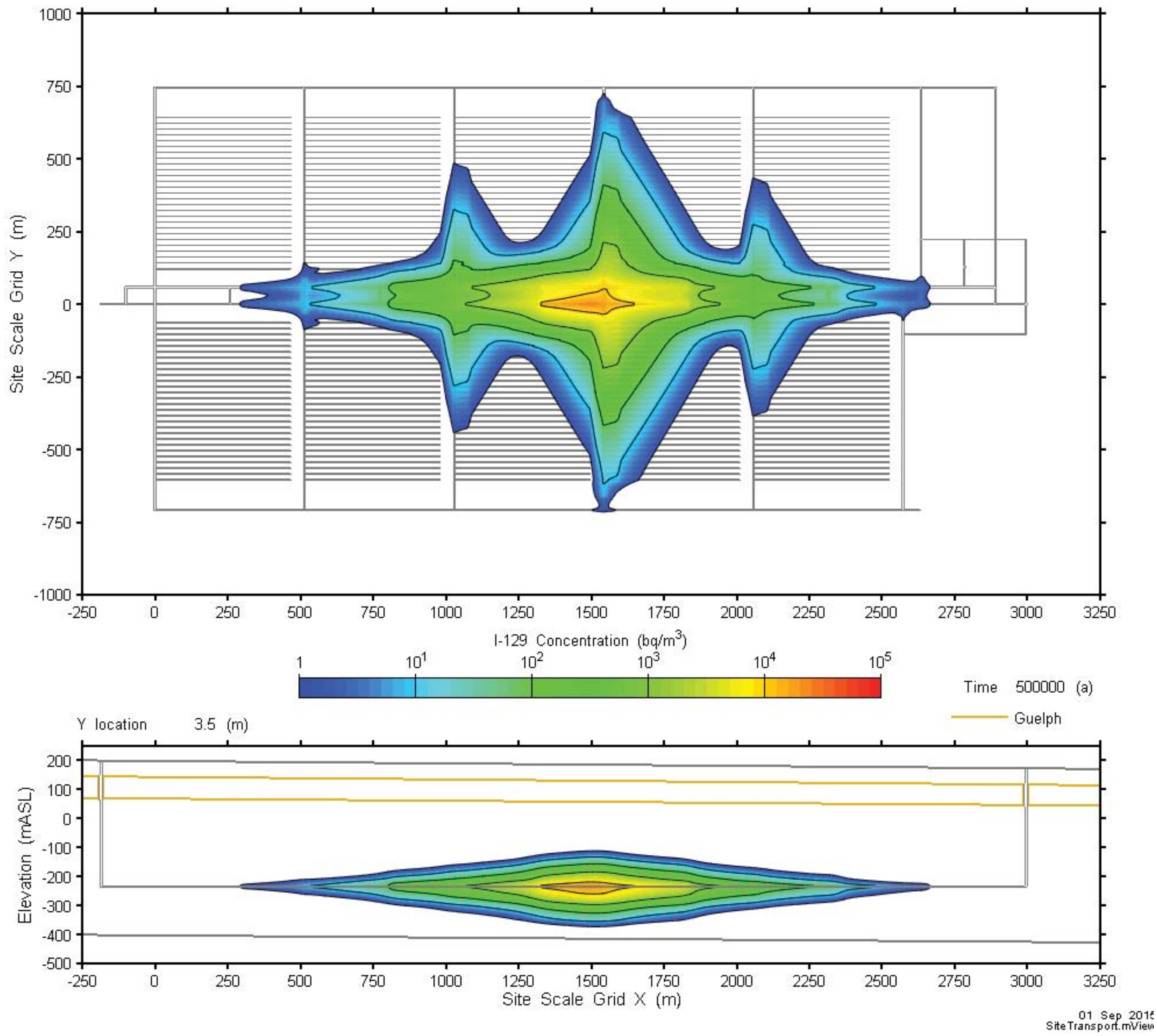

Figure 4-99: Site-Scale Model: Centre Well – I-129 Transport at 500 ka

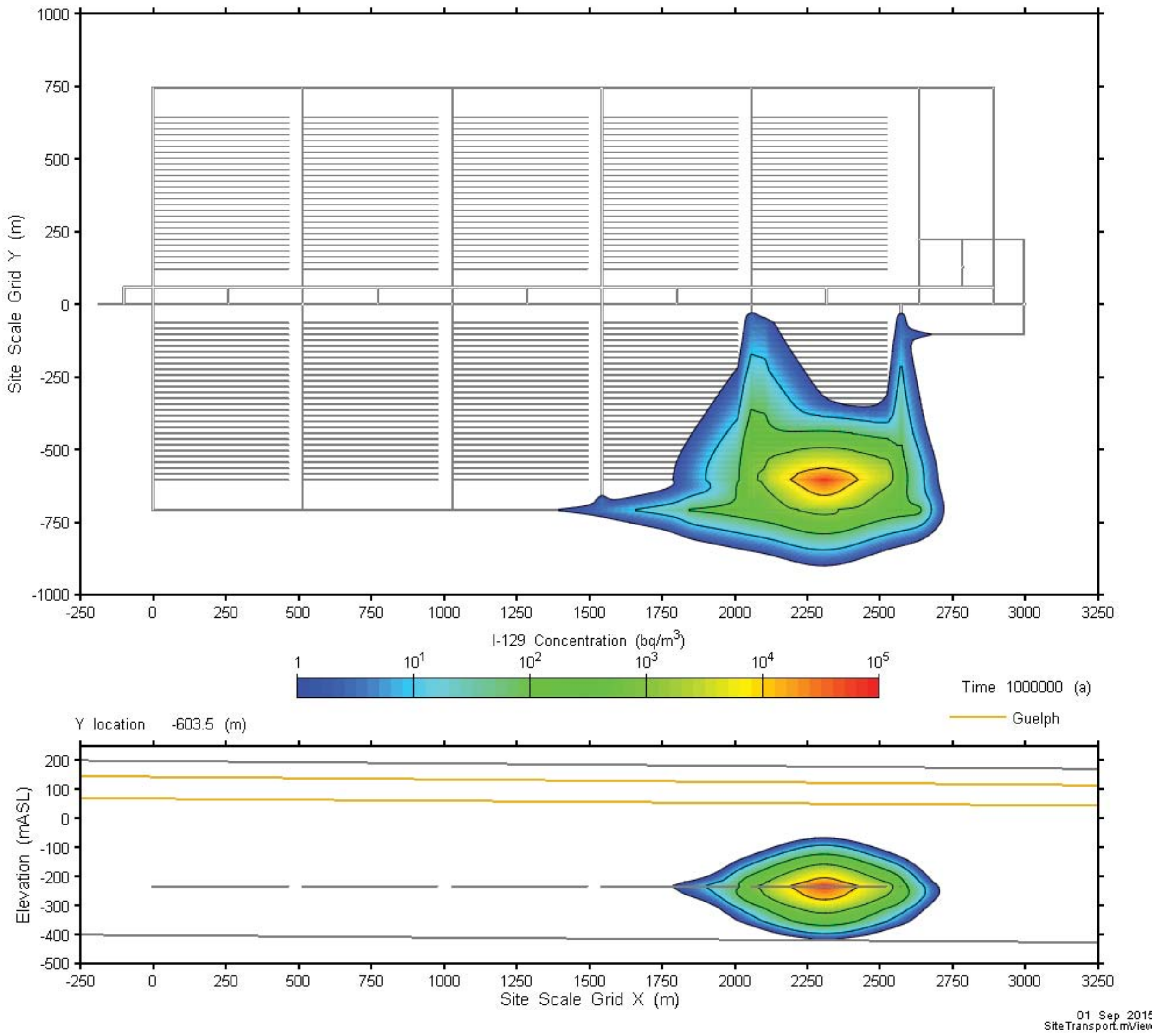

Figure 4-100: Site-Scale Model: Reference Well – I-129 Transport at 1 Ma

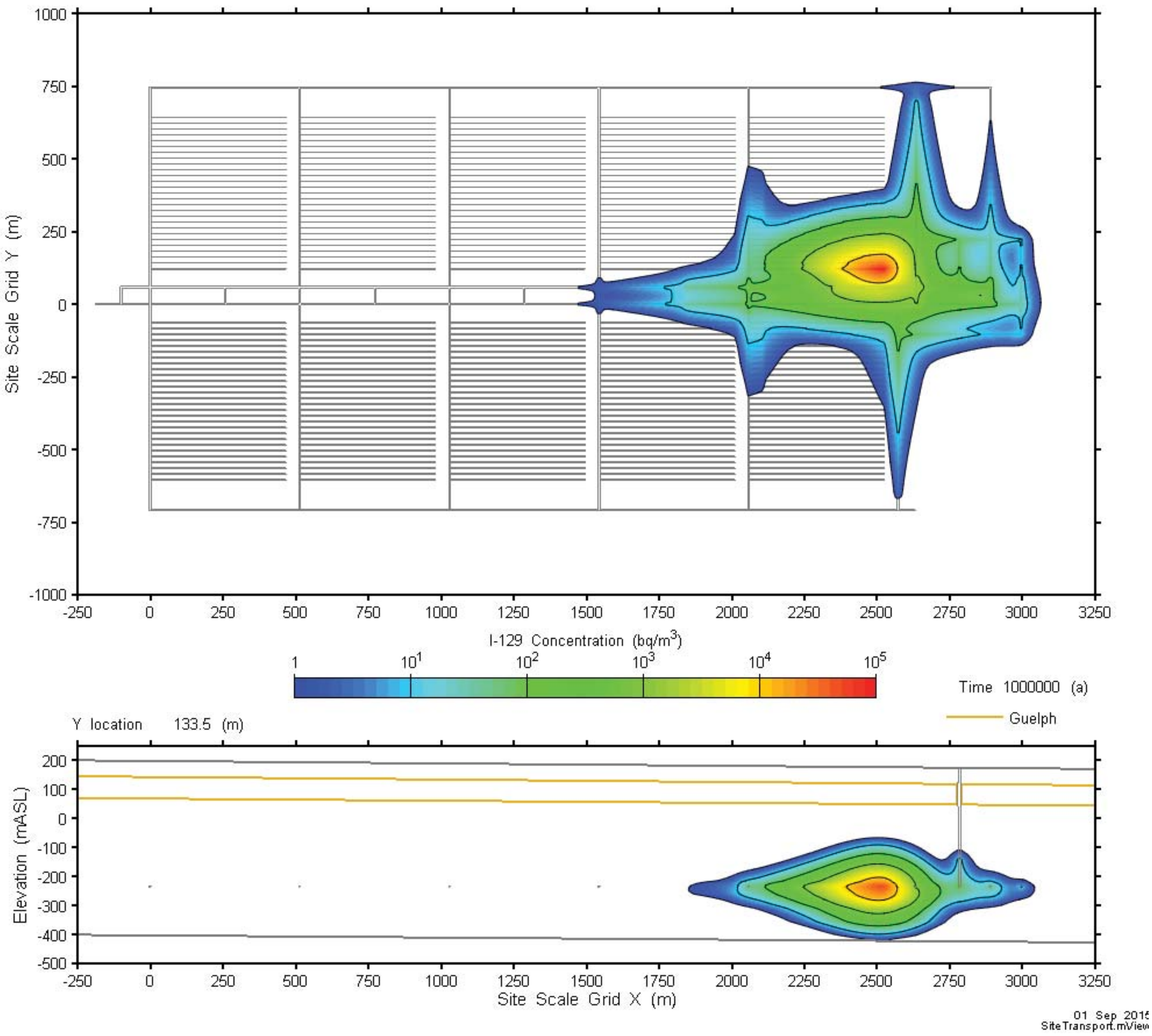

Figure 4-101: Site-Scale Model: Shaft Well – I-129 Transport at 1 Ma

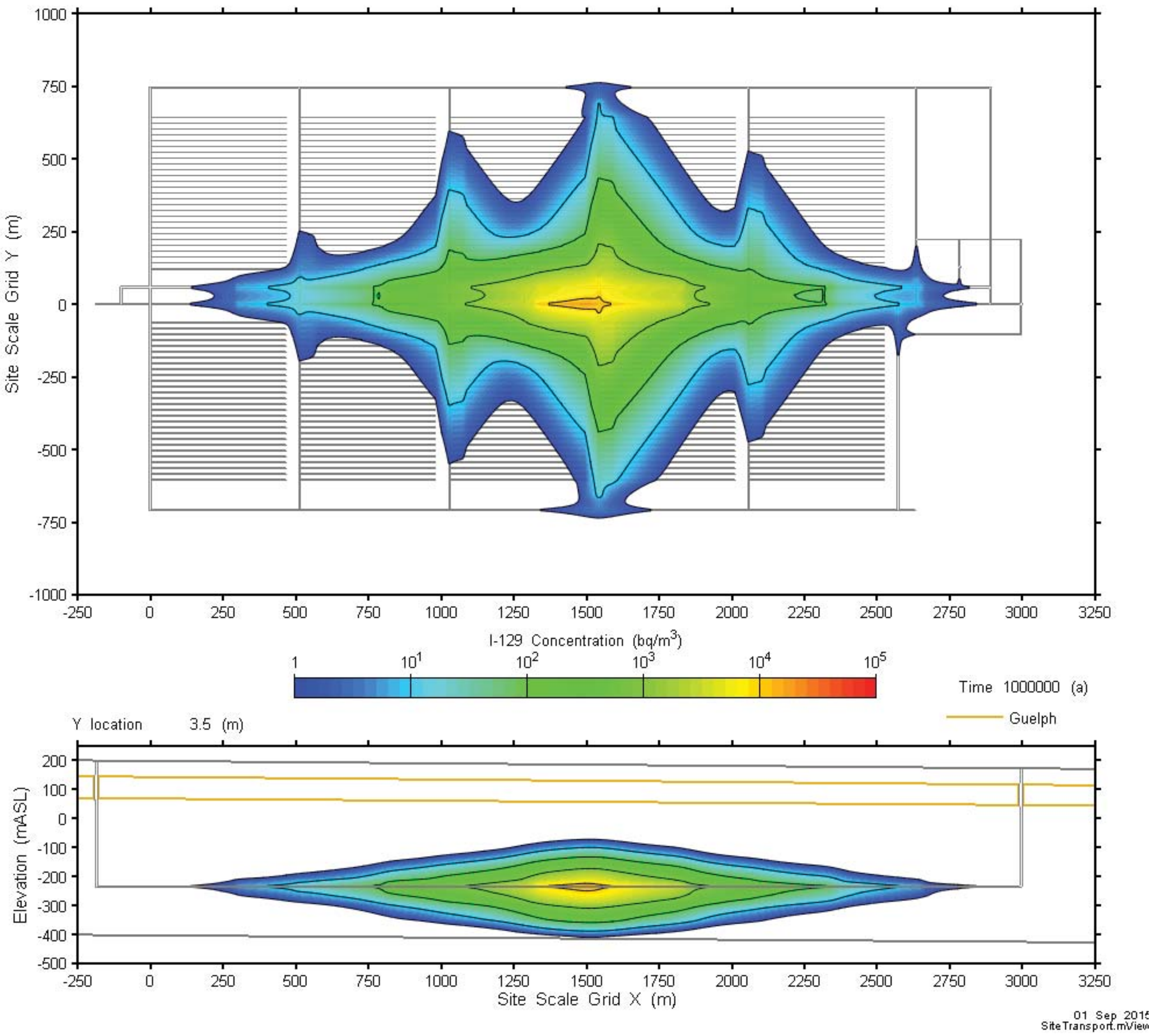

Figure 4-102: Site-Scale Model: Centre Well – I-129 Transport at 1 Ma

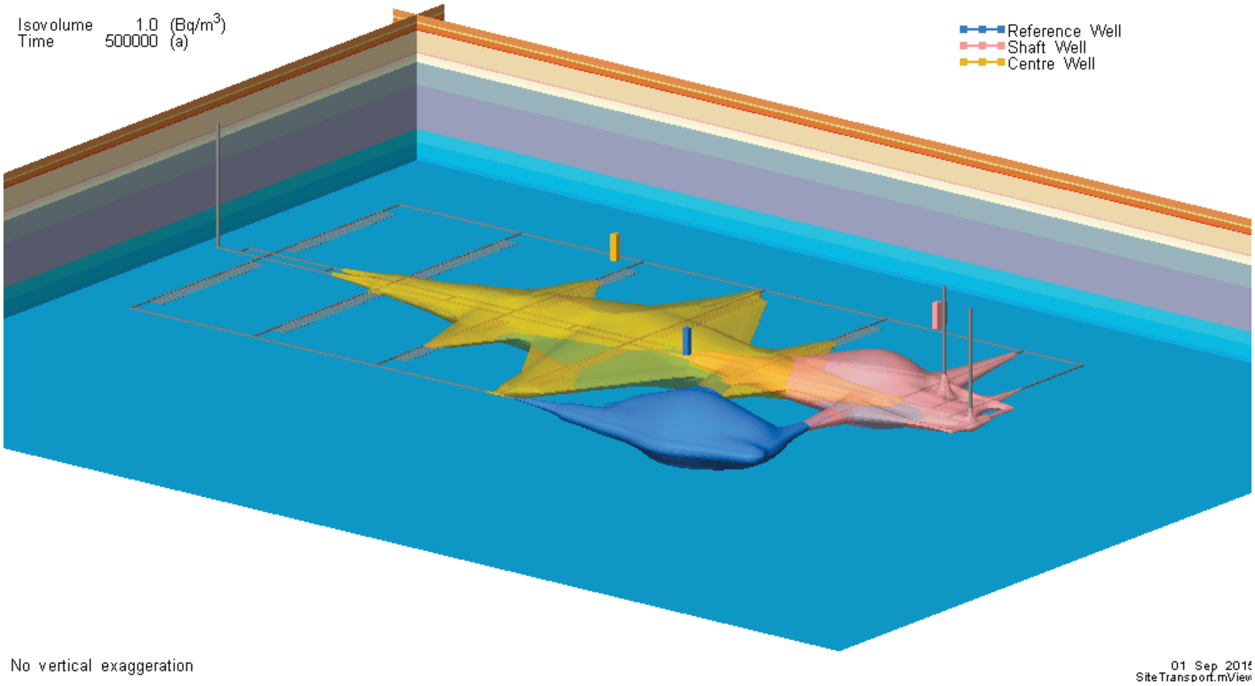

Figure 4-103: Site-Scale Model: All Results – 1 Bq/m^3 Isovolumes of I-129 at 500 ka

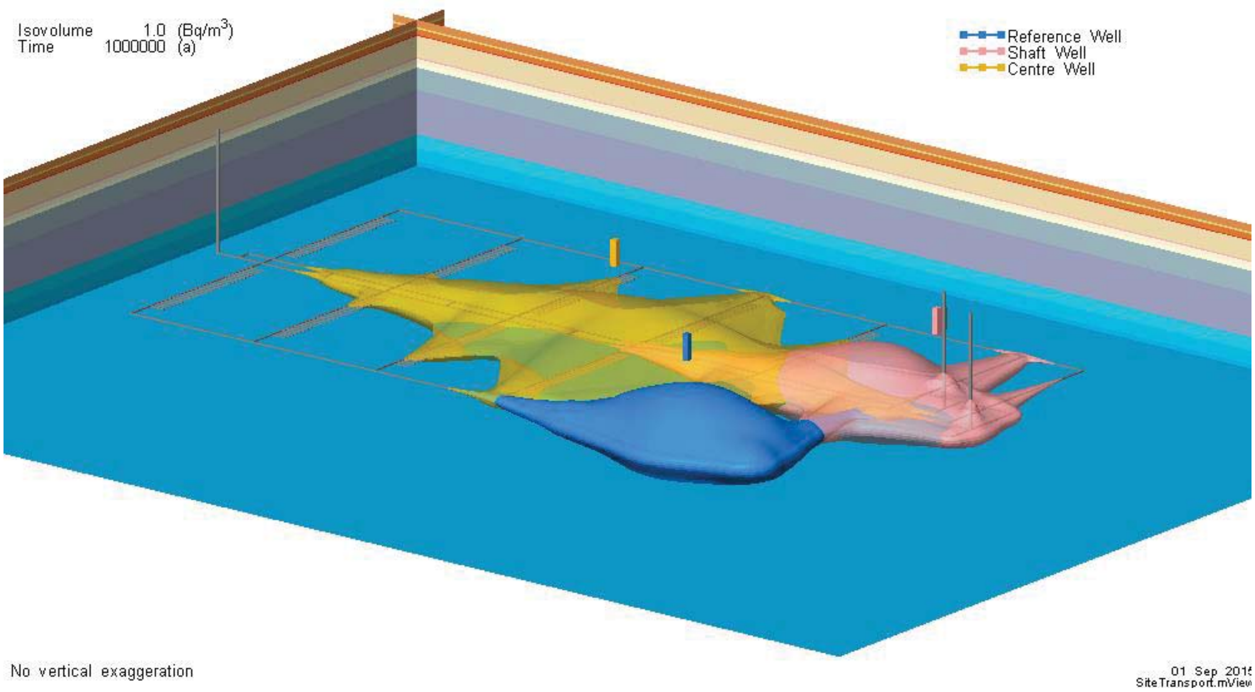

Figure 4-104: Site-Scale Model: All Results – 1 Bq/m^3 Isovolumes of I-129 at 1 Ma

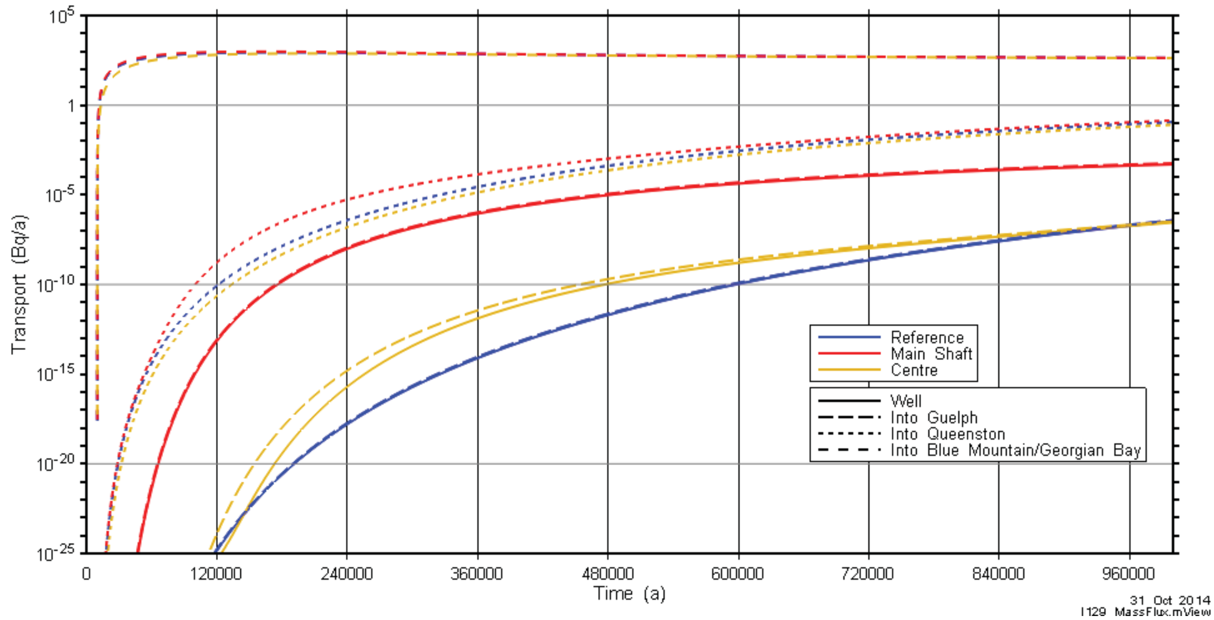

Figure 4-105: Site-Scale Model: All Results – I-129 Transport at well and Into Selected Formations

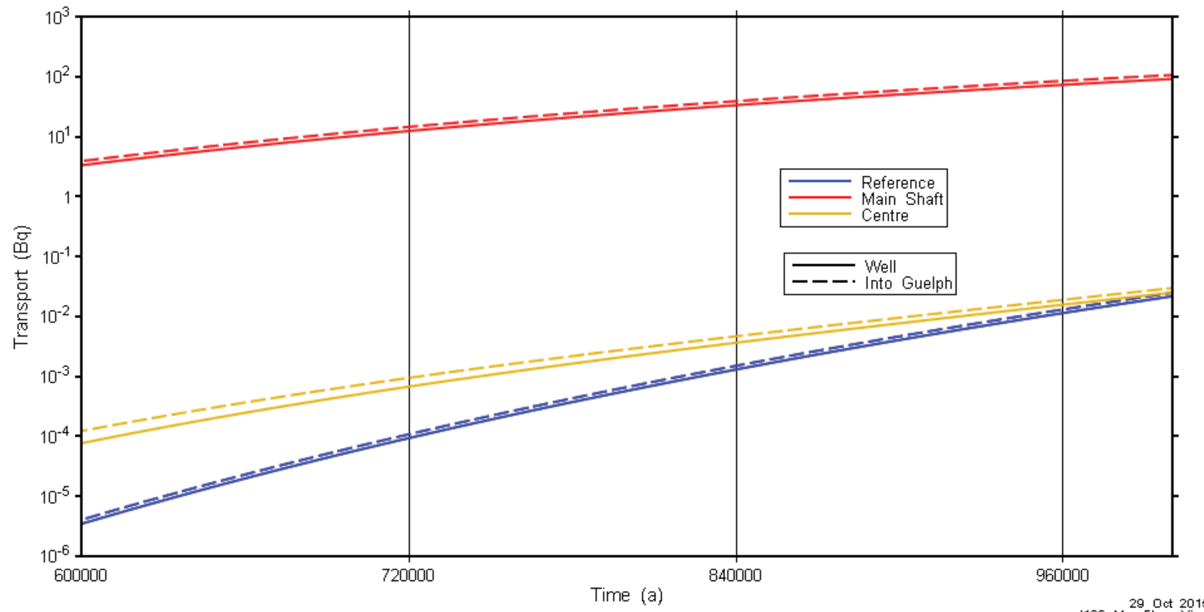

Figure 4-106: Site-Scale Model: All Results – I-129 Integrated Transport at Well and Into Guelph Formations

4.2.3.3 Comparison to 5CS

Transport model spatial results for the reference well case at 1 Ma are compared to the corresponding 5CS results in Figure 4-107. Mass flux at the well for reference and shaft case wells are compared in Figure 4-108. Results correspond very well with the current model showing slightly less well transport than the 5CS model. In general, the results are sufficient to verify that the current model represents the overall flow and transport system with good fidelity to previous results.

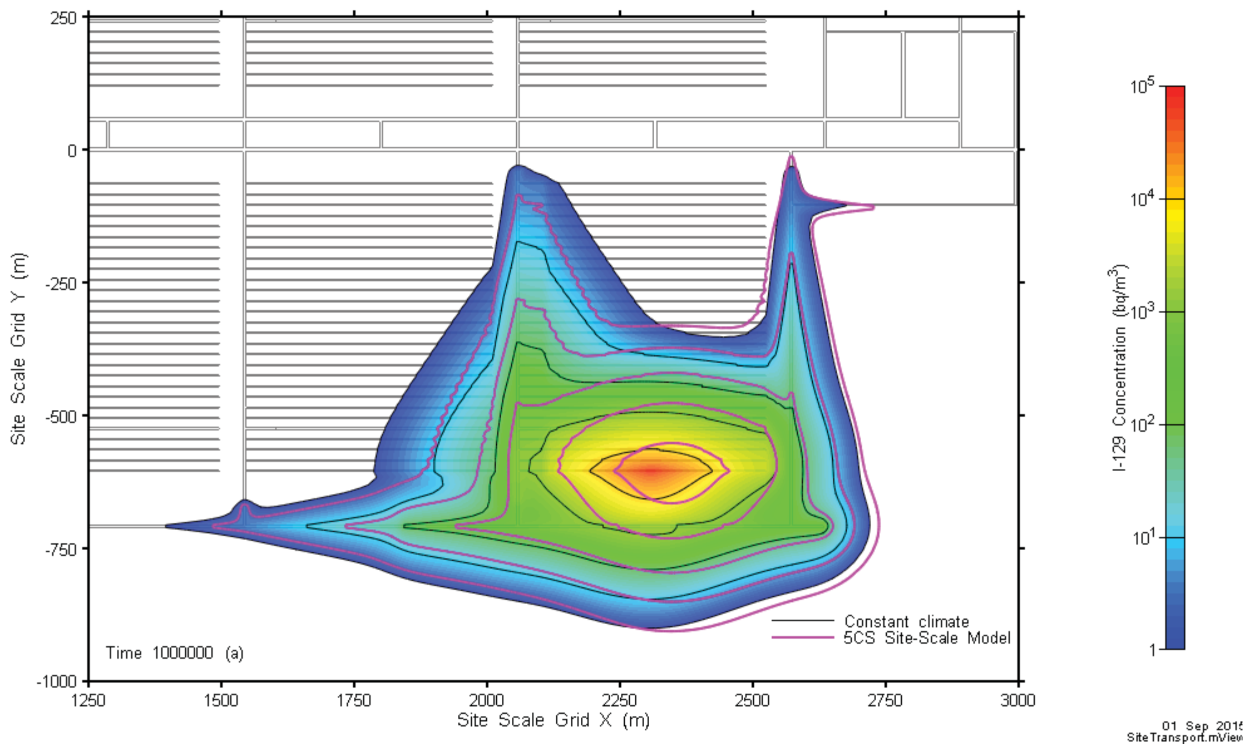

Figure 4-107: Site-Scale Model: Reference Well Plan Section Results at 1 Ma Compared to NWMO (2013)

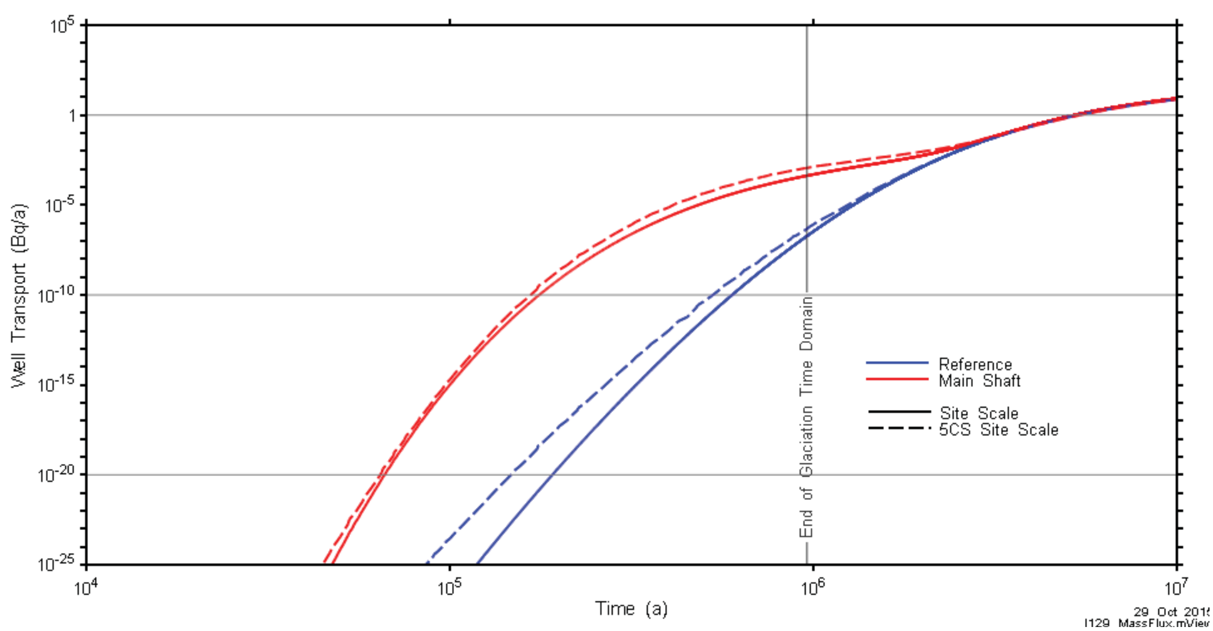

Figure 4-108: Site-Scale Model: I-129 Transport at Well Compared to NWMO (2013)

4.2.4 Glacial Climate Transport Simulations

4.2.4.1 Flow System Verification

Correct implementation of transient glacial boundary conditions is verified by comparing simulated heads and advective velocities. For the site-scale model, heads and velocities were extracted at a grid location some distance from the repository, where Site-Scale and Glaciation Sub-Regional grids were coincident (Figure 4-109). Simulated heads and velocity magnitude in the fifth glacial cycle are shown in Figure 4-110 and Figure 4-111. A spatial comparison of heads along a vertical slice at the time of maximum well operation in the fifth glacial cycle is presented in Figure 4-112. Site-Scale velocities in the Guelph are lower at the selected location during well operations as a result of the differences in model plan discretization. Peak glacial velocities at initial ice advance are higher for the Glaciation Sub-Regional model as the regular time discretization of the head boundary condition extraction used for the site scale model does not capture exactly the start time of the advance and retreat. Otherwise, results compare very well, providing confidence that the glacial climate Sub-Regional flow system is adequately represented within the Site-Scale transport model.

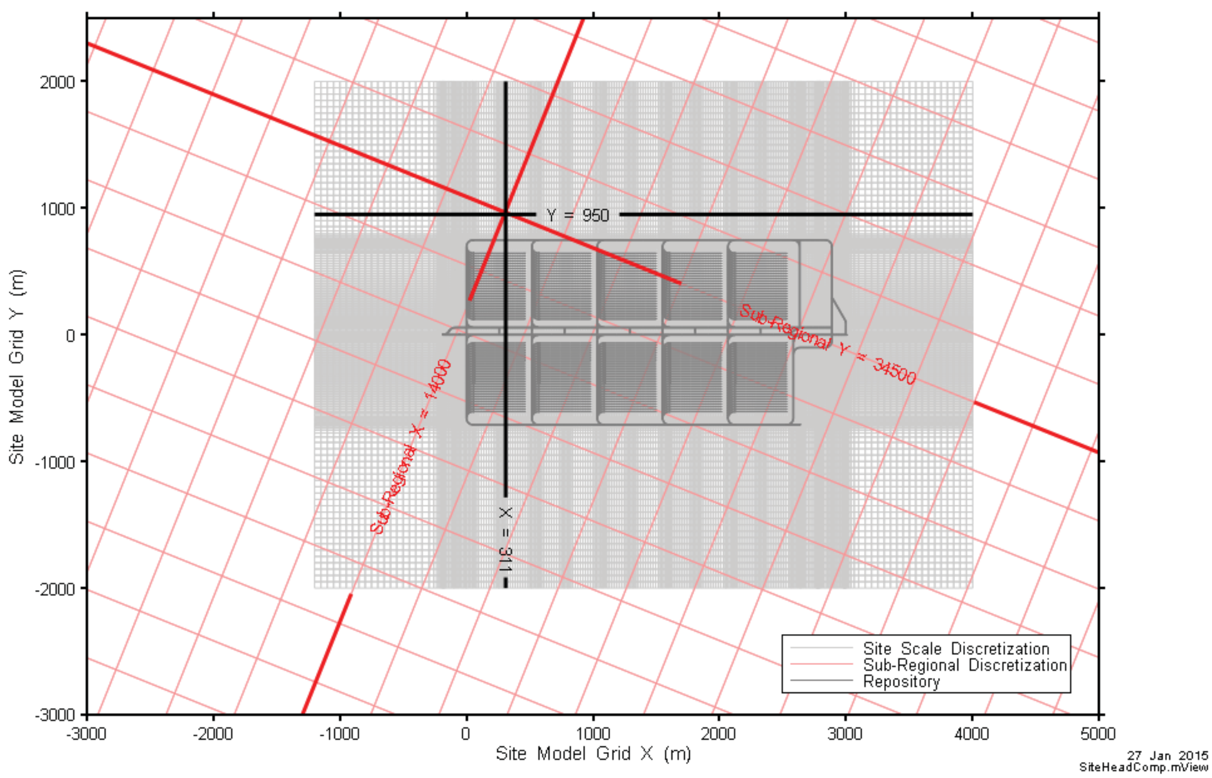

Figure 4-109: Site-Scale to Glaciation Sub-Regional Model Comparison Location

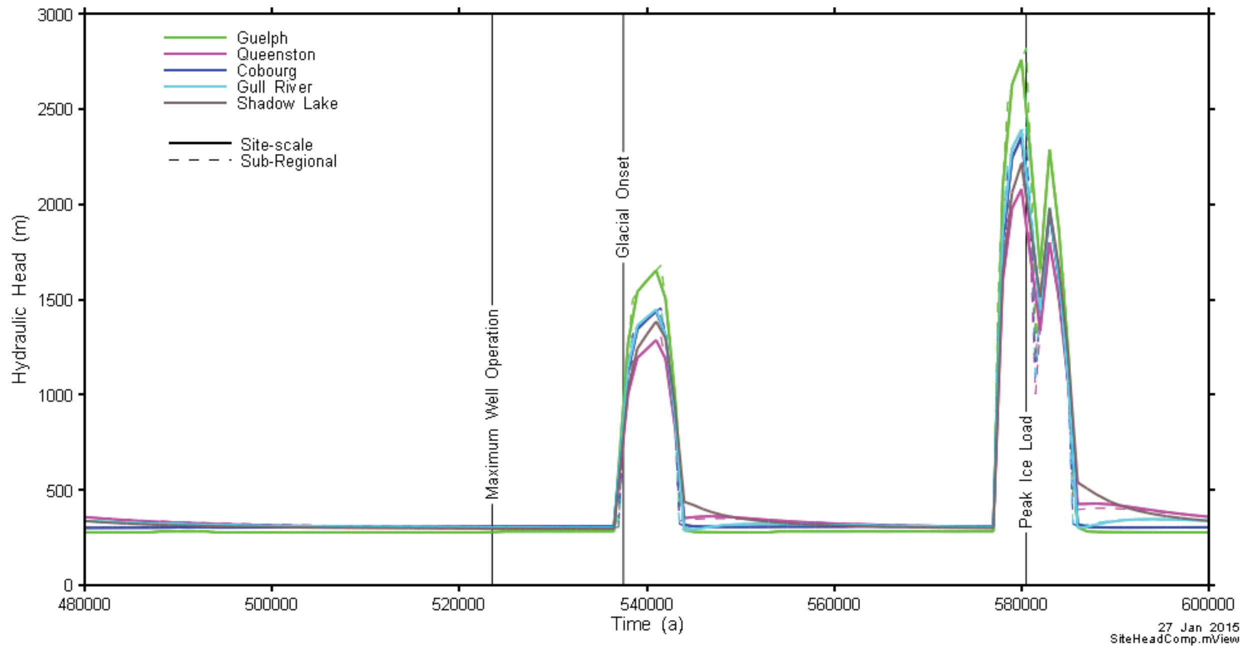

Figure 4-110: Site-Scale – Head Comparison with Glaciation Sub-Regional Model

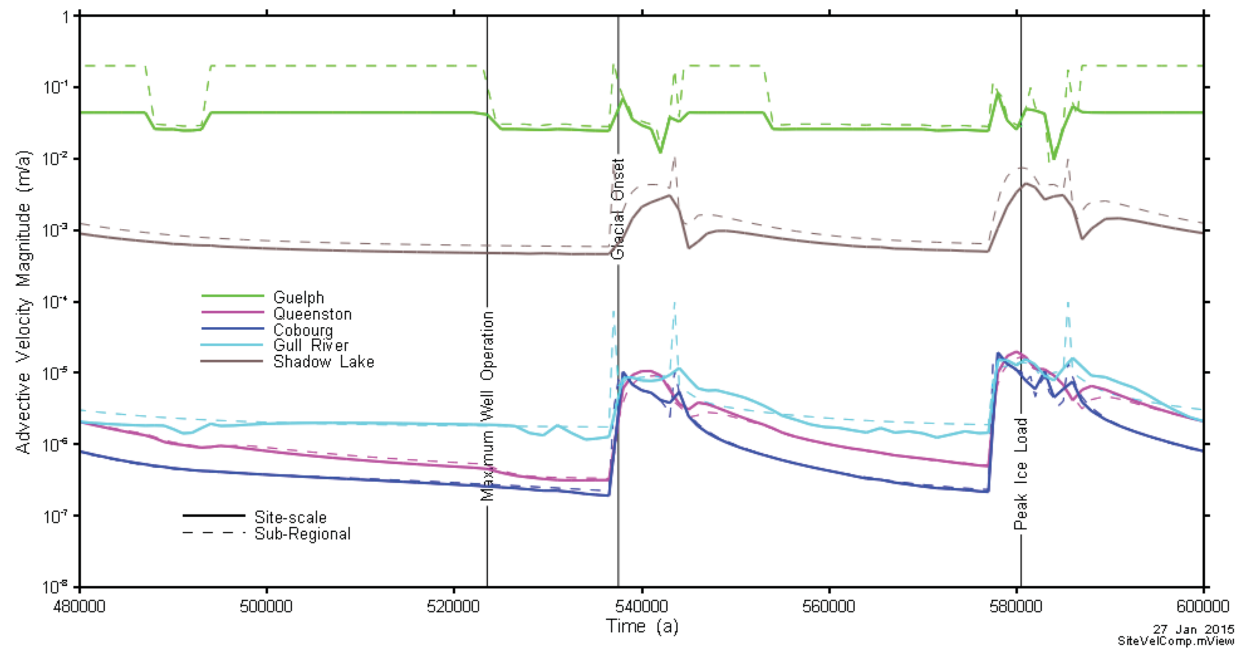

Figure 4-111: Site-Scale – Advective Velocity Comparison with Glaciation Sub-Regional Model

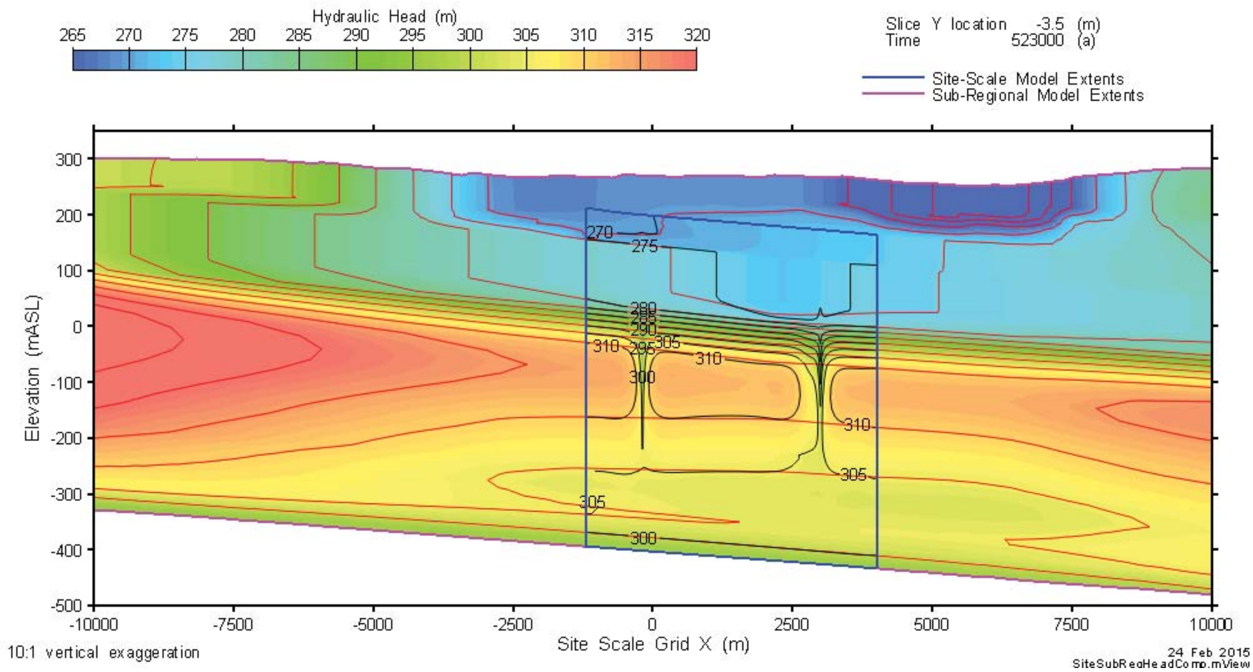

Figure 4-112: Site-Scale – Head Comparison with Glaciation Sub-Regional Model on Vertical Slice

4.2.4.2 Results

Spatial representations of transport model results at 1 Ma for the reference and shaft well glacial climate cases are shown in Figure 4-113 and Figure 4-114, and compared to results from the constant climate cases. The figures indicate very minor differences in transport, providing further evidence of the diffusion dominated nature of transport from the repository.

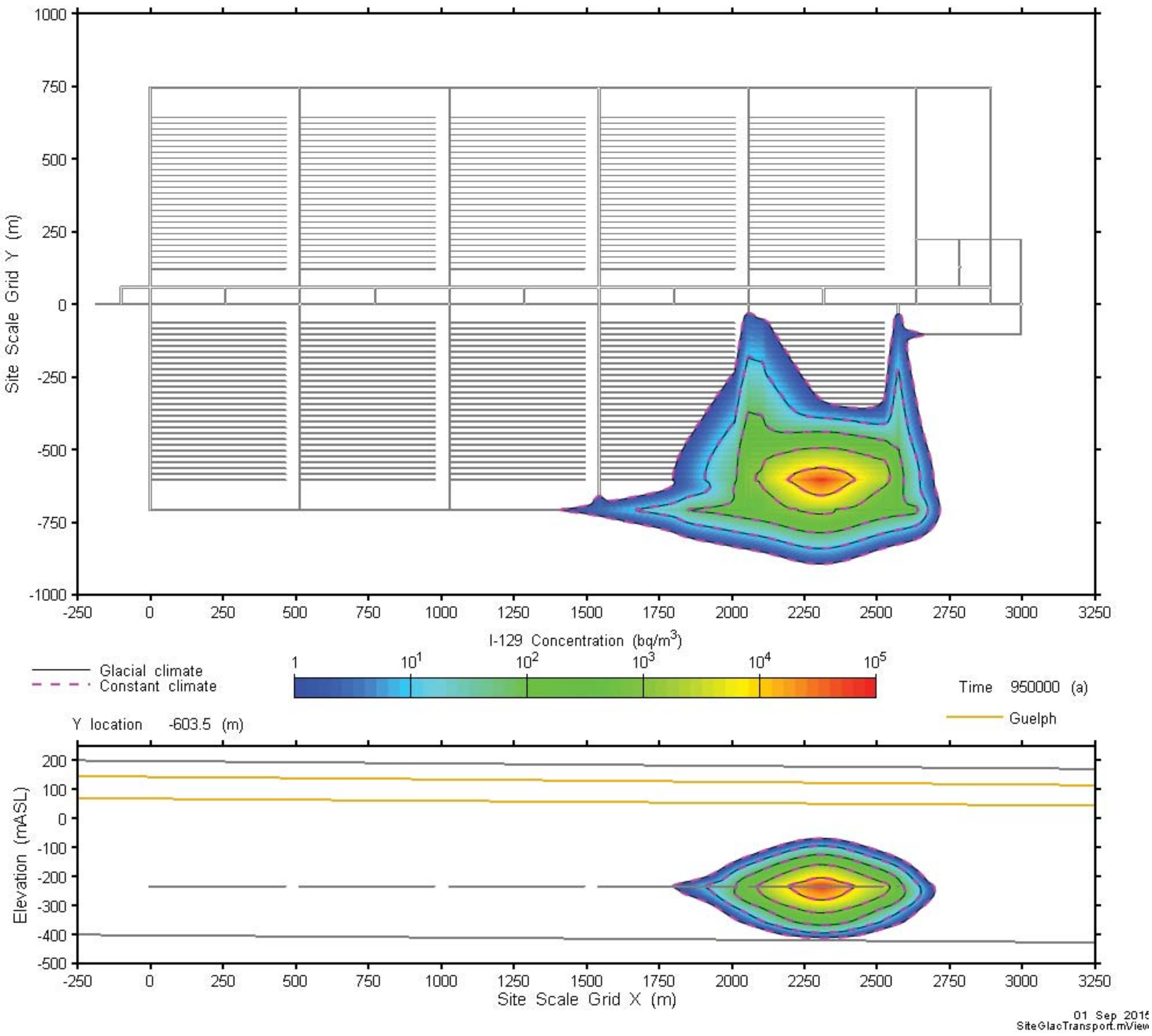

Figure 4-113: Site-Scale Model: Reference Well – Comparison of Constant and Glacial Climate I-129 Transport at 950 ka

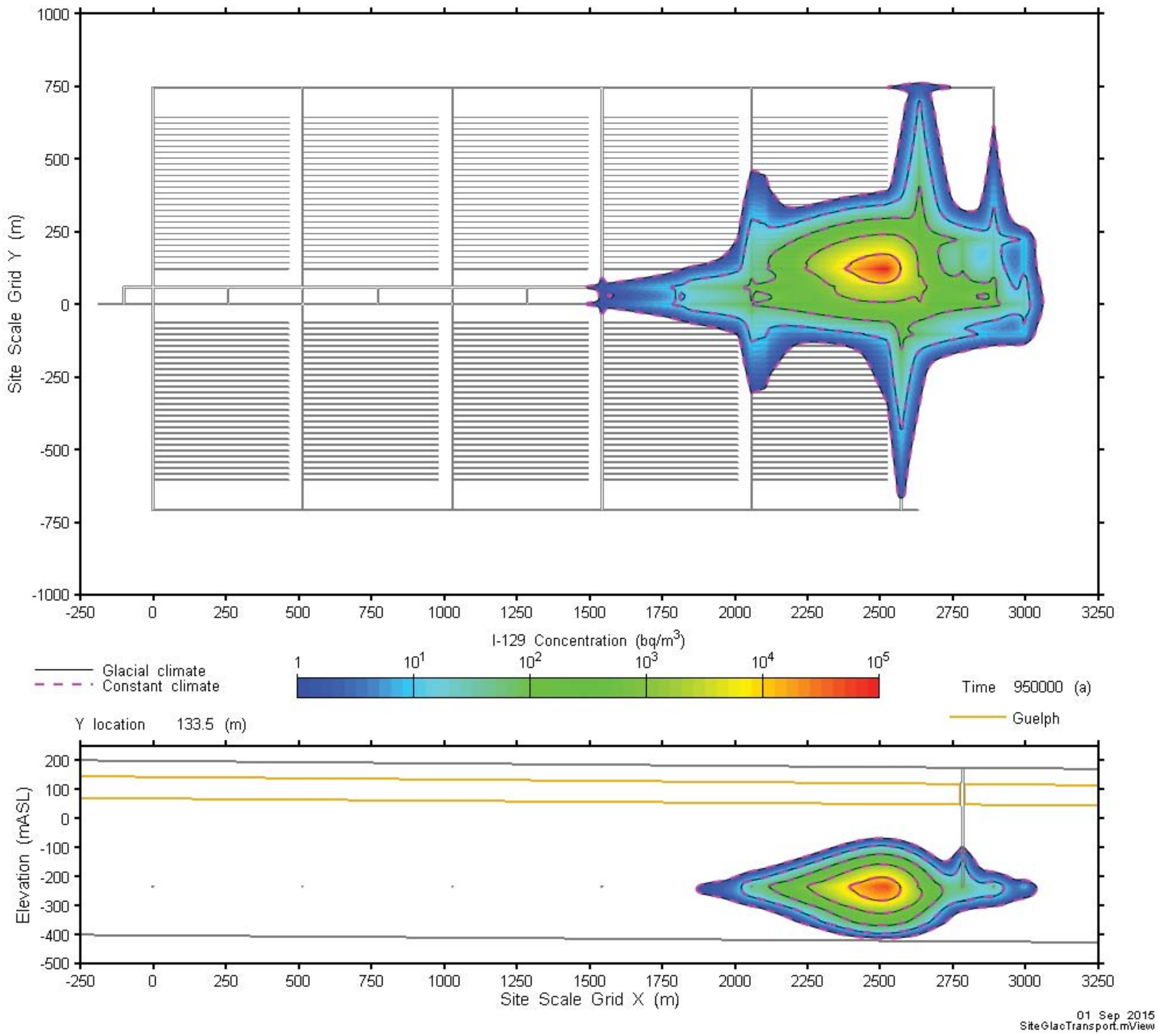

Figure 4-114: Site-Scale Model: Shaft Well – Comparison of Constant and Glacial Climate I-129 Transport at 950 ka

For the shaft well case, the glacial climate results in a very small increase in transport up the shaft relative to the constant climate case. This is shown in Figure 4-114 and below in Figure 4-115 where transport up the vent shaft is also shown to slightly increase (note slight blue cone at shafts where glacial isovolume is above the constant climate isovolume).

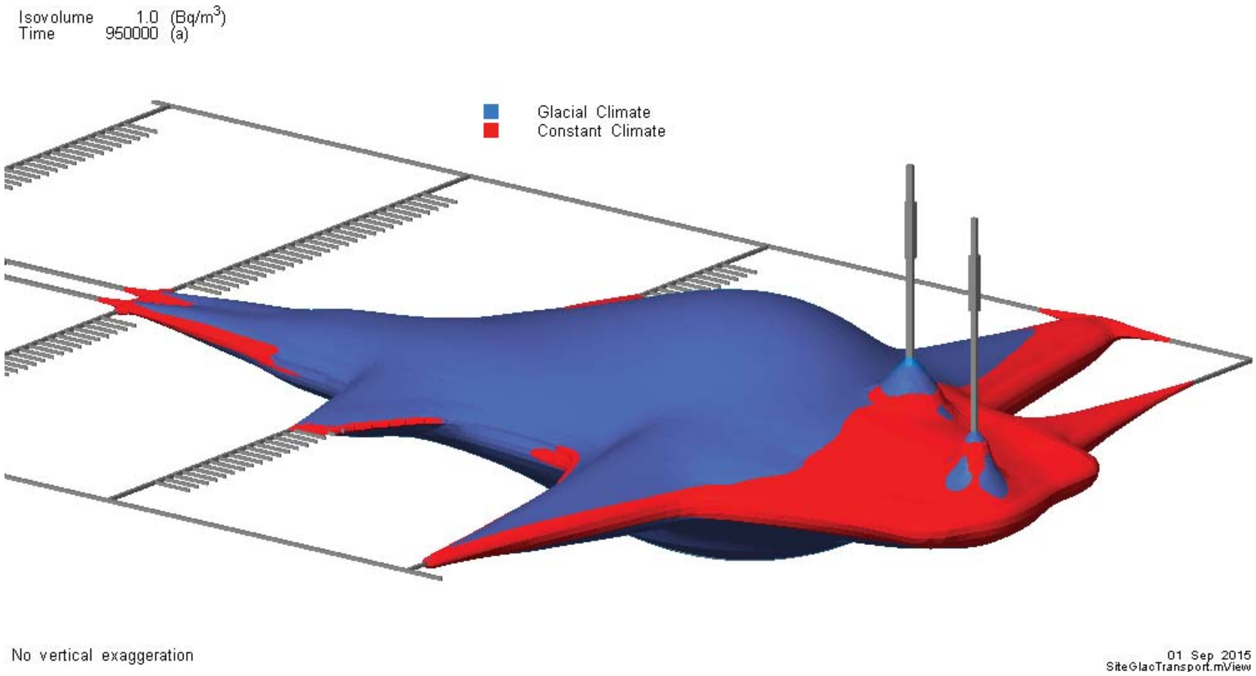

Figure 4-115: Site-Scale Model: Shaft Well – 3D Comparison of Constant and Glacial Climate I-129 Transport at 950 ka

Transport to the well is an important metric for evaluating system performance. In previous studies (NWMO, 2013) and for steady-state flow transport simulations in the current study, well mass flux calculations have been numerically stable. However, for initial transport simulations with the transient glacial climate, concentrations in the immediate vicinity of the pumping well were subject to oscillations each time the pumping well started operation. While the oscillations declined over the duration of the pumping period they were not completely eliminated. All previous transport simulations (NWMO, 2013; steady-state flow in the current report) have used centred-in-time (CIT) temporal discretization, a method that minimizes errors due to numeric dispersion. However, CIT is known to increase instability in strongly advective portions of the grid. Consequently, all glacial-climate site-scale transport cases were simulated with fully implicit time weighting. This eliminated the well oscillations with no other discernible impact. A comparison of CIT and fully implicit results is provided later in this sub-section.

Figure 4-116 compares glacial and constant climate I-129 mass flows into various formations for the reference well case. The glacial well results (solid line in figure) are intermittent, reflecting the time period that the well is operating. The high initial mass flux as the well is turned on is the capture of transport into the Guelph over the previous period of no well operation. After the initial peak, the well mass flux is virtually identical to the transport rate into the Guelph. Figure 4-117 compares glacial climate and constant climate I-129 mass flows into the Guelph and the well for the reference and shaft well cases. Calculated peak ratios of glacial climate to constant climate well flow for the last glacial period are approximately 140 and 155 for reference and shaft well cases respectively during the initial well uptake period, diminishing to a ratio of approximately five for both cases.

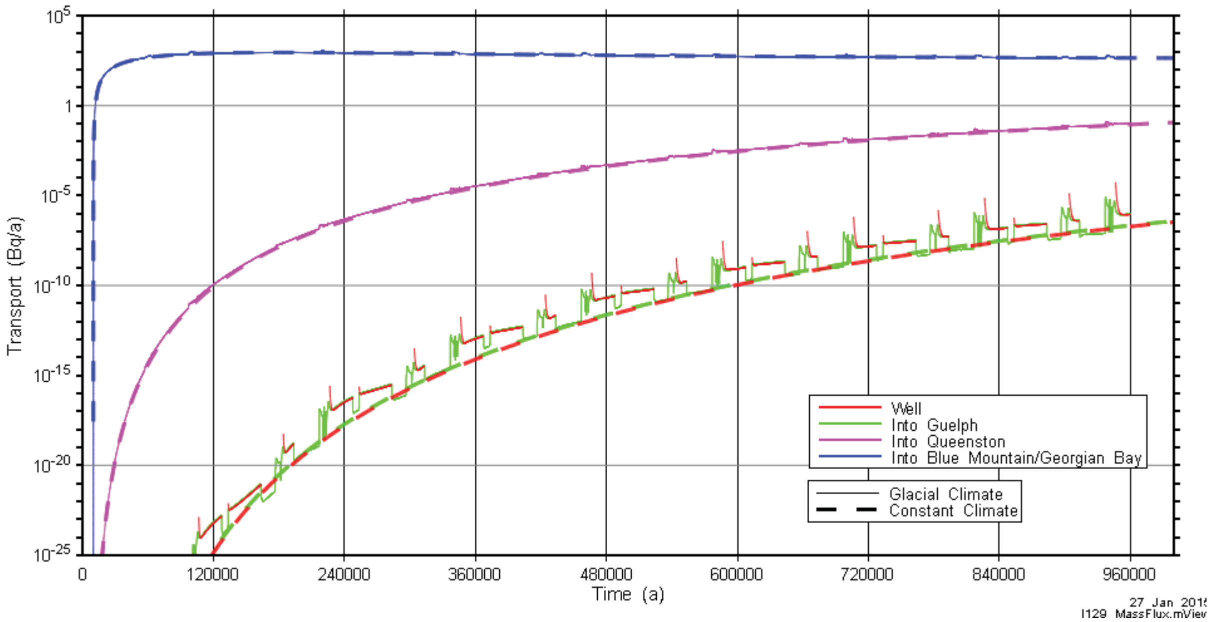

Figure 4-116: Site-Scale Model: Reference Well Results – I-129 Transport Into Well and Formations for Constant and Glacial Climate Cases

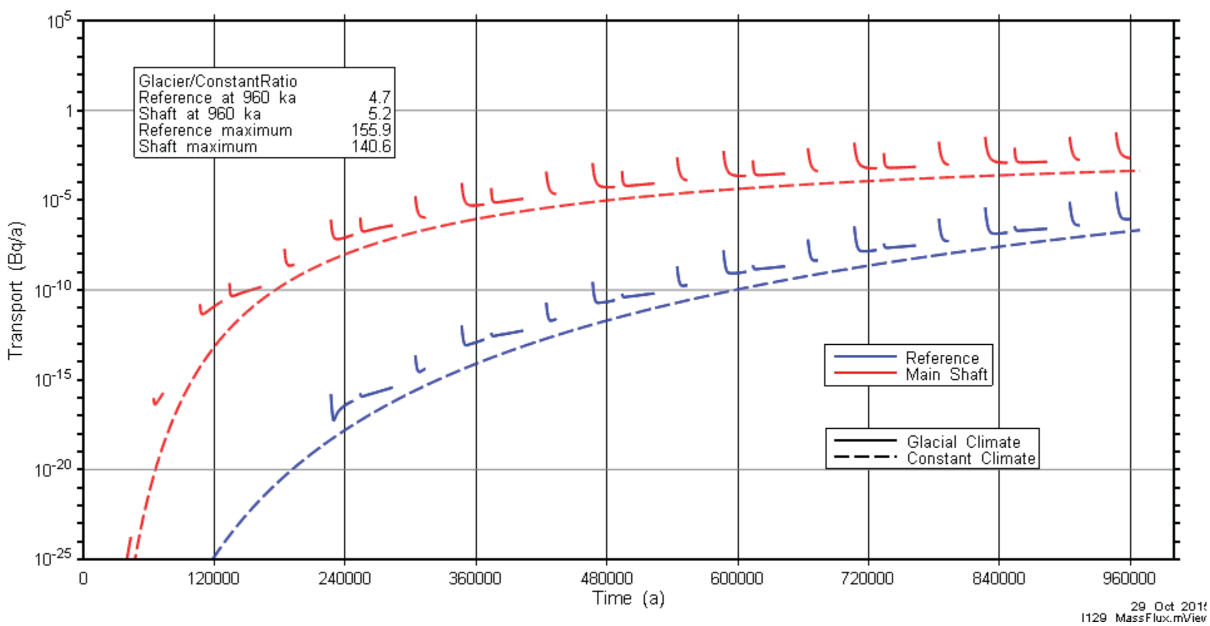

Figure 4-117: Site-Scale Model: Reference and Shaft Well Results – I-129 Well Transport for Constant and Glacial Climate Cases

Figure 4-118 shows the integrated flux into the Guelph and the well for the reference well and shaft well cases for the final three glacial cycles. Cumulative well flux closely follows the transport into the Guelph, showing that even intermittent well operation effectively captures all transport.

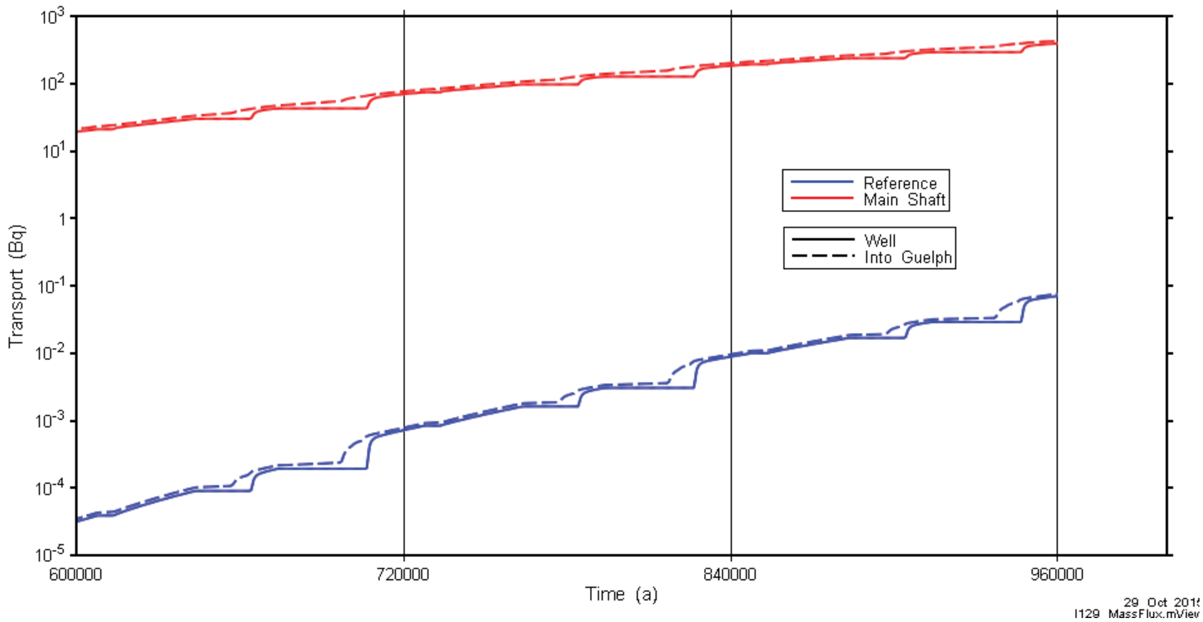

Figure 4-118: Site-Scale Model: Reference and Shaft Well Results – Integrated I-129 Well and Guelph Transport

4.2.4.3 Shaft Failure Sensitivity Case

Well and geosphere transport results for the shaft failure sensitivity case are compared to the shaft well results in Figure 4-119 and Figure 4-120 respectively. The effect of shaft failure parameters is clear, with significantly increased maximum well transport (factor of 90) compared to the shaft well case.

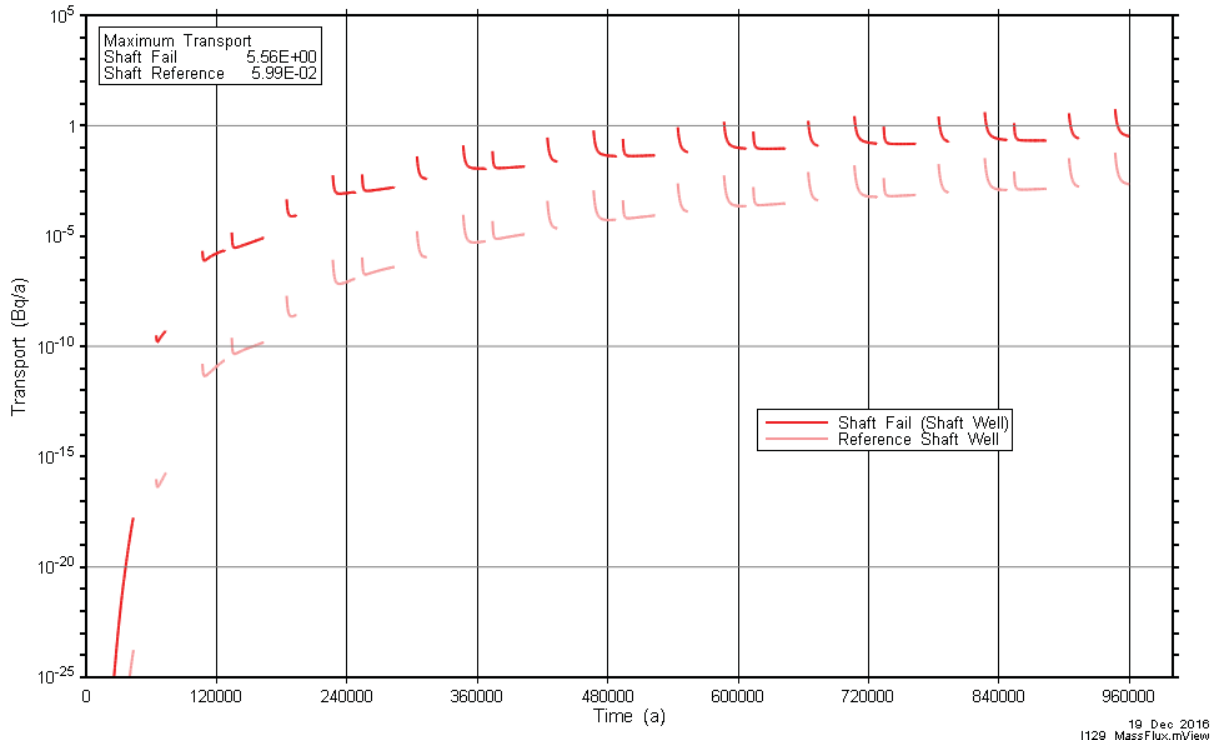

Figure 4-119: Site-Scale Model: Shaft Failure Sensitivity Case – Well Transport for Glacial Climate Sensitivity Cases

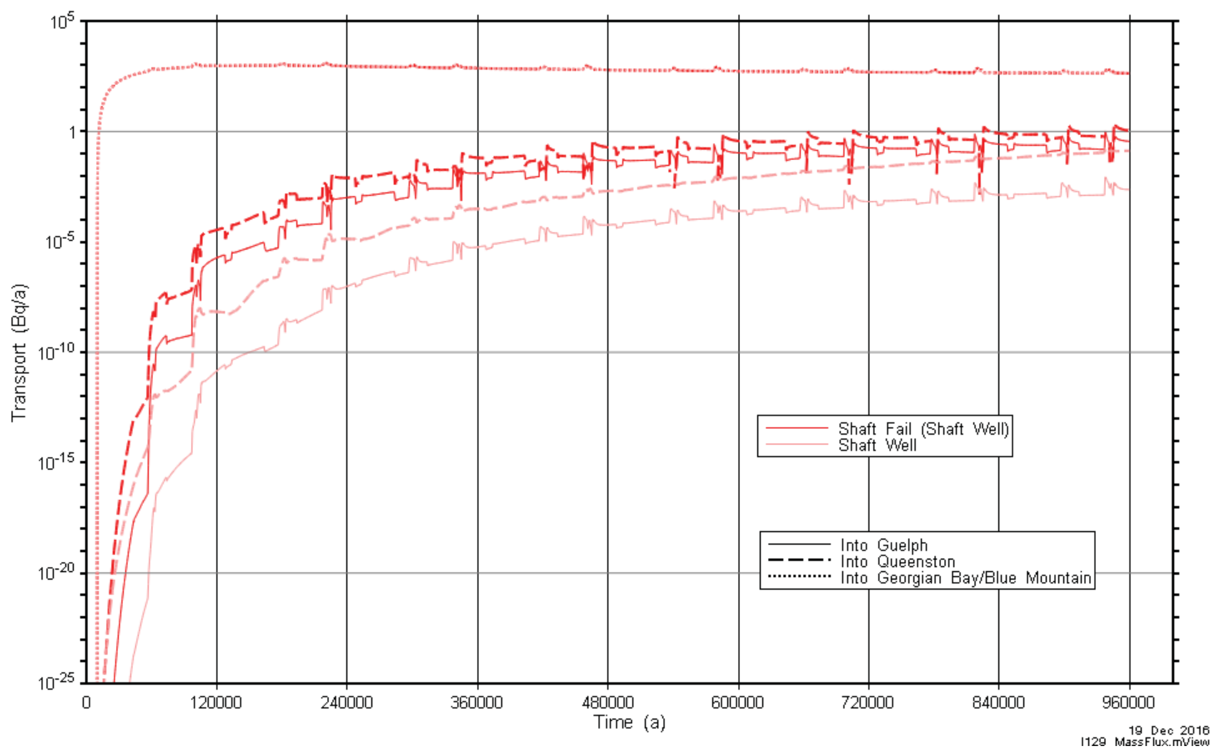

Figure 4-120: Site-Scale Model: Shaft Failure Sensitivity Case – Geosphere Transport for Glacial Climate Sensitivity Cases

Figure 4-121 shows the clear increase in concentrations near the shafts for the Shaft Fail case with higher concentrations in the shaft extending down into the Ordovician formations.

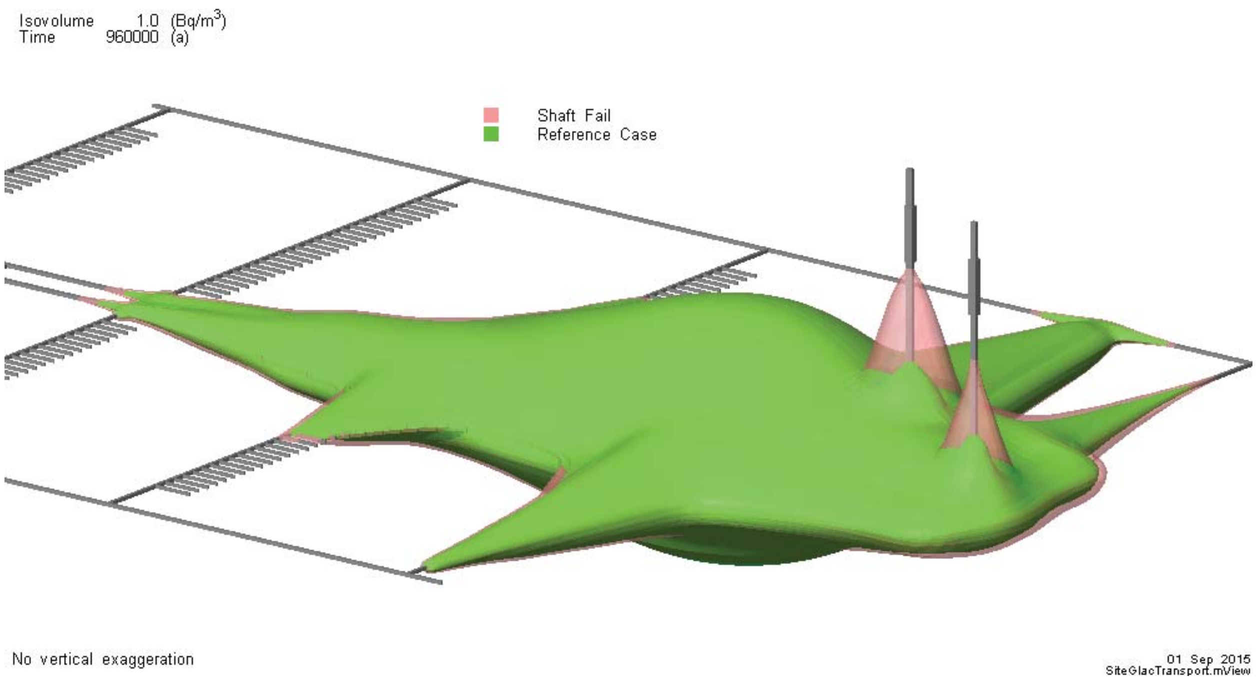

Figure 4-121: Site-Scale Model: Shaft Well – 3D Comparison of Shaft Well Reference Case and Shaft Fail Case Results at 1 Ma.

4.2.4.4 Geosphere and Transport Parameter Sensitivity Cases

Geosphere and transport parameters sensitivity results are compared to the reference well results in Figure 4-122 and Figure 4-123. Increased diffusion has the greatest impact with a factor of 2000 increase in peak well transport relative to the reference case. Increased hydraulic conductivity results in a factor of 7 increase, while increased dispersivity leads to a factor of 14 increase. The increased dispersivity and increased hydraulic conductivity cases are very similar to each other, which is to be expected as each parameter has a similar impact on the advective/dispersive term of the transport equation. Both cases also show some early-time oscillations in results at the well and into the Guelph. As shown in section 4.2.4.5, this can be ameliorated with reduced time steps, but does not affect results beyond the second glacial cycle.

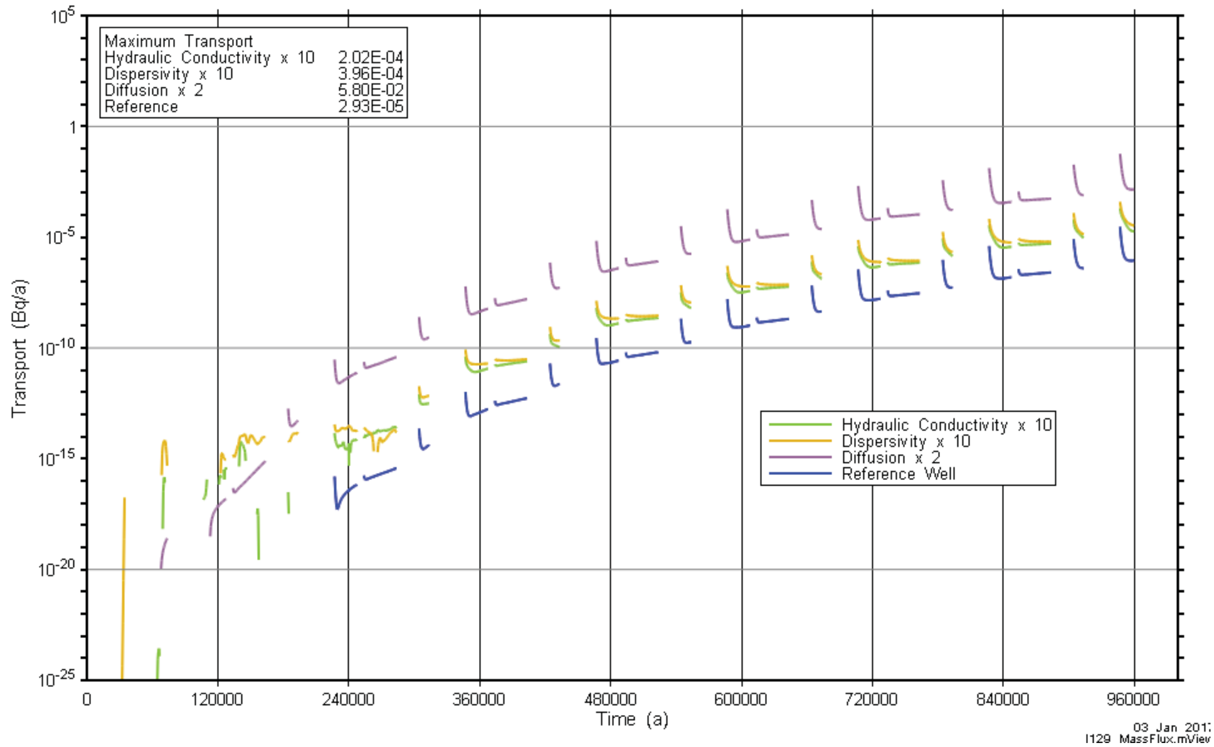

Figure 4-122: Site-Scale Model: Geosphere and Transport Parameters Sensitivity Cases – Well Transport for Glacial Climate Sensitivity Cases

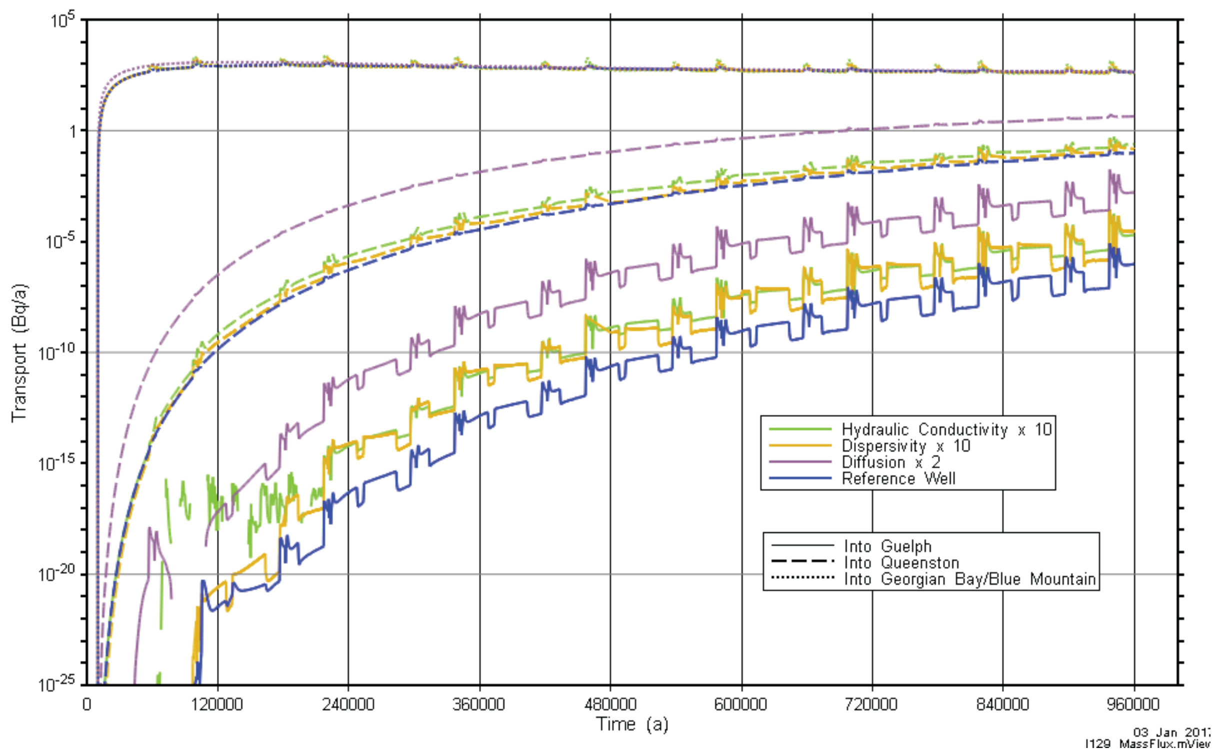

Figure 4-123: Site-Scale Model: Geosphere and Transport Parameters Sensitivity Cases – Geosphere Transport for Glacial Climate Sensitivity Cases

The increased transport for the High Diffusion case is primarily due to the extremely low concentrations at the edge of the radionuclide plume. A small increase in diffusion rate causes a large relative increase at the far edges of the plume, where well transport occurs. Concentrations closer to the source do not increase to as great an extent (Figure 4-124). The relative difference decreases over the duration of the simulation.

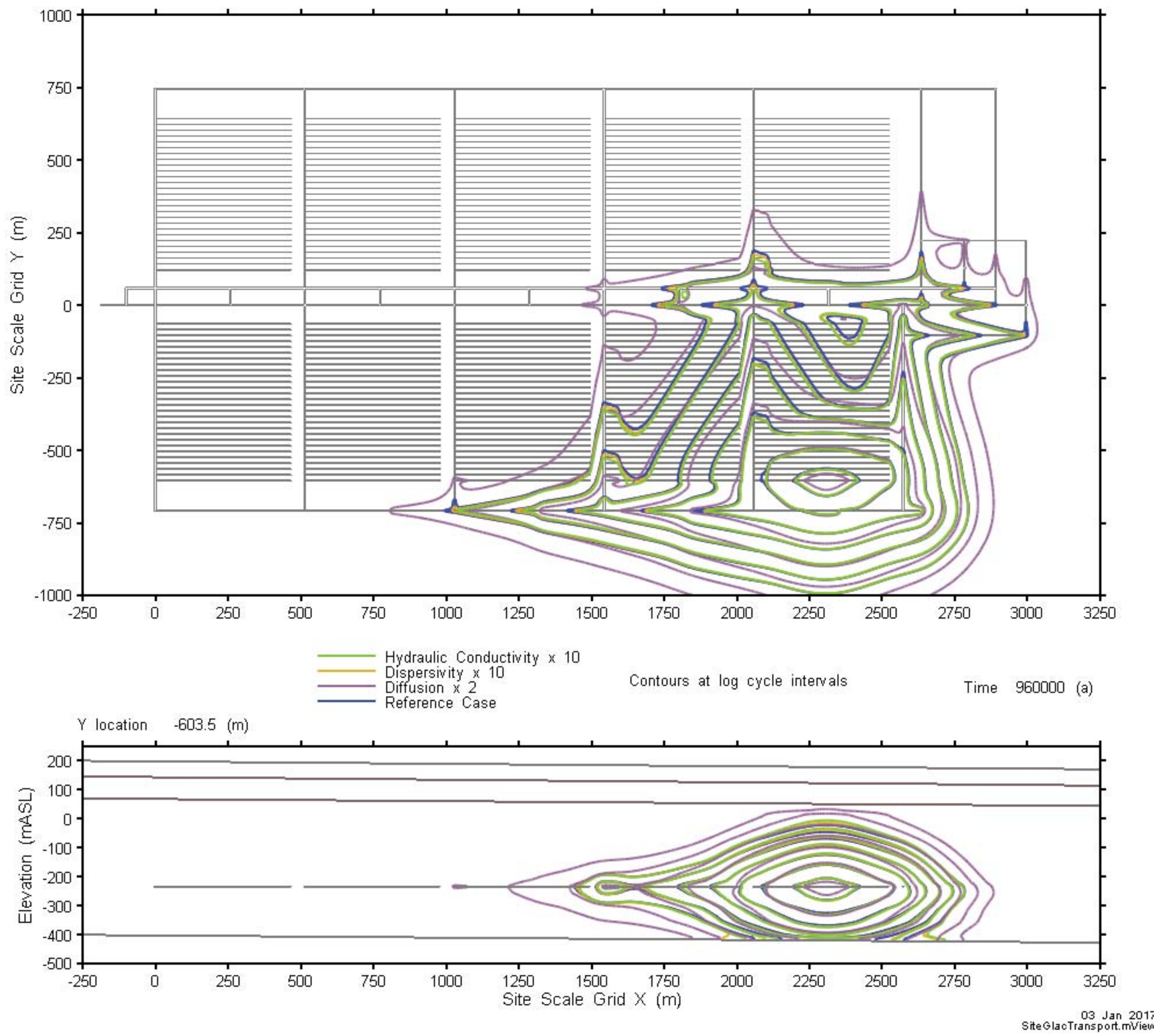

Figure 4-124: Site-Scale Model: Geosphere and Transport Parameters Sensitivity Cases – Comparison of I-129 Transport at 960 ka

4.2.4.5 Numerical Sensitivity

Two numerical sensitivity cases were simulated: reduced maximum time step; and the previously mentioned comparison of CIT and fully implicit results.

Time step sensitivity was assessed by limiting the maximum time step size to 100a, compared to the 500a used for all other transport simulations, for the Shaft Well Reference Case and the High Dispersivity Case (Figure 4-125 and Figure 4-126). An additional simulation with 1000 a maximum time step was simulated for the High Dispersivity Case. Results show that there are no significant differences for the reference case, but the minor early time oscillations previously noted for the High-Dispersivity case are eliminated with the smaller time steps.

As would be expected, there is an impact on execution time, with the Shaft Well Reference Case 100 a time step case taking 42 days, compared to 13 days for the 500 a maximum time step case. A hybrid approach with 100 a maximum for the first two glacial cycles and 500 a for the remainder would offer a good trade-off between accuracy and execution time.

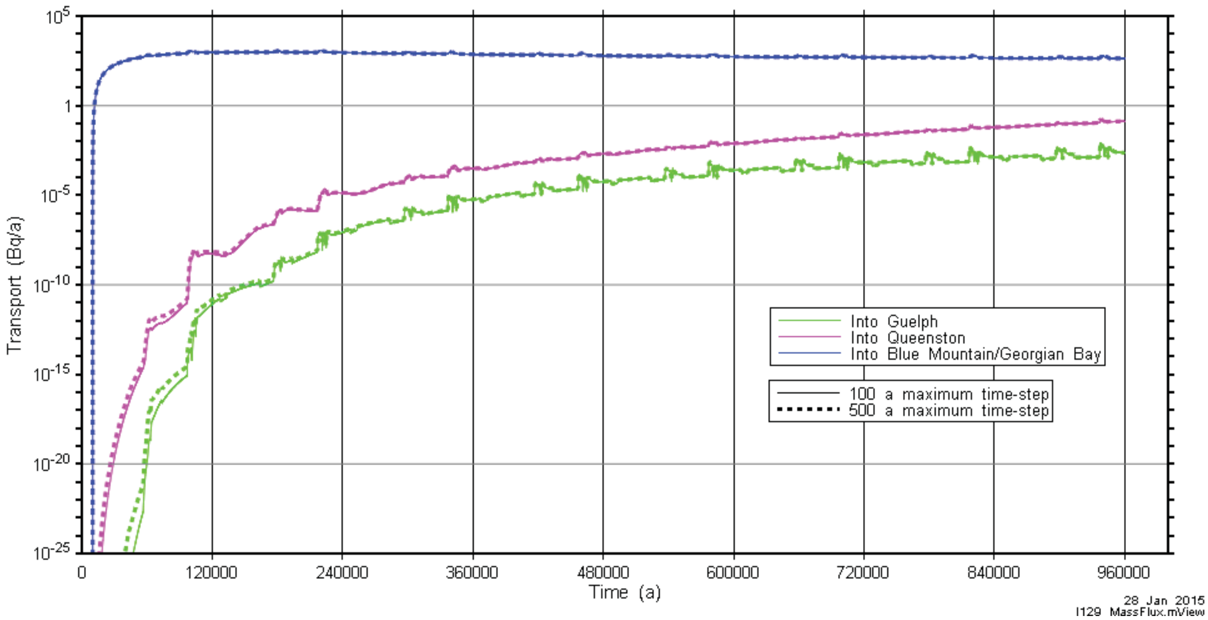

Figure 4-125: Site-Scale Model: Numeric Sensitivity Cases – Maximum Time Step - RC Shaft Case

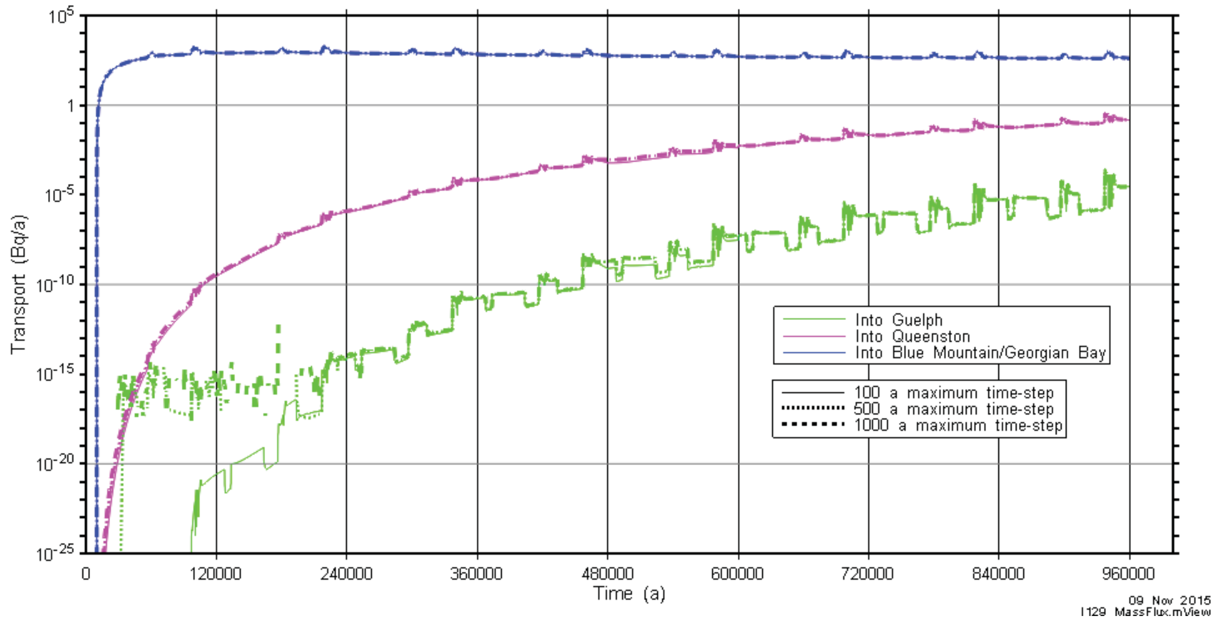

Figure 4-126: Site-Scale Model: Numeric Sensitivity Cases – Maximum Time Step – High Dispersivity Case

Temporal discretization sensitivity simulations (CIT or fully implicit) showed significantly differences only in the well response (see Figure 4-127), with improved stability in the well response for the fully-implicit temporal discretization. Figure 4-128 shows the oscillating nature of the well mass flux during the final well operation period.

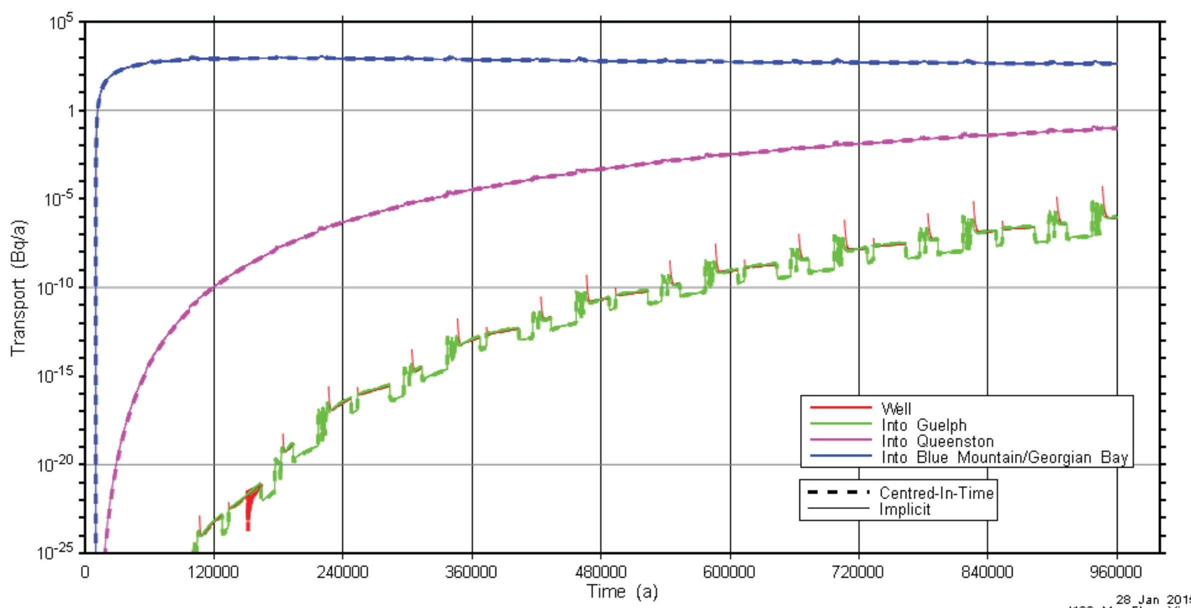

Figure 4-127: Site-Scale Model: Reference Well – Comparison between Centred-in-Time and Fully-Implicit Temporal Transport Discretization Geosphere and Well Transport

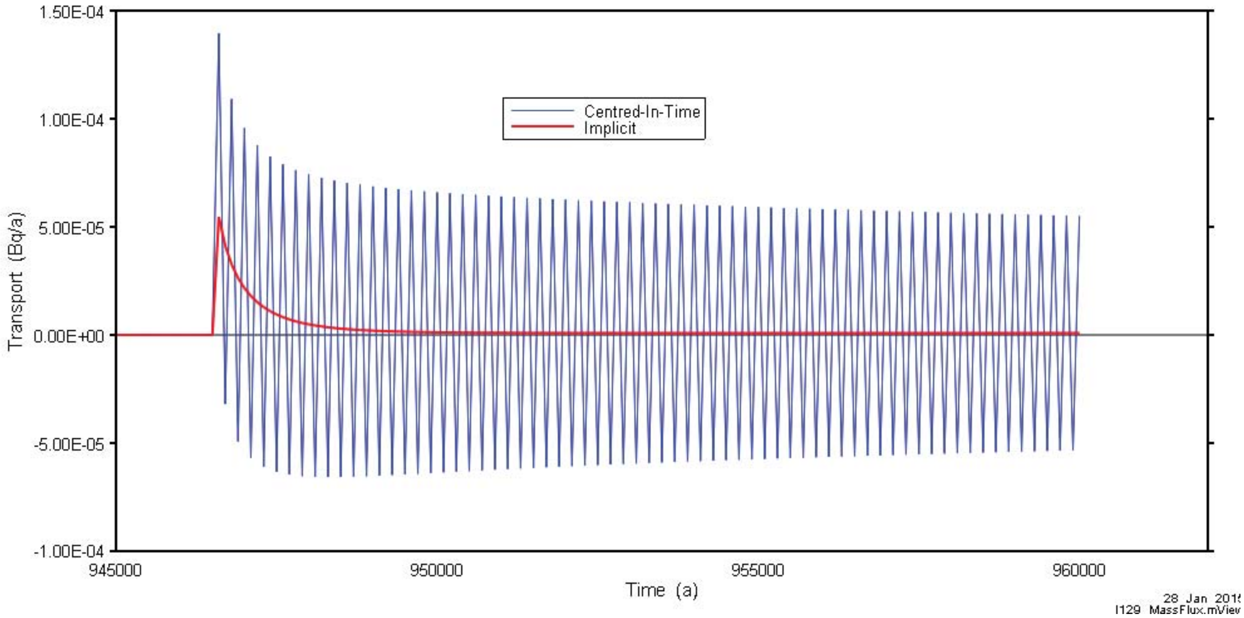

Figure 4-128: Site-Scale Model: Reference Well – Comparing Well Transport of Centred-in-Time and Fully-Implicit Temporal Transport Discretization

4.3 Glaciation Sub-Regional Two-Phase Flow Model

Although not currently considered in the postclosure safety assessment cases, there is evidence of residual gases in the Ordovician rock formations (INTERA, 2011). During a glacial cycle, the greater compressibility of gas, relative to water, would moderate head increases due to glacial loading. Two-phase flow models were generated at the Sub-Regional scale to evaluate the impact of gas on groundwater flow during glacial climate cycles.

The two-phase model is a 2D slice of the Glaciation Sub-Regional Model and uses the code T2GGM. Compared to the 3D FRAC3DVS-OPG model presented in Section 4.1, some differences are expected due to model dimensionality, model code and modelling approach. To minimize and understand these differences due to model implementation, a stepped approach was taken to generate the 2D T2GGM model:

1. a 2D FRAC3DVS-OPG model was generated from the 3D FRAC3DVS model;
2. a fully water saturated 2D T2GGM model was developed from the 2D FRAC3DVS slice; and
3. initial gases were introduced to the Ordovician formations to produce the 2D T2GGM two-phase flow model.

Section 4.3.1 describes the 2D FRAC3DVS-OPG model and Section 4.3.2 describes the fully water saturated 2D T2GGM models. Section 4.3.3 provides results for the two-phase flow 2D T2GGM model with an initial gas saturation of 10%. Section 4.3.4 examines the sensitivity of results to the initial gas saturation, comparing the 10% initial gas saturation results to different initial gas saturations of 5% and 1%.

It should be emphasized that the model results presented in this section are extracted at the same times and location as results for the 3D single phase models presented in previous sections of this report. The location is selected based on the well location and some of these times are chosen and labelled based on effects of the well and permafrost, despite the fact that the well and permafrost are NOT present in any of the 2D models presented here. The names of these reporting times and location were not changed, for consistency and comparison with other sections of this report.

4.3.1 2D FRAC3DVS Model: Single Water-Phase

The 2D FRAC3DVS model is a 2D slice of the 3D Glaciation Sub-Regional Model at X = 12500 m, as shown in Figure 4-129, with the same discretization and boundary conditions as the 3D model. Property assignment for the 2D slice is illustrated in Figure 4-130. The resulting model has 11,918 nodes and 5,800 elements. The model does not include the well and permafrost was ignored, which should have minimal impact on results based on the 3D model results described above.

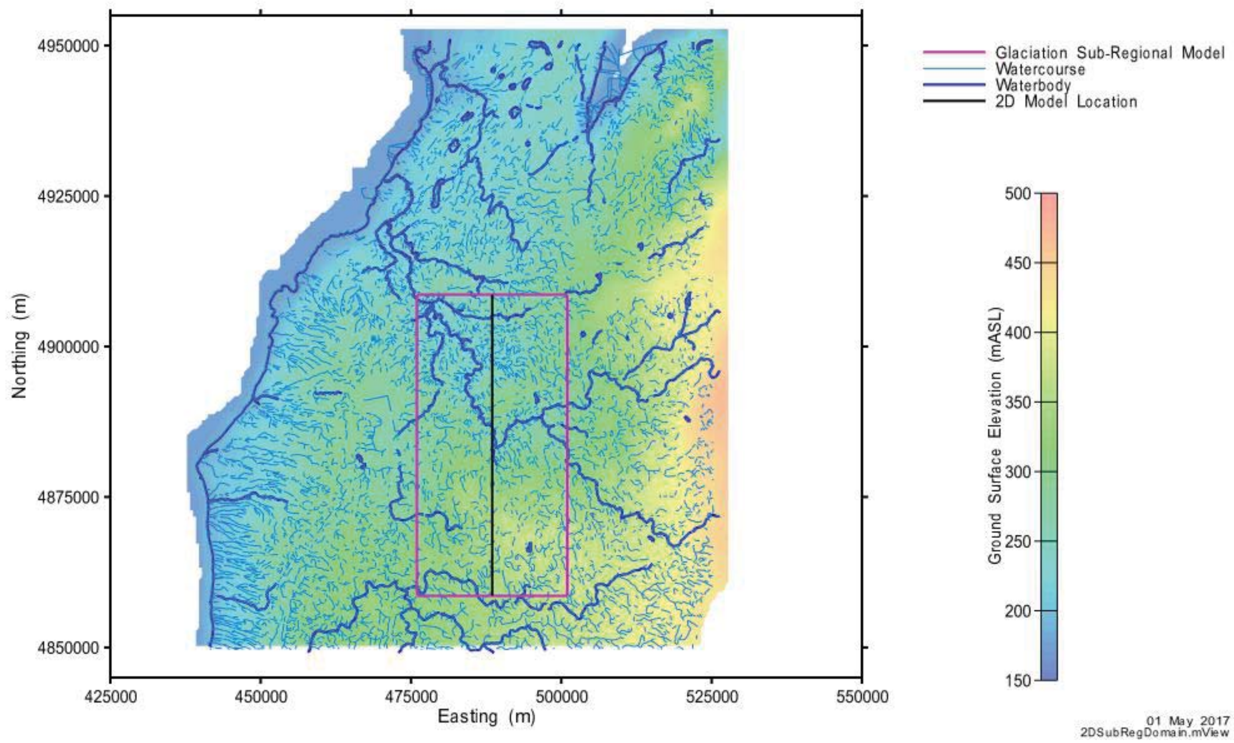

Figure 4-129: 2D Glaciation Sub-Regional Model Location

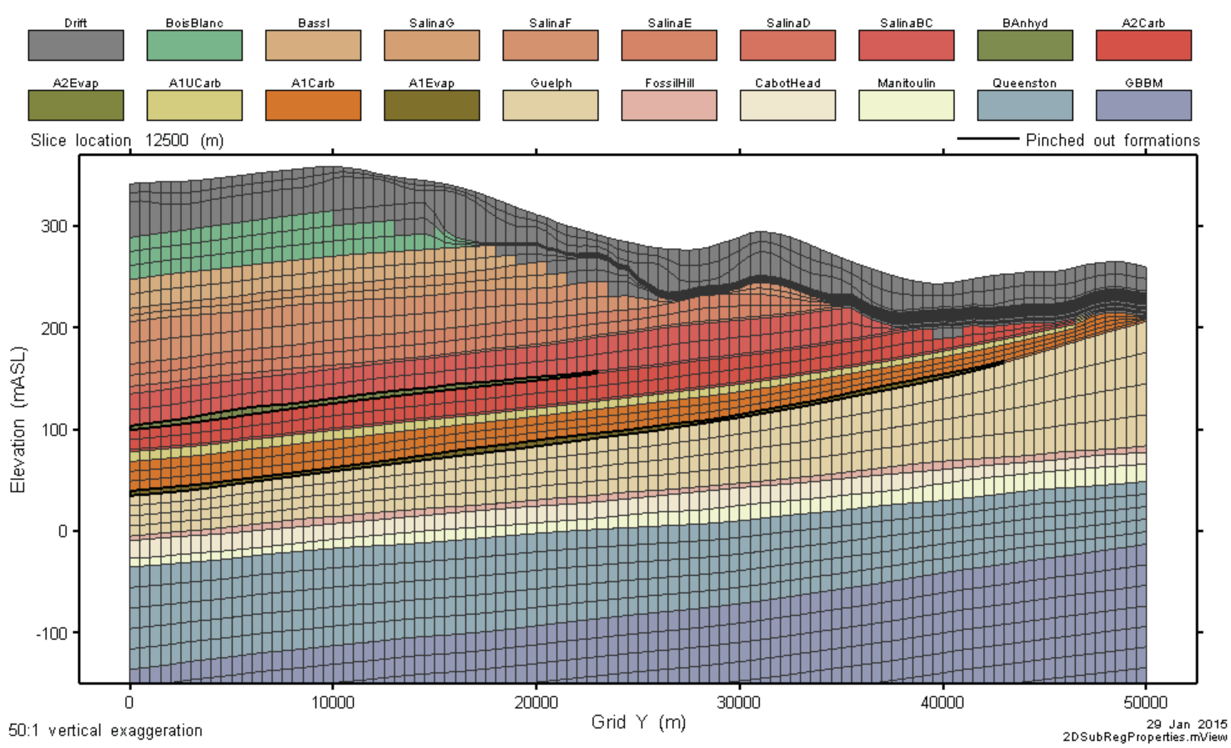

Figure 4-130: 2D Glaciation Sub-Regional Model Property Assignment

A comparison of results between the 2D and 3D FRACDVS-OPG model are provided in Figure 4-131 through Figure 4-136. For consistency, locations in space and time are the same as shown for the Reference Case Glacial Climate Simulation in Section 4.1.4, even though the 2D model does not include the well or consider permafrost. These results show that the 2D vertical slice provides a good representation of the 3D model. While there are minor differences between results, the general trends are the same for both models. It also confirms previous conclusions that the well and permafrost included in the 3D model have only minor and local impacts on the groundwater flow regime.

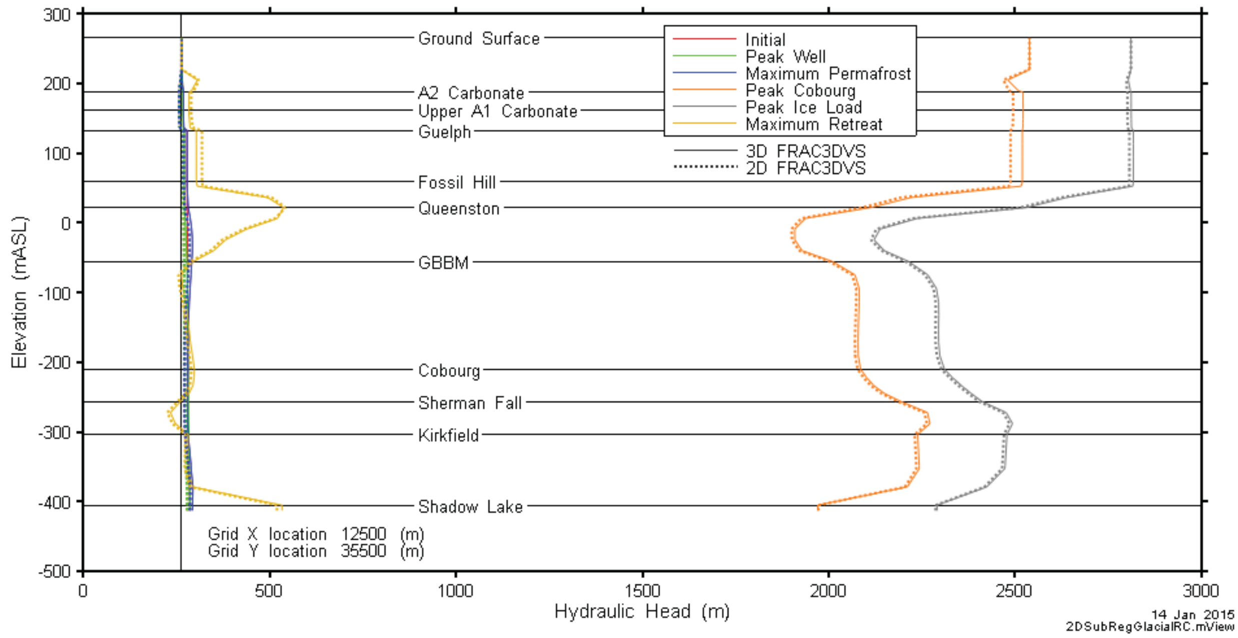

Figure 4-131: 2D and 3D Glaciation Sub-Regional Glacial Cycle Simulations: Hydraulic Head Profiles at Water-Supply Well Location for the First Cycle

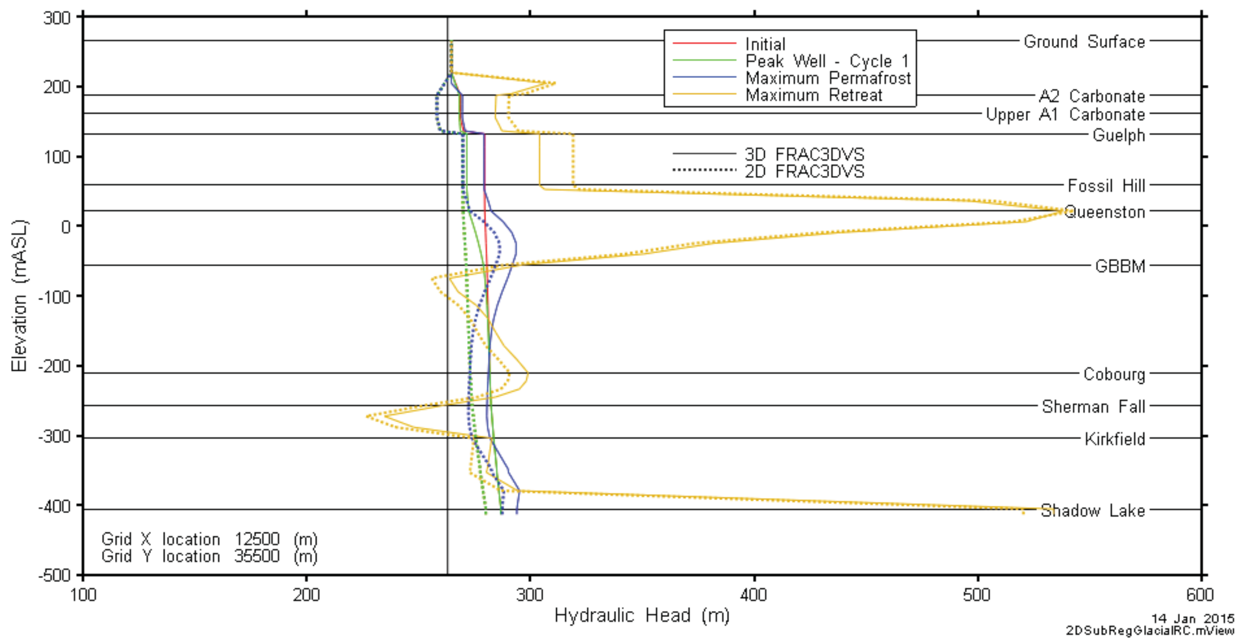

Figure 4-132: 2D and 3D Glaciation Sub-Regional Glacial Cycle Simulations: Hydraulic Head Profiles at Water-Supply Well Location (Detail) for the First Cycle

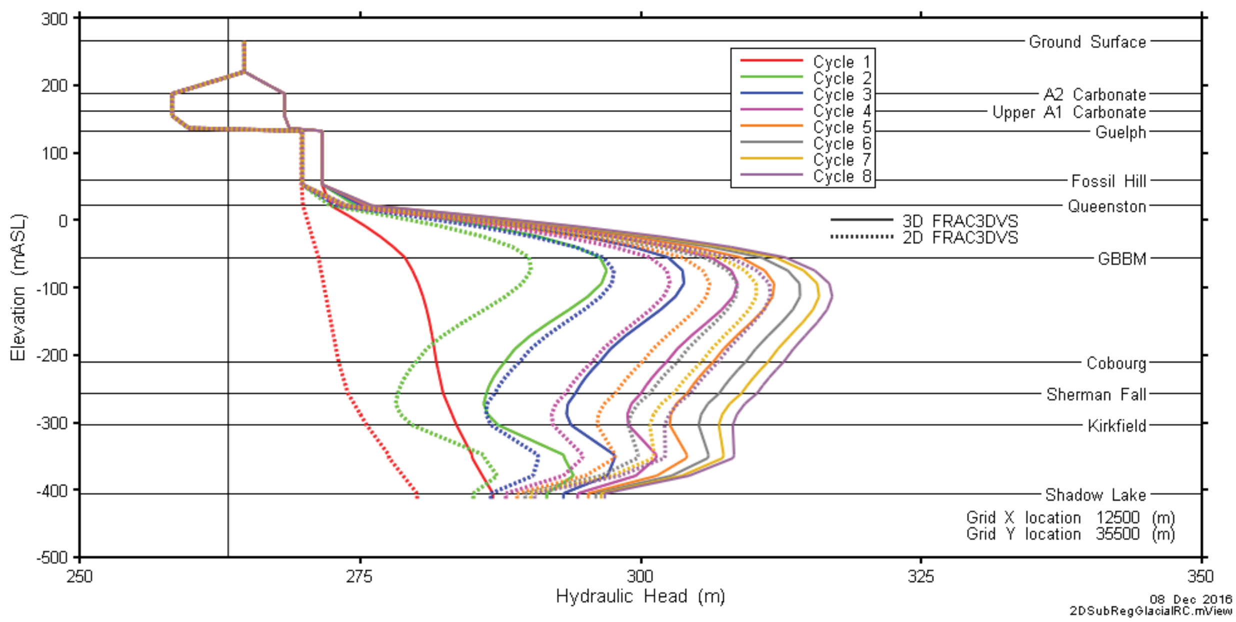

Figure 4-133: 2D and 3D Glaciation Sub-Regional Glacial Cycle Simulations: Hydraulic Head Profiles at Water-Supply Well Location at Time of Maximum Well Impact for All Cycles

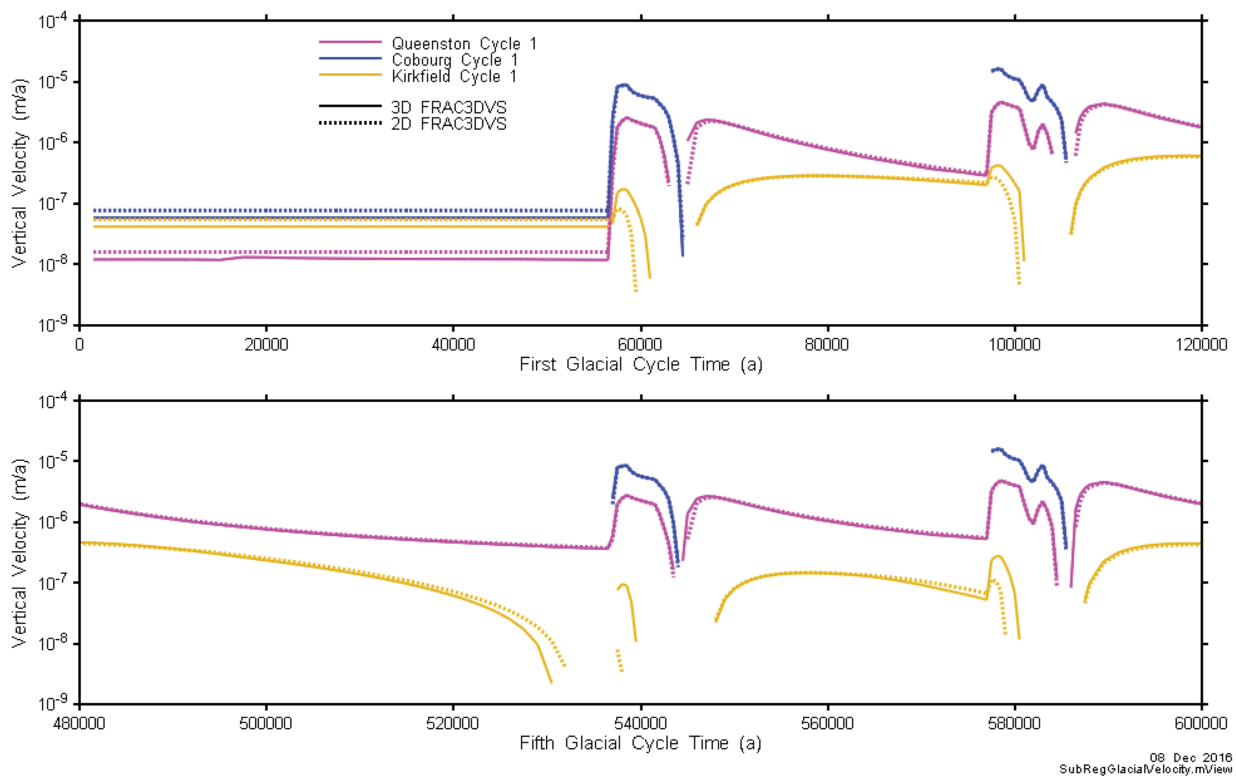

Figure 4-134: 2D and 3D Glaciation Sub-Regional Glacial Cycle Simulations: Maximum Vertical Velocity in Repository Vicinity and Selected Formations for the First and Fifth Cycles

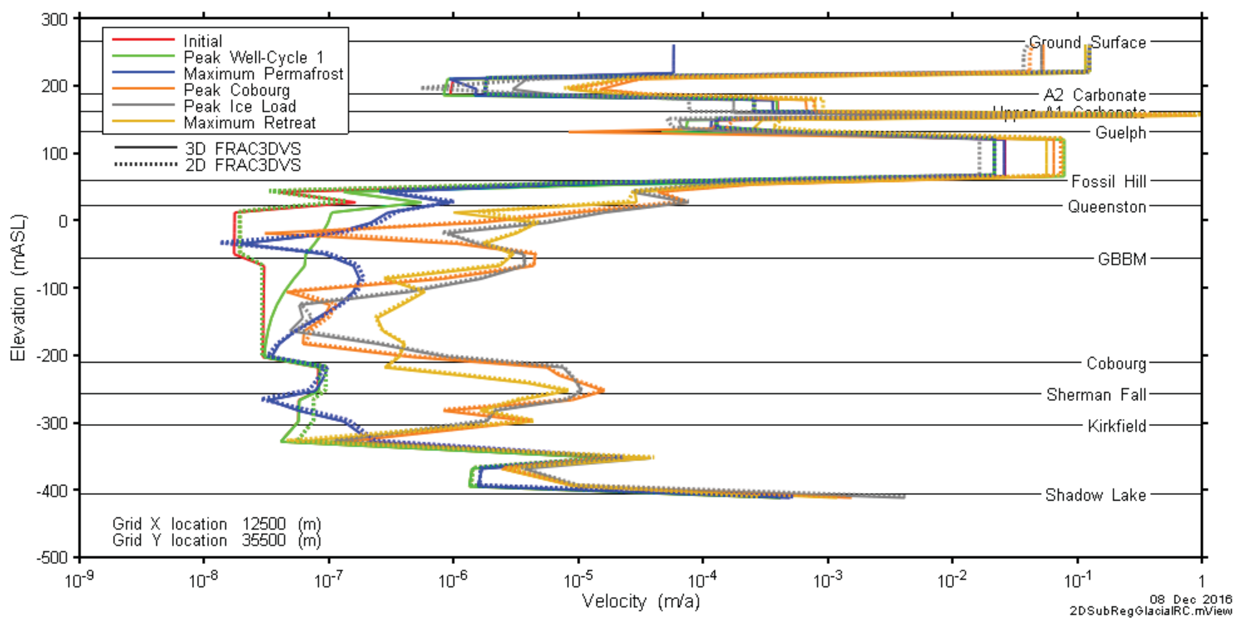

Figure 4-135: 2D and 3D Glaciation Sub-Regional Glacial Cycle Simulations: Velocity Magnitude Profiles at Water-Supply Well Location for the First Cycle

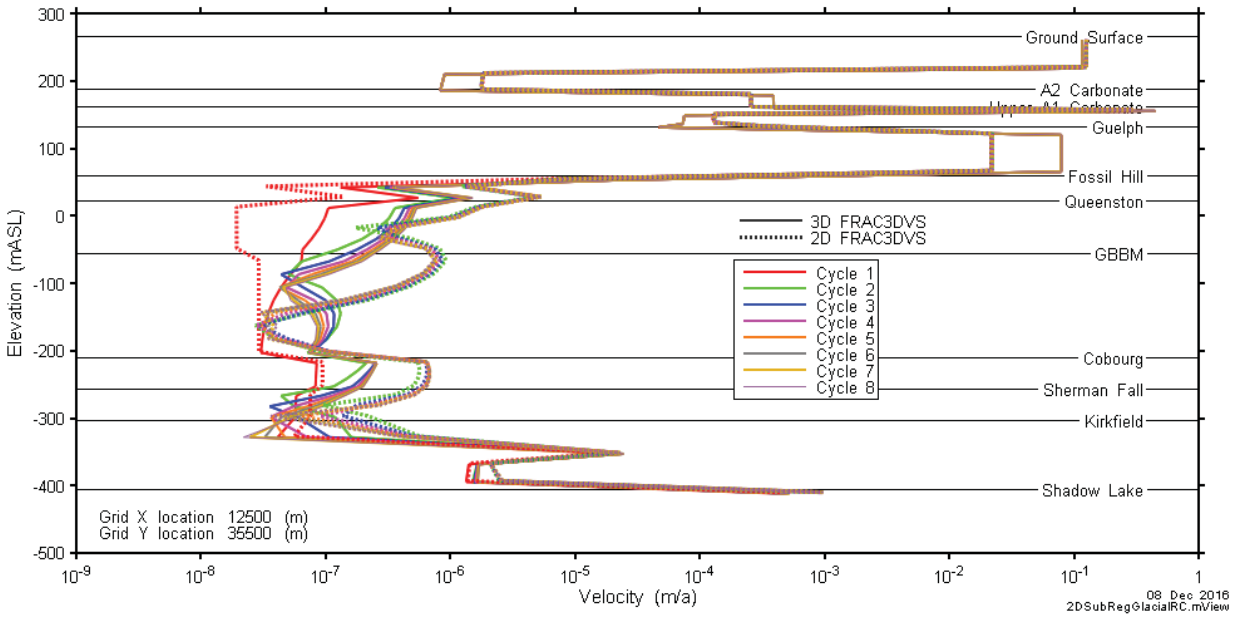

Figure 4-136: 2D and 3D Glaciation Sub-Regional Glacial Cycle Simulations: Velocity Magnitude Profiles at Water-Supply Well Location at Time of Maximum Well Impact for All Cycles

As a final test, MLE calculations were performed using the 2D model. Steady-state MLE are compared in Figure 4-137, while snapshot MLE for the fifth glacial cycle are compared in Figure 4-138. Results are very similar, leading to the conclusion that the 2D representation of the 5CS flow system captures the essential flow attributes of the much more computationally demanding 3D model. The largest differences in Repository MLE are due to well operation in the 3D model. There is no pumping well in the 2D model.

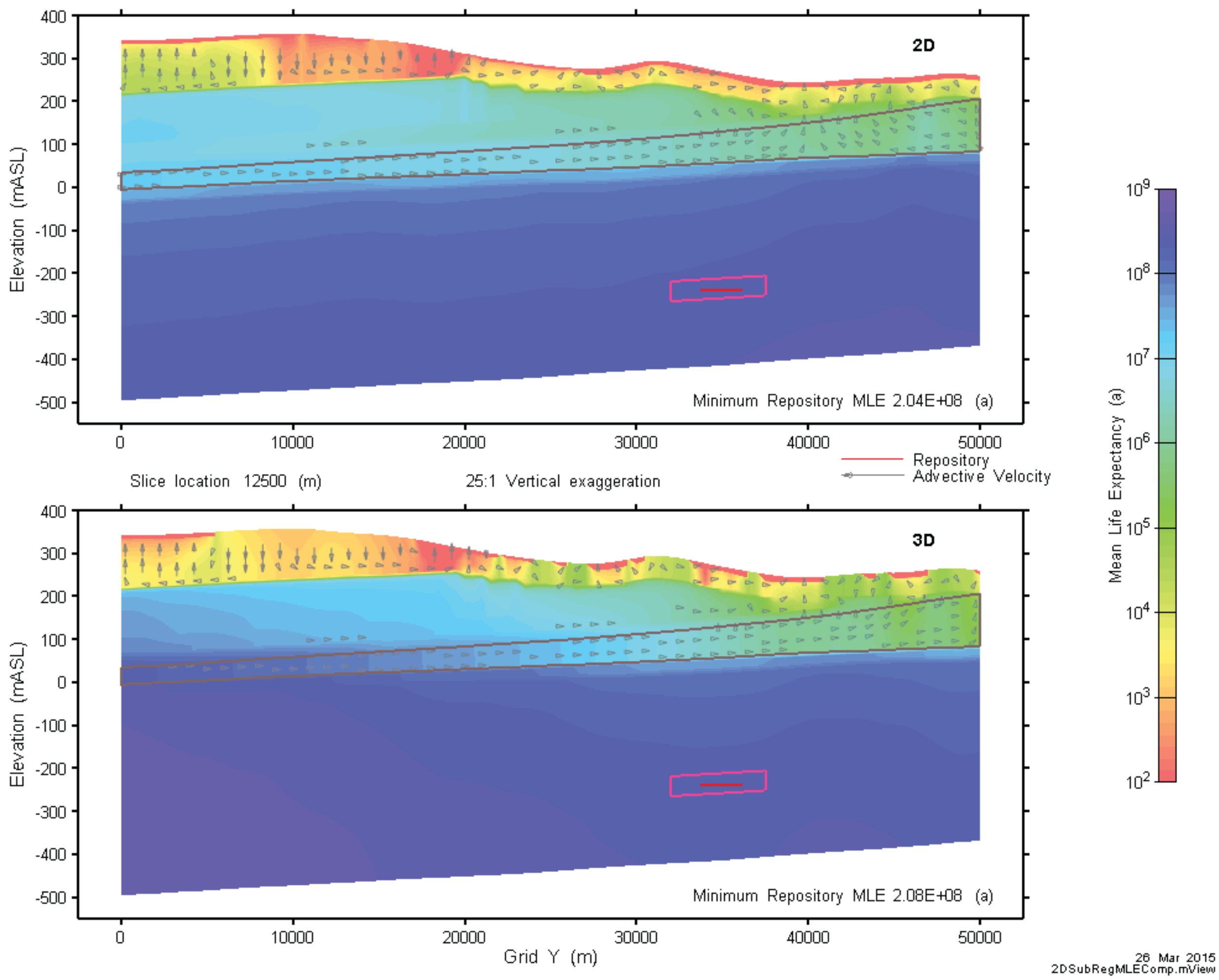

Figure 4-137: 2D Sub-Regional Flow: Comparison of Mean Life Expectancy to 3D model at time of Peak Glacial Load

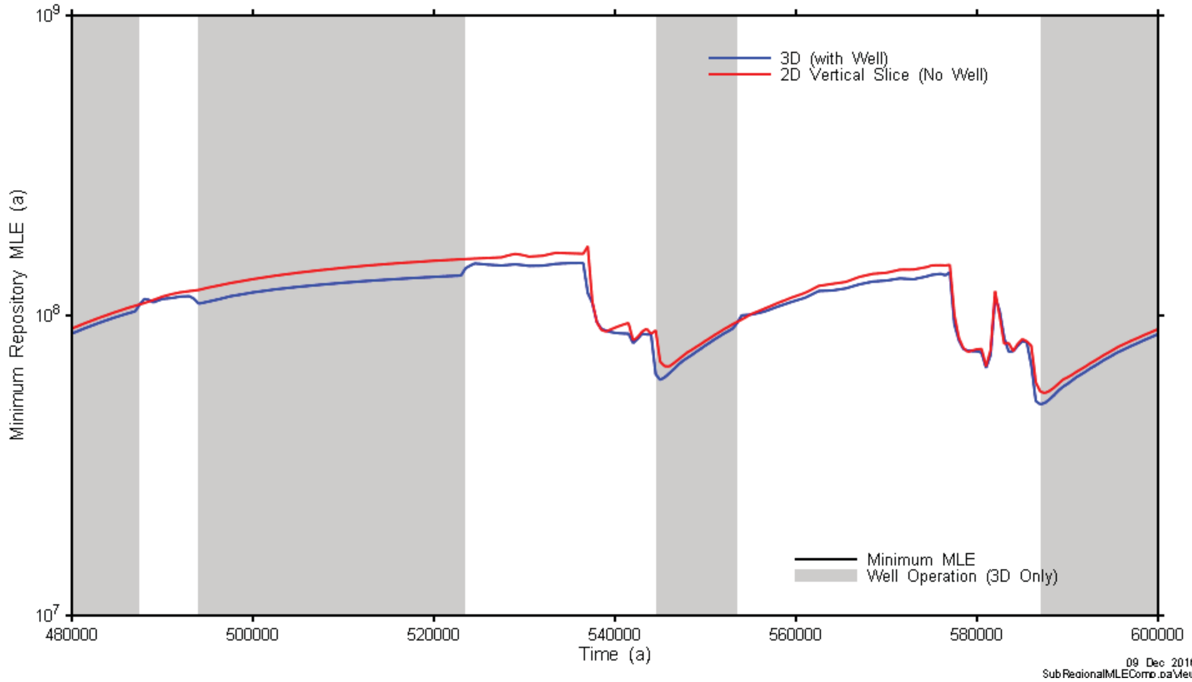

Figure 4-138: Glaciation 2D Sub-Regional Glacial Cycle Simulations: Repository MLE for Fifth Glacial Cycle – Comparison to 3D Reference Case

4.3.2 2D TGGM Model: Single Water-Phase

The 2D T2GGM model is based directly on the 2D FRAC3DVS-OPG model. Some differences in discretization occur due to differences in approach between T2GGM and FRAC3DVS-OPG. T2GGM is a node-centered integral finite difference model, and the element centres of the FRAC3DVS model are defined as the nodes for the T2GGM model. FRAC3DVS elements are roughly equivalent to the T2GGM blocks, the main difference being that all T2GGM block surfaces are flat whereas some FRAC3DVS element surfaces are sloped, following the the surfaces defining the geologic formations. Boundary conditions are time-variable fixed pressure and fully water saturated at the top and sides of the model.. The resulting grid has 5,916 nodes.

Results for the T2GGM and FRAC3DVS 2D Glaciation Sub-Regional models are very similar, as shown in Figure 4-139 though Figure 4-144.

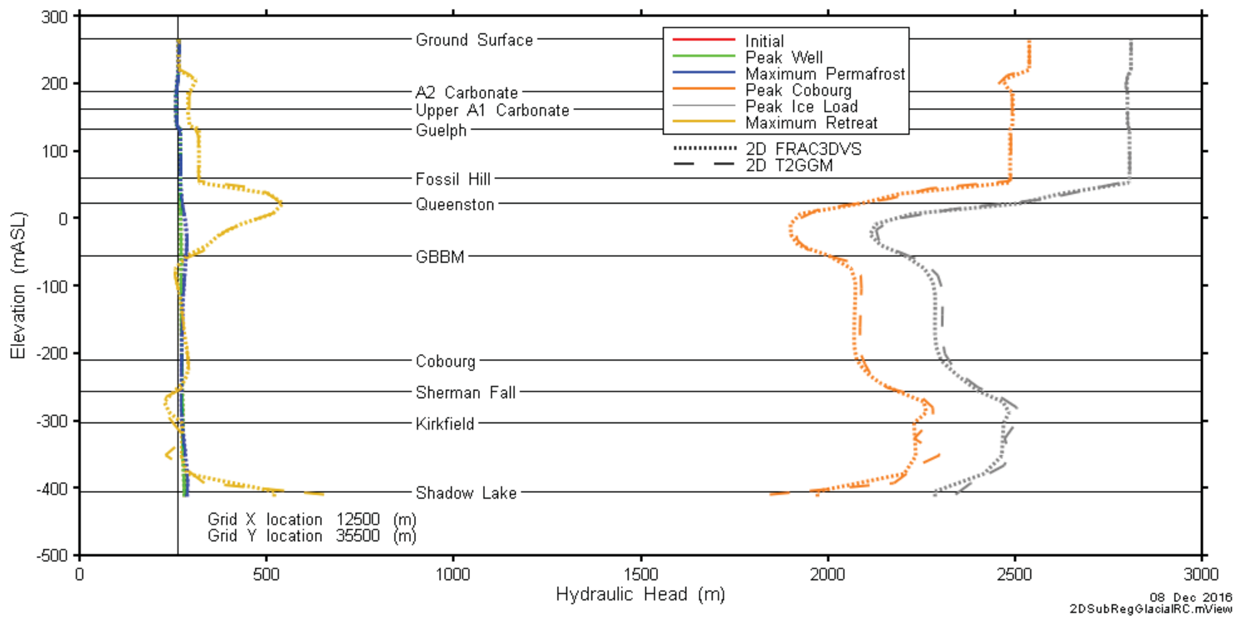

Figure 4-139: 2D Glaciation Sub-Regional Glacial Cycle Simulations: Hydraulic Head Profiles at Water-Supply Well Location for the First Cycle

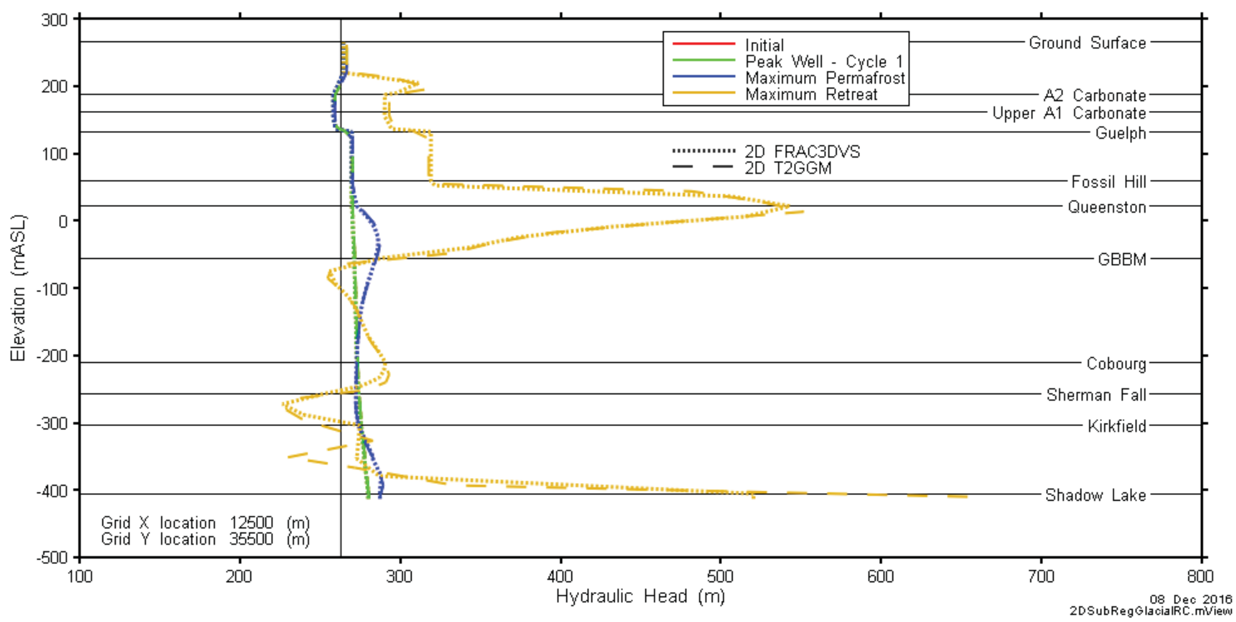

Figure 4-140: 2D Glaciation Sub-Regional Glacial Cycle Simulations: Hydraulic Head Profiles at Water-Supply Well Location (Detail) for the First Cycle

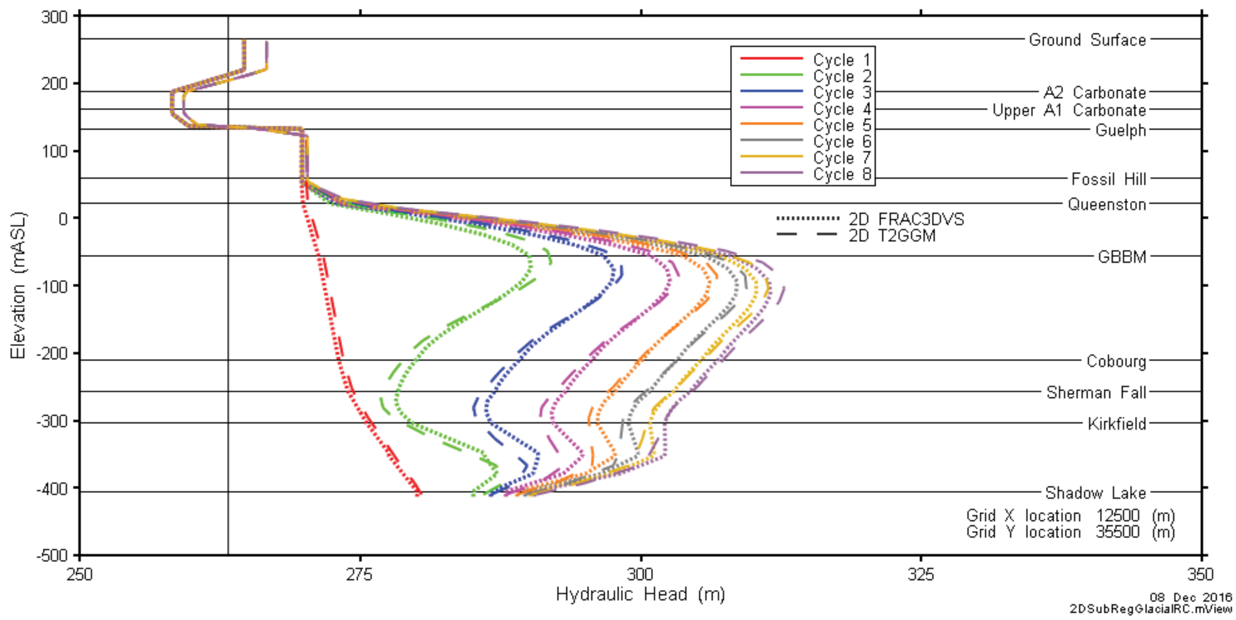

Figure 4-141: 2D Sub-Regional Glacial Cycle Simulations: Hydraulic Head Profiles at Water-Supply Well Location at Time of Maximum Well Impact for all Cycles

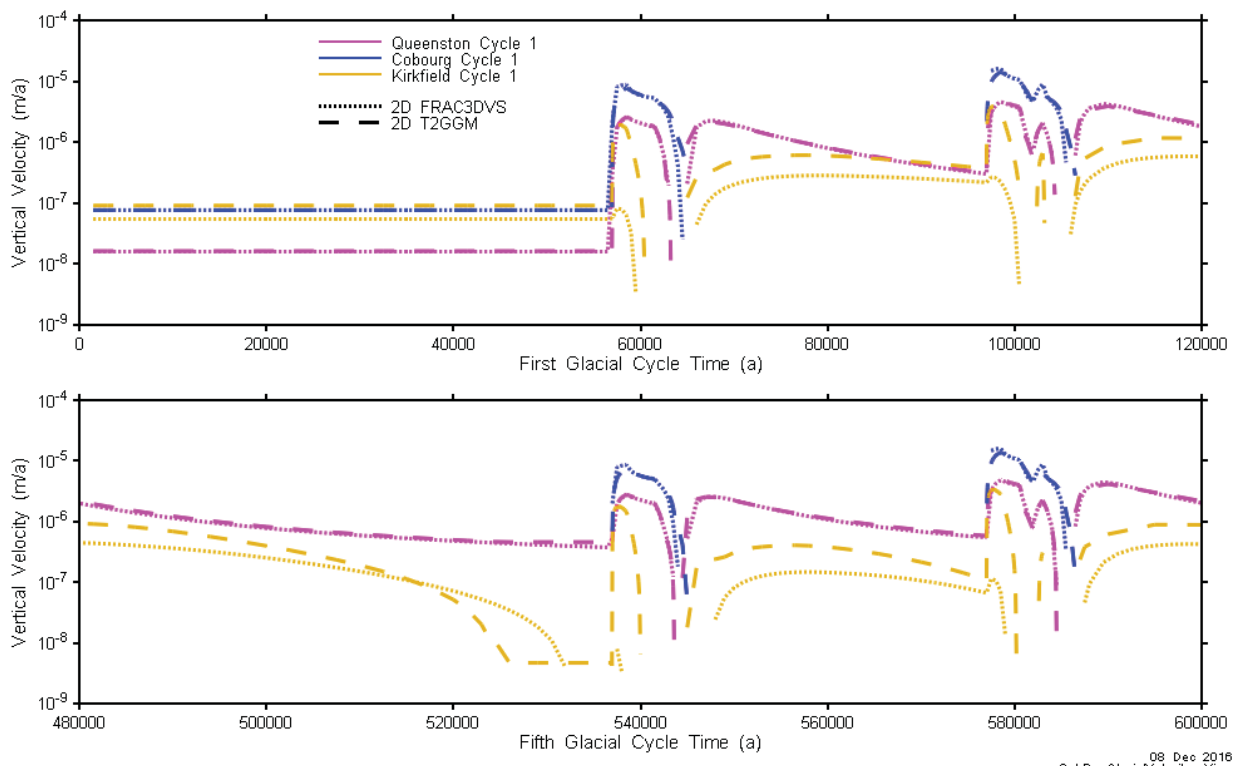

Figure 4-142: 2D Glaciation Sub-Regional Glacial Cycle Simulations: Maximum Vertical Velocity in Repository Vicinity and Selected Formations for the First and Fifth Cycles

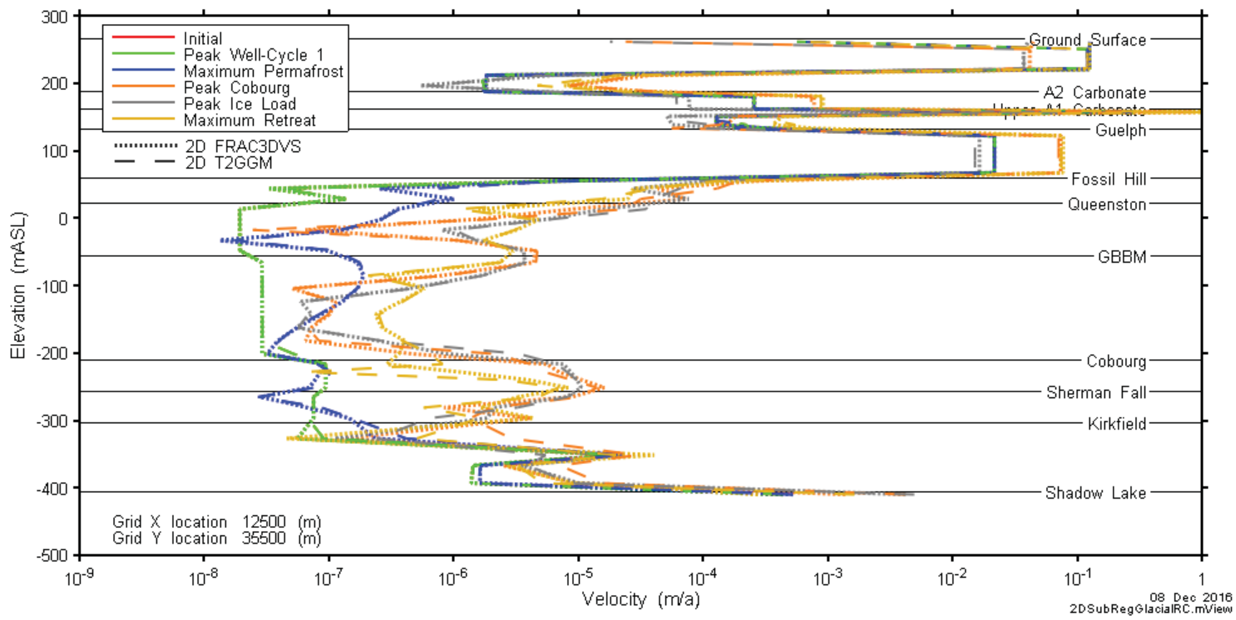

Figure 4-143: 2D Glaciation Sub-Regional Glacial Cycle Simulations: Velocity Magnitude Profiles at Water-Supply Well Location for the First Cycle

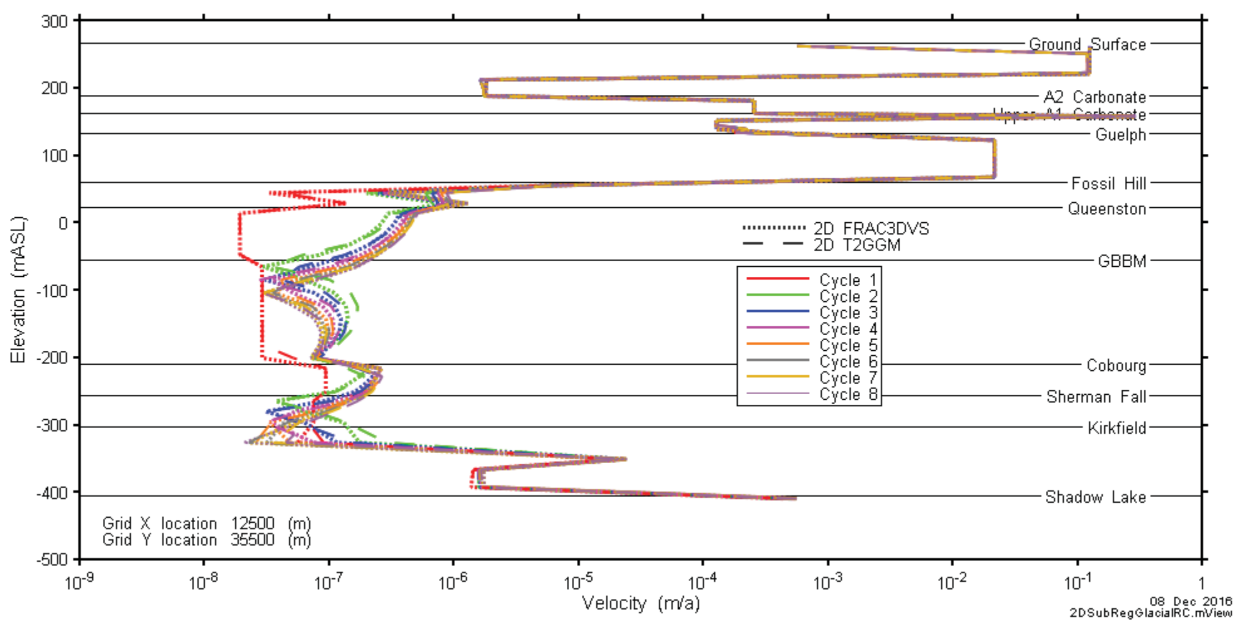

Figure 4-144: 2D Glaciation Sub-Regional Glacial Cycle Simulations: Velocity Magnitude Profiles at Water-Supply Well Location at Time of Maximum Well Impact for All Cycles

4.3.3 Two-Phase Flow with 10% Gas in the Ordovician

The two-phase flow model takes the 2D T2GGM model described in Section 4.3.2 and adds initial gases in the Ordovician units at a gas saturation of 10%. Sensitivity cases exploring different initial gas saturations are presented in the following section. The gas in the Ordovician is assumed to be methane, with a Henry's coefficient of 7.2×10^{-11} Pa^{-1} (Quintessa and Geofirma, 2011). Two-phase formation parameters are detailed in Appendix A.

As expected, the greater compressibility of gas significantly moderates the increase in head during glacial loading, as shown in Figure 4-145 for the first glacial cycle, where the times coinciding with glacial loading are the time of Peak Cobourg (orange) and Peak Ice load (grey). Gas saturations during glacial loading also decrease, as shown in Figure 4-146, due to the greater compression of gas relative to water during loading, resulting in a smaller volumetric ratio of gas (gas saturation is a volumetric ratio of gas to pore volume). Gas saturations begin to vary between formations, due to different capillary pressures in each zone, with gas preferring formations with lower capillary pressure.

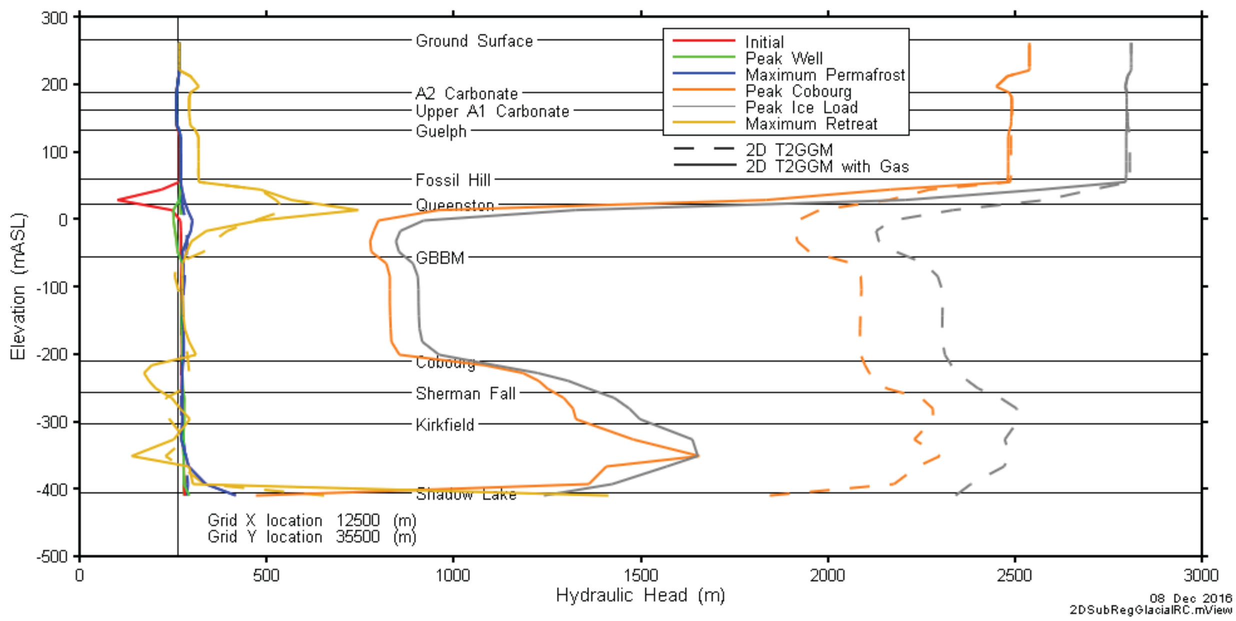

Figure 4-145: 2D Glaciation Sub-Regional Glacial Cycle Simulations with 10% Gas in the Ordovician: Hydraulic Head Profiles at Water-Supply Well Location for the First Cycle

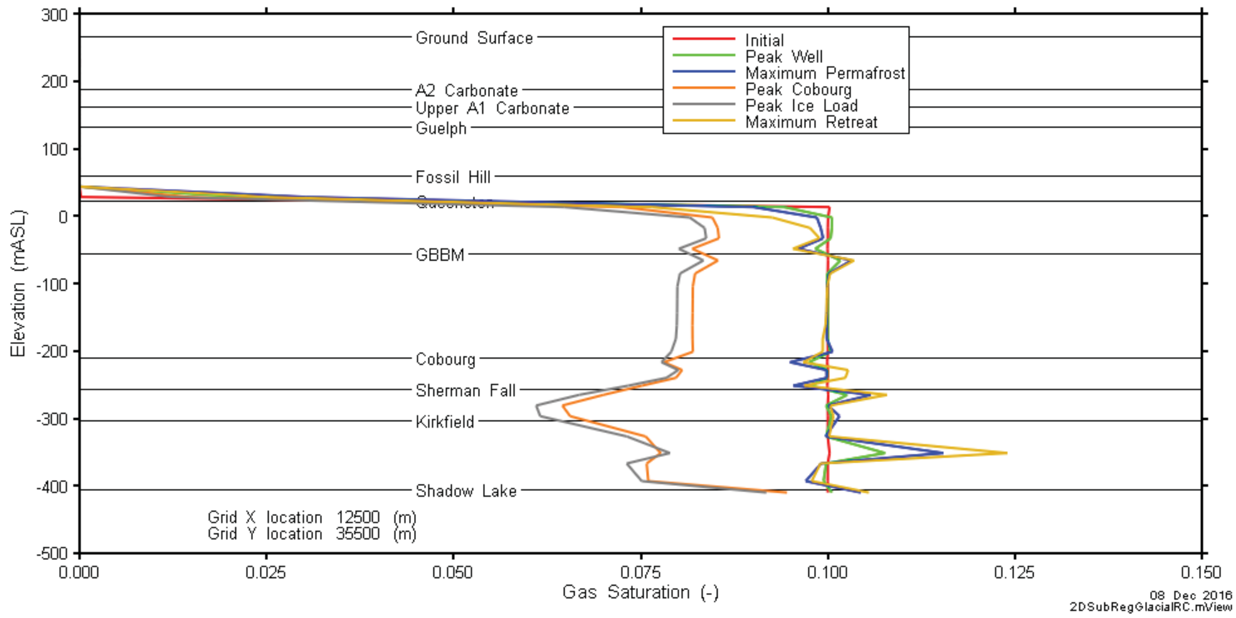

Figure 4-146: 2D Glaciation Sub-Regional Glacial Cycle Simulations with 10% Gas in the Ordovician: Gas Saturation Profiles at Water-Supply Well Location for the First Cycle

Moderation of heads during glacial cycles does not translate to a moderation of vertical velocities. Upward vertical velocities are of interest from a transport perspective. Figure 4-147 provides the maximum vertical velocities in three Ordovician formations during the first and fifth cycles. The pattern in velocity is similar between the first and fifth cycles, excepting differences prior to the first glacial cycle, attributed to the effects of initial conditions. Upward vertical velocities are increased in the Cobourg and Kirkfield formations, due to differences in the vertical head profile, such as an increase in head gradient during glacial loadings seen in Figure 4-145. Upward velocities are also greater in the Queenston, except during glacial loading when upward velocities are actually decreased.

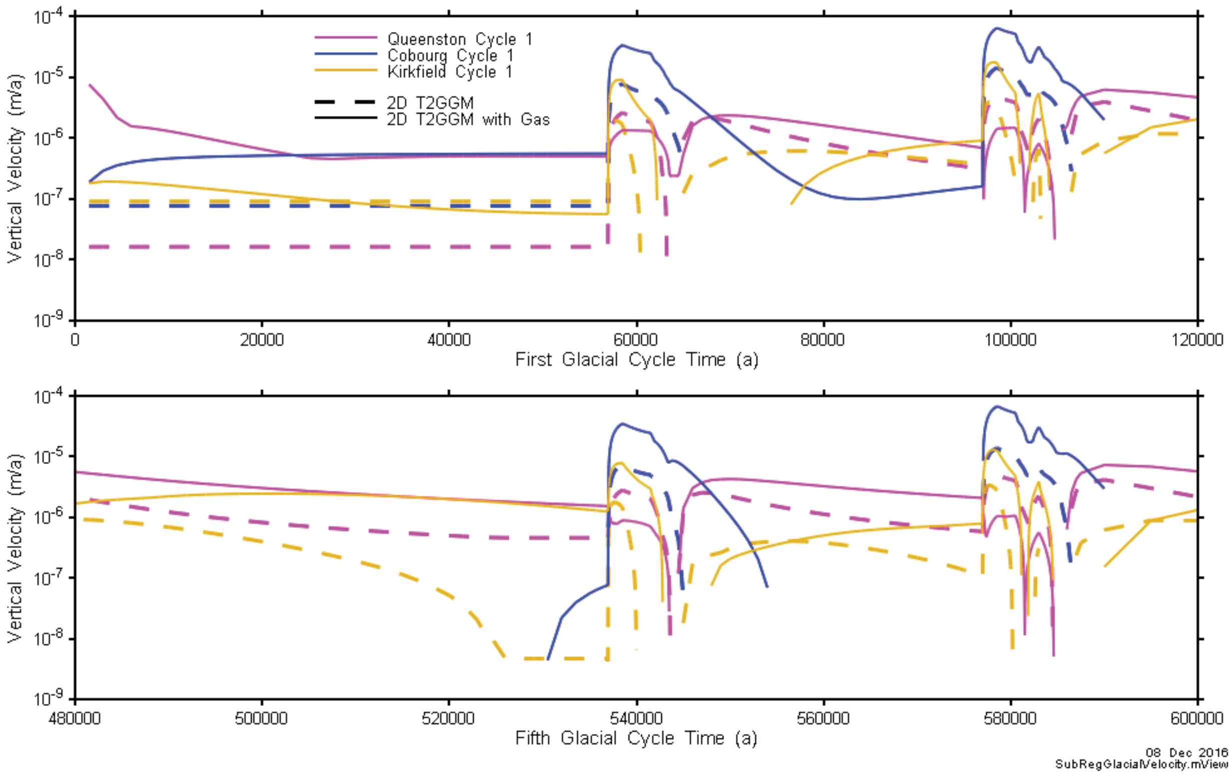

Figure 4-147: 2D Glaciation Sub-Regional Glacial Cycle Simulations with 10% Gas in the Ordovician: Maximum Vertical Velocity in Repository Vicinity and Selected Formations for the First and Fifth Cycles

Figure 4-148 through Figure 4-152 show the velocity field at event times within the first glacial cycle. Figure 4-153 provides the velocity profile at the well location during the first cycle at the same event times and compares it to the results from the fully water saturated case. As with maximum vertical velocities shown above, compared to the fully water saturated case velocities are increased in many formations, including the Cobourg formation.

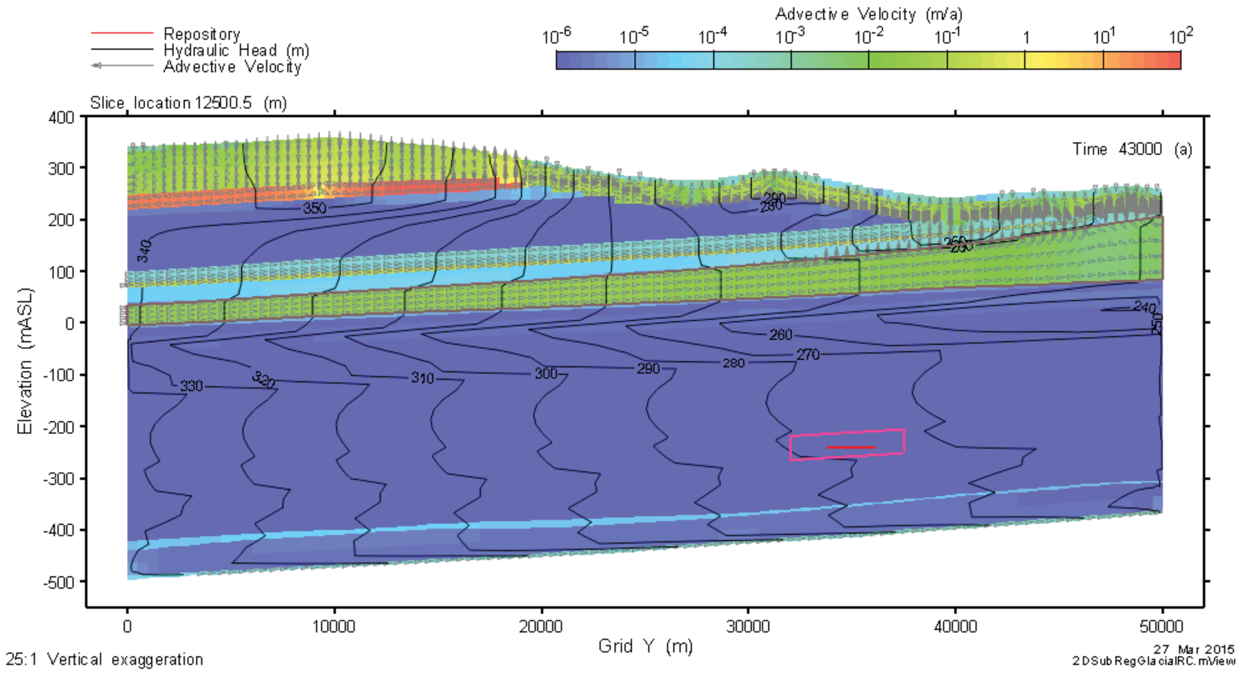

Figure 4-148: 2D Glaciation Sub-Regional Glacial Cycle Simulations with 10% Gas in the Ordovician: Advective Velocity and Hydraulic Head at Time of First Cycle Peak Well Operation (T = 43,000 a)

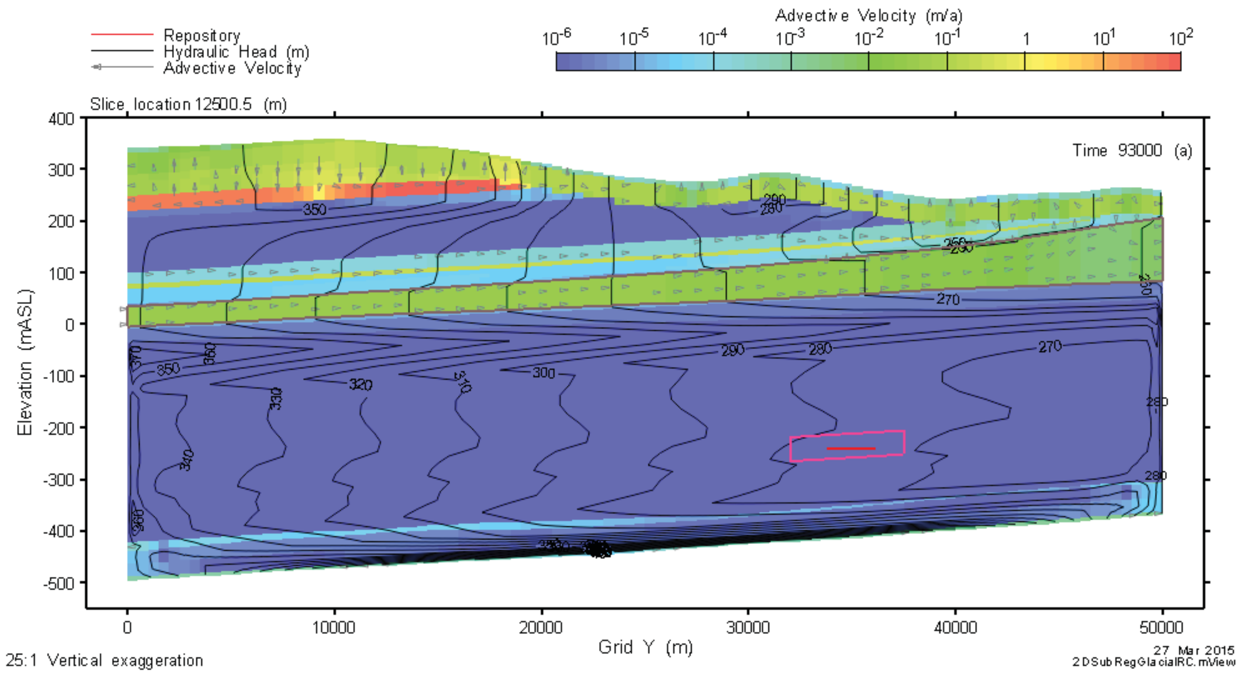

Figure 4-149: 2D Glaciation Sub-Regional Glacial Cycle Simulations with 10% Gas in the Ordovician: Advective Velocity and Hydraulic Head at Time of Maximum Permafrost (T = 93,000 a).

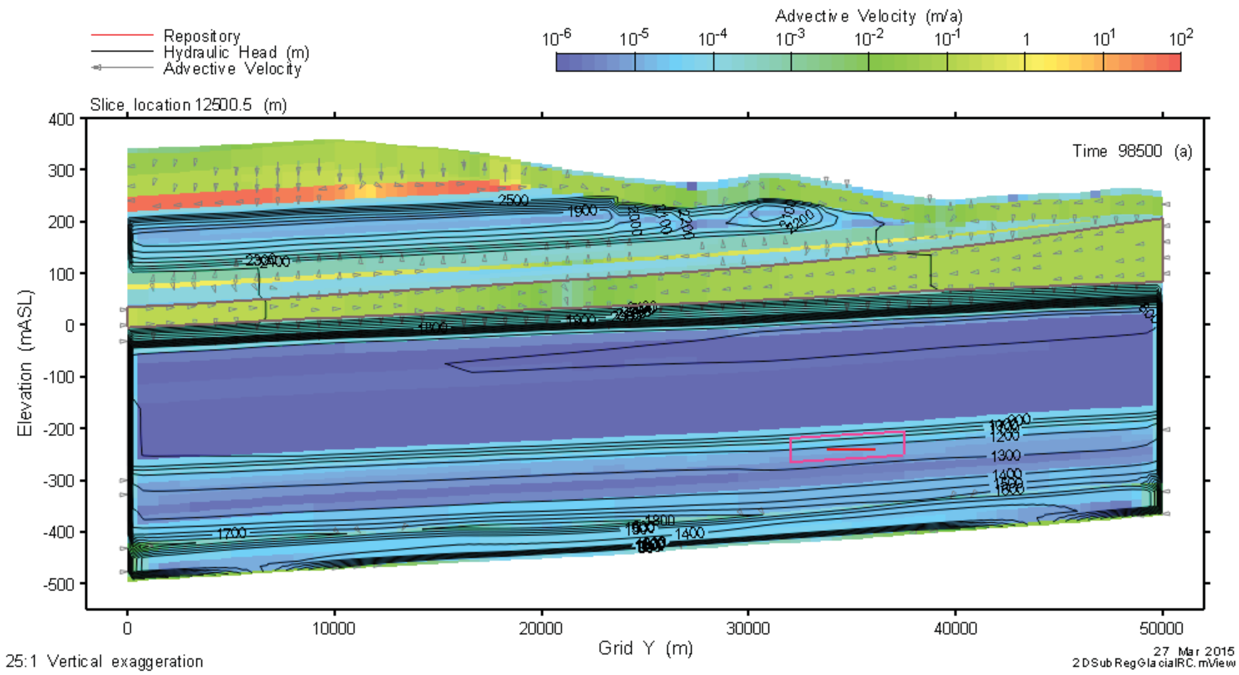

Figure 4-150: 2D Glaciation Sub-Regional Glacial Cycle Simulations with 10% Gas in the Ordovician: Advective Velocity and Hydraulic Head at Time of Peak Upward Velocities in Cobourg Formation at Repository (T = 98,500 a)

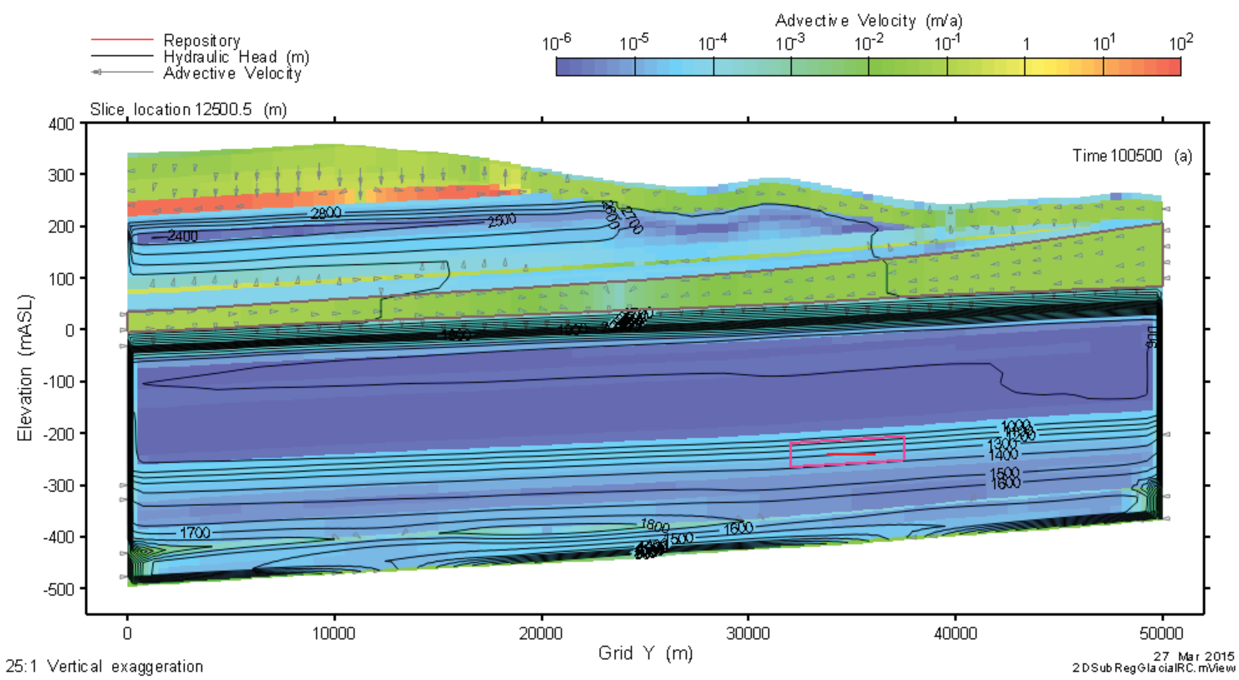

Figure 4-151: 2D Glaciation Sub-Regional Glacial Cycle Simulations with 10% Gas in the Ordovician: Advective Velocity and Hydraulic Head at Time of Maximum Glacial Load at Repository (T = 100,500 a)

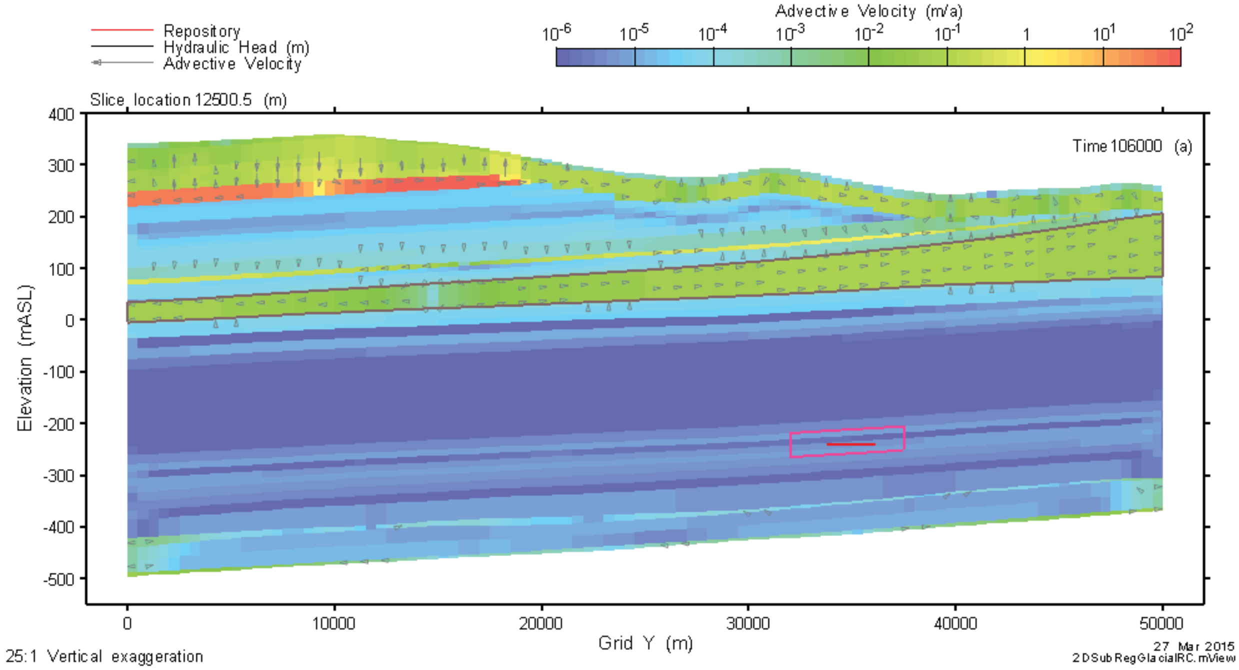

Figure 4-152: 2D Glaciation Sub-Regional Glacial Cycle Simulations with 10% Gas in the Ordovician: Advective Velocity and Hydraulic Head at Time of Maximum Glacial Retreat at Repository (T = 106,000 a)

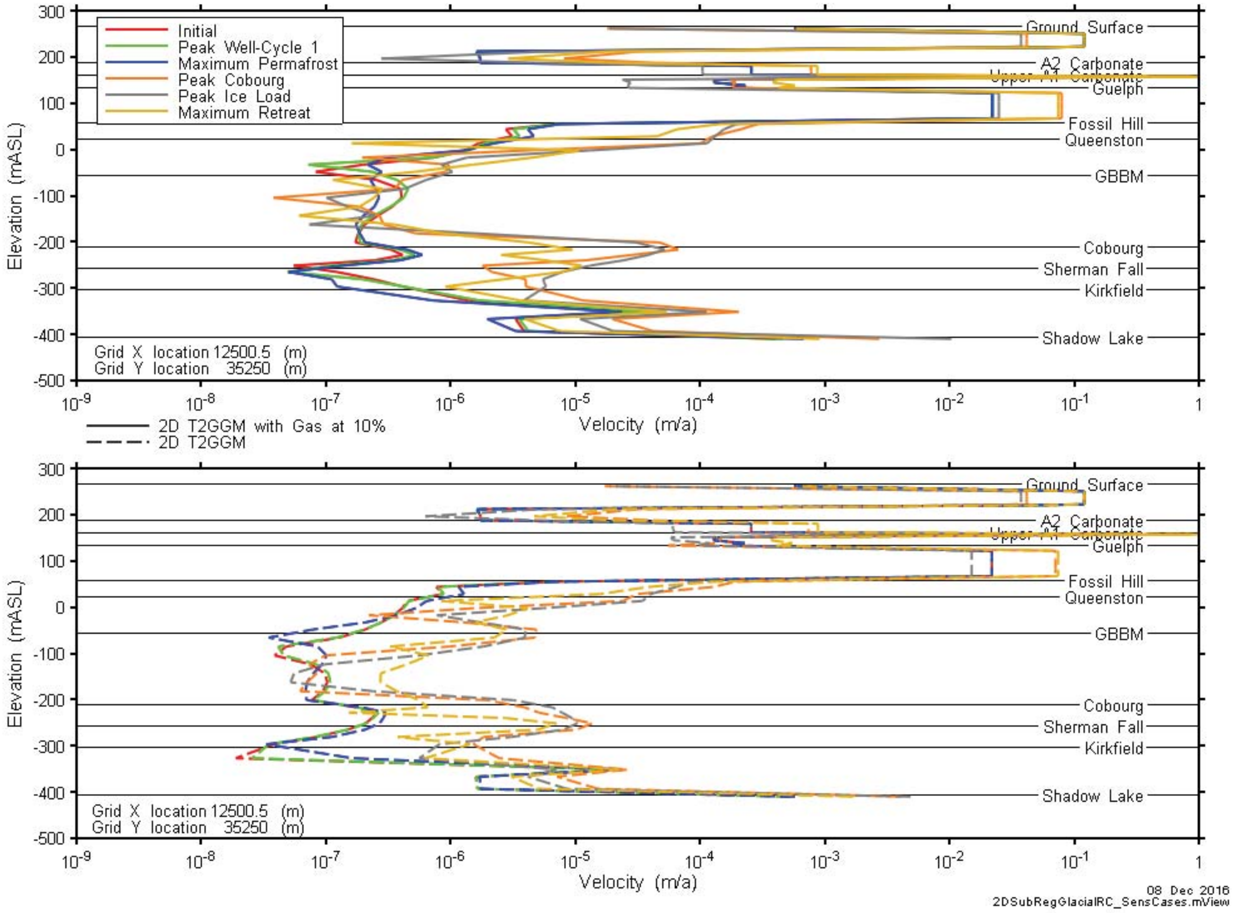

Figure 4-153: 2D Glaciation Sub-Regional Glacial Cycle Simulations with 10% Gas in the Ordovician Compared to Water-Saturated Case: Velocity Magnitude Profiles at Water-Supply Well Location for the First Cycle

Two-phase flow not only impacts the groundwater flow regime, but adds an additional potential pathway for transport through the flow of the gas phase. Figure 4-154 shows upward gas flow at the Cobourg and Queenston formation tops. Gas flows steadily decrease during the course of the simulation, with additional reductions in gas flow during glacial loading events. In the Queenston formation, gas flow direction reverses for a short time during the second glacial loading of each cycle, flowing downward during this time. Gas flow in the Kirkfield formation is not shown as the flow is effectively zero.

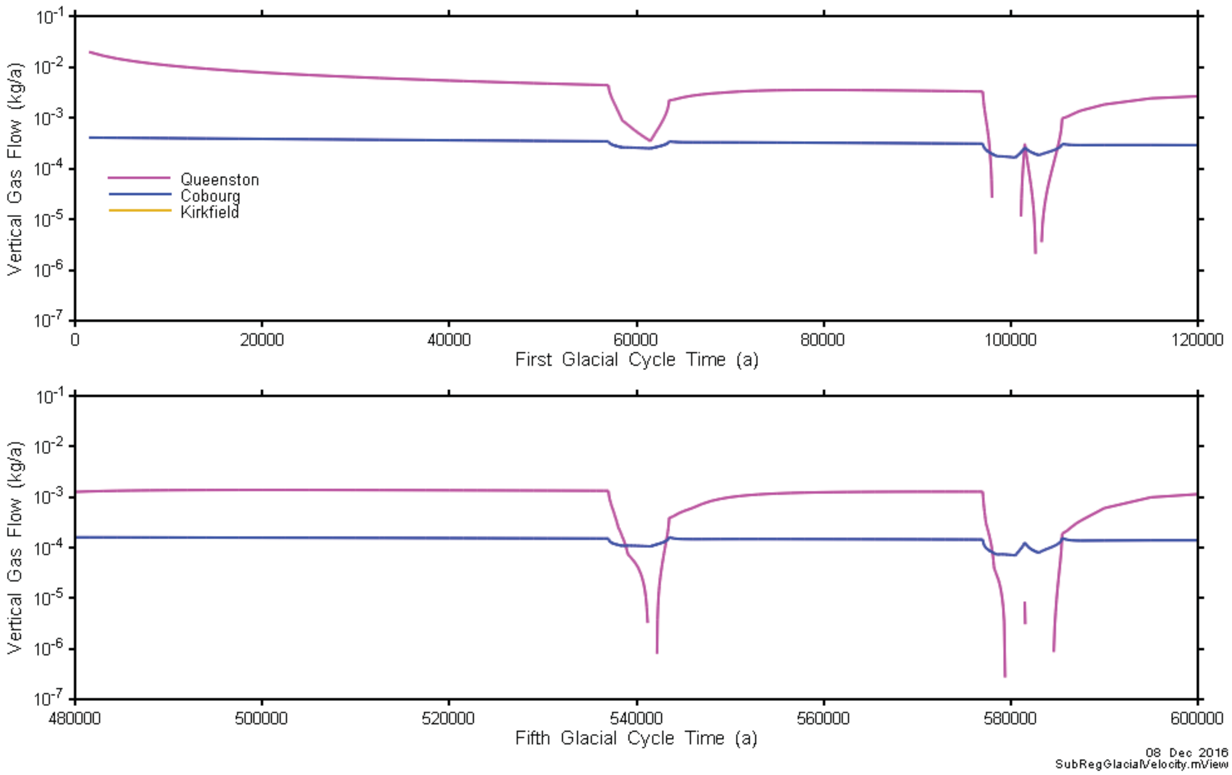

Figure 4-154: 2D Glaciation Sub-Regional Glacial Cycle Simulations with 10% Gas in the Ordovician: Maximum Vertical Gas Flow in Repository Vicinity and Selected Formations for the First and Fifth Cycles

Cumulative effects of glacial loading on hydraulic head are slightly greater with gas present, but are still small relative to the fluctuations in head due to glacial loading. After the first cycle, heads do not return to values near the initial heads, as in the case with no gas present, and there is a small increase in head with each cycle. Figure 4-155 shows the heads at various depths with time. Figure 4-156 shows the head profile at the time of maximum well operation for each glacial cycle. There is no well in the 2D model, but the time of maximum well operation occurs during the longest period of recovery between glacial loadings, and is used for consistency with previous results. Figure 4-156 shows the cumulative head change which follows a similar pattern to the fully water saturated case, but with greater overpressures generated by the successive glacial cycles. The cumulative head change in the Cobourg formation is approximately 65 m, compared to 30 m in the fully water saturated case.

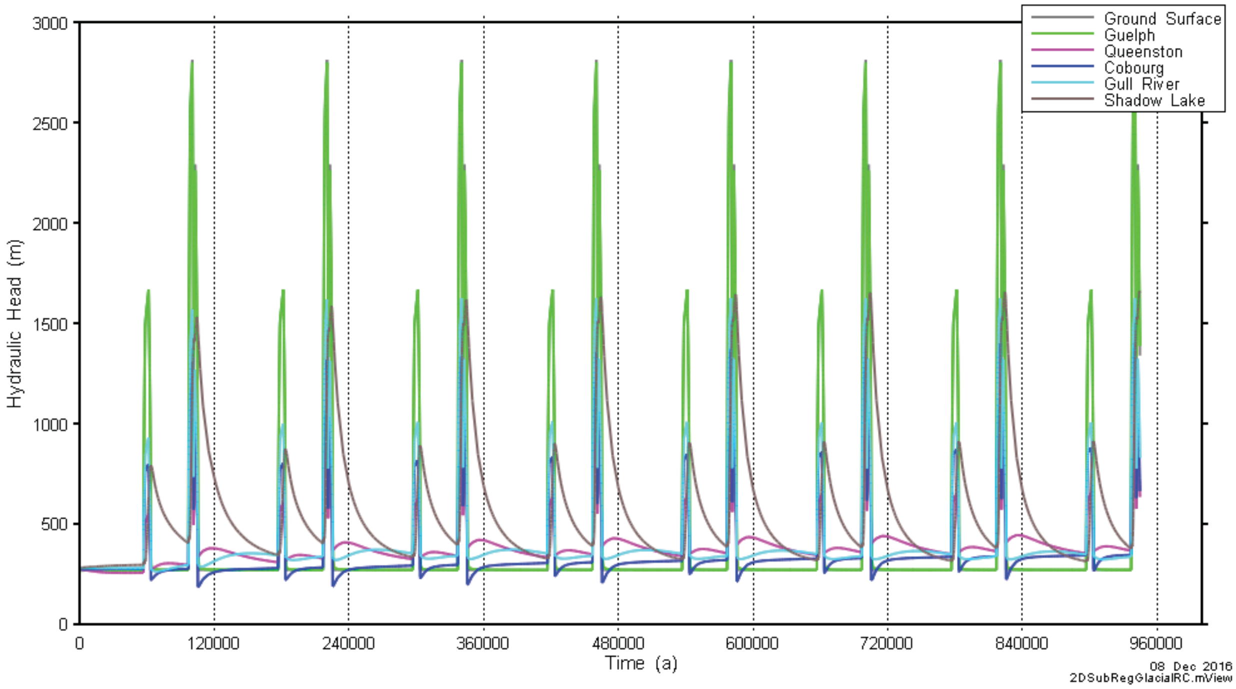

Figure 4-155: 2D Glaciation Sub-Regional Glacial Cycle Simulations with 10% Gas in the Ordovician: Hydraulic Head at Repository Location (X = 12,500.5 m, Y = 35,000 m) and Selected Formations

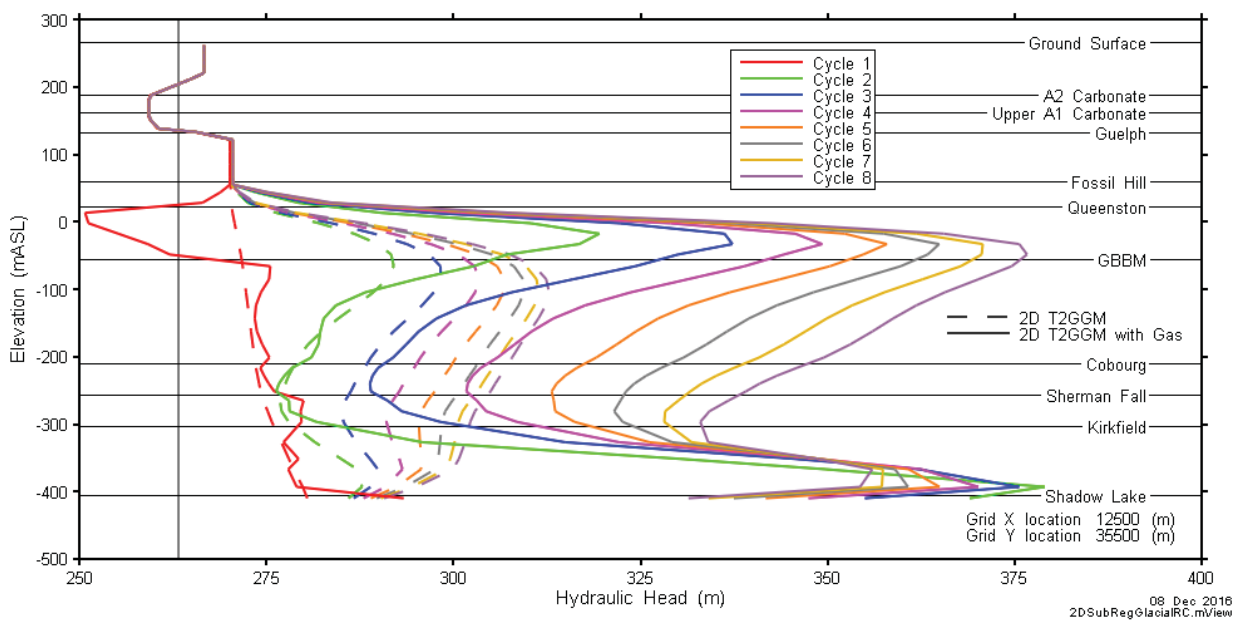

Figure 4-156: 2D Glaciation Sub-Regional Glacial Cycle Simulations with 10% Gas in the Ordovician: Hydraulic Head Profiles at Water-Supply Well Location at Time of Maximum Well Impact for All Cycles

There is little cumulative impact of glacial cycles on gas saturation, with the gas saturation in most formations remaining near 10% at the time of maximum well operation in each cycle, as illustrated in Figure 4-157. The biggest cumulative change in gas saturation occurs in the formations with the greatest or lowest capillary pressures. Formations with greater gas saturations have relatively low capillary pressures, and similarly, formations with low gas saturations have relatively high capillary pressures. For example, at the time of maximum well operation in Cycle 8, the Coboconk formation has a gas saturation of 0.18, and a capillary pressure of 20 MPa. The Kirkfield formation above the Coboconk has a capillary pressure of 24 MPa and gas saturation of 0.1, and the Gull River Formation below has a capillary pressure of 26 MPa and a gas saturation of 0.09. Some of the formations have variable gas saturations, with the gas saturation at the transition between formations having a higher or lower gas saturation, depending on the differences in capillary pressure between formations. For example, the Cobourg formation has a gas saturation of 0.09 in the middle two layers, and a gas saturation of 0.075 at the top and bottom of the formation.

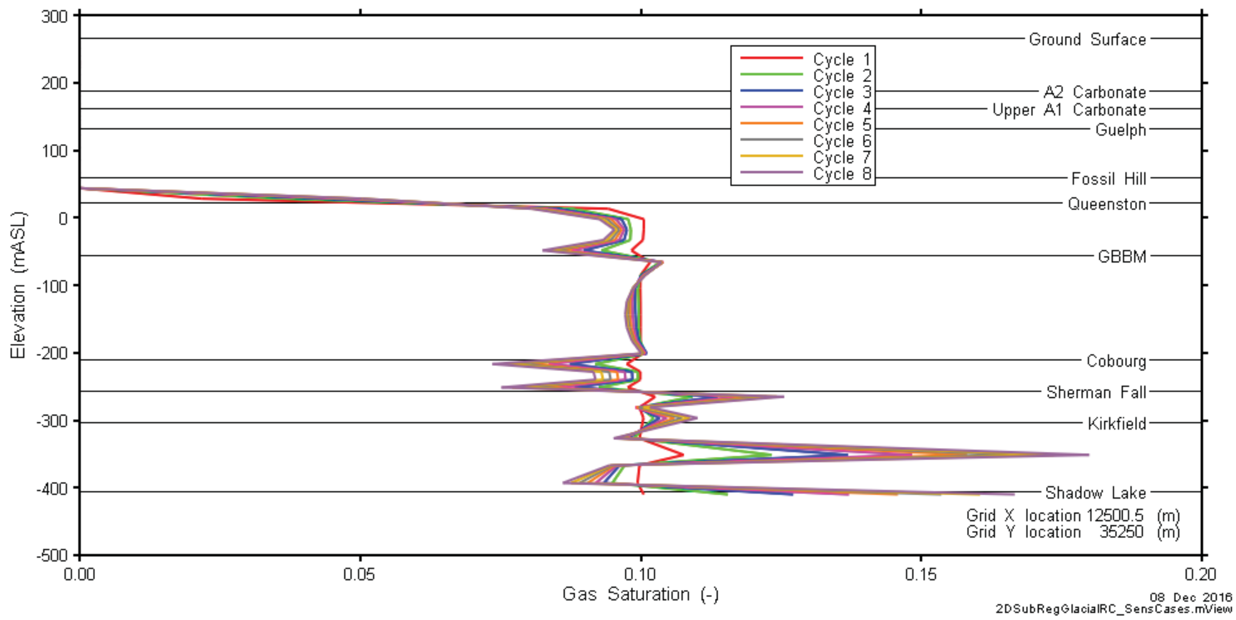

Figure 4-157: 2D Glaciation Sub-Regional Glacial Cycle Simulations with 10% Gas in the Ordovician: Gas Saturation Profiles at Water-Supply Well Location at Time of Maximum Well Impact for All Cycles

There is also little cumulative impact on velocities, as shown in Figure 4-158. Particularly in the Georgian Bay and Blue Mountain Formation, there is an increase in velocity between the first and third cycles, after which the velocity change is small. Within the Cobourg, the velocity profile changes between each cycle, making changes in magnitude more difficult to discern; However, there is a five-fold increase in velocity in the middle of the Cobourg between the first and eighth cycle. In the fully-water saturated case, the velocity in the middle of the Cobourg increases by approximately 2.5 between the first and eighth cycle (see Figure 4-144).

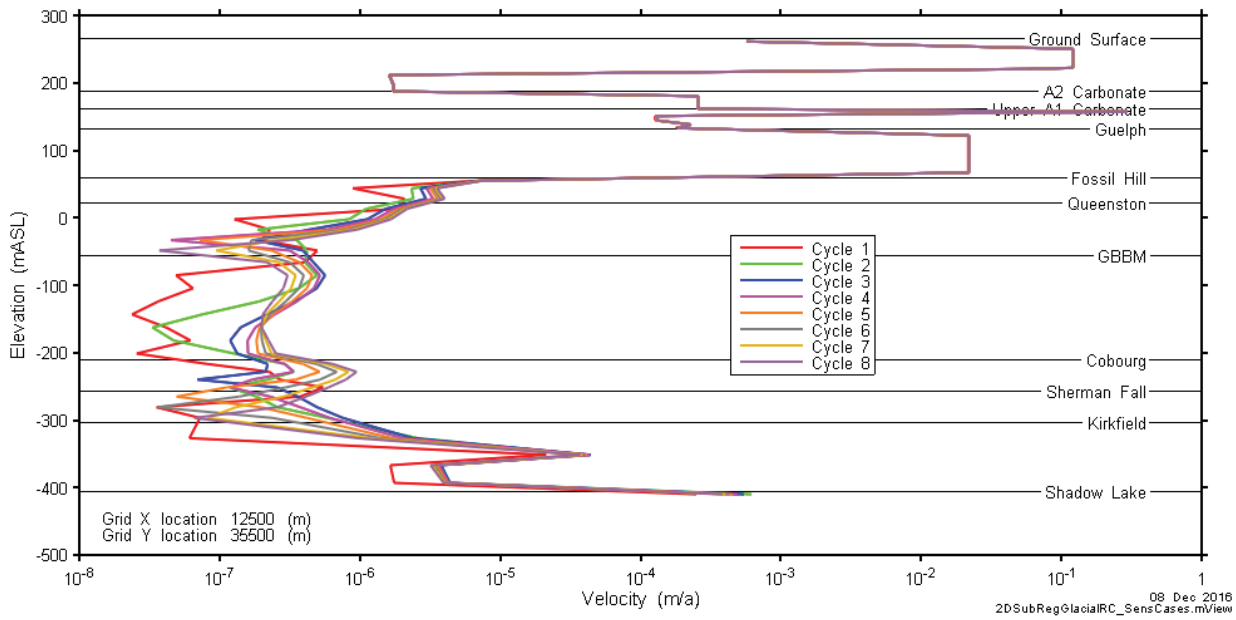

Figure 4-158: 2D Glaciation Sub-Regional Glacial Cycle Simulations with 10% Gas in the Ordovician: Velocity Magnitude Profiles at Water-Supply Well Location at Time of Maximum Well Impact for All Cycles

4.3.4 Two-Phase Flow Sensitivity Cases

The sensitivity of the groundwater flow regime to initial gas saturations in the Ordovician units was investigated by applying initial gas saturations of 15%, 5% and 2%.

Figure 4-159 provides the head in the middle of the repository during the fifth glacial cycle for all four initial gas saturation cases and the fully-water saturated case. Figure 4-160 and Figure 4-161 provide the head profile for the fifth cycle, and Figure 4-162 provides the gas saturation profile for the fifth cycle, for all four initial gas saturations (15%, 10%, 5% and 2%). As expected, the 2% and 5% gas saturation cases moderate glacially induced heads less than the 10% gas saturation case, whereas the 15% case moderates the heads even further. In all cases, gas moves between formations, with final gas saturations greatest in formations with low capillary pressures. The differences in gas saturation are most marked at the bottom of the model in the 15% initial gas saturation case where the post-glacial retreat gas saturation in the Coboconk (the formation below the Kirkfield formation) is almost 30%, twice the initial gas saturation, and gas saturation in the Gull River (between Shadow Lake and Coboconk) decreased to 11%.

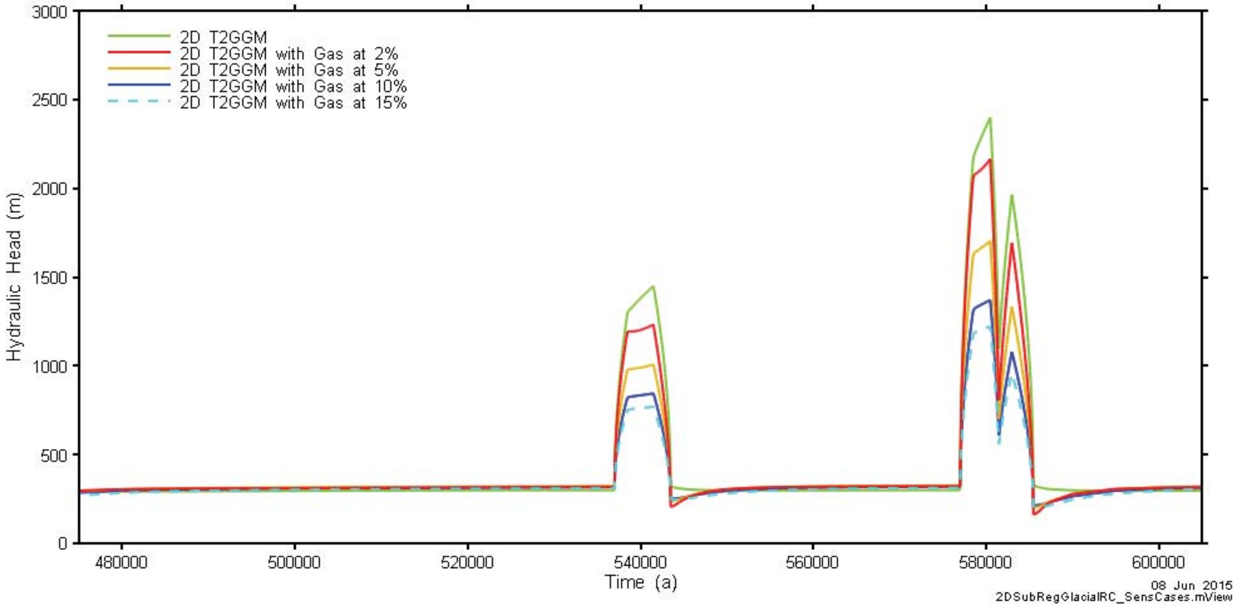

Figure 4-159: 2D Glaciation Sub-Regional Glacial Cycle Simulations with 15%, 10%, 5% and 2% Gas in the Ordovician – Parameter Sensitivity Detail: Hydraulic Head in Centre of Repository Over Fifth Glacial Cycle

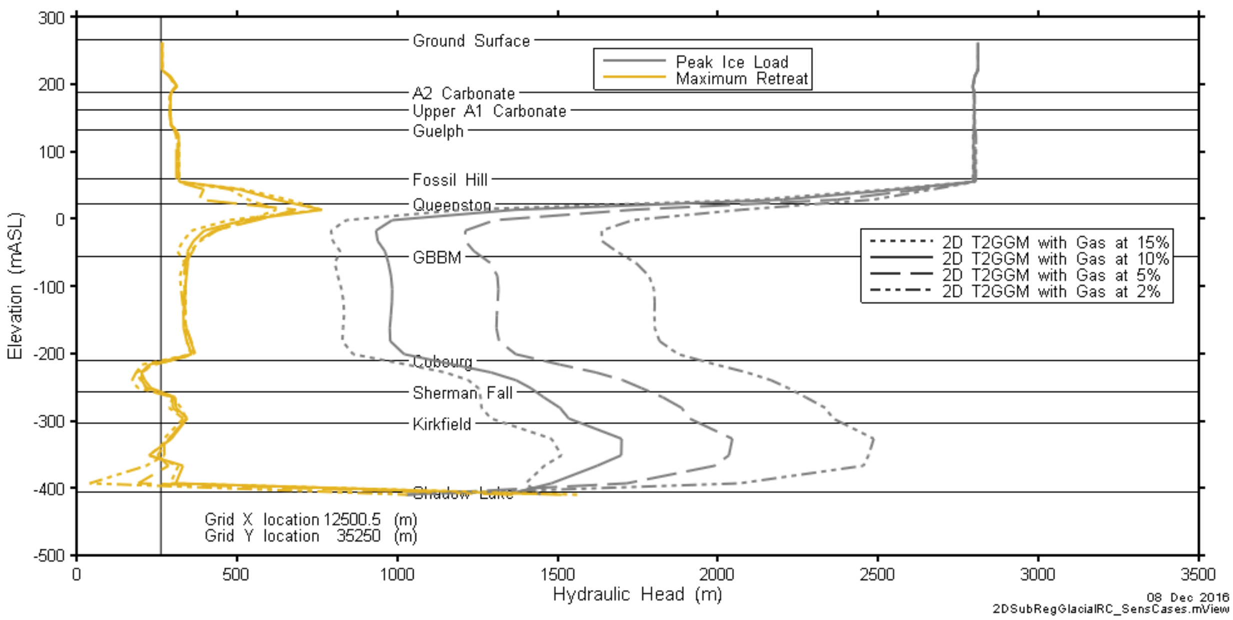

Figure 4-160: 2D Glaciation Sub-Regional Glacial Cycle Simulations with 10%, 5% and 2% Gas in the Ordovician: Hydraulic Head Profiles at Water-Supply Well Location for the Fifth Cycle

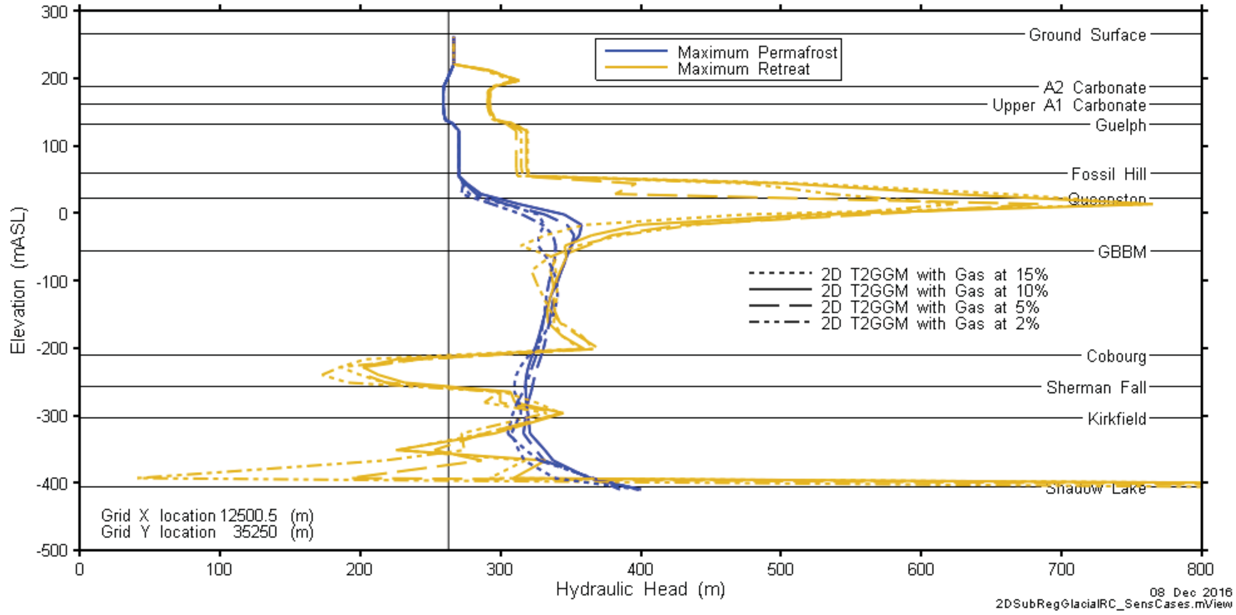

Figure 4-161: 2D Glaciation Sub-Regional Glacial Cycle Simulations with 10%, 5% and 2% Gas in the Ordovician: Hydraulic Head Profiles at Water-Supply Well Location (Detail) for the Fifth Cycle

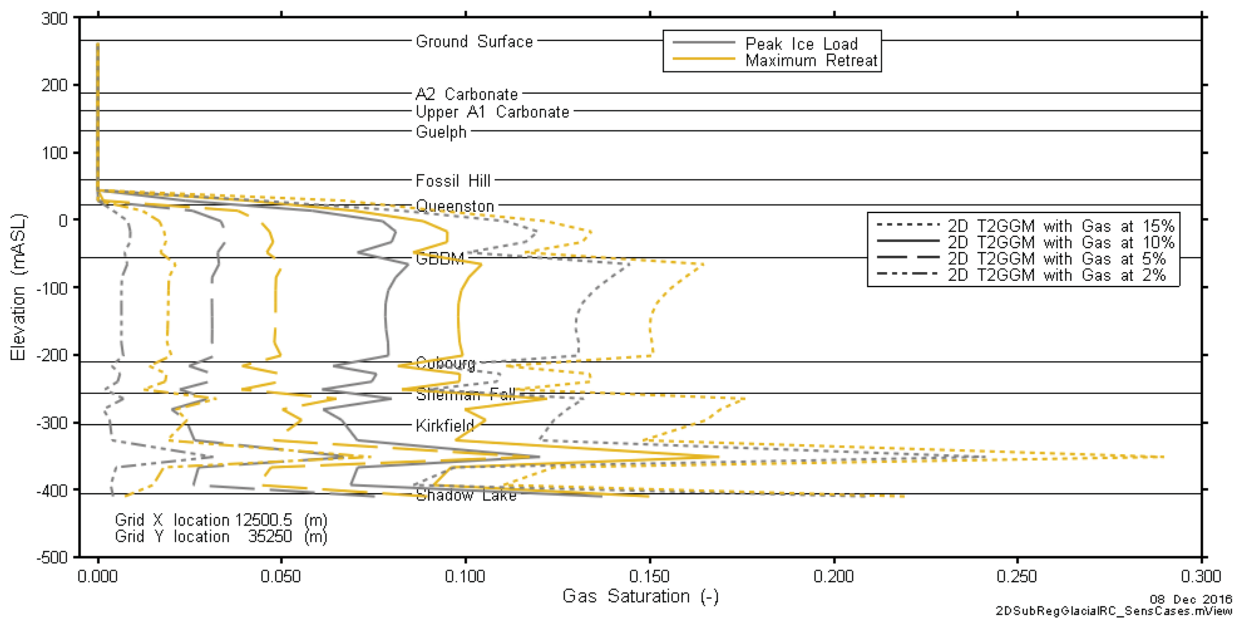

Figure 4-162: 2D Glaciation Sub-Regional Glacial Cycle Simulations with 10%, 5% and 2% Gas in the Ordovician: Gas Saturation Profiles at Water-Supply Well Location for the Fifth Cycle

Figure 4-163 shows the maximum advective velocity in the repository for the three gas saturation cases compared to the fully-water saturated cases, and Figure 4-164 shows the maximum upward vertical advective velocity in the repository for the fifth glacial cycle. The presence of gas causes an increase in velocity, due to the head gradients induced by differences in gas saturation and capillary pressure, with similar peak velocities regardless of the initial gas saturation. Peak velocities occur during periods of glacial loading. The reduction in velocity during non-glacial loading periods approaches the same value with each passing cycle, with the exception of the 15% initial gas saturation case. Maximum vertical velocities during non-glacial loading periods are downwards, and are therefore not shown in the log scale of Figure 4-164 where only upwards velocities are positive.

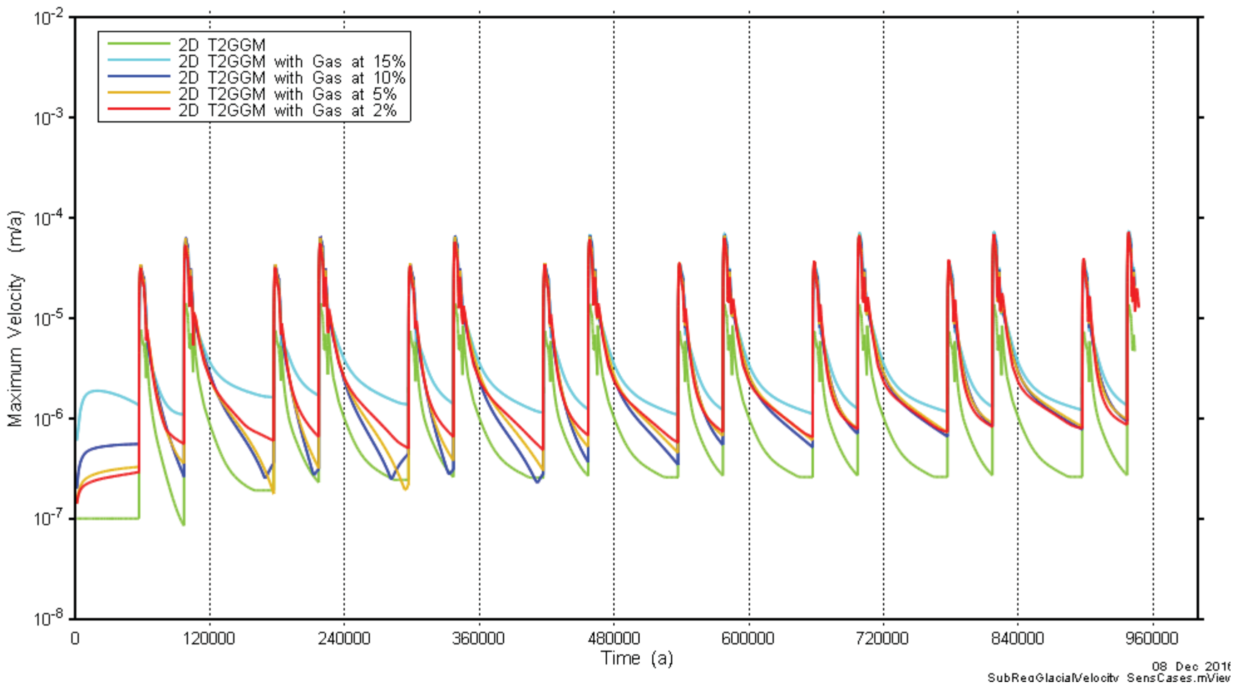

Figure 4-163: 2D Glaciation Sub-Regional Glacial Cycle Simulations with 15%, 10%, 5% and 2% Gas in the Ordovician: Maximum Advective Velocity Magnitude in Vicinity of Repository in Cobourg Formation

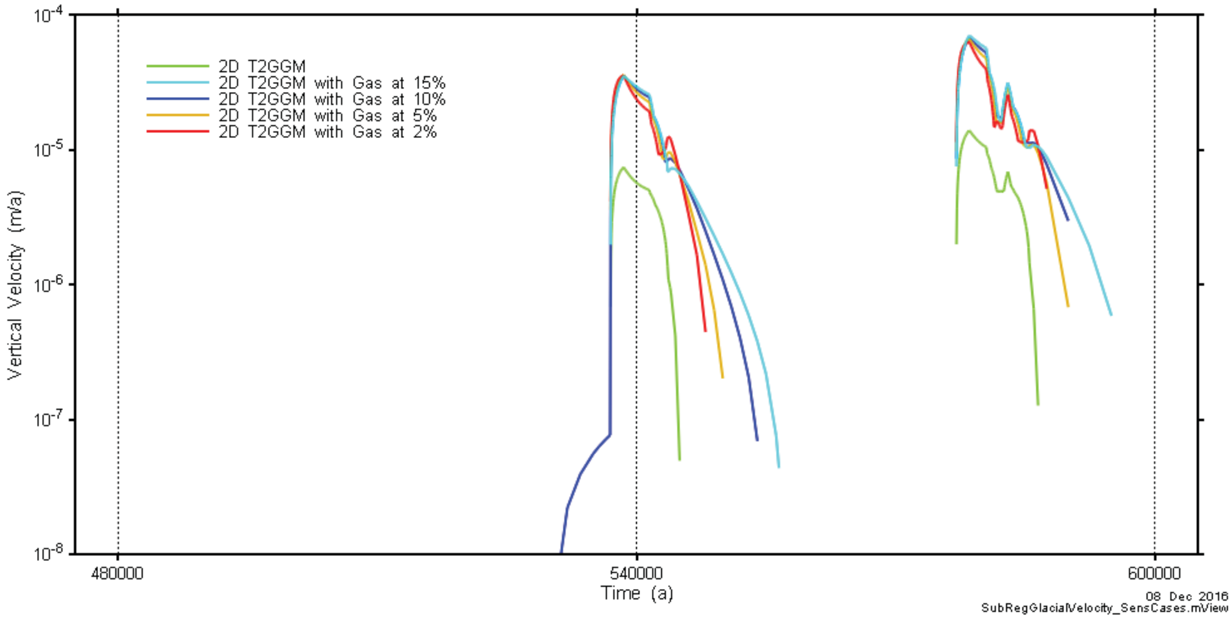

Figure 4-164: 2D Glaciation Sub-Regional Glacial Cycle Simulations with 10%, 5% and 2% Gas in the Ordovician: Maximum Vertical Advective Velocity Magnitude in Vicinity of Repository in Cobourg Formation Over Fifth Glacial Cycle

The cumulative impacts of glacial cycles on head, gas saturation and velocity are illustrated in Figure 4-165, Figure 4-166 and Figure 4-167, respectively. The cumulative head impact of the glacial cycles is similar for the four initial gas saturation cases, with the exception of the early cycles of the 15% case which show significant underpressures that dissipate after three cycles. These underpressures can be attributed to the movement of gas between formations to align with the capillary properties of each formation. The cumulative impacts on gas saturation are also similar for each case, with the magnitude of change during each cycle increasing with increasing gas saturation. Velocity profiles are more variable for cases with higher gas saturation, with the greatest changes occurring in the first few cycles.

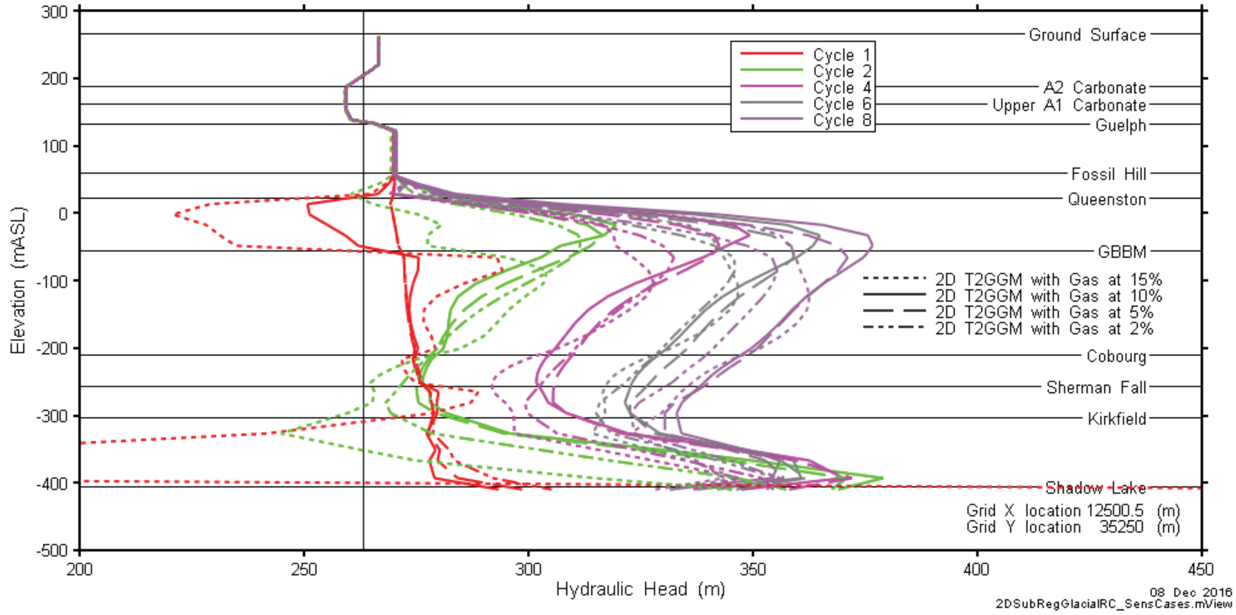

Figure 4-165: 2D Glaciation Sub-Regional Glacial Cycle Simulations with 10%, 5% and 2% Gas in the Ordovician: Hydraulic Head Profiles at Water-Supply Well Location at Time of Maximum Well Impact for Select Cycles

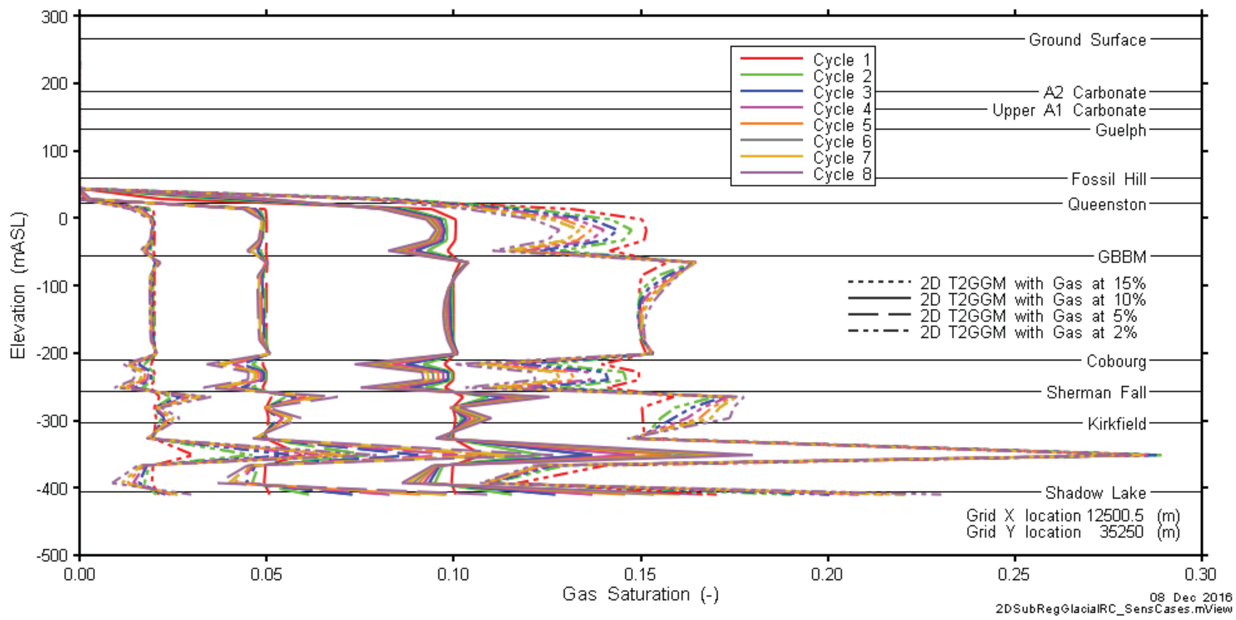

Figure 4-166: 2D Glaciation Sub-Regional Glacial Cycle Simulations with 10%, 5% and 2% Gas in the Ordovician: Gas Saturation Profiles at Water-Supply Well Location at Time of Maximum Well Impact for All Cycles

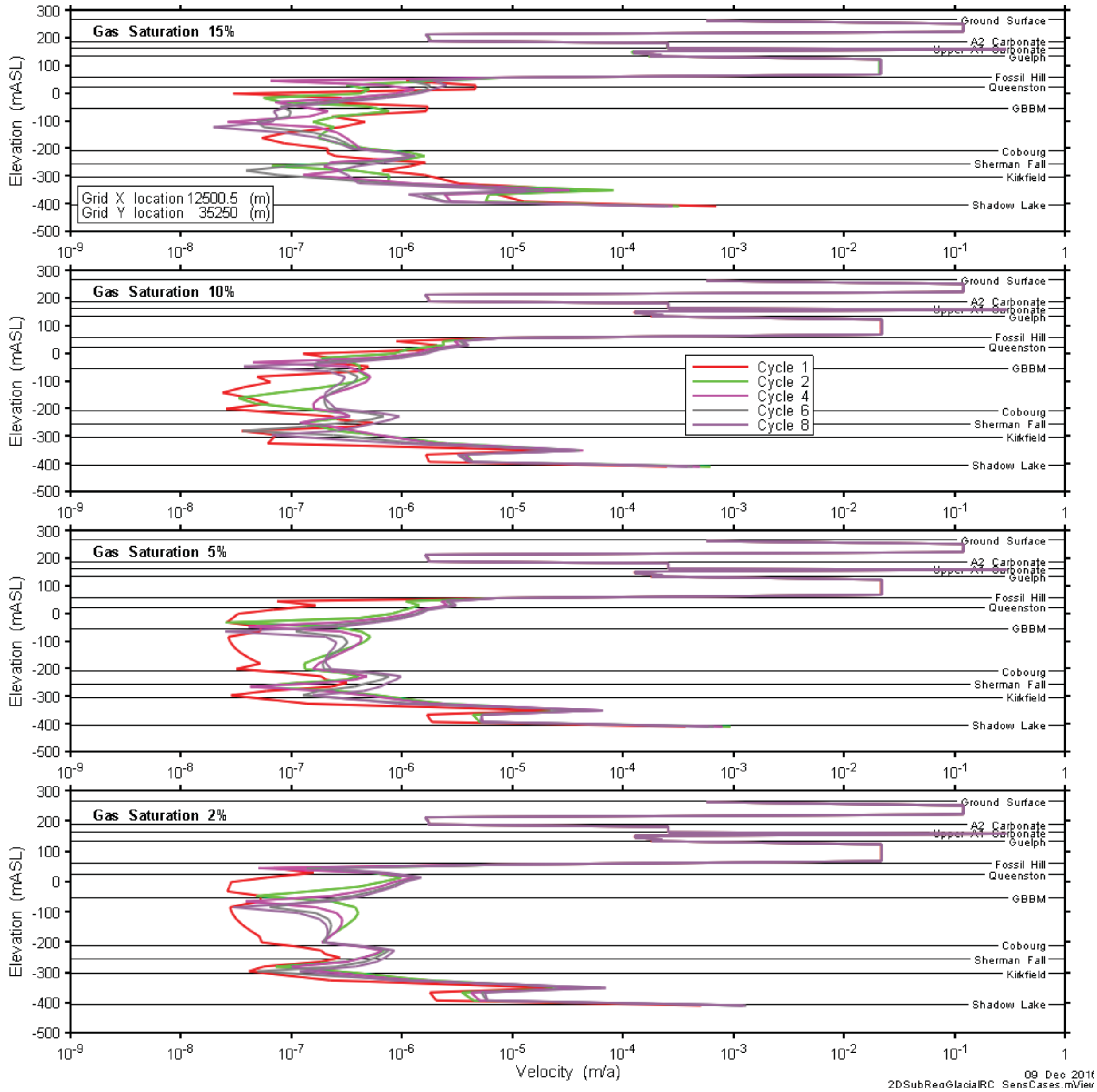

Figure 4-167: 2D Glaciation Sub-Regional Glacial Cycle Simulations with 15%, 10%, 5% and 2% Gas in the Ordovician: Velocity Magnitude Profiles at Water-Supply Well Location at Time of Maximum Well Impact for Select Cycles

5. EROSION SCENARIO

The erosion scenario expands the glaciation scenario to account for 100 m of erosion occurring over the 1 Ma performance period. This scenario assumes glacial cycles every 120 ka, with approximately 12.5 m of upper bedrock being removed each cycle. This will reduce the thickness of confining material isolating the repository from surface and will cause additional hydro-mechanical unloading due to overburden material removal. Two cases are assessed: uniform erosion, and valley erosion. Uniform erosion assumes each glacial retreat removes a constant thickness of material over the entire model domain. Valley erosion limits erosion by locally increased glacial scouring and creation of a valley directly above the repository due to channeling of the ice flow through local topographic variability. Assumptions for the erosion scenario were based on possible erosion phenomena applied conservatively for the purposes of this study.

The scenario is implemented similarly to the base glaciation scenario with two scales of modelling:

1. Erosion Sub-Regional Flow Model – the domain of the Erosion Sub-Regional Flow model differs from the Glaciation Sub-Regional Flow model in grid orientation and domain area, and has an increased number of layers to support adequate resolution of erosion processes. The model definition (discretization, property assignment, boundary conditions) and results are described in Section 5.1

2. Erosion Site-Scale Transport Model – the Site-Scale Model domain and initial properties are identical to the Glaciation Site Scale Transport model described in Section 4.2. Properties, boundary conditions, and execution sequencing are modified to implement the erosion processes. These modifications and results are described in Section 5.2.

Four reference cases were simulated: all permutations of the reference and shaft well with uniform and valley erosion.

5.1 Erosion Sub-Regional Scale Flow Model

The Erosion Sub-Regional flow models expand upon the Glaciation Sub-Regional flow modelling by accounting for erosion occurring over the 1 Ma performance period. The effects of erosion on the flow domain are expected to be driven by two factors: 1) the reduced elevation of ground surface will result in lower elevations for the fixed head surface boundary conditions, possibly resulting in overpressures at depth, and 2) the additional hydro-mechanical unloading due to the removal of surface sediments, possibly resulting in underpressures at depth.

Erosion is incorporated as an additional process, added to the Glaciation Sub-Regional modelling previously described in Section 4.1. Initial property assignments are identical to the previously described glaciation model. Erosion is assumed to occur at each glacial retreat, at which time model properties are modified. A new ground surface elevation is calculated as the initial ground surface minus the total erosion to that time. All model elements located above the revised ground surface are set to inactive. A new weathered zone is calculated as extending to 50 m below the revised ground surface. All elements in the revised weathered zone are set to the “Drift” material property type (see Appendix A).

In extreme erosion cases, the removal of the low-permeability Ordovician units will reduce the thickness of the diffusion dominated barrier formations, enhancing mass flux into the newly formed weathered zone with biosphere access. However, the scenarios evaluated in this report have a total erosion of 100 metres, which does not reach the Ordovician units in the vicinity of the repository.

Two variant cases were evaluated: 1) uniform erosion (UE) occurs over the entire model domain; while 2) valley erosion (VE) considers ice flow channeling through local topographic variability, resulting in locally increased glacial scouring and creation of a 15 km wide valley directly above the repository.

The Erosion Sub-Regional Scale Flow modelling provides boundary conditions for the Erosion Site-Scale Transport modelling, discussed in Section 5.2.

5.1.1 Modelling Approach

The general approach can be described as follows:

1. Material is removed incrementally, temporally coincident with glacial retreats. For UE, the 100 m total depth was removed across the entire model domain. For VE, erosion describes a “V” shaped valley 15 km wide and a total depth of 100 m, with the centre of the valley located directly above the repository. The valley traverses the full length of the model in the Y direction with the “V” centred on the model domain in the X direction.

2. The same base model grid was used for both cases. Compared to the glaciation only model, the grid is more finely discretized in the upper layers to more accurately resolve each material removal event. To effectively model the VE case, the grid also has increased horizontal resolution perpendicular to the valley. The grid orientation is modified from the glaciation only model for improved consistency of valley erosion processes with topographic features.

3. The eight glacial cycles each contain two erosion events, each of which results in removal of material from the entire domain (UE) or from the floor of the valley (VE) at the end of each event. For VE, removal rates vary linearly from a maximum at the valley centre to zero at the full width.

4. After each erosion event, the grid properties were redefined with “null” or inactive elements replacing the eroded material. The weathered surface zone was also redefined based on the new surface location. Head and loading boundary conditions were calculated for the next event using the new surface.

5. Simulations for each event were linked by way of head restart files.

6. Responses from each event simulation were combined.

5.1.2 Model Description

5.1.2.1 Model Domain and Discretization

The Erosion Sub-Regional flow model domain was determined from the repository location and the local topography. Glacial steering by existing topography is assumed to cause valley erosion, with the advance/retreat direction orthogonal to prevailing topography, as shown in Figure 5-1. The grid roughly parallels the Lake Huron shoreline at a rotation of 35 degrees clockwise from North-South. At 35 km wide (X direction) by 40 km long (Y direction), the grid is wider than the Glaciation Sub-Regional grid to extend boundaries beyond the valley edges for the VE case. Glacial advance and retreat is parallel to the Y axis. The grid is centred on the repository to simplify the grid rotation. An area of Guelph formation sub-crop extends across nearly the entire grid to the North-East of the repository.

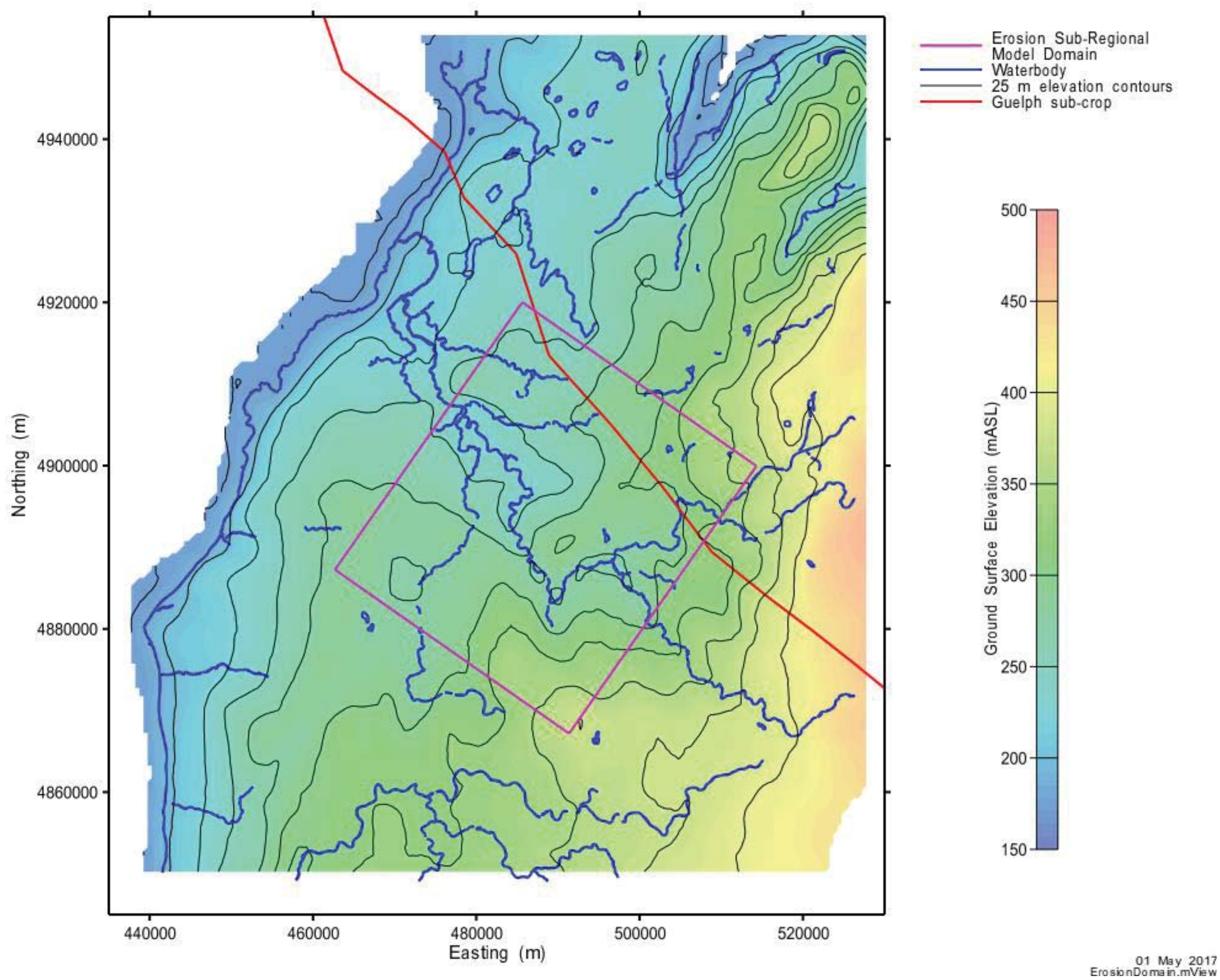

Figure 5-1: Erosion Sub-Regional Model Domain

Figure 5-2 illustrates the plan discretization, with constant 500 m element lengths in the Y direction. X direction discretization varies to support the VE case, with a higher resolution (250 to 100 m) in the 15 km wide valley region.

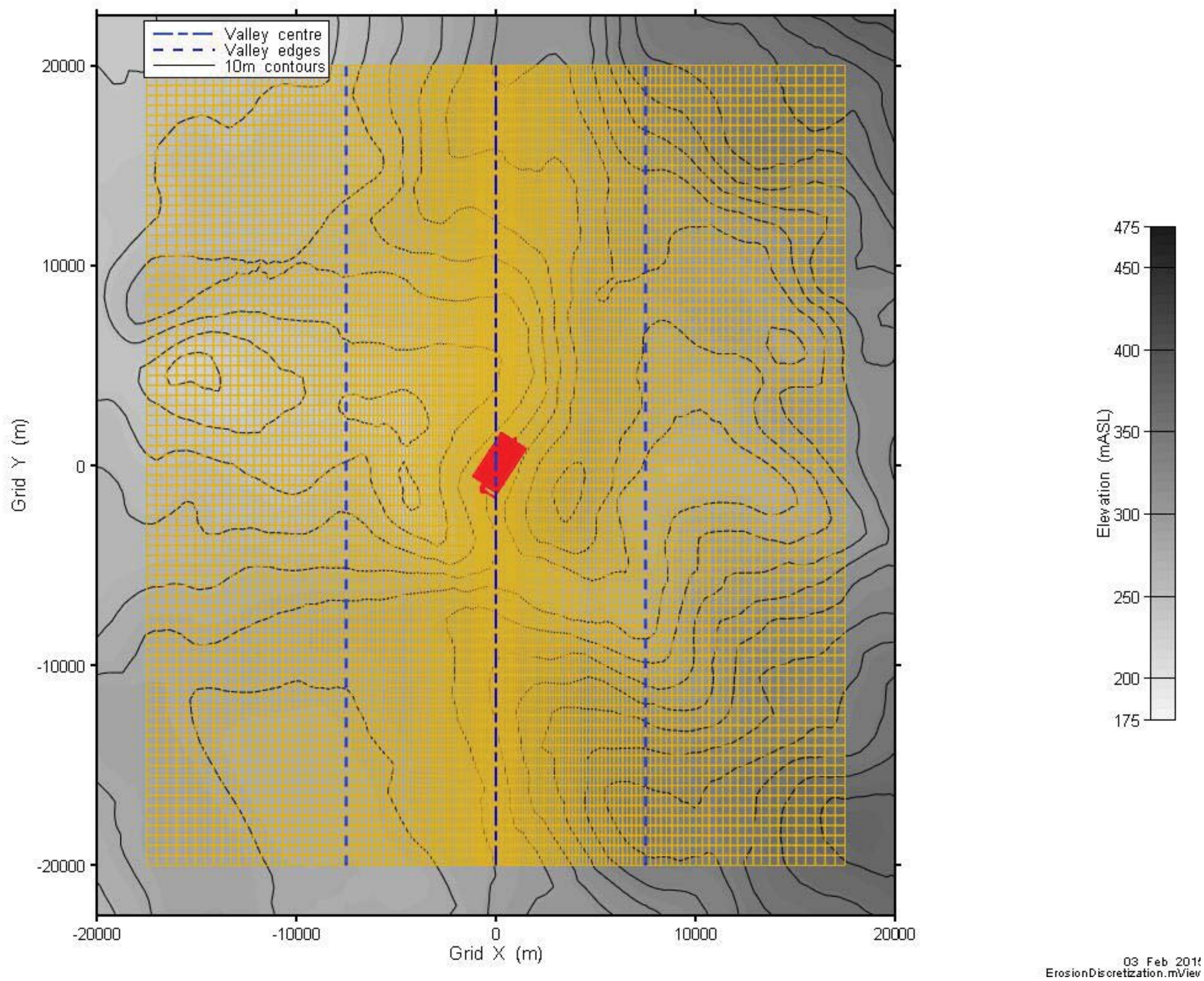

Figure 5-2: Erosion Sub-Regional Horizontal Discretization

Vertical discretization was based on the geological surfaces described in Section 3.1 and illustrated in Figure 5-3 and Figure 5-4. Upper layer discretization was modified so that a minimum of 50 m thickness weathered bedrock/overburden zone could be assigned for each erosion event. A minimum grid layer thickness of 0.1 m was enforced in the northern end of the grid where sub-cropping layers were merged into the drift/weathered bedrock zone.

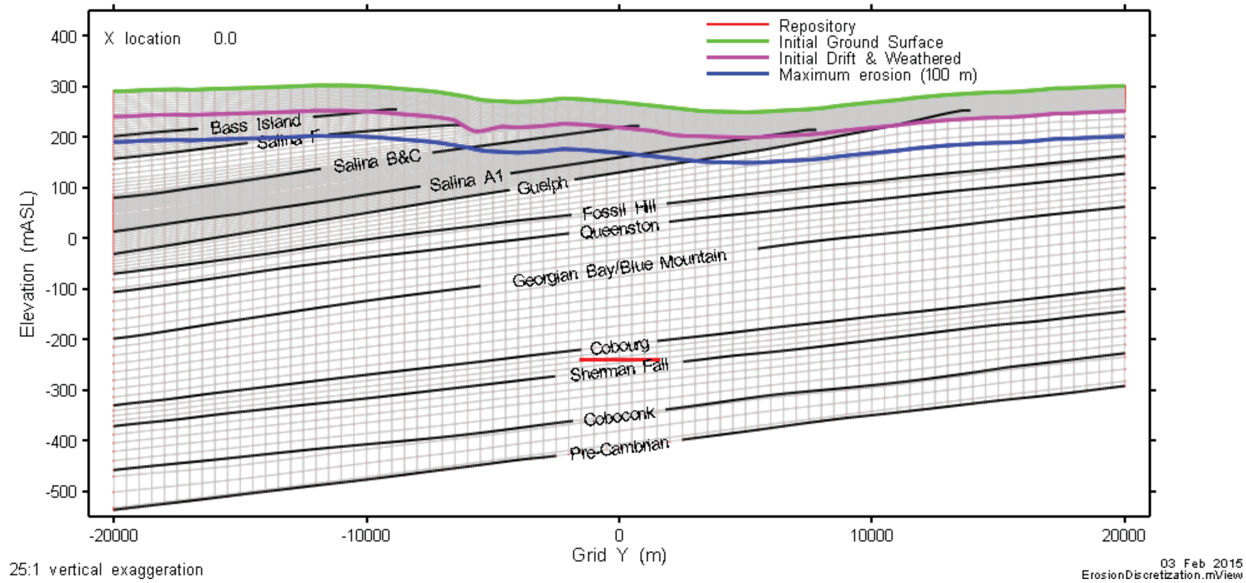

Figure 5-3: Erosion Sub-Regional Model Discretization on Vertical Slice Through X = 0 m

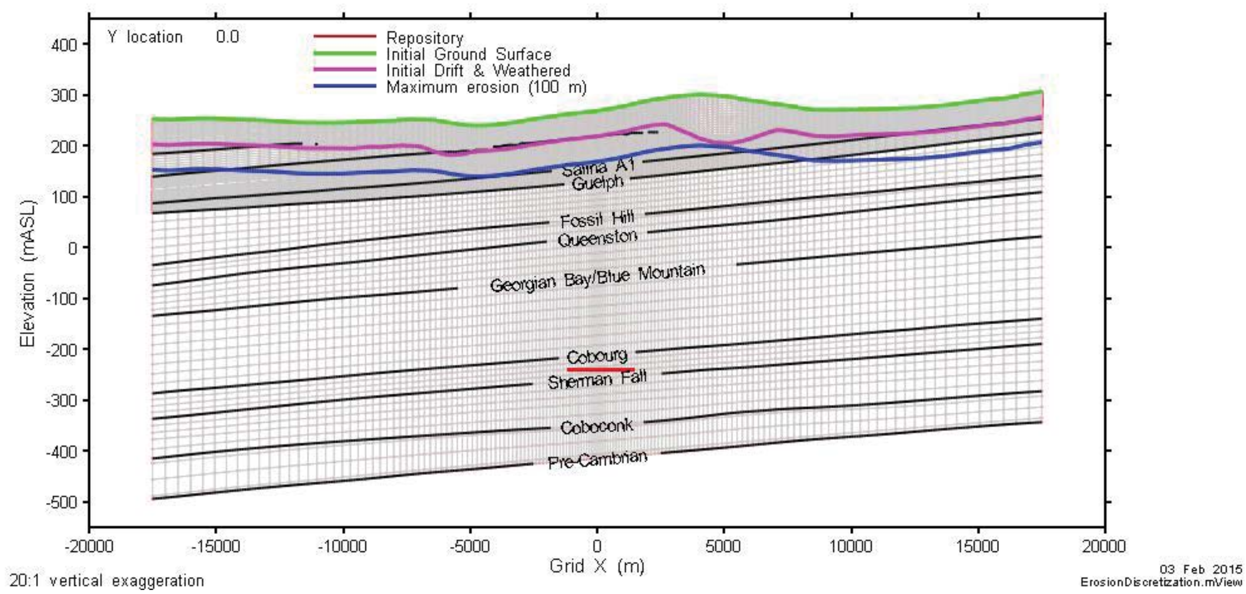

Figure 5-4: Erosion Sub-Regional Model Discretization on Vertical Slice Through Y = 0 m

The resulting model domain consists of 149 nodes in the X direction, 81 in the Y direction and 105 node layers, for a total of 1,267,245 nodes and 1,231,360 elements, or approximately a factor of four larger than the Glaciation Sub Regional Flow model.

5.1.2.2 Property Assignment

Initial model properties were assigned based on element position relative to geological surfaces (Figure 5-5 with vertical exaggeration, Figure 5-6 with no vertical exaggeration). Figure 5-7 details pinch outs (A1 Evaporite, A2 Evaporite and B Anhydrite) and sub-cropping.

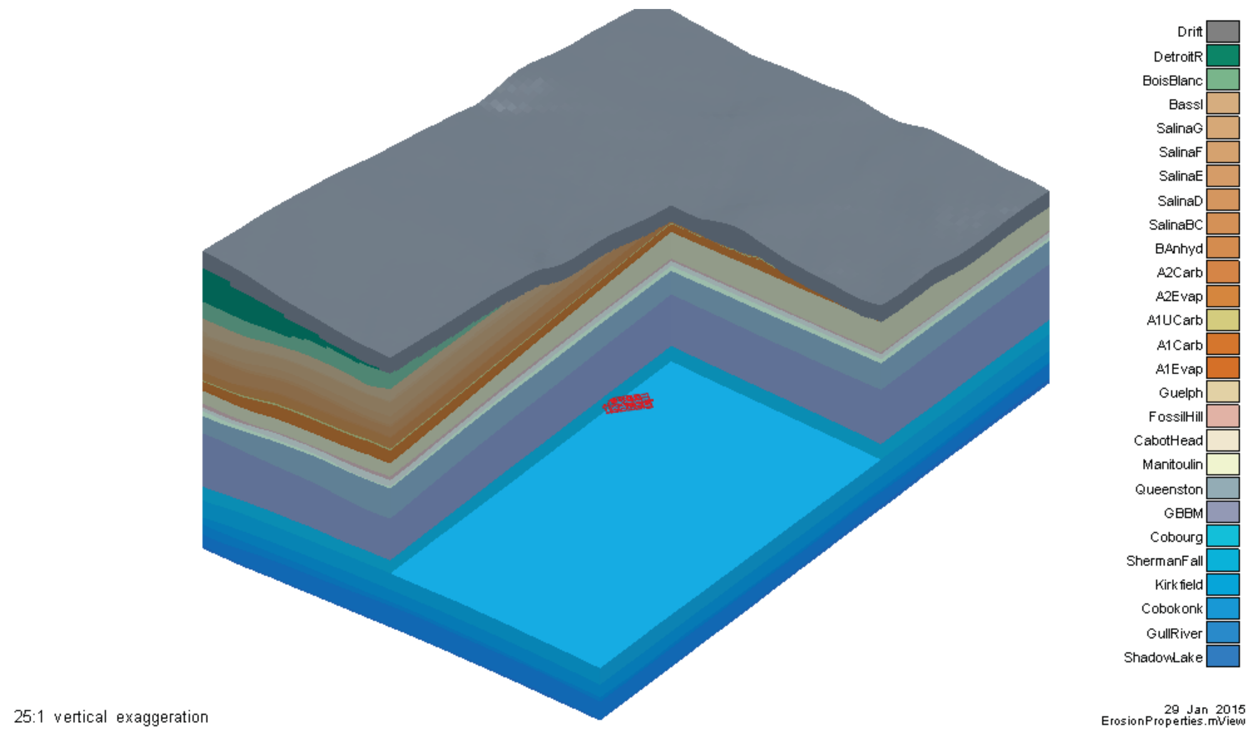

Note: Repository shown for location reference only

Figure 5-5: Erosion Sub-Regional Model Property Assignment

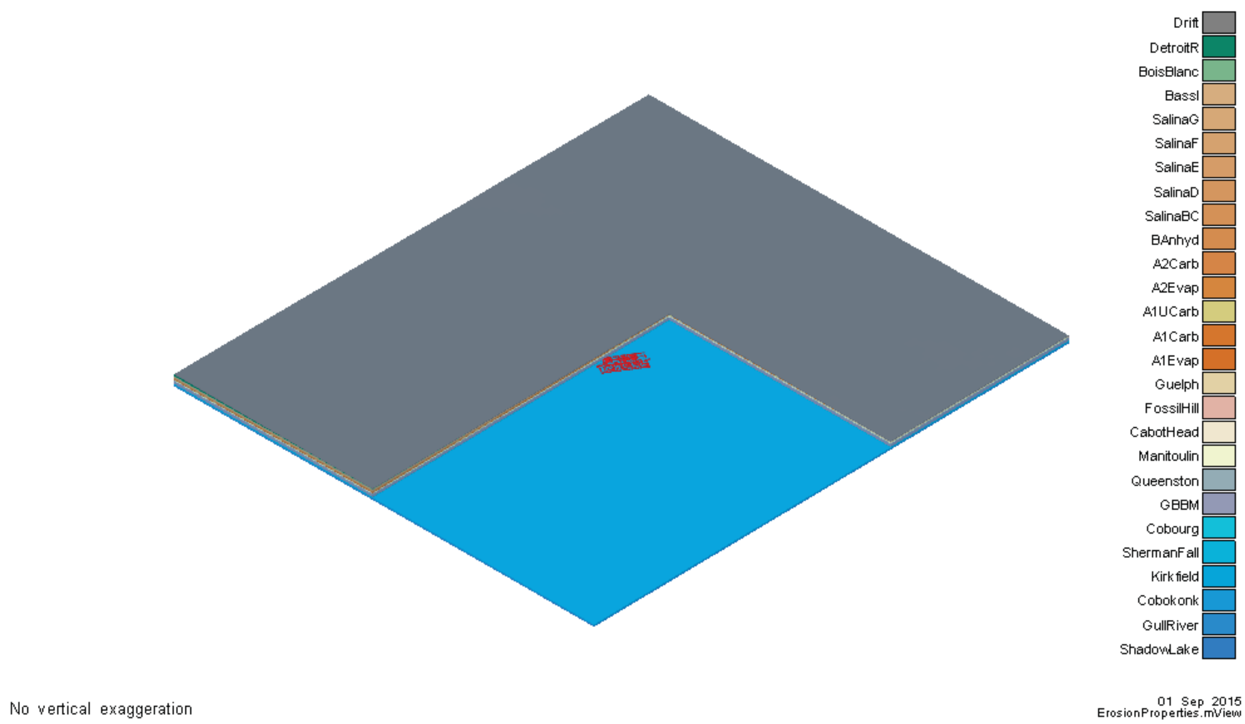

Note: Repository shown for location reference only

Figure 5-6: Erosion Sub-Regional Model Property Assignment– no vertical exaggeration

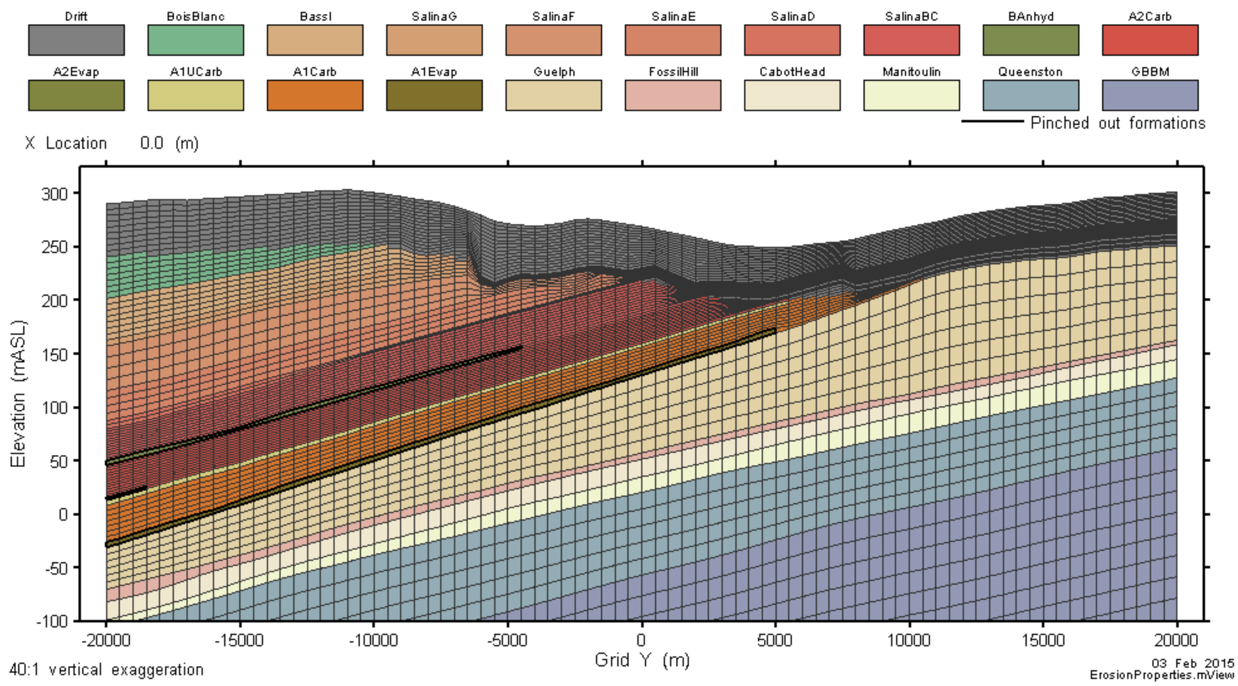

Figure 5-7: Erosion Sub-Regional Model Property Assignment on Vertical Slice Through X = 0

Modification of properties to implement erosion is illustrated in Figure 5-8 and Figure 5-9. In Figure 5-8, the eroded material has been removed, but the revised weathered zone has not been applied. Figure 5-9 is a cross-section through the repository centre showing erosion and weathering.

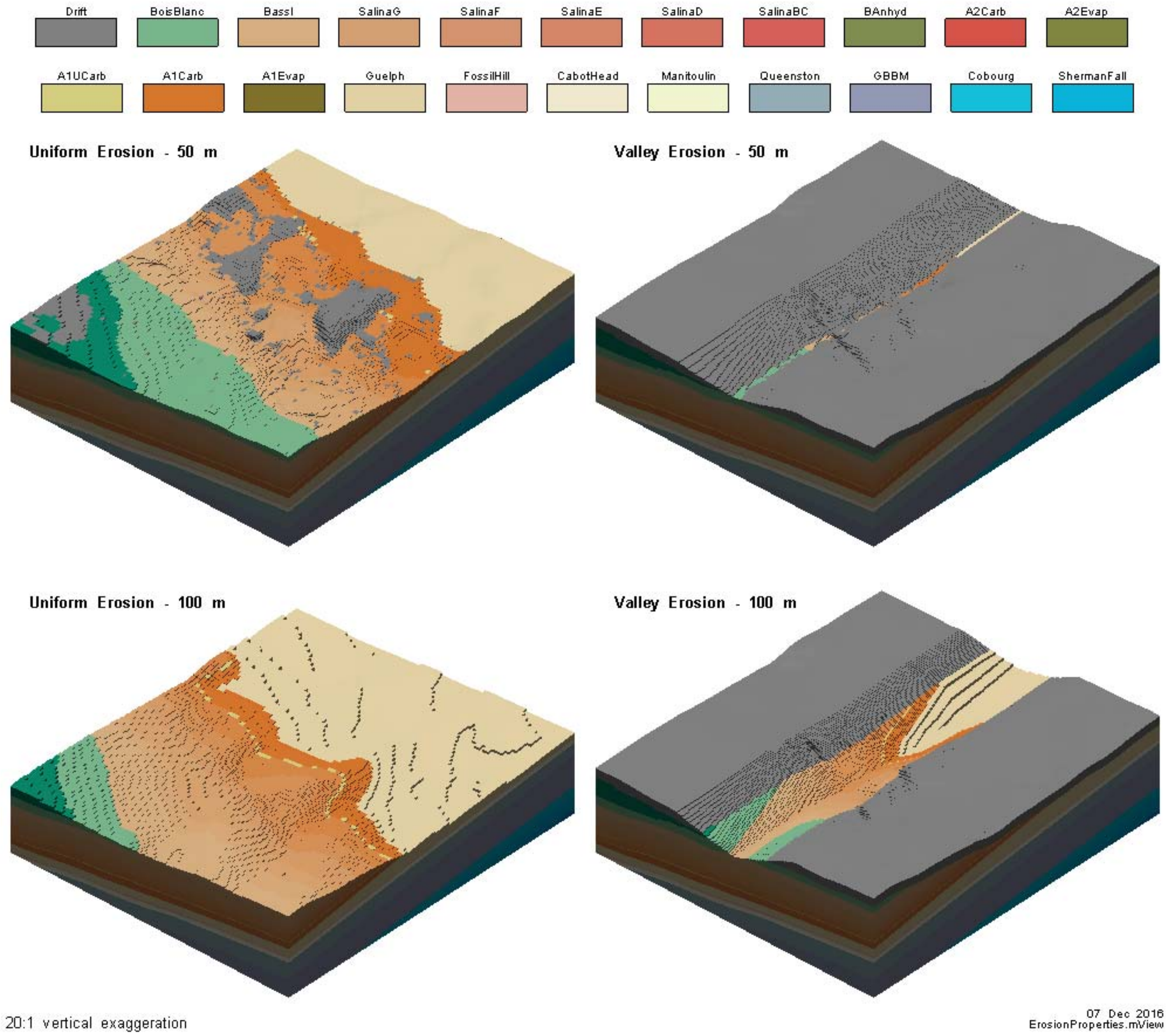

Figure 5-8: Erosion Sub-Regional Model Property Assignment Before Weathered Zone Reassignment

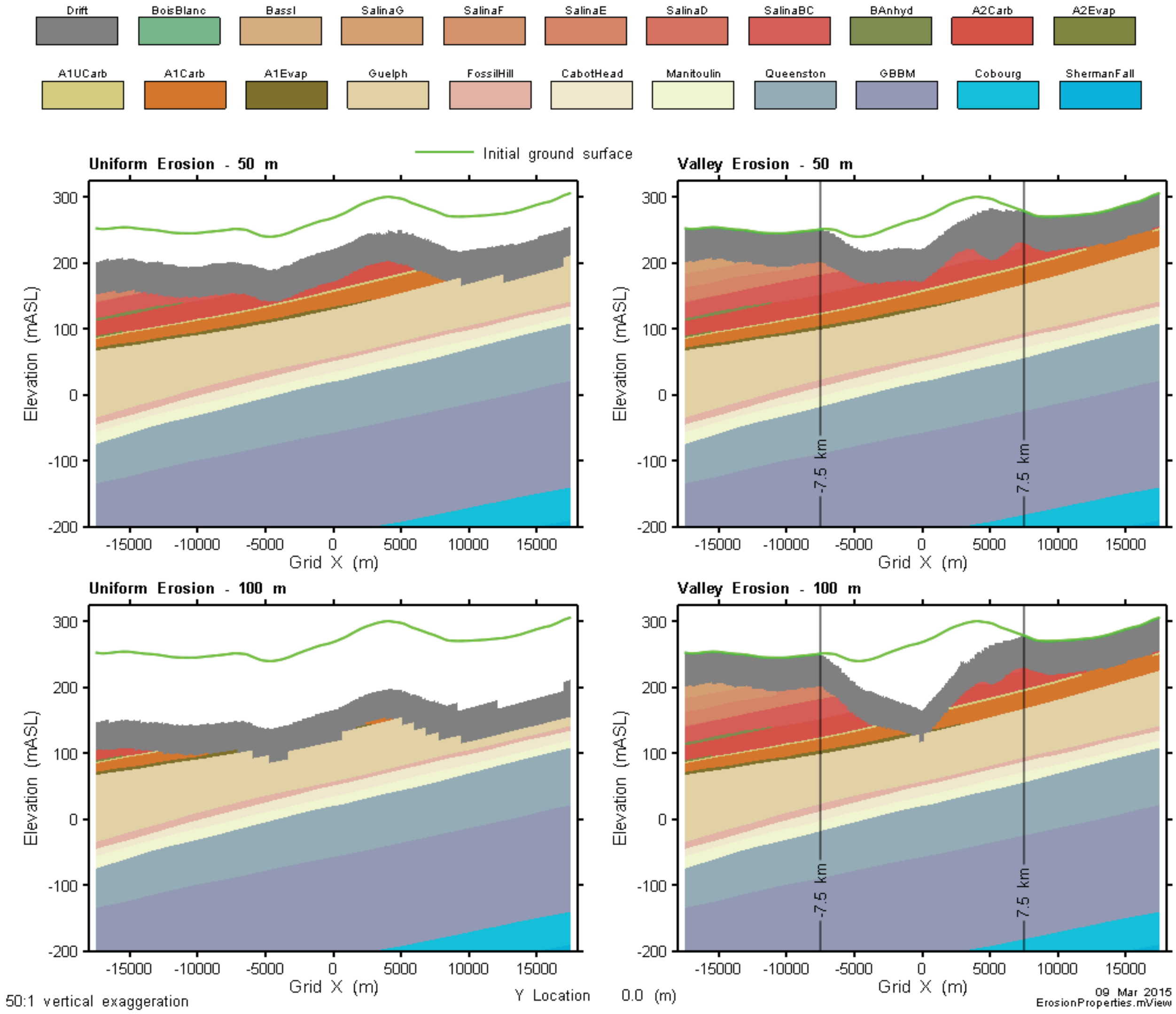

Figure 5-9: Erosion Sub-Regional Model Property Assignment on Vertical Slice Through Y = 0

Separate property assignments are required for each erosion event and each case (UE or VE). The 100 m total erosion is applied equally to each glacial cycle at 12.5 metres per cycle. Within each cycle, erosion is applied at the end of each of the two full retreats. Allocation of the total cycle erosion between the two retreats is 35:65 based on the differences in peak ice load for each advance, resulting in 4.375 m removed at the end of the first retreat, and 8.125 m at the end of the second. These are the nominal values; the actual value at any location depends on the vertical resolution of the grid at that location.

Erosion periods were designated using the cycle number and “A” or “B” for first and second retreat in each cycle respectively (see Figure 5-10). For implementation convenience, each cycle ends at the second full retreat. This results in a shorter duration for the 1A period and the requirement of a 9A period from the end of the last retreat to 960 ka, for a total of 17 simulation periods. Each period was simulated separately, with initial head conditions copied from the final simulated head of the previous period. Initial conditions for the first period were based on the no-well, steady-state flow simulation results.

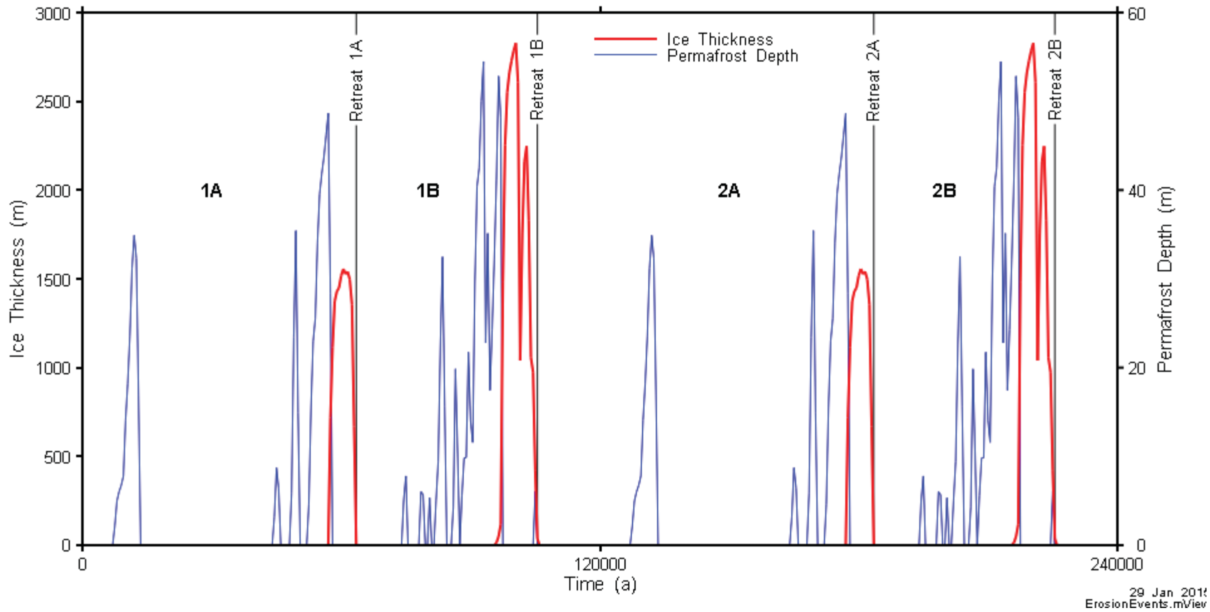

Figure 5-10: Erosion Sub-Regional Model Erosion Events for Single Cycle

Ground surface elevations at the repository and approximately half-way up the valley side to the South-East of the repository are shown in Figure 5-11 for both uniform and valley erosion cases. Note that the total difference in elevation at the repository is 97 m, rather than the 100 m specified, reflecting discretization related adjustments. The uniform erosion case at the valley side mid-point is also approximately 100 m, while the valley erosion case at the same point has a total removal of just under 50 m, as expected. Note that for the valley case at the valley side mid-point, a number of erosion events show no change in elevation (e.g. 3A, 4A, 6A, 7A) due to discretization related effects.

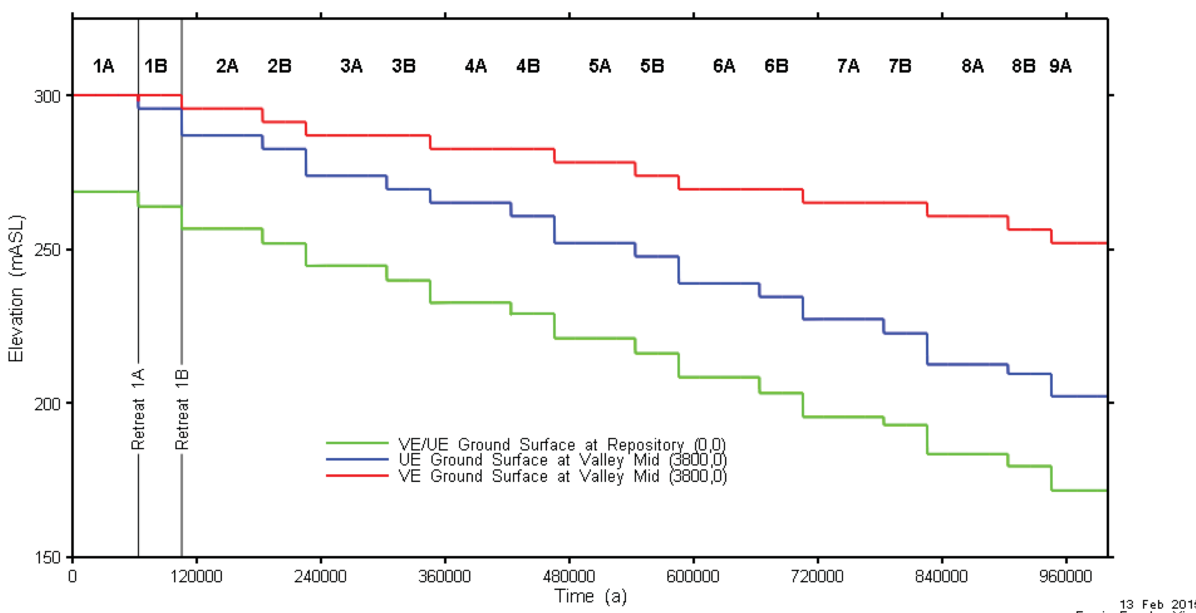

Figure 5-11: Erosion Sub-Regional Model – Ground Surface Elevation at Repository and Valley Mid-Point Location

Discretization related spatial variation from the nominal 100 m total erosion at 960 ka for the UE and VE cases are shown in Figure 5-12 and Figure 5-13, respectively.

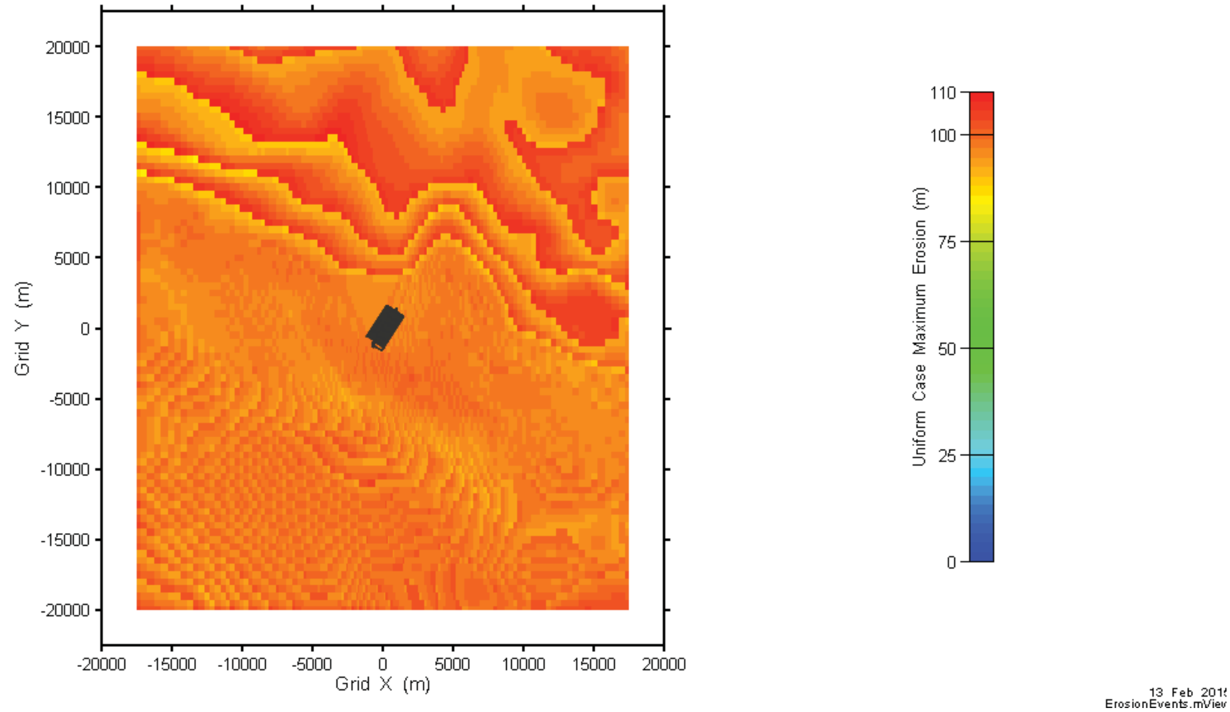

Figure 5-12: Erosion Sub-Regional Model – UE Case Total Erosion at 960 ka

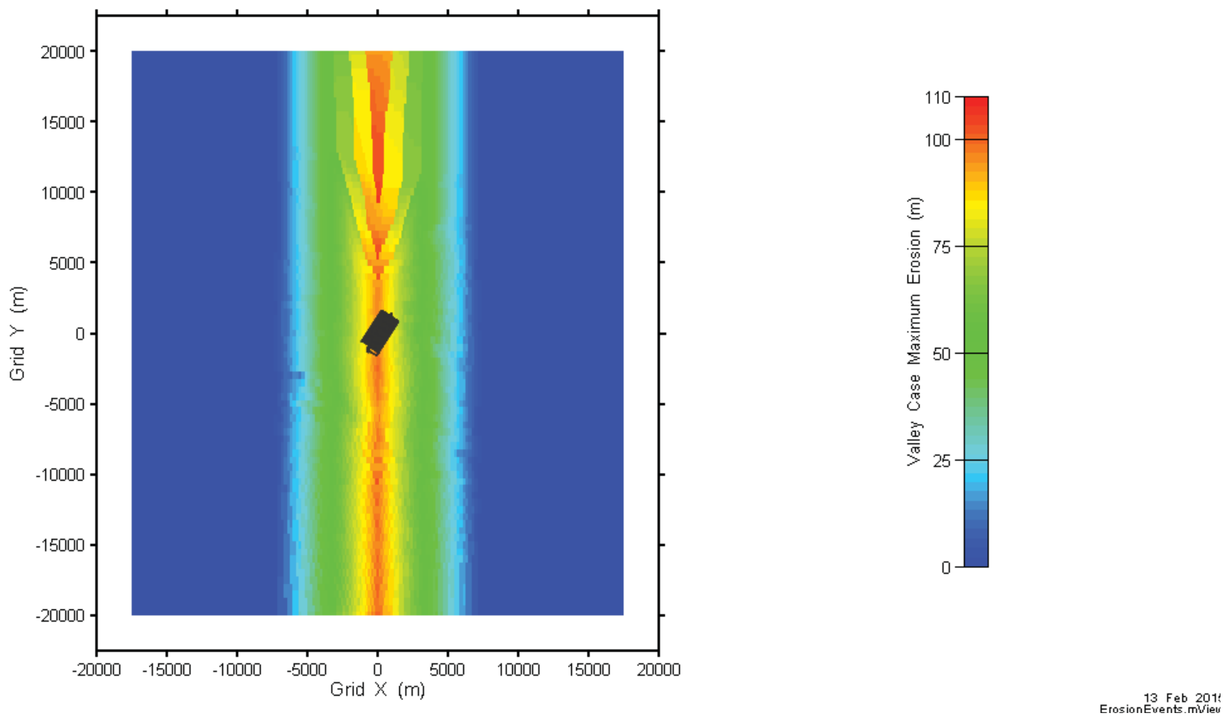

Figure 5-13: Erosion Sub-Regional Model – VE Case Total Erosion at 960 ka

5.1.2.3 Boundary Conditions

The fixed head glacial boundary conditions were calculated for each erosion period to reflect the different ground surface node elevations (see Figure 5-14). Boundary conditions were applied at ground surface only, with zero flow boundaries on all sides. This simplification reduced computational effort required for boundary condition calculations and was justified given results from the glacial boundary condition sensitivity case (Surface BC in Section 4.1.5.3) which showed no significant differences between reference case and Surface BC results.

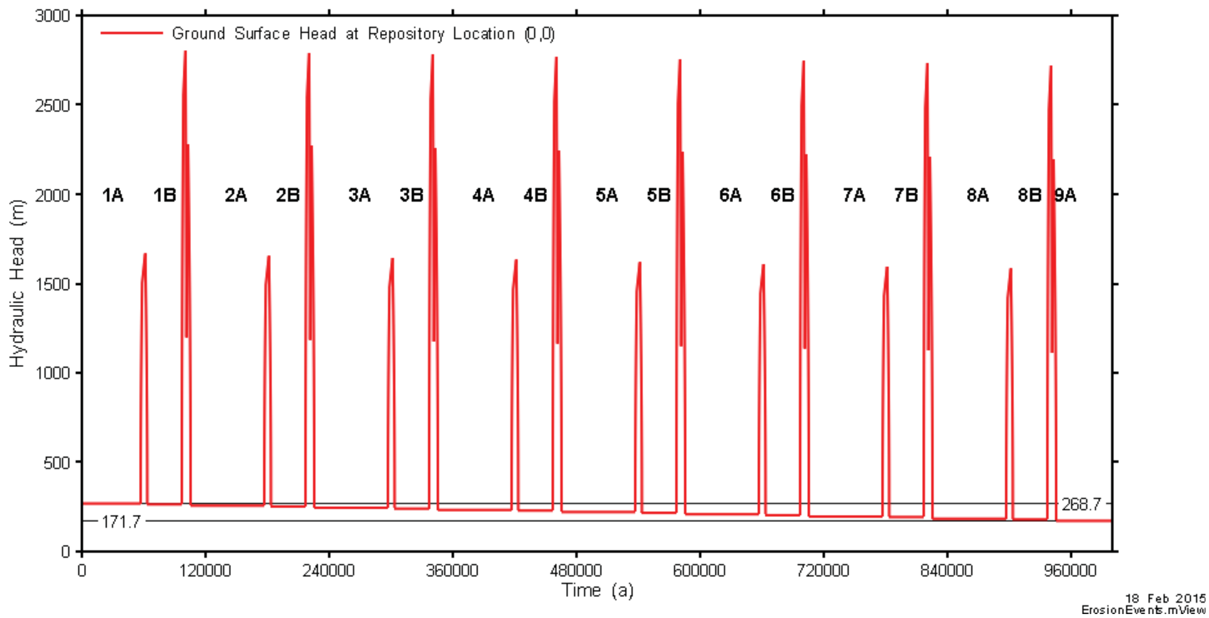

Figure 5-14: Erosion Sub-Regional Model - Glacial Surface Boundary Condition

The hydraulic head change of the final retreat portion of each period was increased to incorporate the calculated erosion (4.375 m for period A, 8.125 m for period B). As a result of the change, the head at the glacier toe is lower at the end of the retreat than at the start of each period. This ensures continuity of surface fixed head boundary conditions. For valley erosion, the head change was scaled according to position within the valley, with a multiplier of 1.0 at the valley centre and 0.0 at the valley edges, and varying linearly from the edge to centre, with no change applied outside of the valley.

The hydro-mechanical loading rate boundary condition is calculated from the head boundary condition (change in head divided by time step equals loading rate). A separate hydraulic head profile was used in calculating the hydro-mechanical boundary conditions to include the weight of eroded material in the unloading. The hydraulic head change at the end of the retreat portion of the profile was increased by a factor of 2.5 (10.9375 m for period A, 20.3125 m for period B), assuming an average density of 2500 kg/m^3 for eroded material. This increases the hydro-mechanical unloading in the retreat beyond that applied in the advance to account for removal of eroded material. As with the head boundary condition, the loading increase for valley erosion was scaled according to position within the valley, with a multiplier of 1.0 at the valley centre and 0.0 at the valley edges and outside the valley, and varying linearly from the edge to centre.

5.1.2.4 Permafrost

Permafrost was calculated separately for each erosion period, using the same approach as described in Section 4.1.1.4. Maximum permafrost depths in selected erosion periods are shown in Figure 5-15.

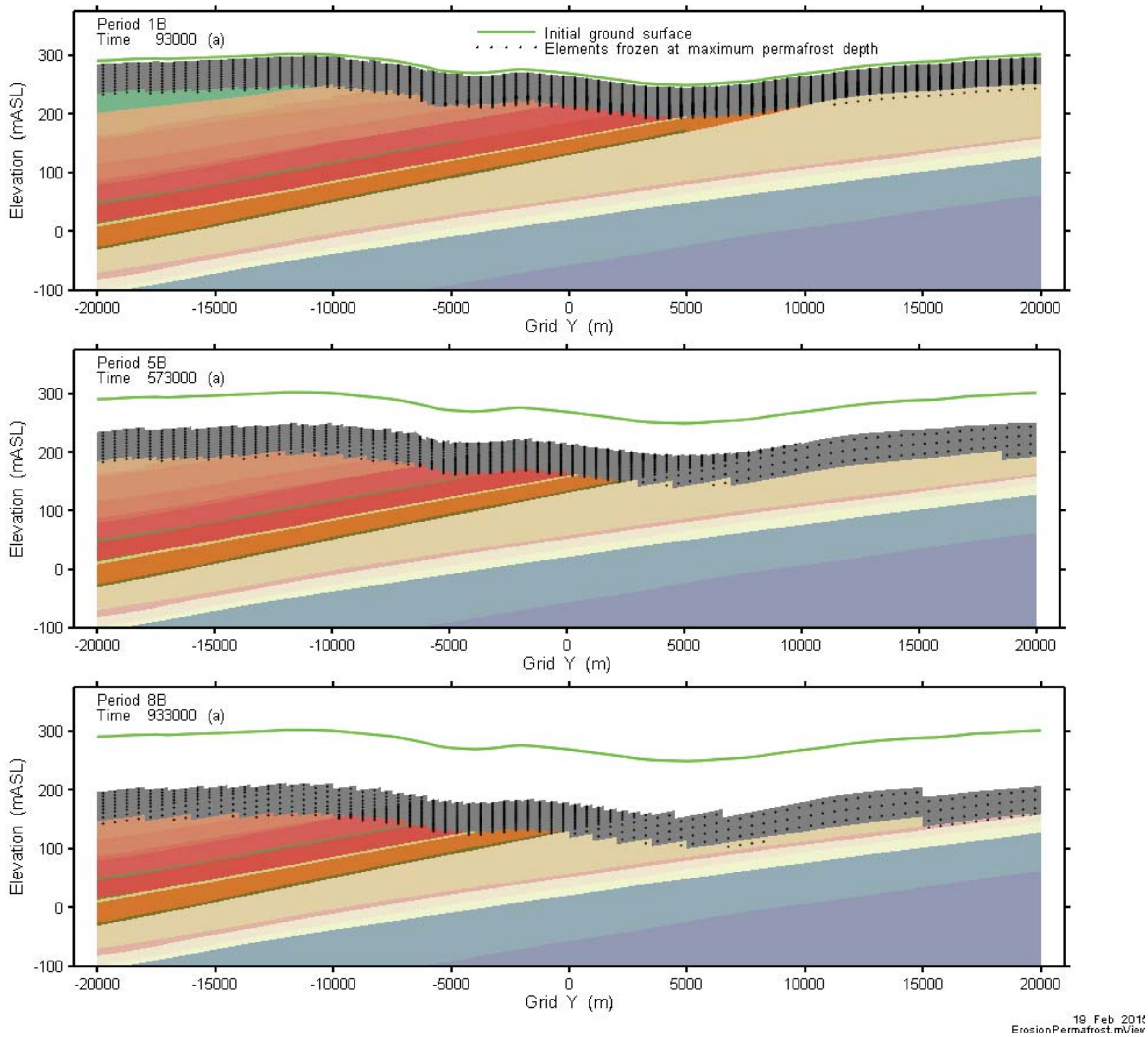

Figure 5-15: Erosion Sub-Regional Model - maximum Permafrost Depth on Vertical Slice Through X = 0

5.1.2.5 Well Locations

Reference and shaft wells are used in the erosion simulations, as shown in Figure 5-16. Well locations were selected to be as close as possible to the corresponding Site-Scale model wells.

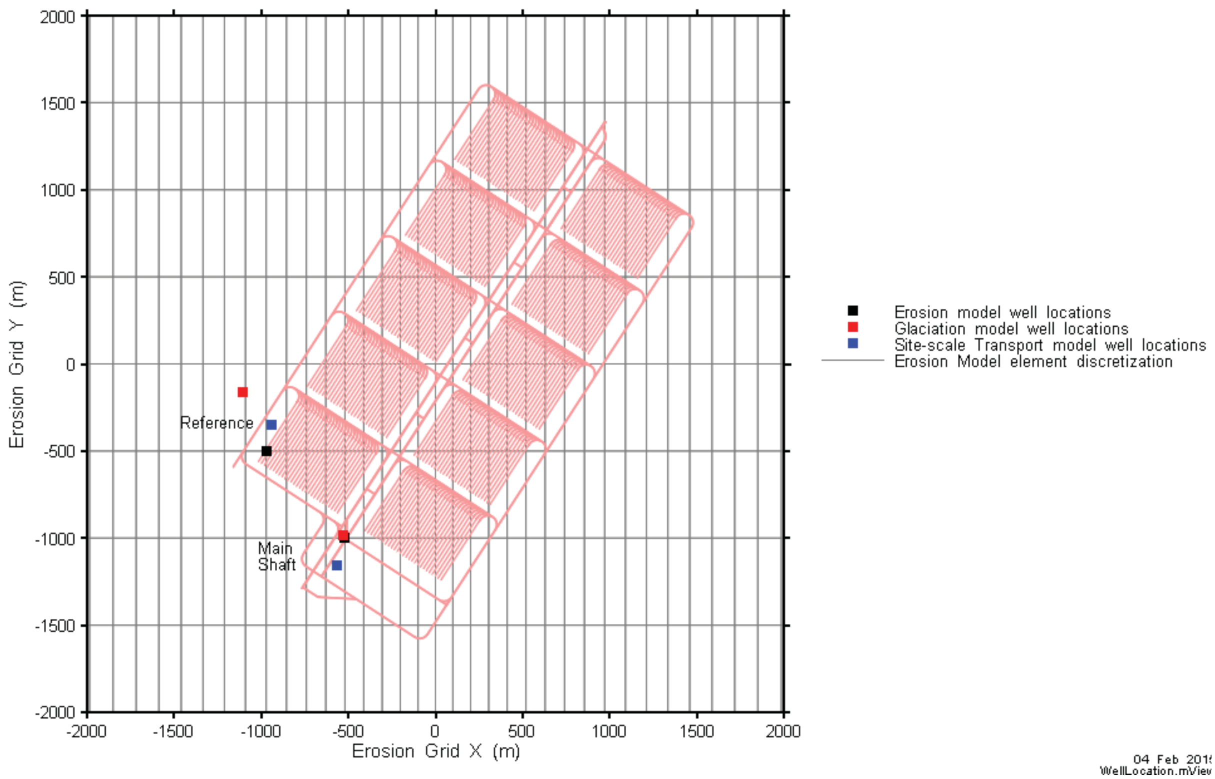

Figure 5-16: Erosion Sub-Regional Model: Well Locations

5.1.3 Steady-State Flow Simulations

Constant density steady-state (constant climate) flow simulations with reference properties (period 1A) were performed to provide initial conditions for the transient erosion cases. Results were also compared to glaciation model steady-state simulations with zero flow vertical boundary conditions to determine model sensitivity to differences in grid orientation and discretization. Hydraulic head, repository velocity and MLE results for the no-well case are compared in Figure 5-17 through Figure 5-19. Results are comparable, indicating no significant impact from the discretization differences.

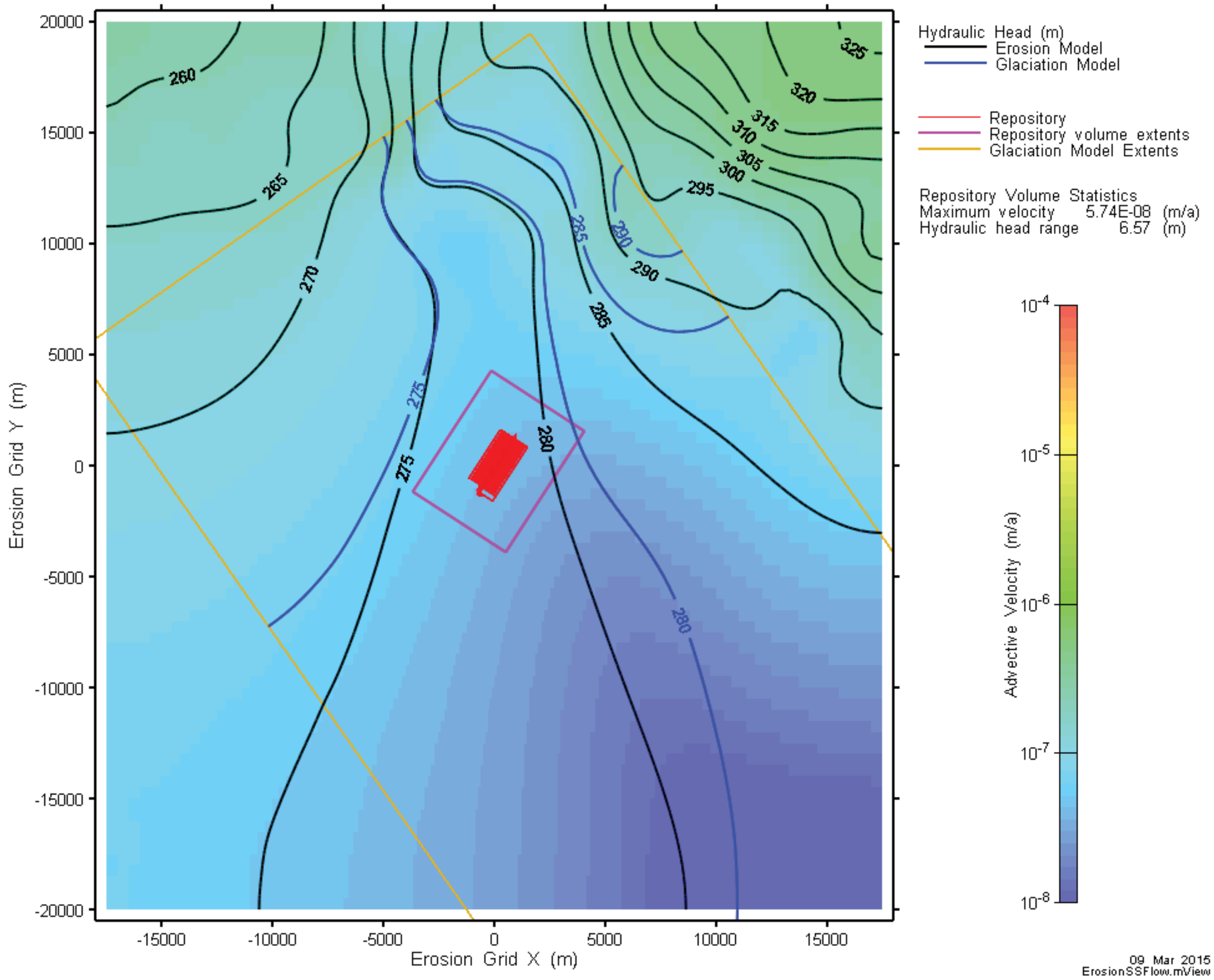

Figure 5-17: Steady-State Sub-Regional Flow: Comparison of Erosion and Glaciation Model Hydraulic Head Distribution on Model Layer Through Cobourg Formation

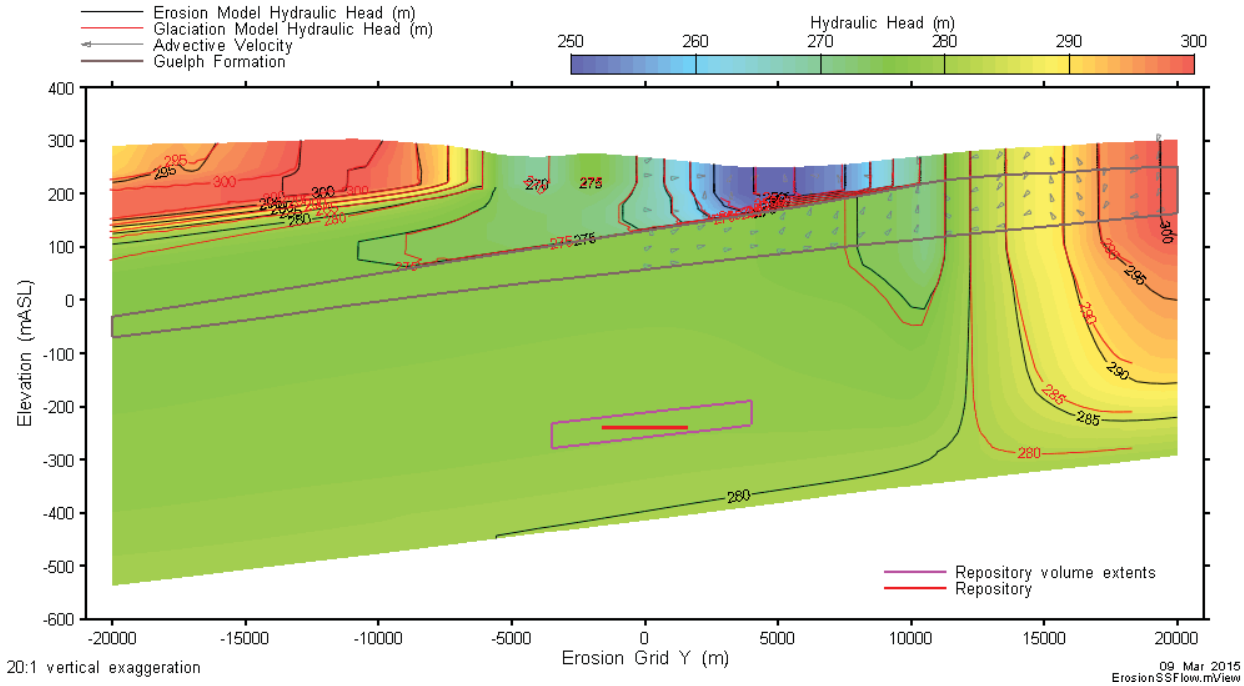

Figure 5-18: Steady-State Sub-Regional Flow: Comparison of Erosion and Glaciation Model Hydraulic Head Distribution on Vertical Slice Through Repository

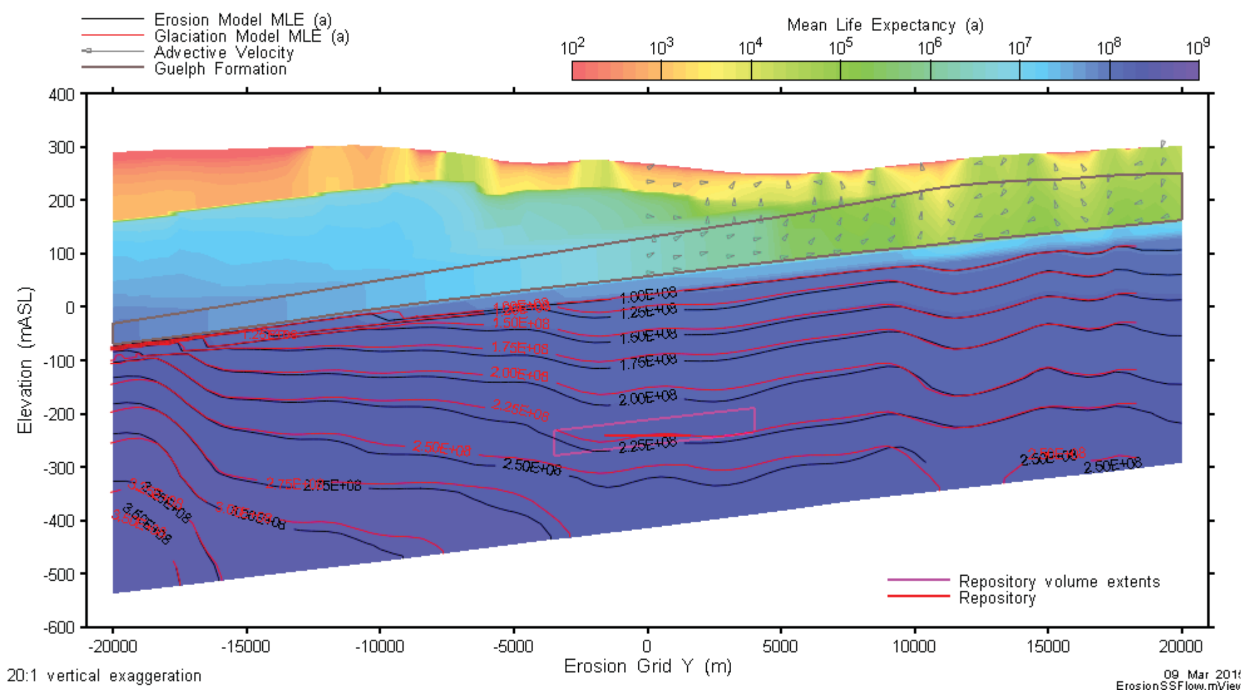

Figure 5-19: Steady-State Sub-Regional Flow: Comparison of Erosion and Glaciation Model MLE on Vertical Slice Through Repository

Additional steady-state simulations with constant water supply well operation were compared to the corresponding glaciation model results to further verify correct model implementation, as shown in Figure 5-20.

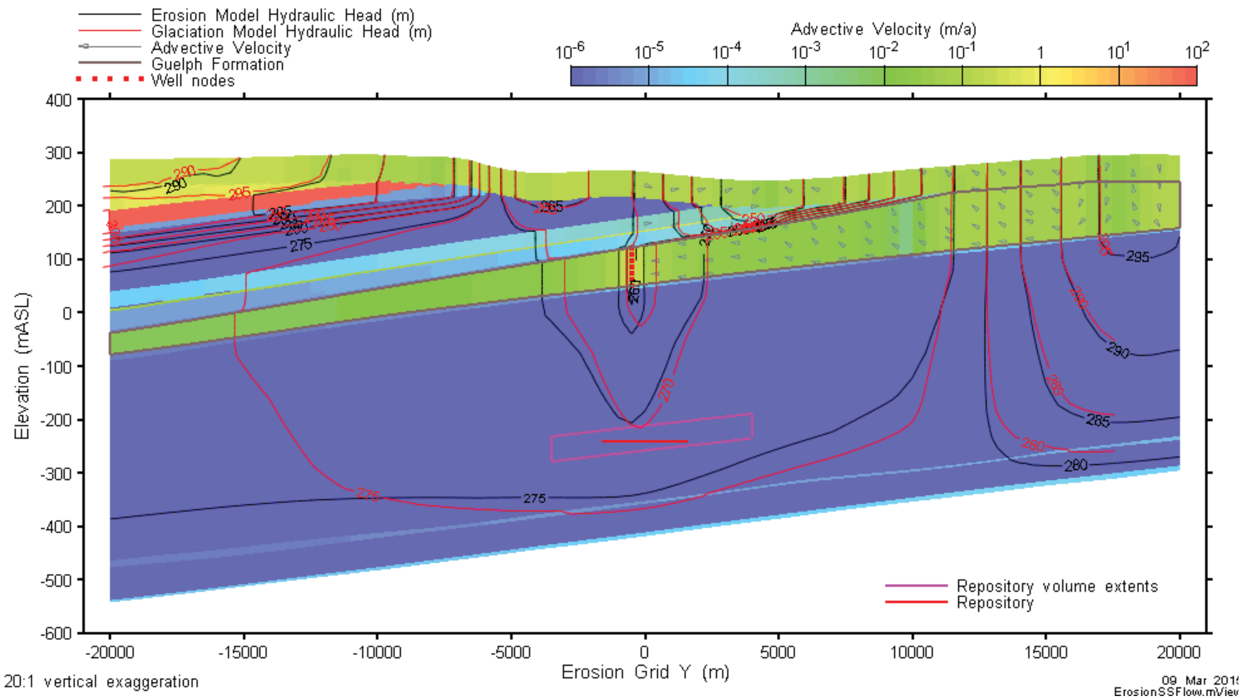

Figure 5-20: Steady State Flow: Comparison of Erosion and Glaciation Model Hydraulic Head Distribution on Vertical Slice Through Repository With Reference Well

5.1.4 Glacial Climate Flow Simulations

As a final comparison to verify model implementation, the 17 period erosion model was simulated with transient glacial boundary conditions, permafrost specification and water supply well operation schedule but without erosion. Head and velocity results from this simulation are compared to the SurfaceBC case glaciation only model. Time series results below present simulated hydraulic head at the reference well location (Figure 5-21) and maximum advective velocities in the plan vicinity of the repository (Figure 5-22) through a selection of formations. Results are very consistent across both models, providing further confidence in correct implementation of the model structure. Velocities in the Guelph during periods of well operation are slightly higher due to discretization effects. The smaller element sizes lead to higher velocities in elements near the well.

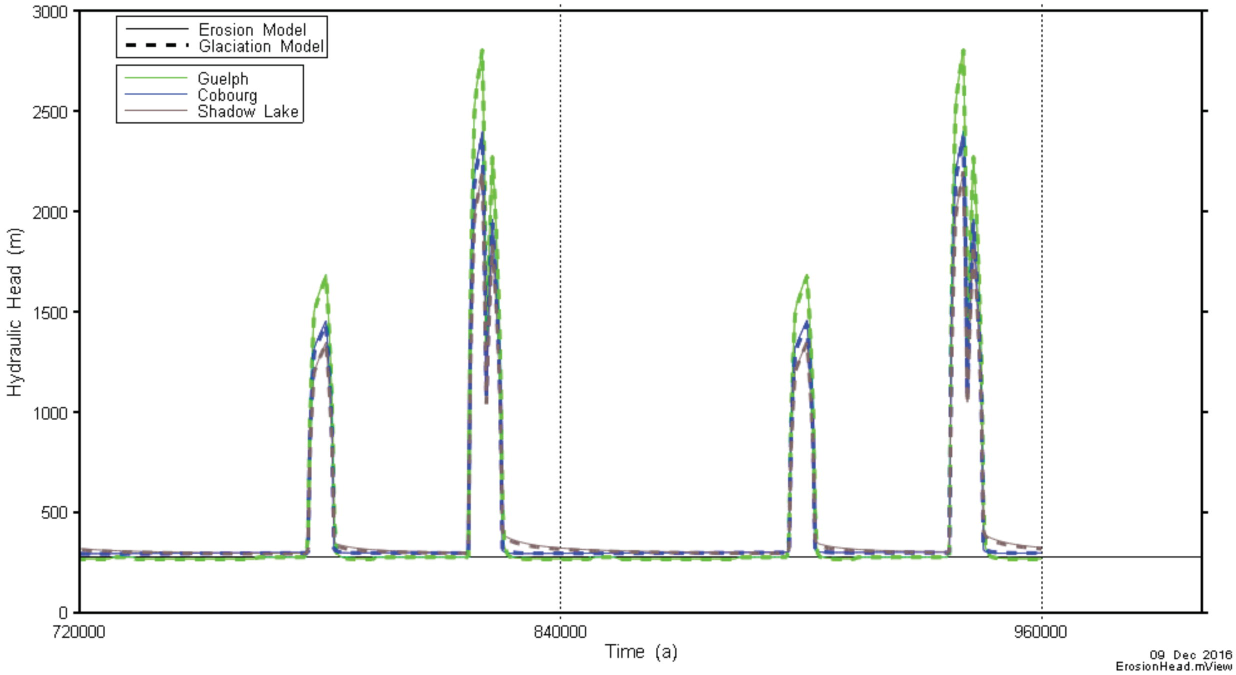

Figure 5-21: Glacial Climate Transient Sub-Regional Flow: Erosion Model With No Erosion and Glaciation Model Comparison of Hydraulic Head During Glacial Cycles Seven and Eight at Repository Location (X = 0 m, Y = 0 m) and Selected Formations

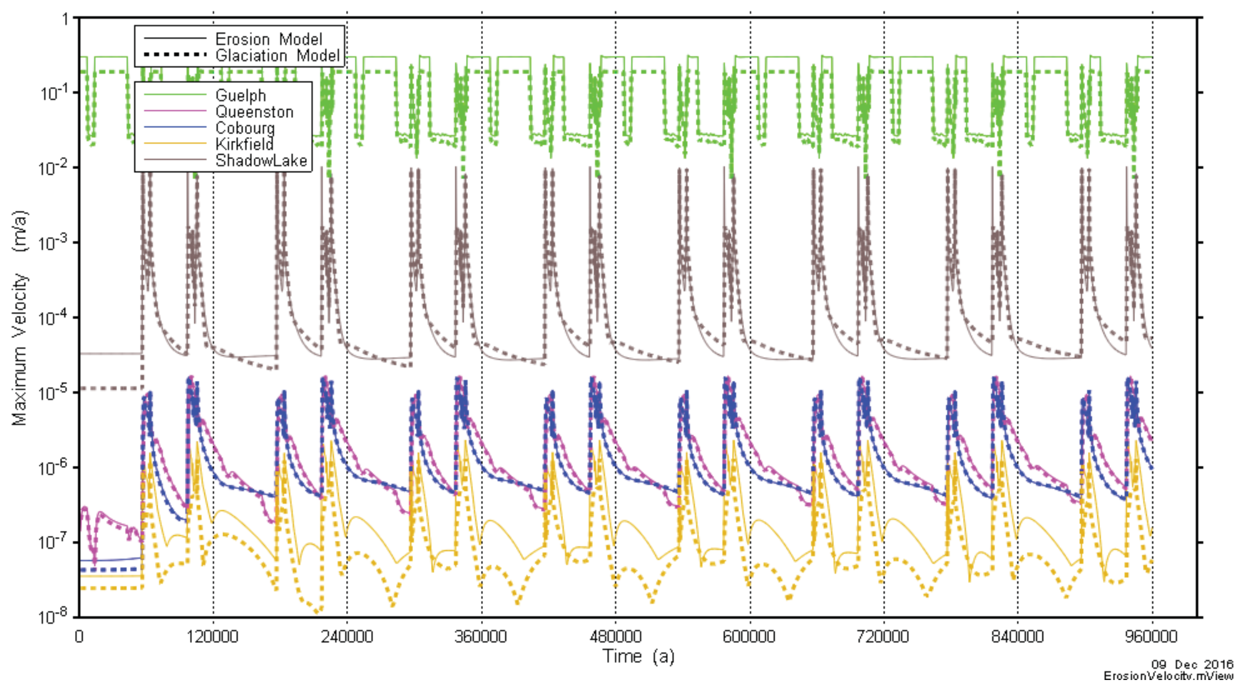

Figure 5-22: Glacial Climate Transient Sub-Regional Flow: Erosion Model With No Erosion and Glaciation Model Comparison of Maximum Advective Velocity in Repository Vicinity and Selected Formations

Hydraulic head profiles for glaciation and erosion models are compared at selected times in the first cycle (Figure 5-23) and at the time of maximum well operation in all cycles (Figure 5-24). The minor discrepancies in the latter figure are due to differences between the grids in ground surface elevation caused by the finer discretization of the erosion model. Head profiles correspond very well if the glaciation model results are shifted by 2.13 m to account for the difference in ground surface elevation, as shown in Figure 5-25.

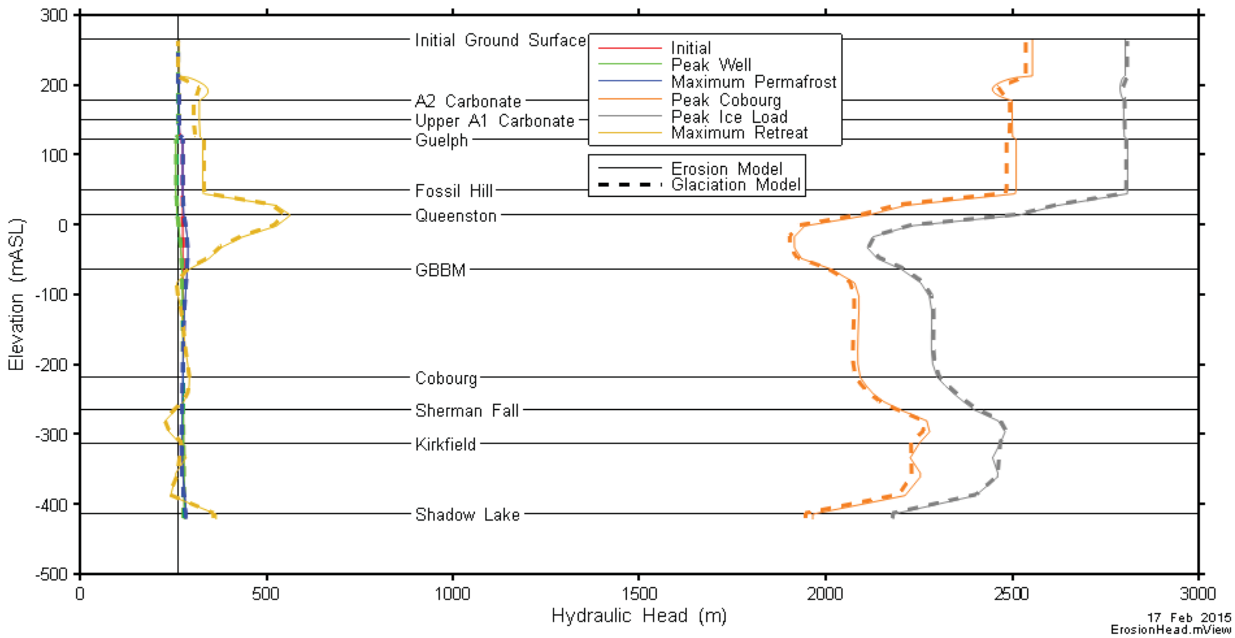

Figure 5-23: Glacial Climate Transient Sub-Regional Flow: Erosion Model With No Erosion and Glaciation Model Comparison of Vertical Hydraulic Head Profiles at Reference Well During First Glacial Cycle

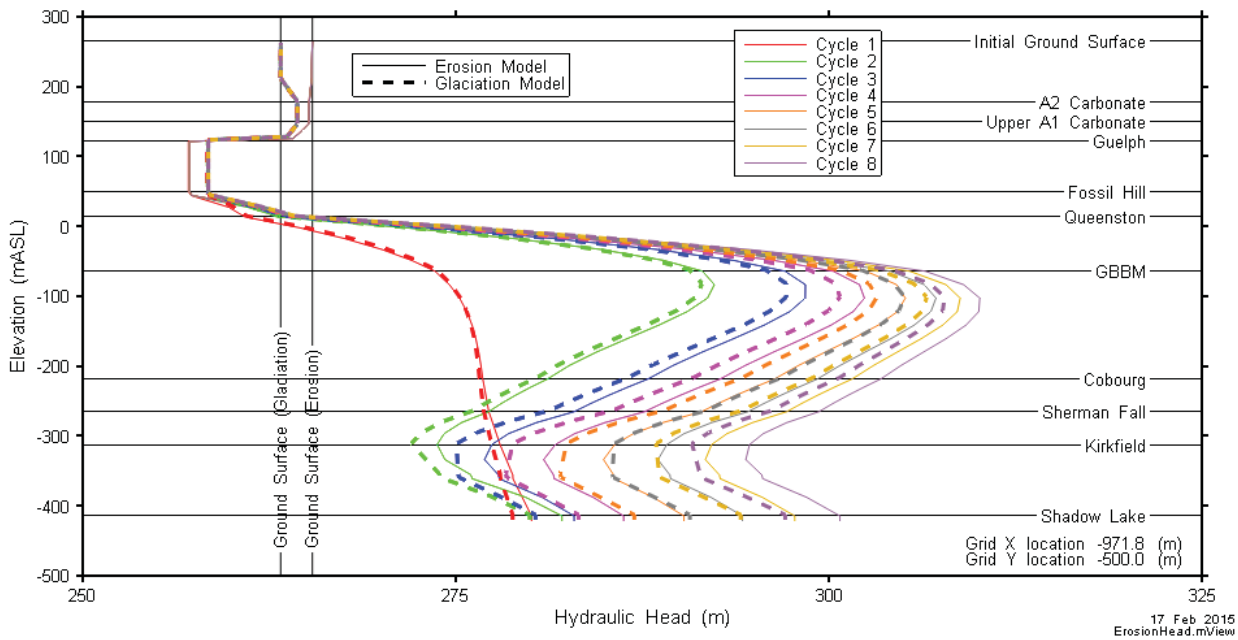

Figure 5-24: Glacial Climate Transient Sub-Regional Flow: Erosion Model With No Erosion and Glaciation Model Comparison of Hydraulic Head Profiles at Water-Supply Well Location at Time of Maximum Well Impact for All Cycles

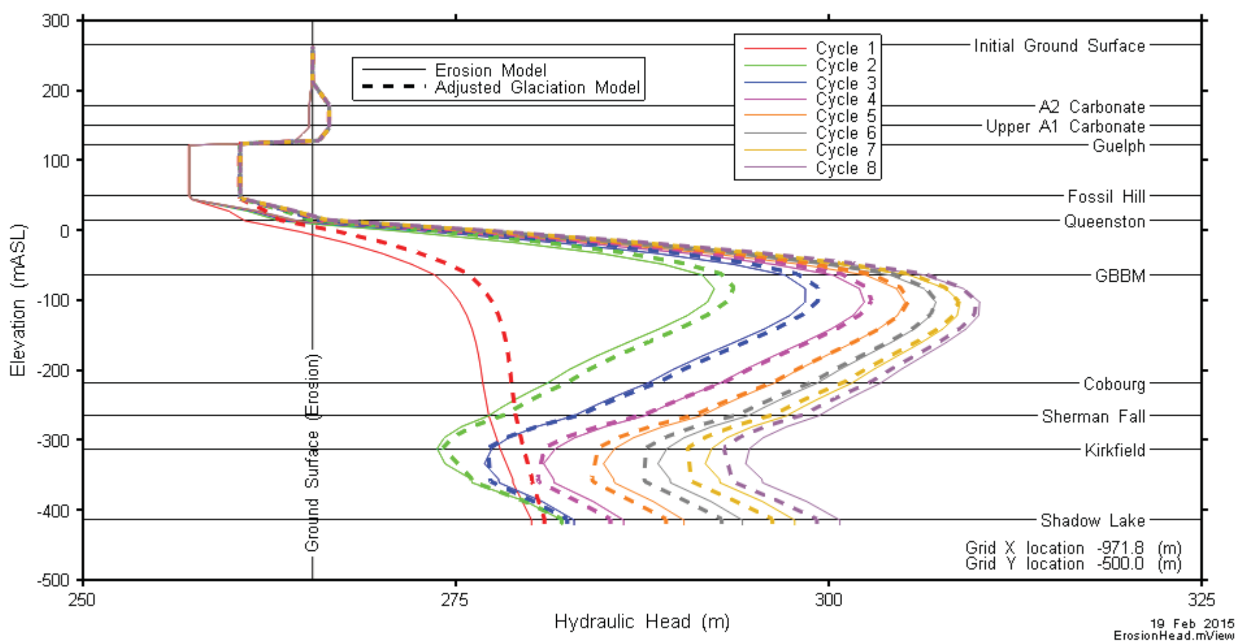

Figure 5-25: Glacial Climate Transient Sub-Regional Flow: Erosion Model With No Erosion and Adjusted Glaciation Model (see text) Comparison of Hydraulic Head Profiles at Water-Supply Well Location at Time of Maximum Well Impact for All Cycles

5.1.5 Erosion Flow Simulations

Uniform and Valley erosion flow simulations were conducted for shaft well and reference well locations.

Velocity comparisons (reference well - no erosion compared to uniform erosion; reference well - no erosion compared to valley erosion; uniform erosion – reference well compared to shaft well) are presented below in Figure 5-26 to Figure 5-28. There are few significant differences in velocities in any of the Ordovician formations between any of the erosion model or wells cases. Kirkfield velocities are higher at the end of the valley erosion cases, but still very low. However, velocities in the Guelph formation increase steadily for the erosion cases, as shown in detail in Figure 5-29.

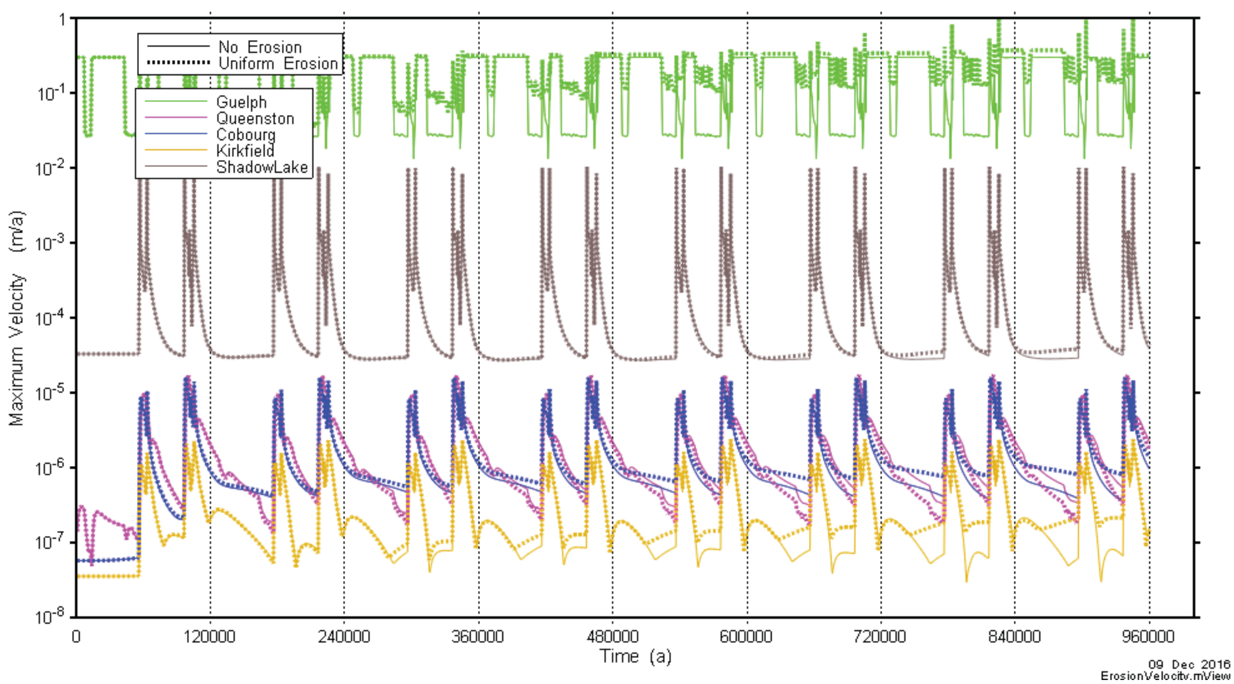

Figure 5-26: Erosion Sub-Regional Flow: No Erosion to Uniform Erosion, Reference Well – Comparison of Maximum Advective Velocity in Repository Vicinity and Selected Formations

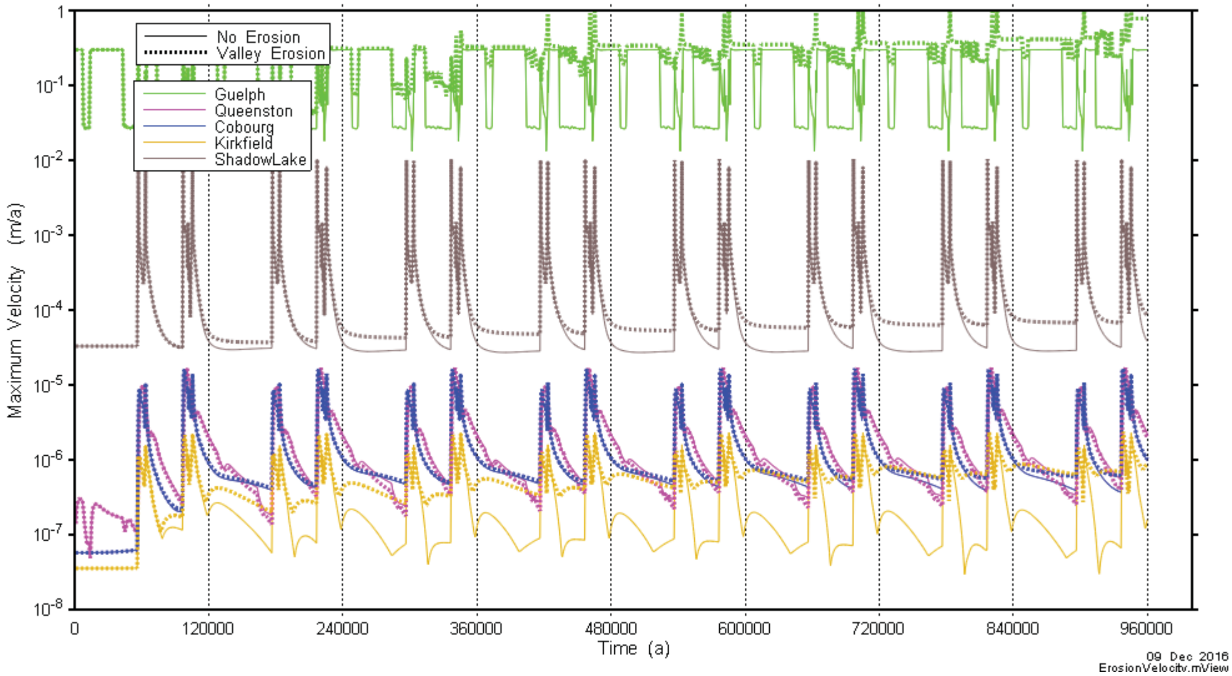

Figure 5-27: Erosion Flow: No Erosion to Valley Erosion, Reference Well - Comparison of Maximum Advective Velocity in Repository Vicinity and Selected Formations

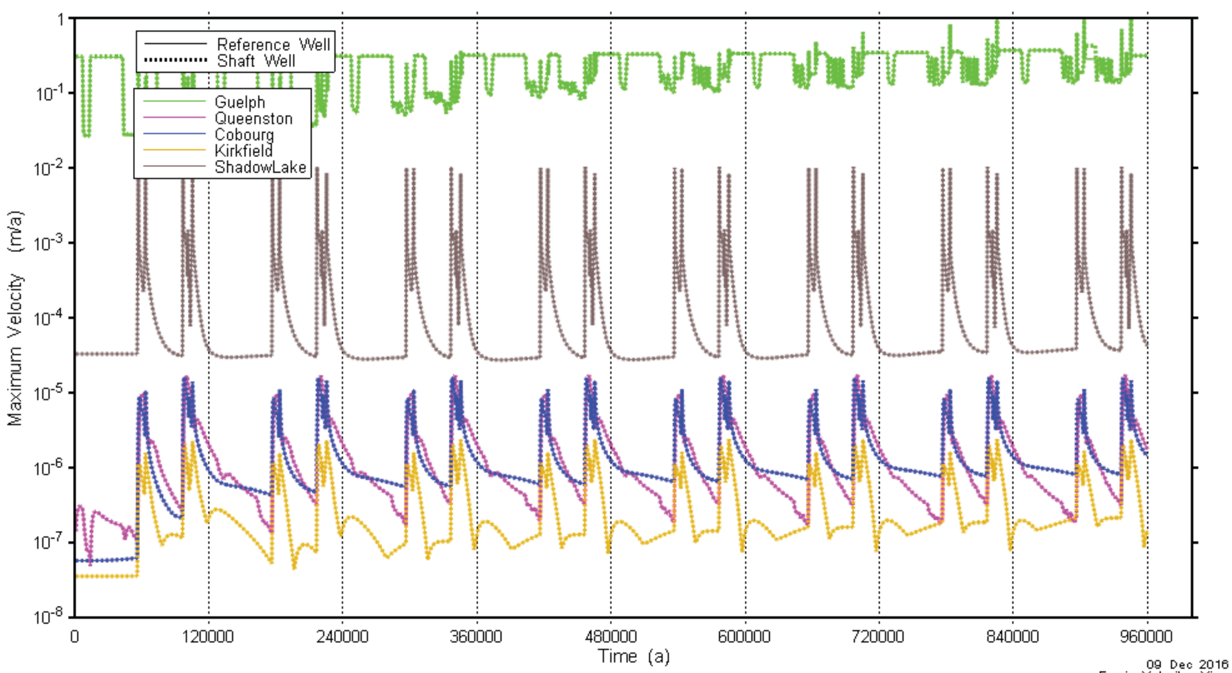

Figure 5-28: Erosion Flow: Reference Well to Shaft Well, Uniform Erosion - Comparison of Maximum Advective Velocity in Repository Vicinity and Selected Formations

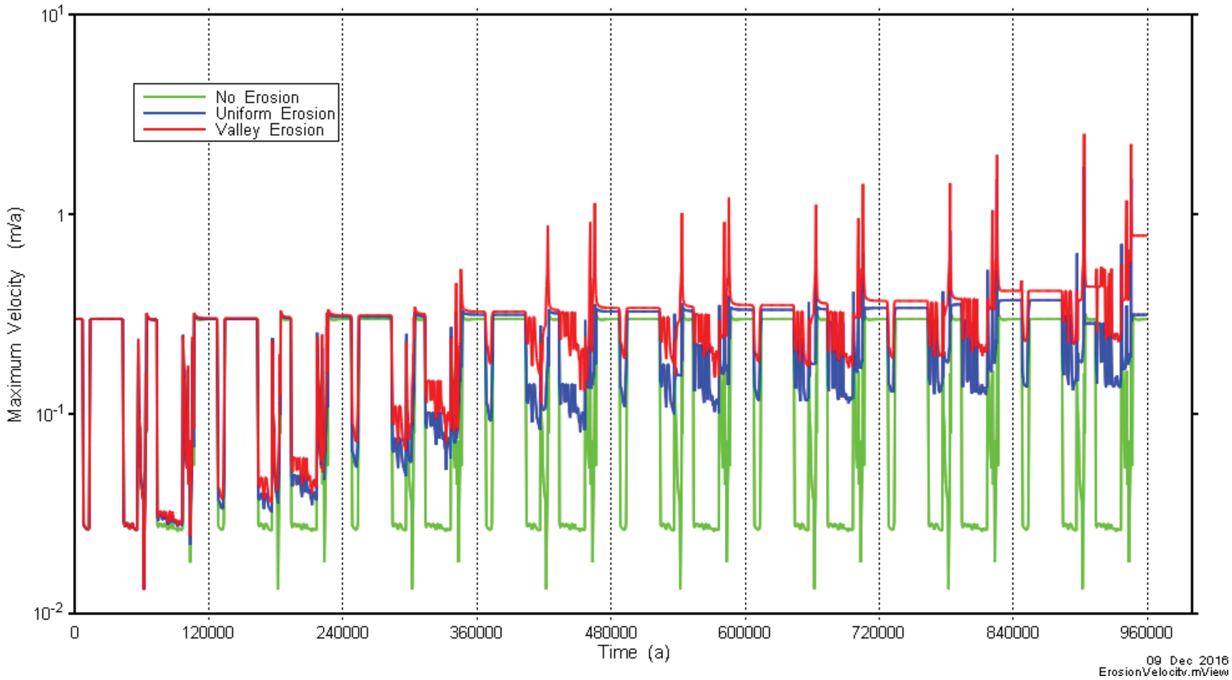

Figure 5-29: Erosion Sub-Regional Flow: Guelph Formation - Comparison of Maximum Advective Velocity in Repository Vicinity for No Erosion, Uniform Erosion and Valley Erosion Cases (All Reference Well)

Velocities in the Guelph during periods of well operation are dominated by the well and are relatively constant. Velocities associated with other periods are generally increased as greater portions of the Guelph are converted into erosion weathered material. Figure 5-30 through Figure 5-33 compare velocities on orthogonal vertical slices at a time between permafrost periods after the "A" retreat in the third cycle and eighth cycle respectively (317,000 a and 917,000 a). Higher velocities in the drift material are communicated over a greater portion of the Guelph as erosion advances, raising velocities above the repository. An interesting effect is evident in Figure 5-33 where discharge above the repository is focussed in the centre of the valley. This may have implications for terrestrial discharge dose calculations.

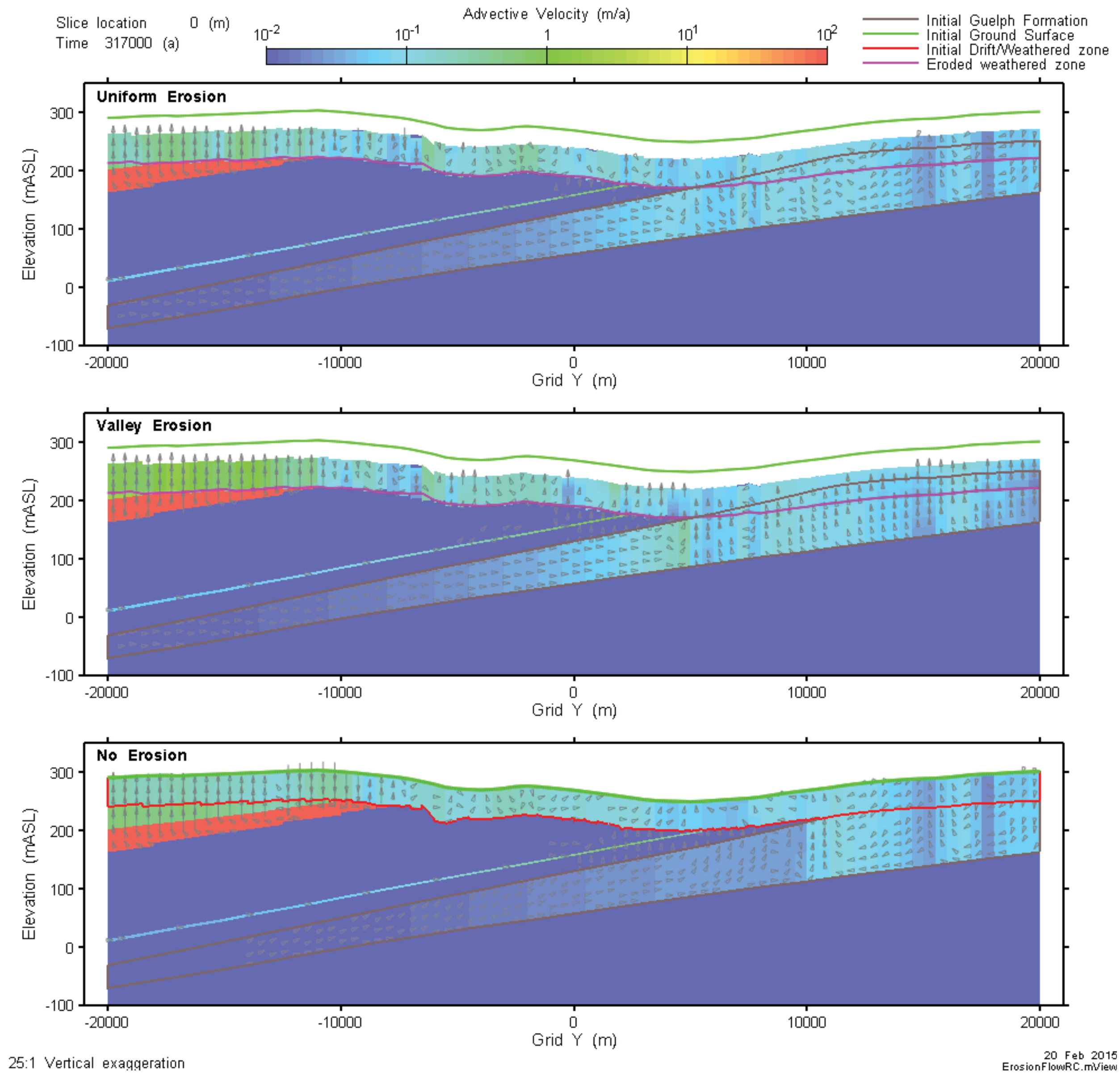

Figure 5-30: Erosion Sub-Regional Flow: Comparison of Advective Velocities for No Erosion, Uniform Erosion and Valley Erosion Cases on YZ Slice Through Repository at 317,000 a (Note: Revised Advective Velocity Scale)

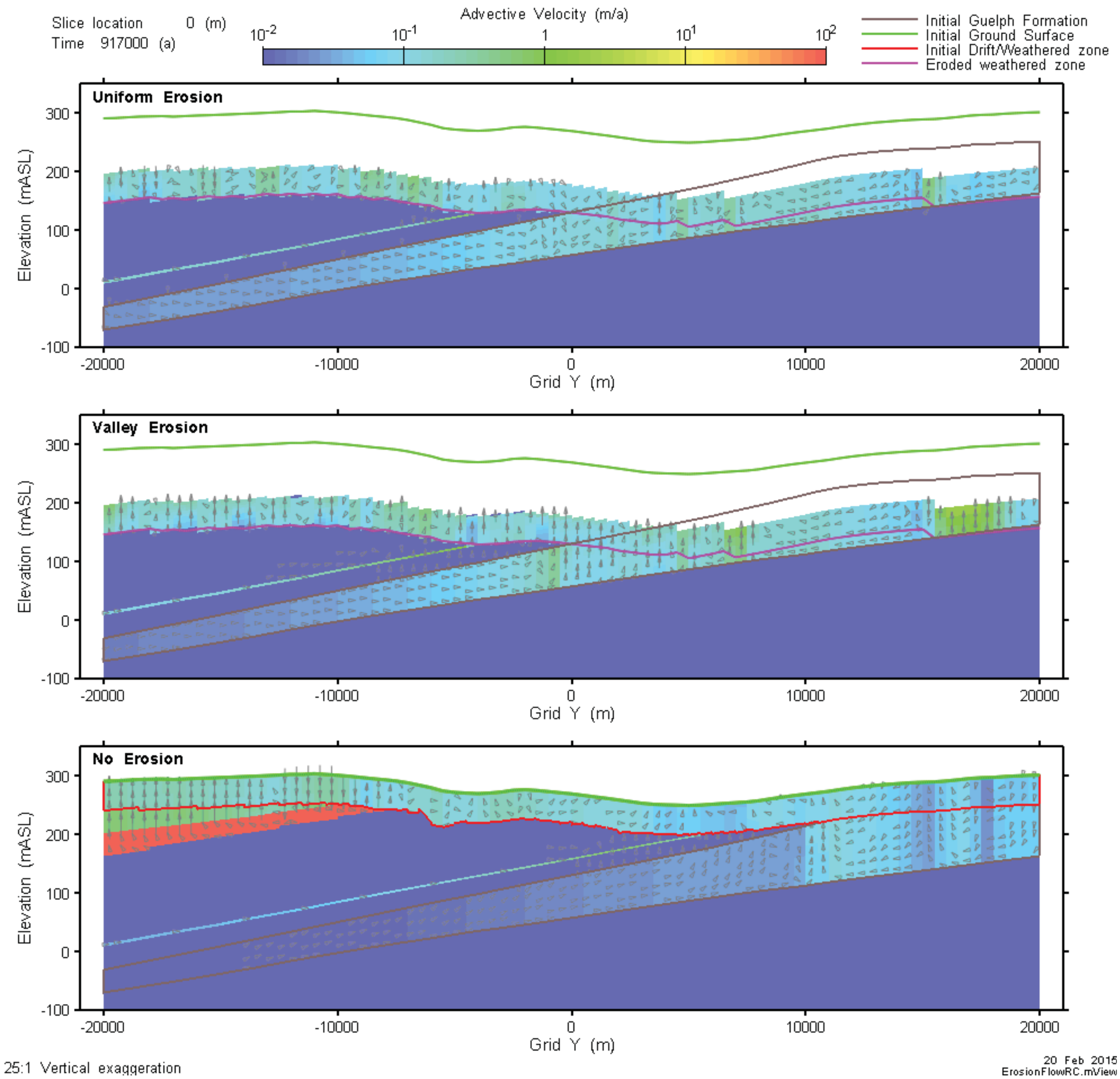

Figure 5-31: Erosion Sub-Regional Flow: Comparison of Advective Velocities for No Erosion, Uniform Erosion and Shaft Erosion Cases on YZ Slice Through Repository at 917,000 a (Note: Revised Advective Velocity Scale)

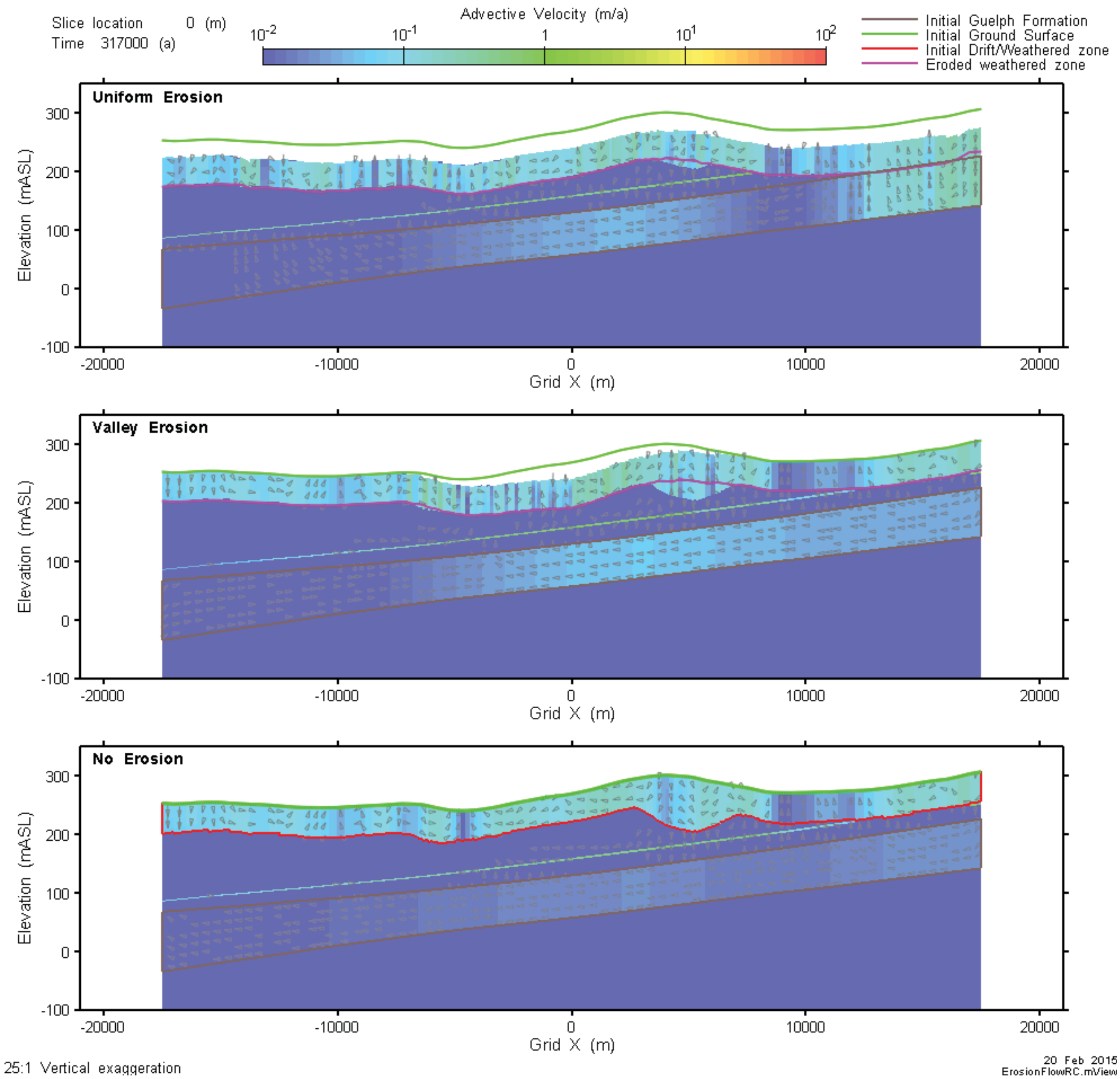

Figure 5-32: Erosion Sub-Regional Flow: Comparison of Advective Velocities for No Erosion, Uniform Erosion and Shaft Erosion Cases on XZ Slice Through Repository at 317,000 a (Note: Revised Advective Velocity Scale)

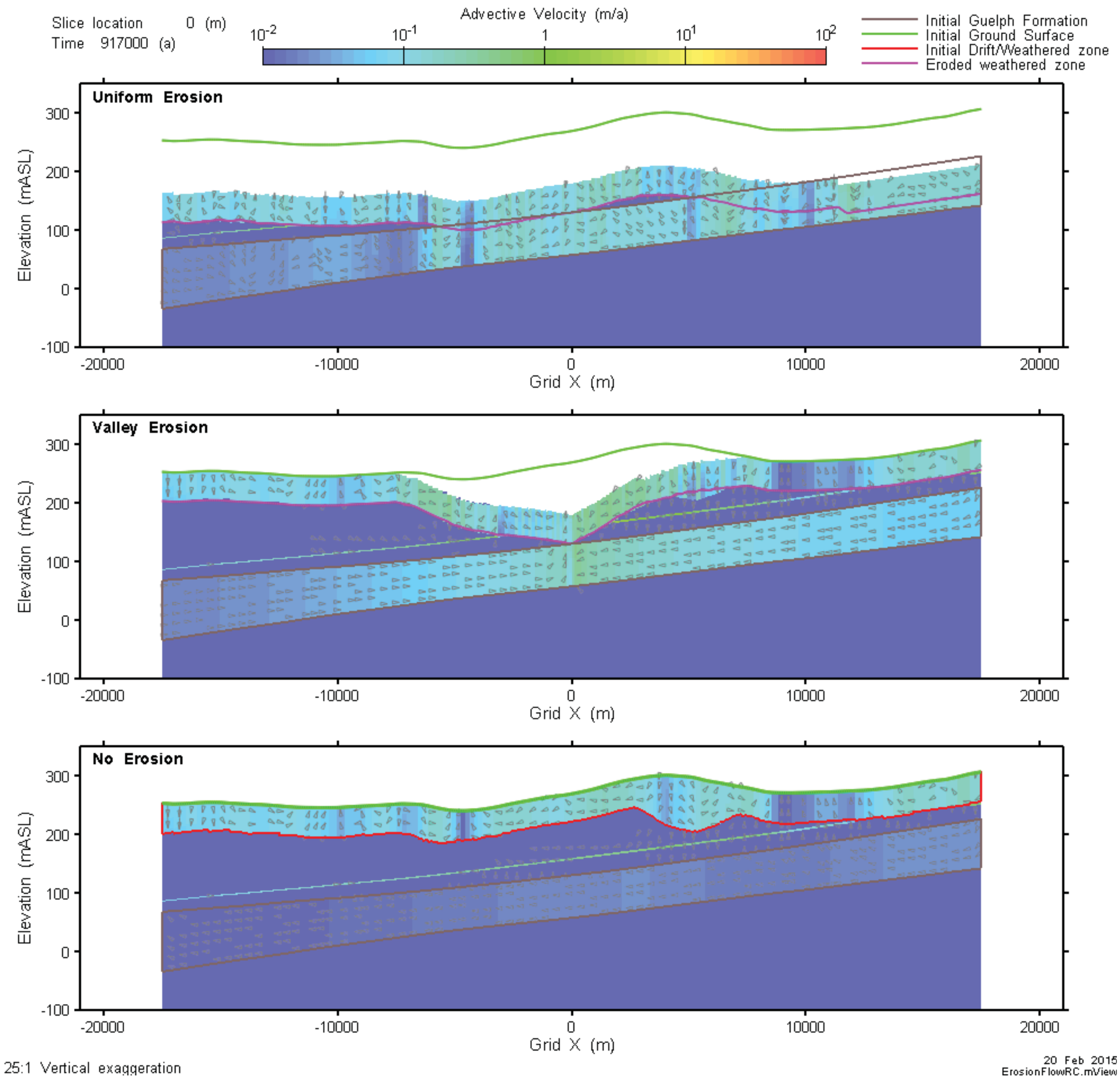

Figure 5-33: Erosion Sub-Regional Flow: Comparison of Advective Velocities for No Erosion, Uniform Erosion and Shaft Erosion Cases on XZ Slice Through Repository at 917,000 a (Note: Revised Advective Velocity Scale)

Cobourg head time series are very similar for all cases. Figure 5-34 compares the No Erosion and four erosion cases over the full glaciation time period. Glacial loading response is similar with a cycle by cycle reduction corresponding to a combination of the eroded ground surface elevation and removal of eroded sediments. A detailed portrayal of heads at the end of the final period within the Cobourg formation (Figure 5-35) illustrates consistent differences between the valley and uniform erosion during non loading periods. The uniform erosion head is approximately 153 m lower than the no erosion head, while valley erosion is 105 m lower. This is consistent with the general larger overall impact expected with uniform erosion.
Within the Guelph formation (Figure 5-36) valley erosion heads respond more strongly to permafrost periods than either no erosion or uniform erosion, resulting in small variations in

head. The difference between final erosion and no erosion heads is 97 m, reflecting the difference in ground surface elevations.

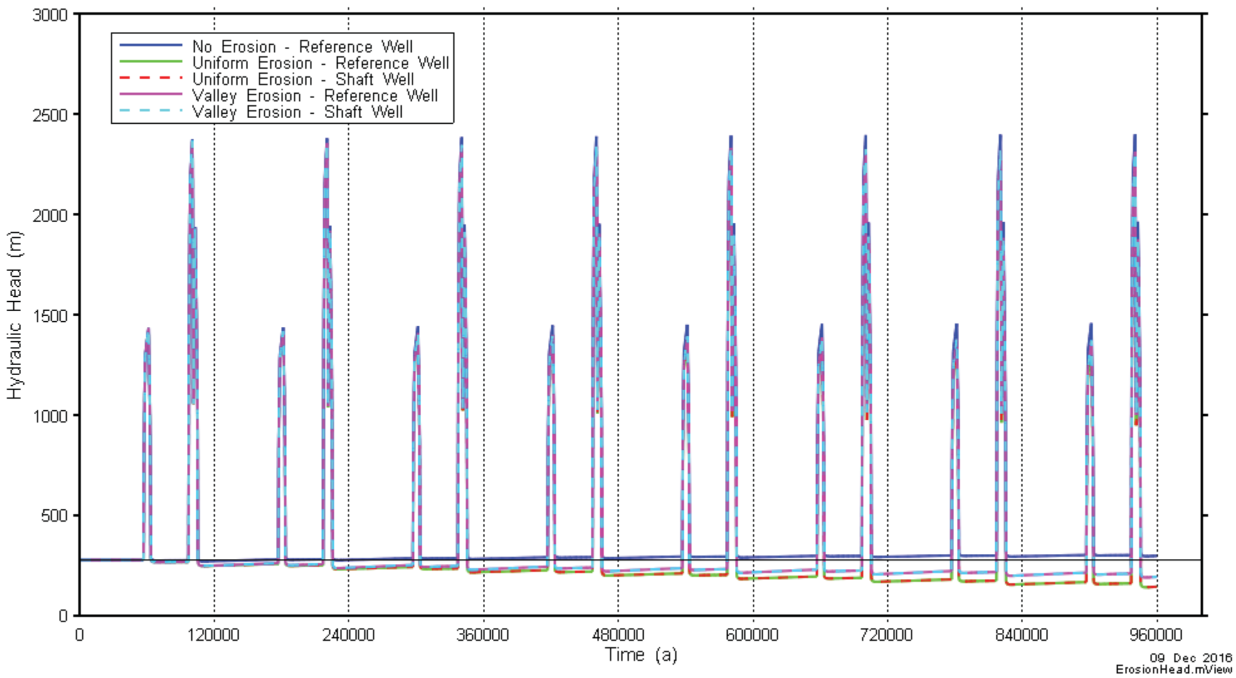

Figure 5-34: Erosion Sub-Regional Flow: Comparison of Cobourg Formation Hydraulic Head Above Repository

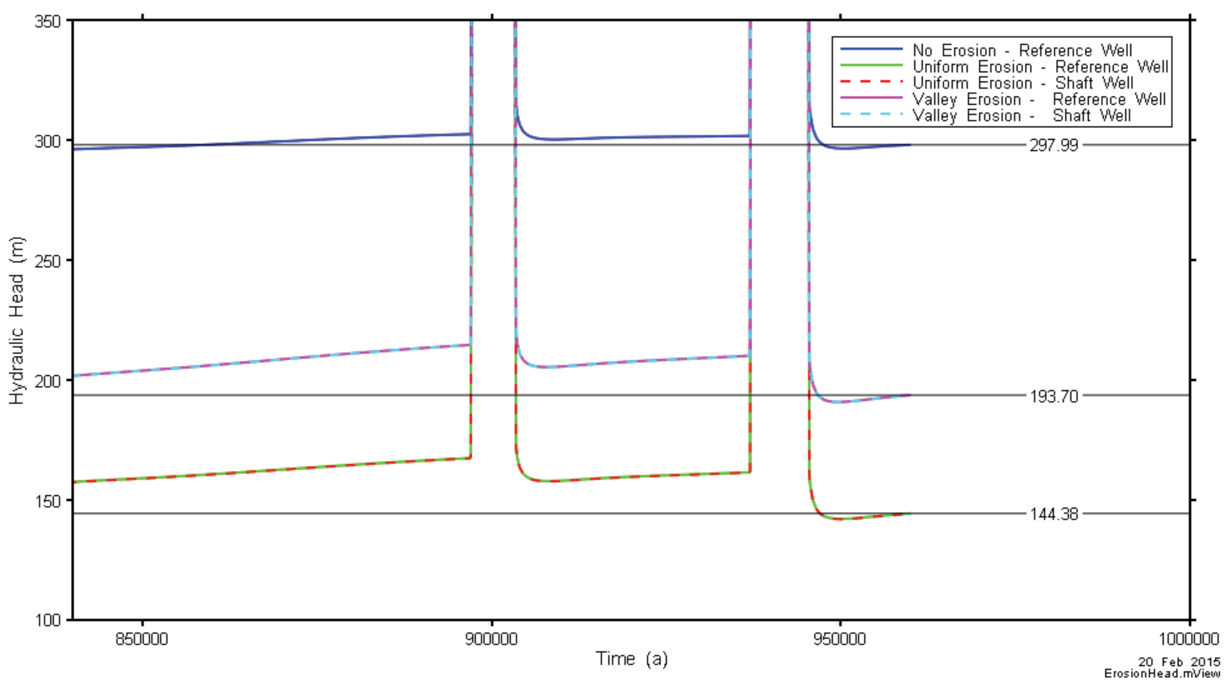

Figure 5-35: Erosion Sub-Regional Flow: Detail of Comparison of Cobourg Formation Hydraulic Head Above Repository at End of Eighth Glacial Cycle

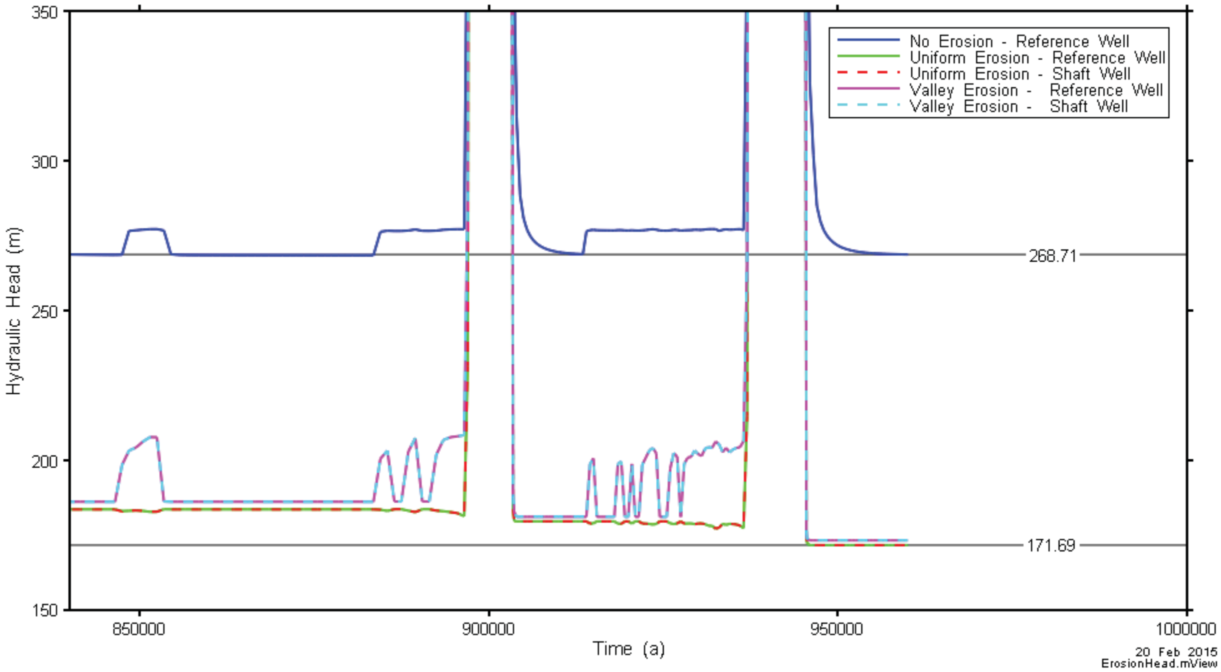

Figure 5-36: Erosion Sub-Regional Flow: Detail of Comparison of Guelph Formation Hydraulic Head Above Repository at End of Eighth Glacial Cycle

Figure 5-37 shows the evolution of head profiles with each glacial cycle at the time of maximum well operation for uniform and valley erosion as compared to the no erosion case. For the no-erosion case, peak heads within the Georgian Bay/Blue Mountain formation increase by approximately 20 m from Cycle two to eight. In contrast, peak erosion heads within the same formation decline relative to ground surface indicating a slight prevalence of erosion processes. A particularly interesting result is the differences in head at the bottom of the model in the more permeable Shadow Lake formation. For uniform erosion, head changes relative to ground surface from being slightly overpressured at the start of the simulation to being underpressured, again indicative of a slight cumulative impact of erosion processes. By contrast, valley erosion Shadow Lake heads are significantly overpressured relative to eroded ground surface as they reflect a combination of non-eroded and eroded behaviour. This overpressured lower formation leads to a higher vertical gradient up to the Sherman Fall, explaining the previously noted higher Kirkfield velocities for the valley case. Although the choice of zero-flow boundary conditions at the vertical model extents may have impacted the permeable formation behaviour, it is still evident that spatial variations in erosion can contribute to anomalous head distributions.

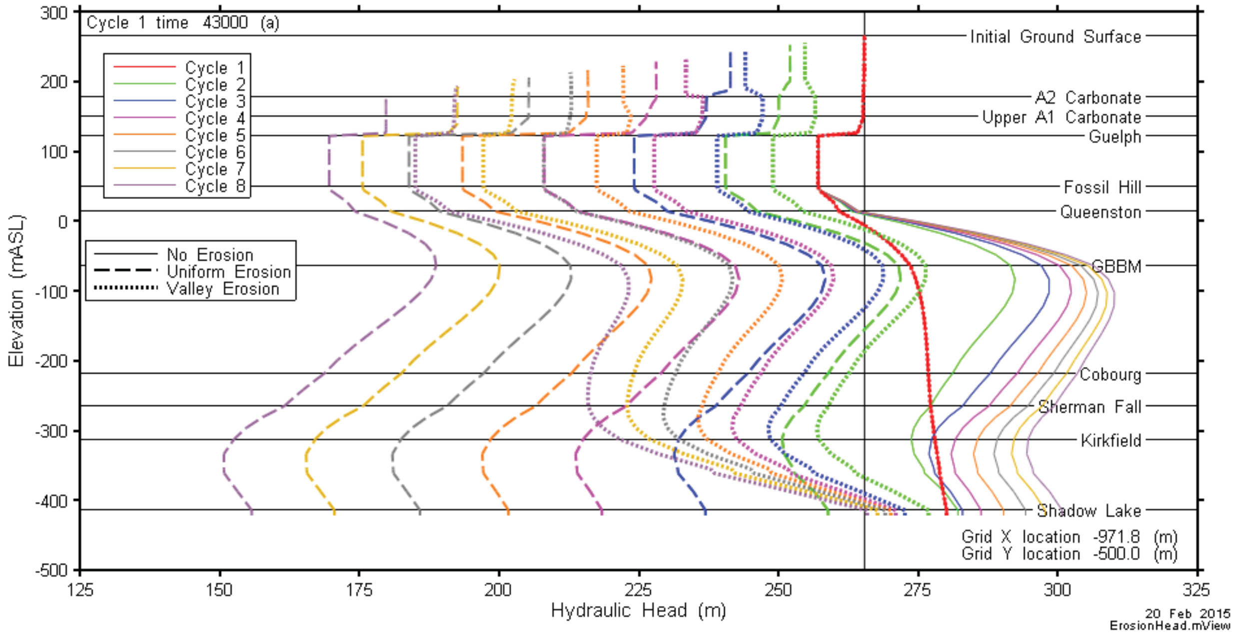

Figure 5-37: Erosion Sub-Regional Flow: Evolution of Head Profiles at Time of Maximum Well Operation Time for Each Cycle at Reference Well Location

5.1.6 Significance of Erosion Flow Systems to Safety Assessment

Repository MLE simulations as described in Section 4.1.6 were performed for Uniform and Valley Erosion Cases. Results are compared to the No Erosion case in Figure 5-38. Erosion MLE decrease steadily, but at a slow rate, due to the reduction in travel distance from the repository to surface. There are no significant differences between the various cases.

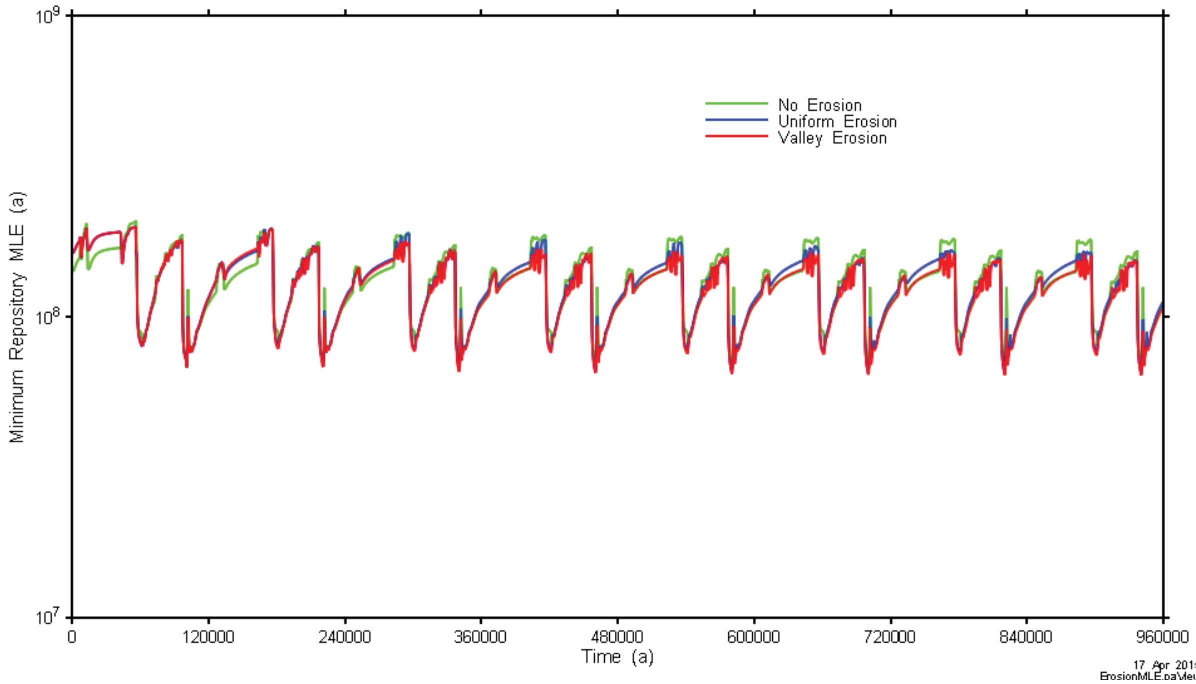

Figure 5-38: Repository MLE for No, Uniform and Valley Erosion

5.2 Erosion Site-Scale Transport Model

Site-Scale transport modelling for the erosion cases uses the grid and approach developed for the Glaciation Site-Scale transport models in Section 4.2, modified slightly to use changing erosion property sets as described in the previous section for erosion flow modelling.

Transport model domain, numeric grid, well and source locations, well operation schedule, repository properties and initial geosphere property assignments are all as presented in Section 4.2.1 and will not be further described here. This section will describe the setting of the Site-Scale model within the Erosion Sub-Regional Flow model, erosion property assignments, boundary conditions, and transport model results.

5.2.1 Model Description

5.2.1.1 Model Setting with Erosion Sub-Regional Model

As described in Section 4.2.1.1, the Site-Scale model extends vertically from the Pre-Cambrian to the top of the Salina A2. The Site-Scale model coordinate system is rotated approximately 123 degrees compared to the Erosion Sub-Regional local coordinate systems. The horizontal model domain and coordinate system are presented with the Erosion Sub-Regional model extents for context in Figure 5-39 and Figure 5-40.

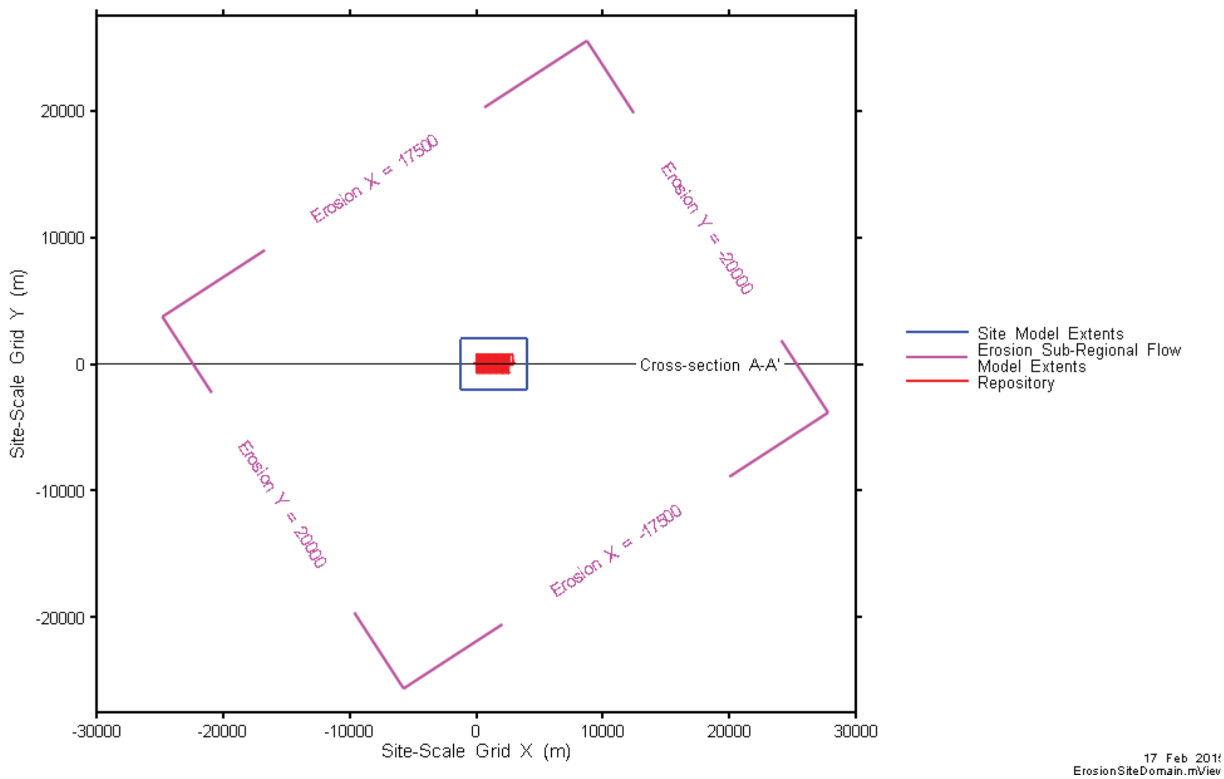

Figure 5-39: Site-Scale Model Domain – Plan View

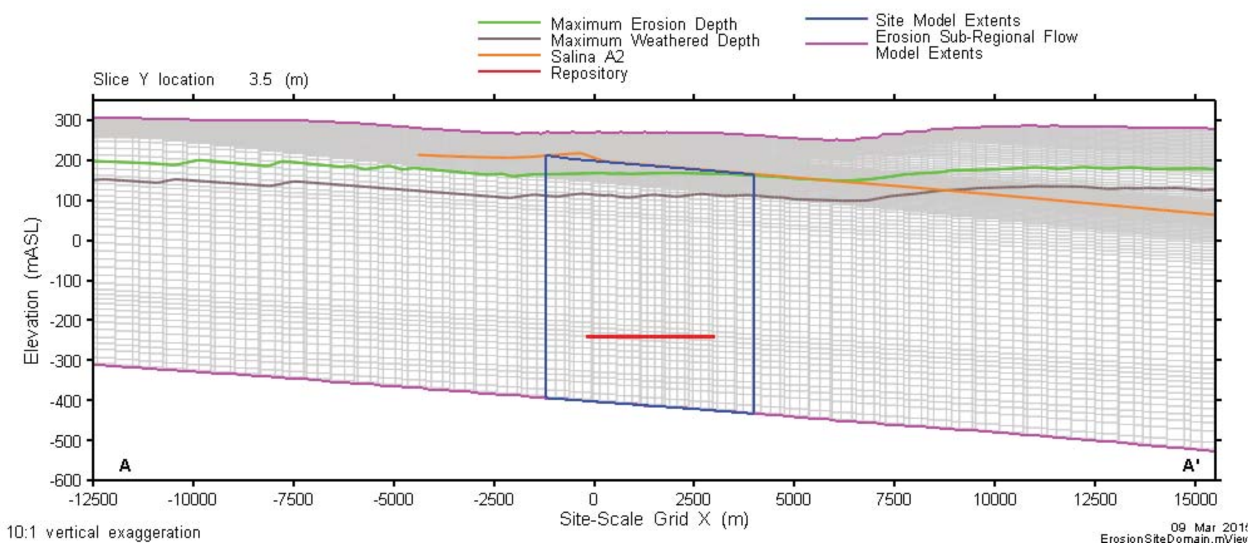

Figure 5-40: Site-Scale Model Domain – Vertical Section Through Site Y = 0

The Site-Scale model geosphere is shown within the surrounding Erosion Sub-Regional geosphere in Figure 5-41. Cross-section A-A' from Figure 4-40 is also shown to assist in orienting the viewpoint.

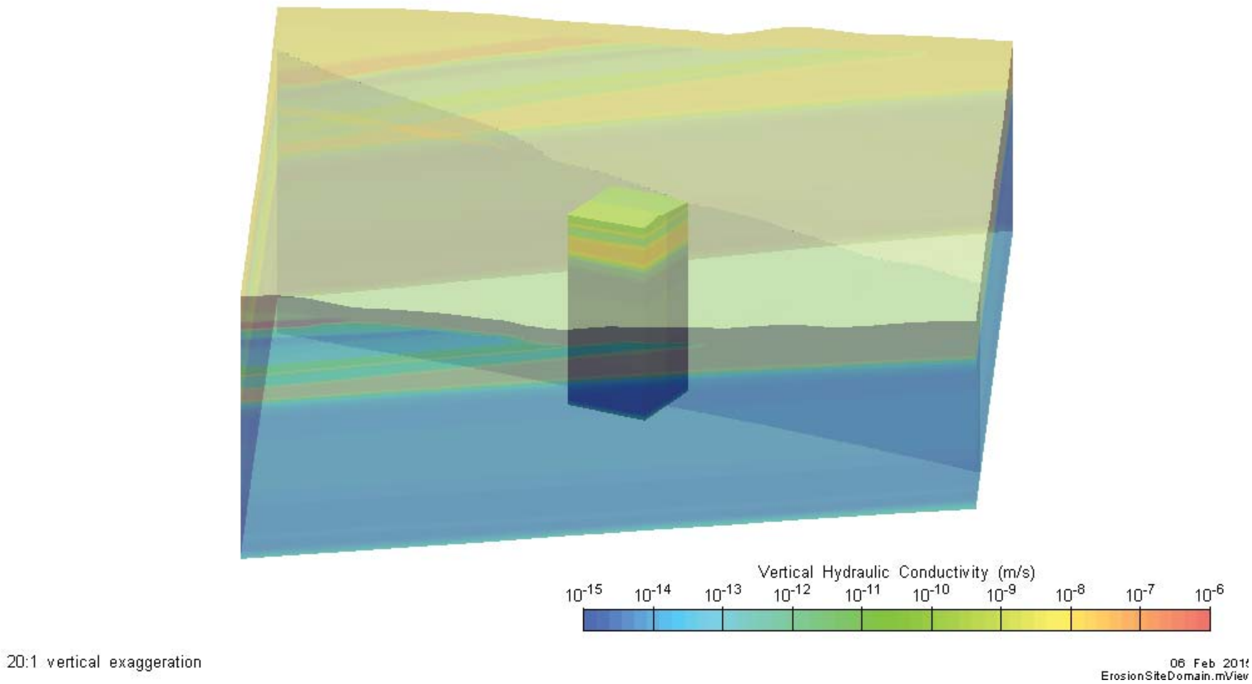

Figure 5-41: Site-Scale and Erosion Sub-Regional Model Domain and Assigned Initial Geosphere Hydraulic Conductivities

Vertical model discretization is shown in Figure 5-42 and Figure 5-43 with maximum extents of erosion and erosion weathered zone indicated.

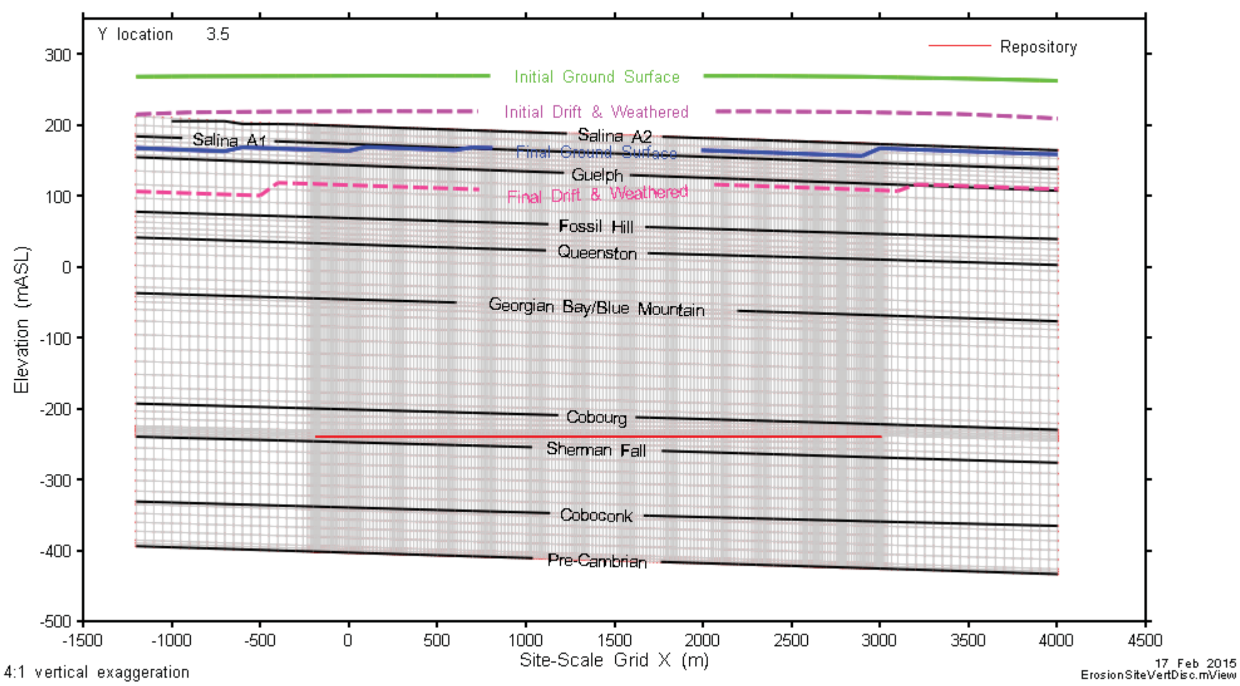

Figure 5-42: Site-Scale Model Discretization in XZ Plane Through Centre of Grid

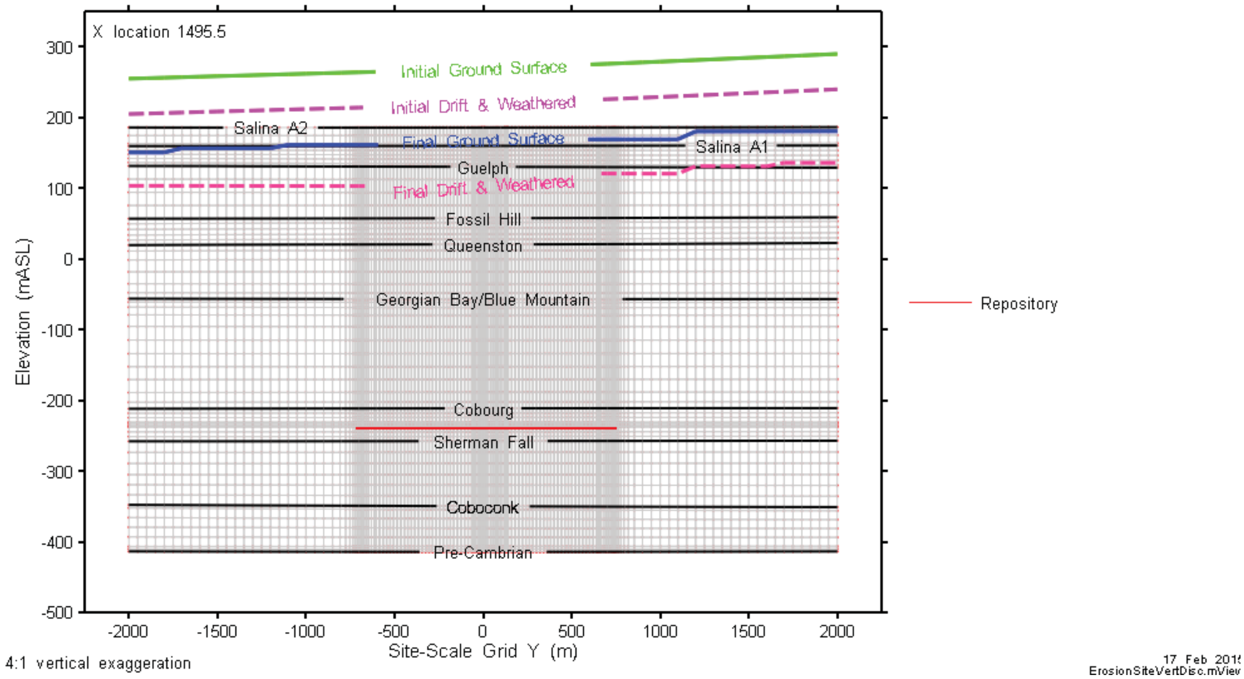

Figure 5-43: Site-Scale Model Discretization in YZ Plane Through Centre of Grid

5.2.1.2 Property Assignment

Properties for each erosion period were calculated as described in Section 5.1.2.2. A new ground surface position was determined based on erosion type (valley or uniform) and period depth and all elements above the revised ground surface were set inactive. All elements less than 50 m below the ground surface were set to a weathered zone, or Drift. Unlike the Erosion Sub-Regional model, which extends to current ground surface, the Site-Scale model vertical domain ends at the top of the Salina A2, which is 55 to 110 m below ground surface. Consequently, the first 9 periods (up to and including 5A) only modify the depth and extent of the weathered zone. The remaining 8 periods also remove material from the model (Figure 5-44 and Figure 5-45).

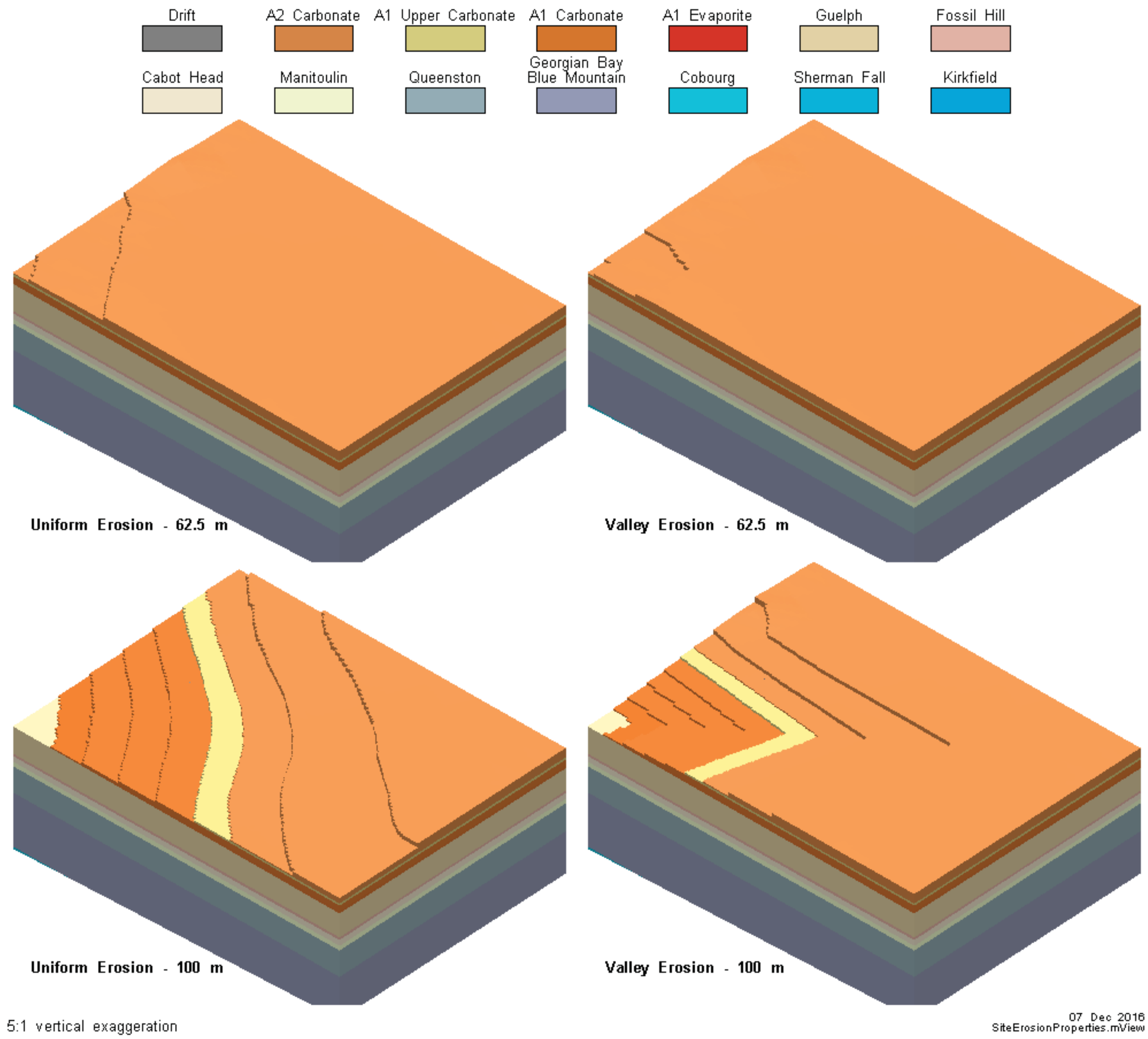

Figure 5-44: Erosion Site-Scale Model Property Assignment Before Weathered Zone (Drift) Reassignment

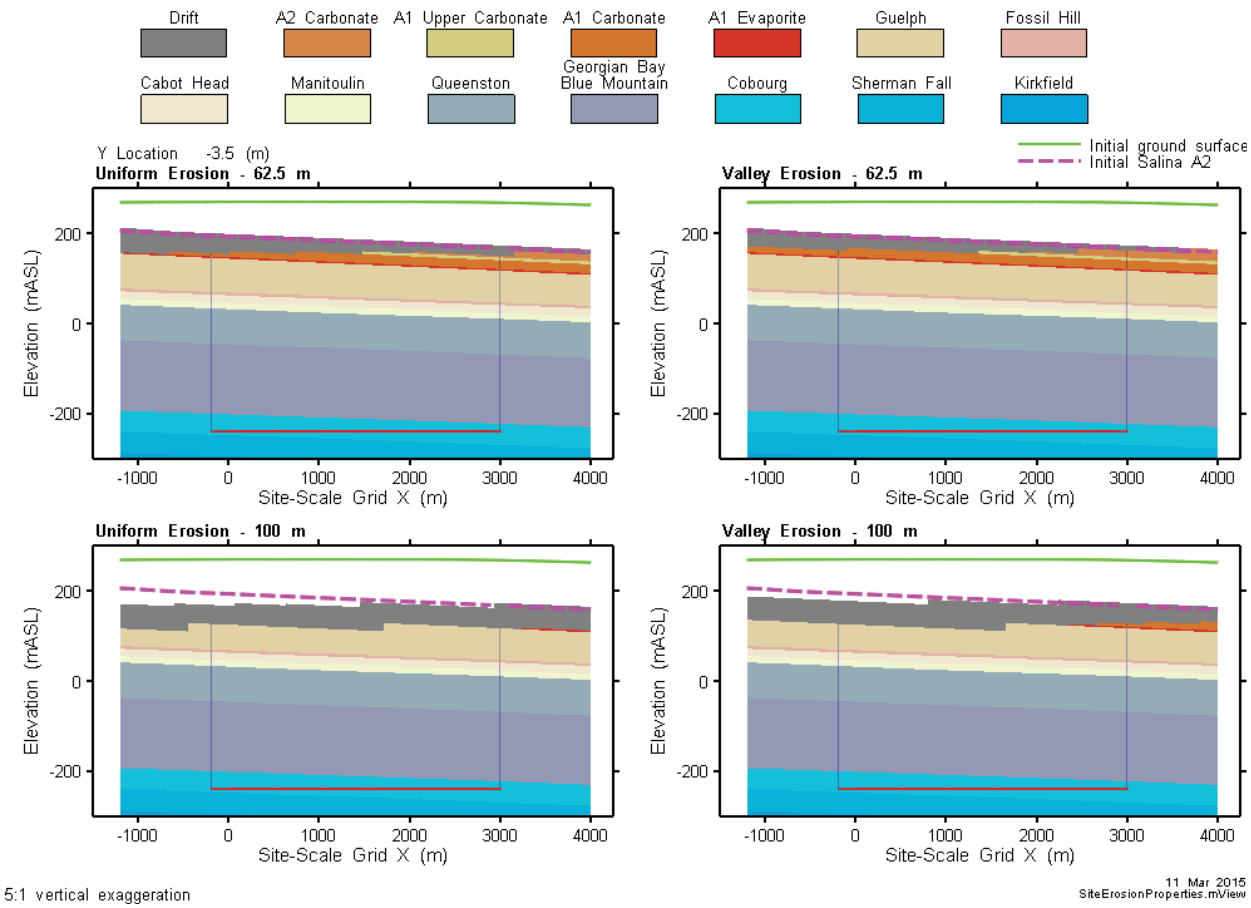

Figure 5-45: Erosion Site-Scale Model Property Assignment on Vertical Slice Through Y = 0

5.2.1.3 Boundary Conditions

Boundary conditions were applied as fixed head on all faces of the model except for the bottom, which was defined as zero flow. Surface loading was applied at the top of the model only. Heads were extracted from the Erosion Sub-Regional model simulation results, while loading stresses were interpolated from Sub-Regional model input loading stresses.

5.2.1.4 Permafrost

As the ground surface erodes, permafrost reaches deeper into the Site-Scale model domain. Figure 5-46 shows the extent of permafrost penetration in the Site-Scale model grid at the time of maximum permafrost depth in each of the first, fifth, and final glacial cycles.

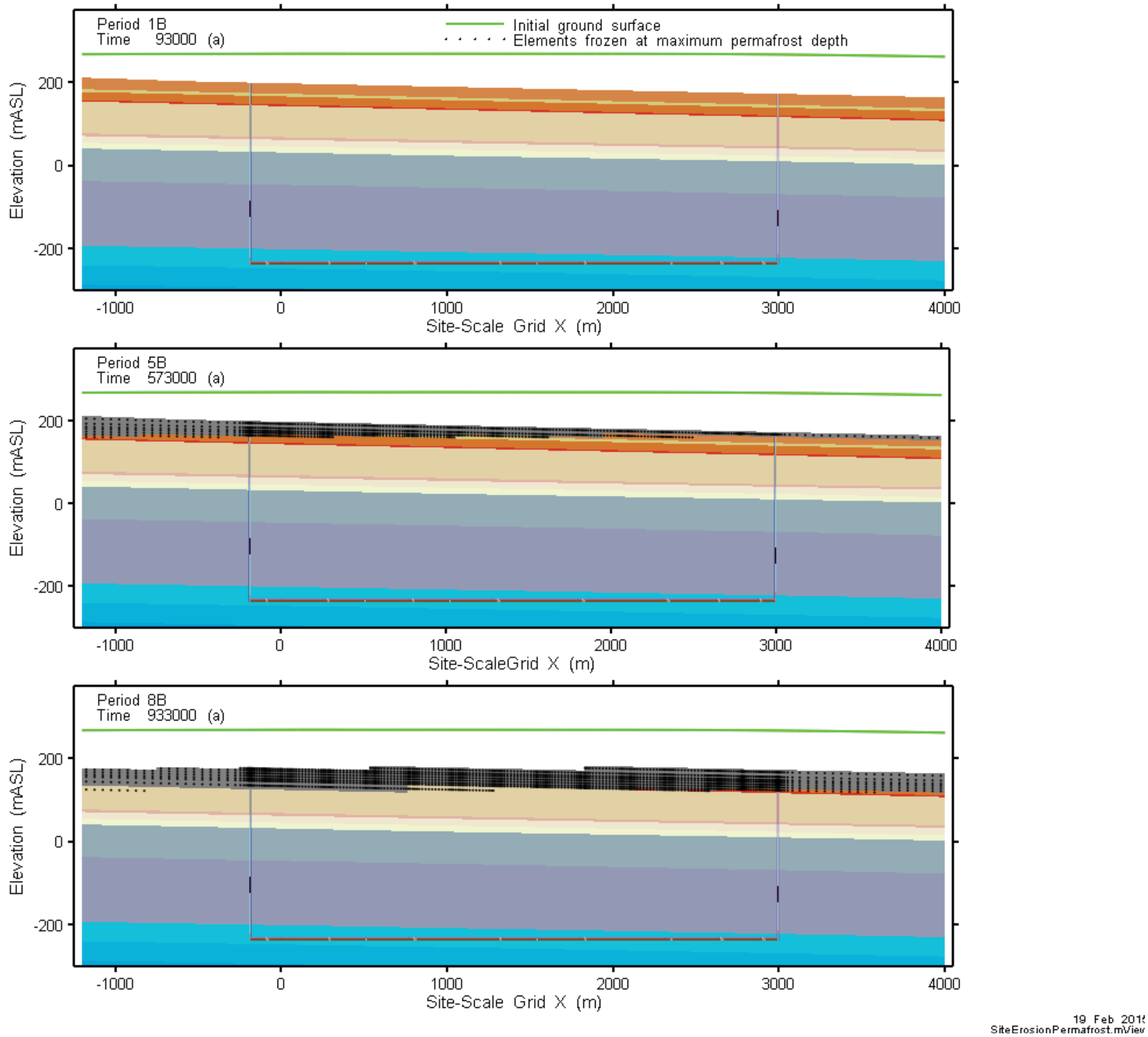

Figure 5-46: Site-Scale Model Permafrost –Specified Permafrost Elements at Time of Maximum Permafrost Depth in the First, Fifth, and Eighth Glacial Cycles on Vertical Slice Through Repository for Uniform Erosion Case

5.2.2 Modelling Cases

Reference case simulations were undertaken for uniform and valley erosion for reference and shaft well and source locations.

5.2.2.1 Flow System Verification

Correct implementation of head and loading boundary conditions was verified by comparing simulated heads from flow and transport models in the final glacial cycle. Figure 5-47 and Figure 5-48 show a clear correspondence of head contours at the Site-Scale model boundary for the UE and VE case respectively. The figures also illustrate the impact of repository shafts and tunnels on the Site-Scale model head distribution.

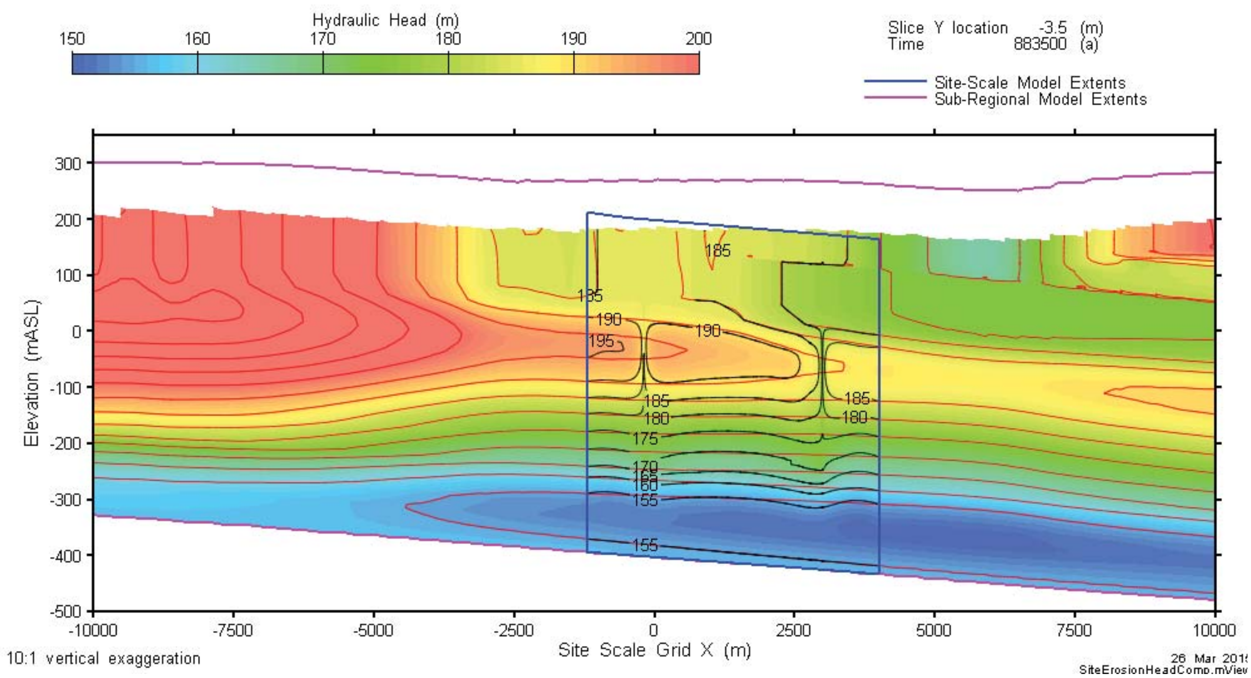

Figure 5-47: Site-Scale Boundary Conditions – Uniform Erosion - Comparison of Hydraulic Heads on Vertical Slice Through Repository at 883.5 ka.

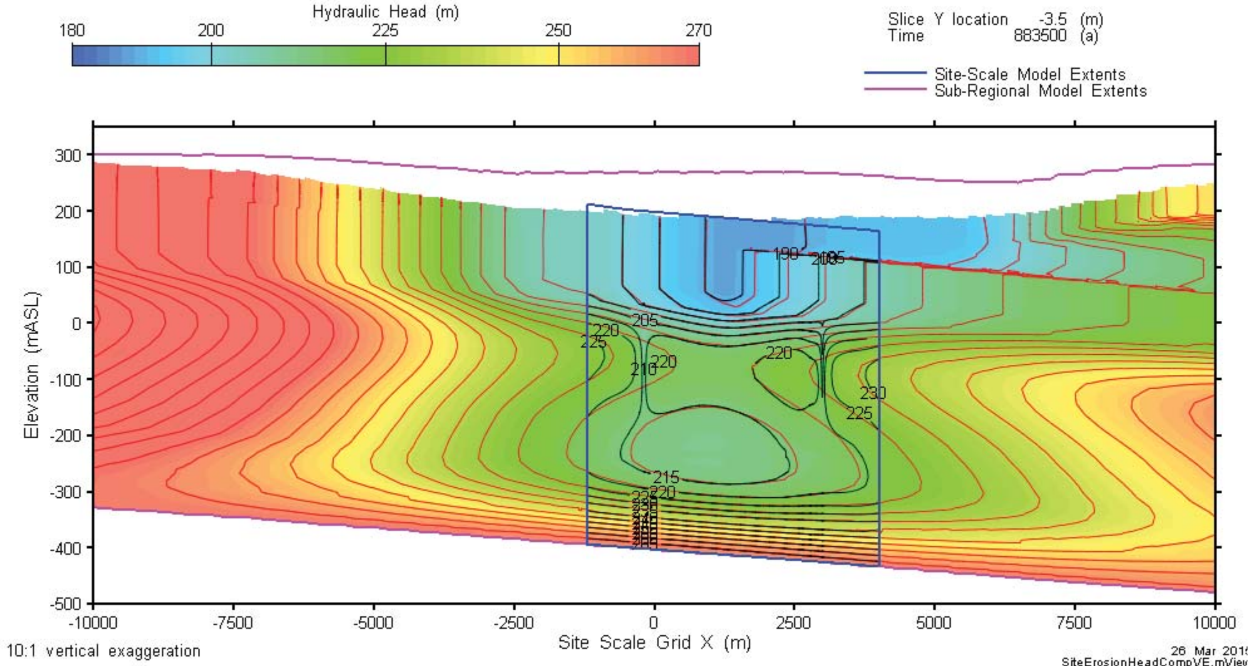

Figure 5-48: Site-Scale Boundary Conditions – Valley Erosion - Comparison of Hydraulic Heads on Vertical Slice Through Repository at 883.5 ka.

5.2.2.2 Results

Spatial representations of transport model results at 1 Ma for the reference and shaft well cases are shown in Figure 5-49 and Figure 5-50. Three-dimensional iso-volumes at 1 Bq/m^3 are presented in Figure 5-51 and Figure 5-52. The figures indicate very minor differences in transport between erosion and no-erosion cases, and virtually no difference between uniform and valley erosion cases. The results further corroborate the evidence of the diffusion dominated nature of transport from the repository.

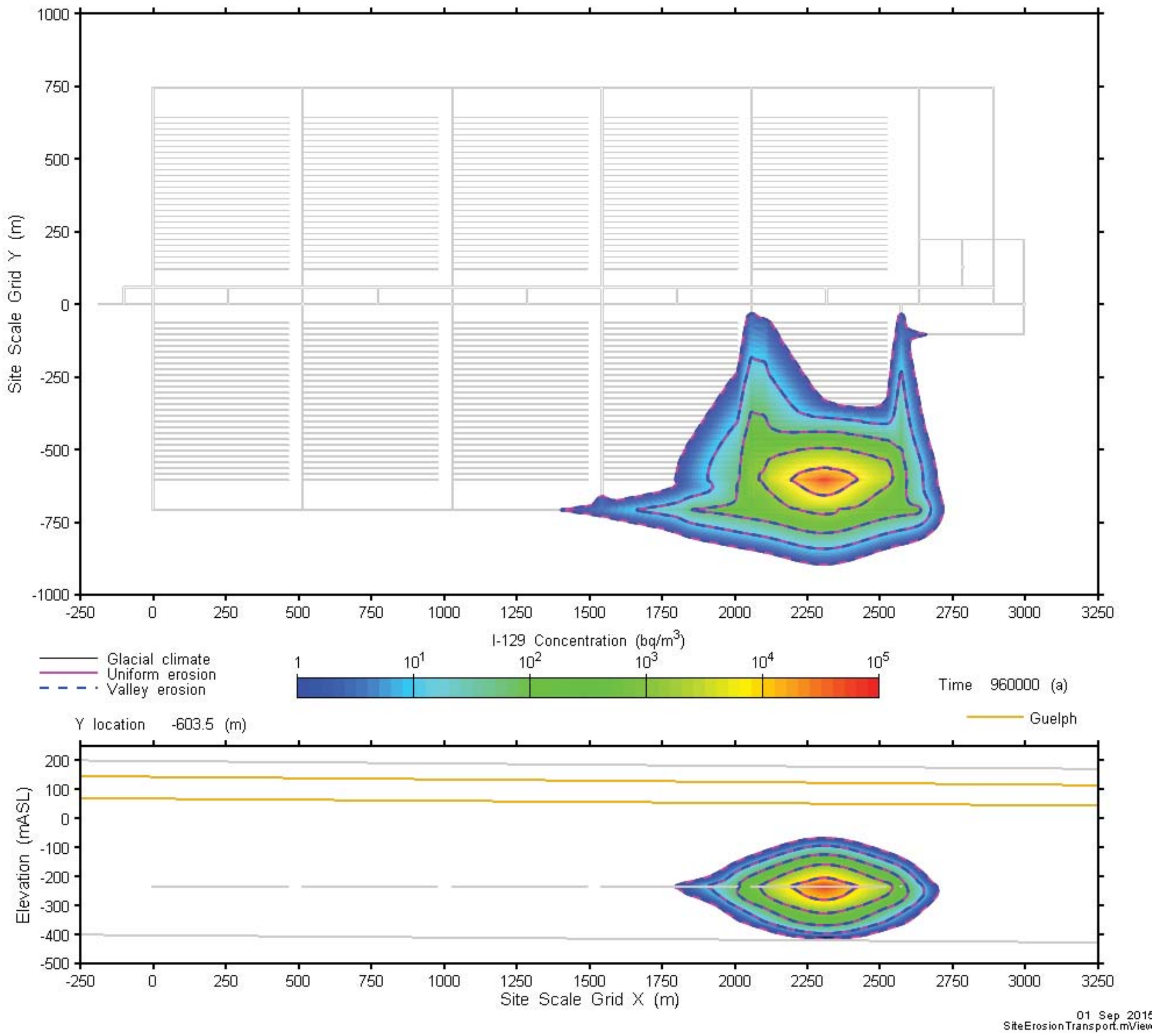

Figure 5-49: Site-Scale Model: Reference Well – Comparison of Erosion and Glaciation Only I-129 Transport at 960 ka

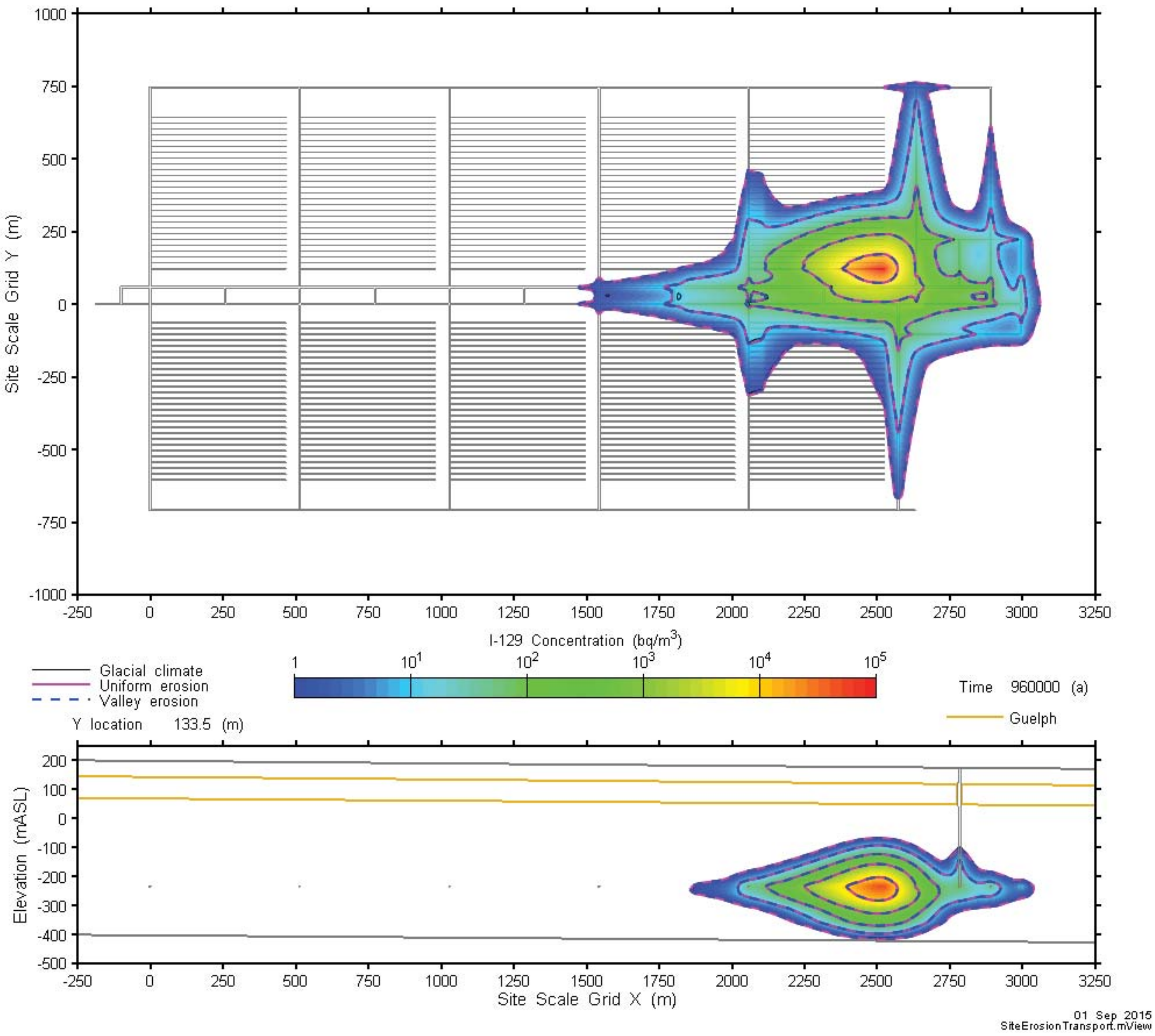

Figure 5-50: Site-Scale Model: Shaft Well – Comparison of Erosion and Glaciation Only I-129 Transport at 960 ka

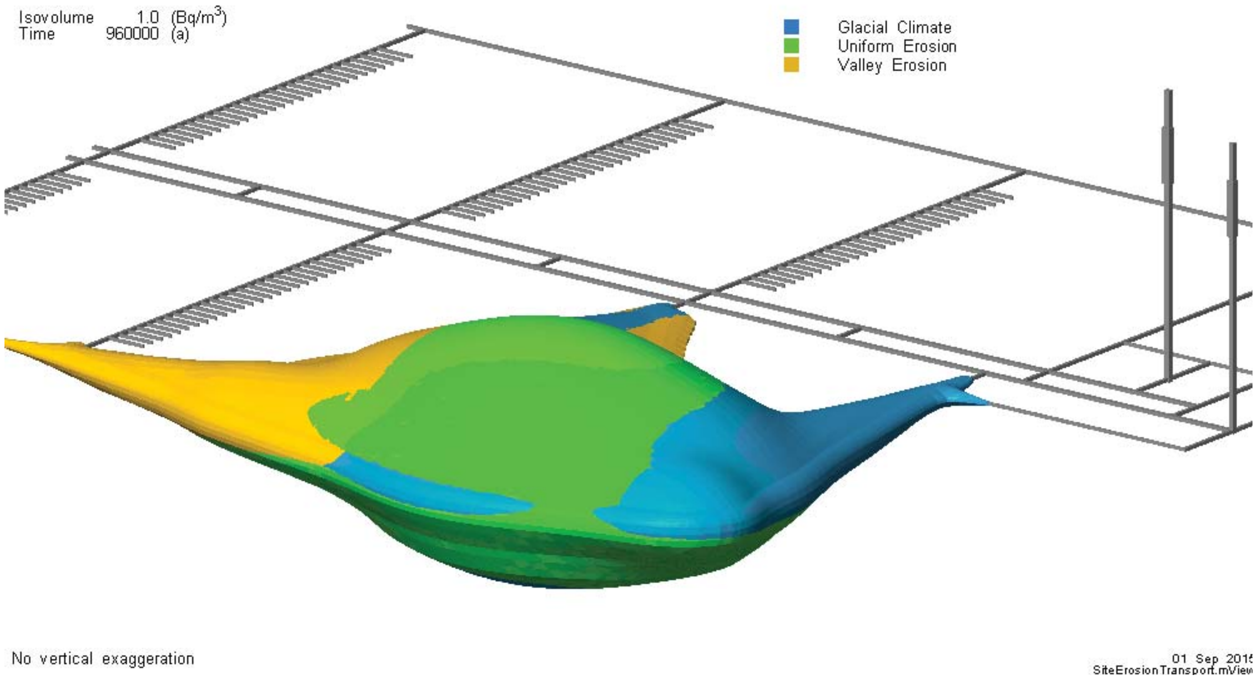

Figure 5-51: Site-Scale Model: Reference Well – 3D Comparison of Erosion and Glaciation Only I-129 Transport at 960 ka

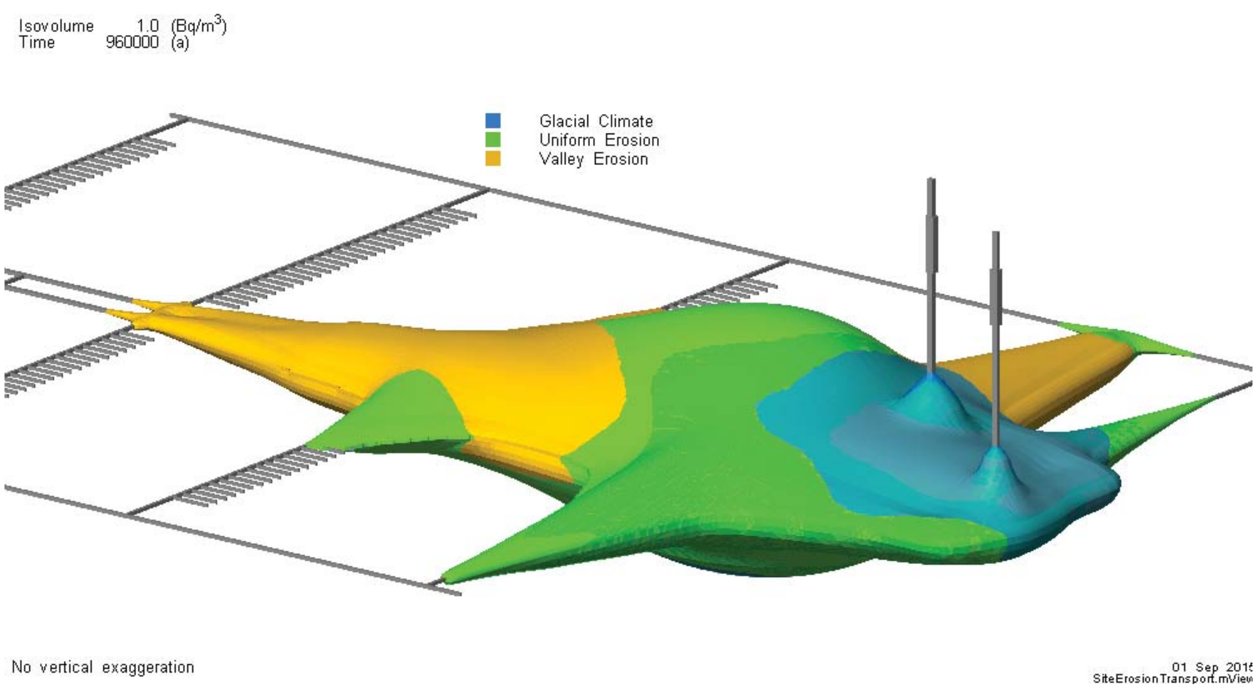

Figure 5-52: Site-Scale Model: Shaft Well – 3D Comparison of Erosion and Glaciation Only I-129 Transport at 960 ka

Transport into formations and uptake by the water supply well for uniform erosion are compared to glaciation only results in Figure 5-53 and Figure 5-54, while valley and uniform erosion case well transport are compared in Figure 5-55.

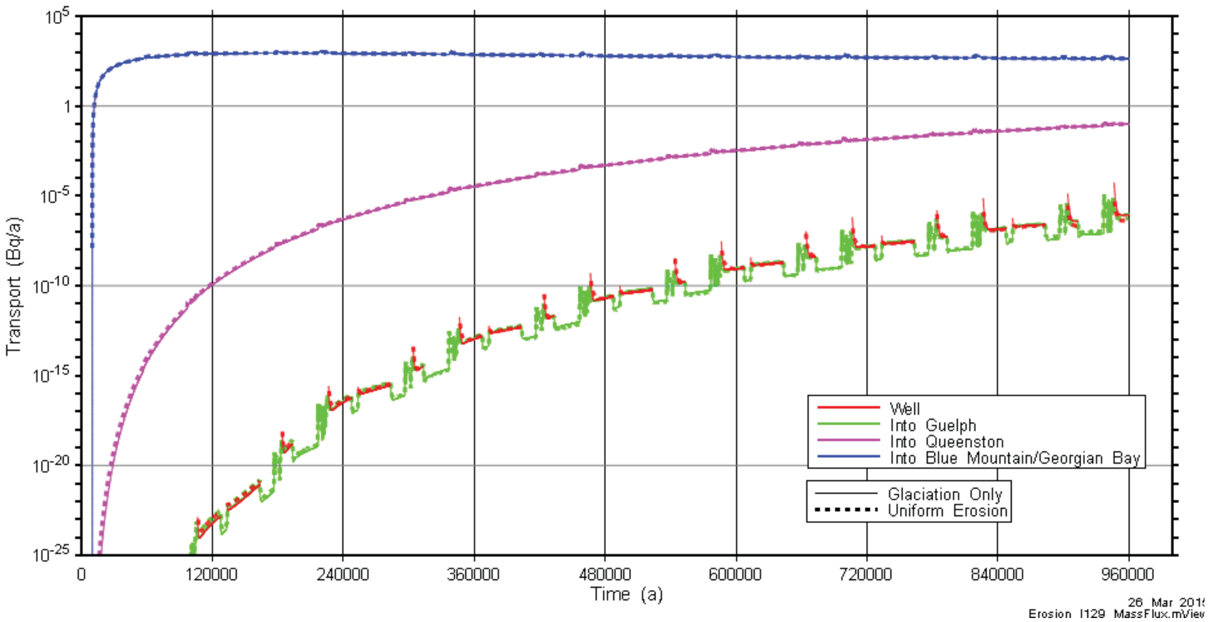

Figure 5-53: Site-Scale Model: Reference Well Results – Mass Flux Into Formations and Water-Supply Well for Uniform Erosion and Glaciation Only Cases

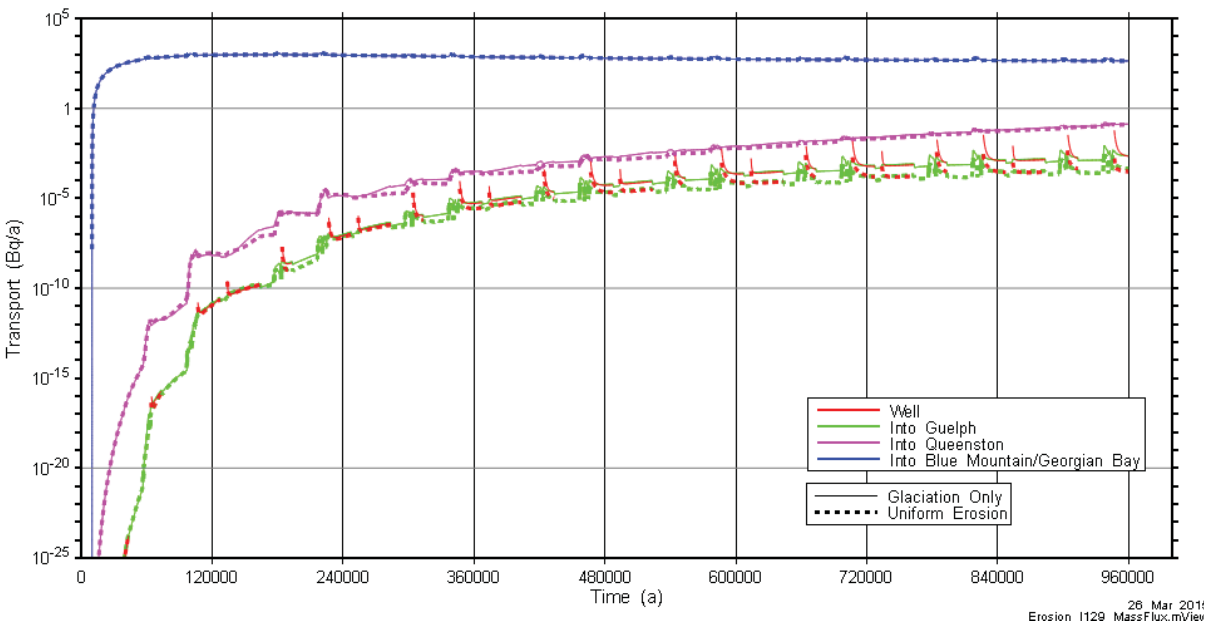

Figure 5-54: Site-Scale Model: Shaft Well Results – Mass Flux Into Formations and Water-Supply Well for Uniform Erosion and Glaciation Only Cases

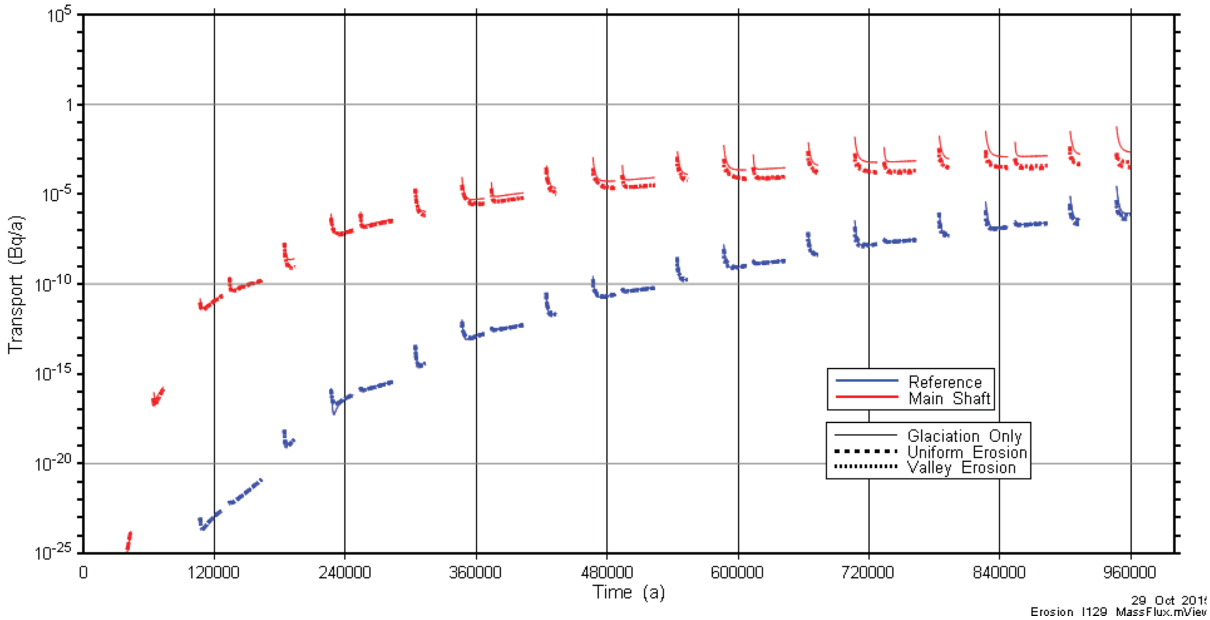

Figure 5-55: Site-Scale Model: Mass Flux Into Water-Supply Well for Uniform and Valley Erosion for Reference and Shaft Well Cases and Compared to Glaciation Only Results

Results for both reference and shaft well cases show negligible impact on transport from either erosion case when compared to the corresponding glaciation (no erosion) case. For the shaft well models, average transport in the erosion model is slightly lower than the corresponding glaciation only cases for the last four glacial cycles. This may be due to reduced well capture or increased dilution by glacial waters because of increased permeability as portions of the Guelph are incorporated in the weathered zone. Peak well transport at the start of each pumping period is lower for the reference well erosion cases, likely for the similar reasons.

6. CONCLUSIONS

A comprehensive 3D numerical modelling exercise has been undertaken to examine the impacts of glacial climate and associated erosion processes on a hypothetical deep geologic repository in the 5CS sedimentary geosphere. The glacial climate has been represented as eight repeating glacial cycles of 120 ka duration, each of which contains two glacial advance and retreat periods. Numerous reference and sensitivity case simulations have been conducted to characterize the behaviour of the flow system using plausible scenarios - as well as some implausible scenarios to improve understanding. The results overwhelmingly indicate that the 5CS geosphere remains a robust barrier with very slow transport under all likely conditions.

Geosphere performance is broadly characterized by advective velocities in the deep Ordovician system and “snap shot” MLE simulations at various times. In these conclusions we use mean MLE and advective velocity within the Cobourg formation in the vicinity of the repository as the primary metrics for evaluating flow system performance. The advective velocity within the deep Ordovician system will control if the flow system deviates from the diffusion dominated transport regime present during constant climate simulations. We used 10^{-5} m/a as a threshold velocity criterion to designate extremely slow, and likely diffusion dominated, transport. At velocities below 10^{-5} m/a, a contaminant particle under advective control will travel 10 m in 1 Ma, less than the thickness of Cobourg formation. Below 10^{-6} m/a, advective transport is under 1 metre in 1 Ma. These two velocities were used to evaluate the change in advective velocities that occur during each glacial cycle.

Transport system performance was characterized by transport of I-129 to the water supply well.

6.1 Glacial Climate Model: Flow

The Glaciation Sub-Regional Flow model was developed to characterize the effect on performance of the 5CS geosphere in the near vicinity (10s of km) of the repository to various reference and sensitivity case parameters, boundary conditions and processes. Surface head boundary conditions and hydro-mechanical loading due to glacial advance and retreat were simulated as were periods of permafrost. In general, sub-regional flow system behaviour was consistent for each glacial cycle. Figure 6-1 and Figure 6-2 show Repository MLE for the reference case and significant plausible sensitivity cases. Cases not supported by regional geosphere data (KHigh100, KHigh1000) and cases with no perceptible impact (discontinuous permafrost (DPF), no permafrost (NoPF), variable density, and Surface BC only) are not shown. The figures show that mean Repository MLE for most cases is in excess of 100 Ma. The figure also shows that all the glacial climate cases have slightly shorter MLE than the constant-climate steady-state no well case.

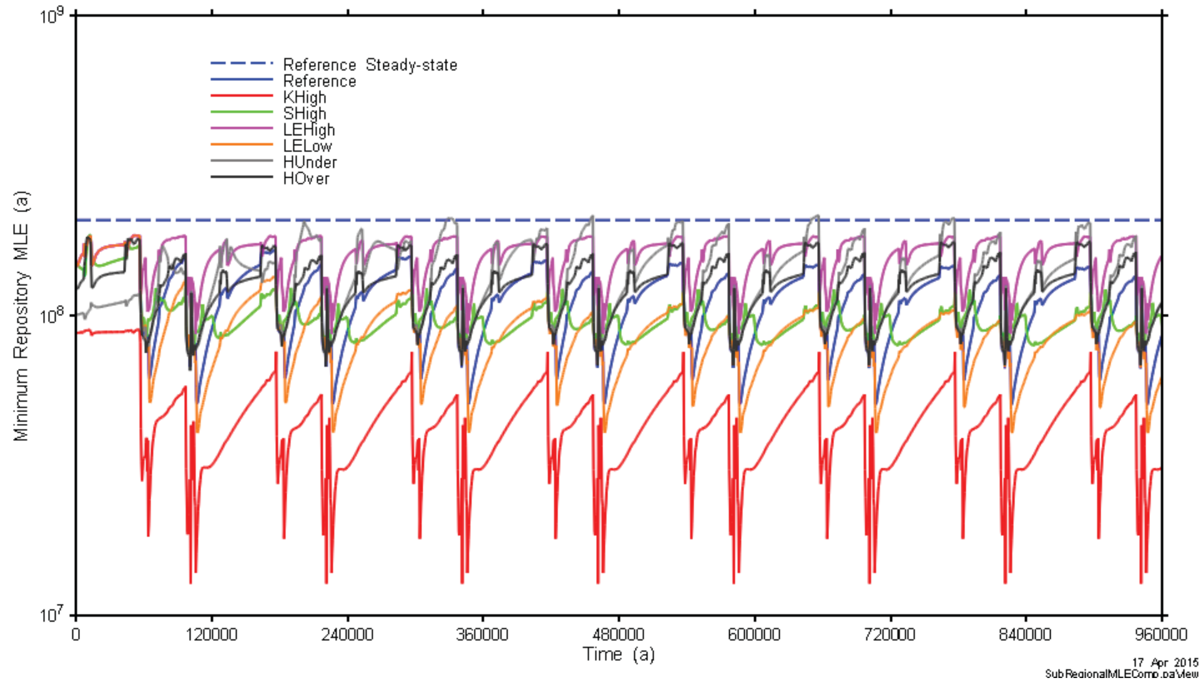

Figure 6-1: Glacial Climate Flow: Minimum Repository MLE for Selected Sensitivity Cases

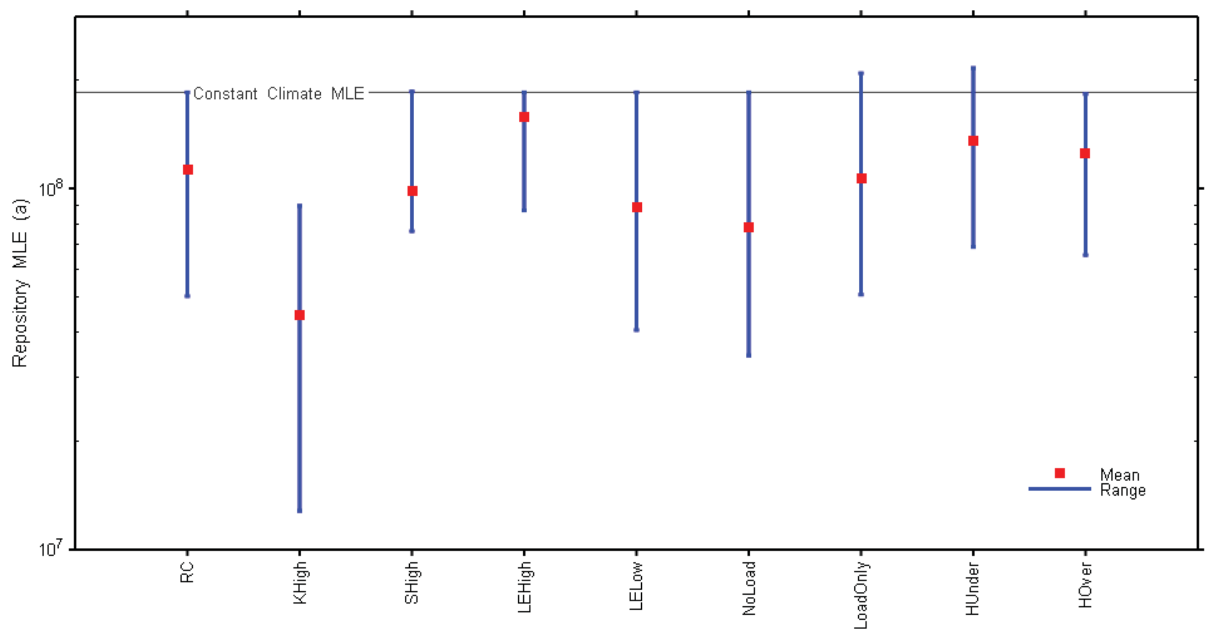

Figure 6-2: Glacial Climate Flow: Repository MLE for Selected Sensitivity Cases

Head profiles at various times illustrate the total and cumulative impact of glacial climate on geosphere pressures. As a reference time, 43 ka from the beginning of each cycle represents the longest period since a previous retreat, and thus shows the most moderation of the glacially induced overpressures. Figure 6-3 shows a steady increase in overpressures in the Ordovician formations. Elevated heads are also present at the bottom of the model, although only on the order of 30 metres above ground surface. Increased conductivity (KHigh case) allows most of the overpressure to dissipate and reduces cumulative effects.

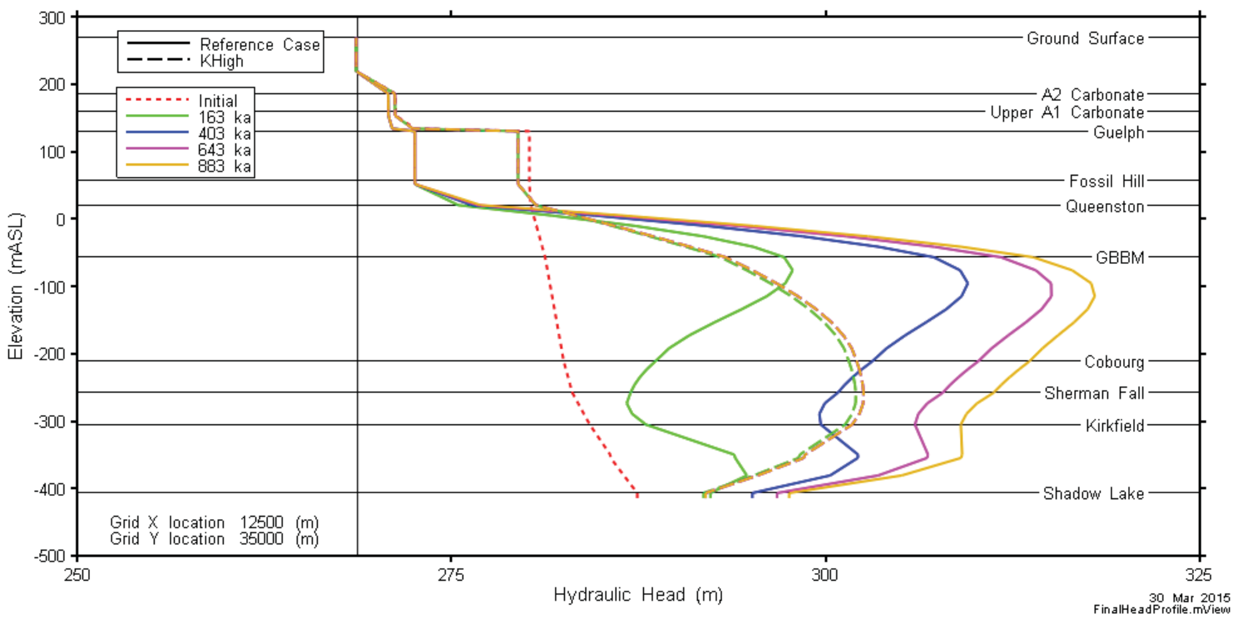

Figure 6-3: Glacial Climate Flow: Head profiles at Time of Maximum Well Operation in Cycles 2, 4, 6, and 8 for Reference and KHigh Cases.

Additional modelling was performed to determine the extent to which the presence of a gas phase will affect glacially induced changes to geosphere flow system behaviour. A simplified 2D model was prepared to simulate the numerically challenging two-phase flow behaviour. Comparisons of 2D single-phase flow to the 3D flow model showed that the reduced dimensionality of the model did not impair its ability to reproduce the 3D velocity field magnitudes and MLEs. The 2D two-phase results (Figure 6-4) show gas saturations causing slight increases in average velocity. However, these velocities are still well below any magnitude of concern.

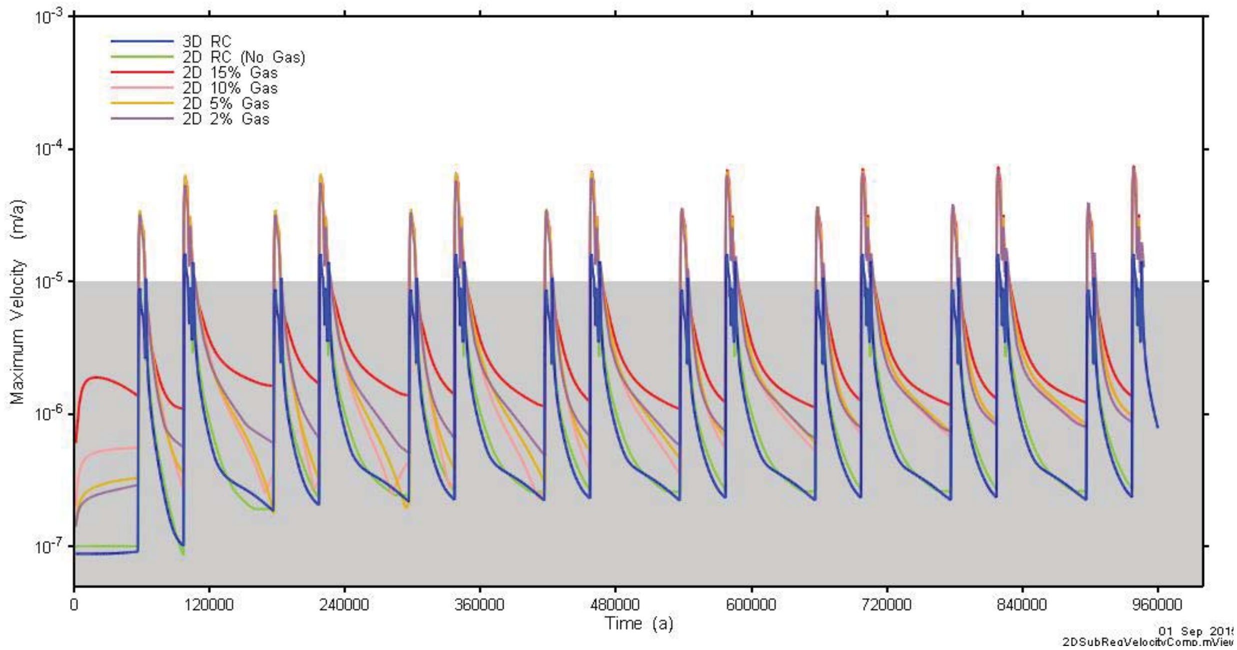

Figure 6-4: Glacial Climate Flow: 2D Two-Phase Advective Velocity in the Vicinity of the Repository for Simulated Gas Saturations.

6.2 Glacial Climate Model: Transport

The Site-Scale Transport model developed for this work is consistent with and compares well to the model used in the Pre-Project report (NWMO, 2013). Transport simulations were conducted for three reference case well and source locations, the KHigh geosphere sensitivity case, a high dispersivity transport sensitivity case, and the Shaft Fail disruptive event case, with boundary conditions extracted from the relevant Glaciation Sub-Regional Flow model.

Glacial climate conditions have only limited impact on well transport. The general development of the plume at depth is almost entirely insensitive to glacial forcing, while glacial advance and retreat cause slightly increased transport into the Guelph formation compared to steady state results. Figure 6-5 shows that transport into the Guelph is very similar to the constant climate results during permafrost periods, when neither well operation or glacial advance and retreat affect the flow system. Transport rates into the Guelph formation increase during ice cover periods. The average well transport during the period when the well is pumping is less than a factor of 10 higher than the steady-state, constant climate results. However, an initial spike in transport occurs when the well is turned on and radionuclides transported into the Guelph formation during the previous ice cover and permafrost periods are captured by the well. Variations in transport into the Guelph occur during glacial loading and unloading.

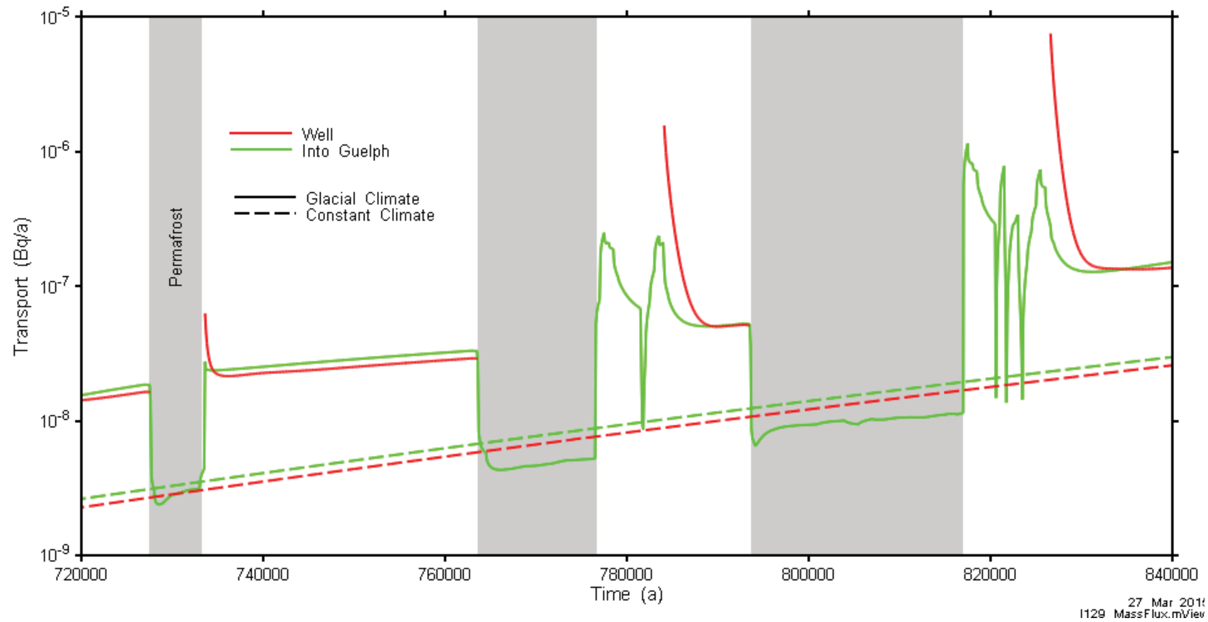

Figure 6-5: Site-Scale Transport: RC Reference Well Comparison of Constant Climate and Glacial Climate Well Transport Results – Seventh Cycle Detail.

Figure 6-6 compares glacial and constant climate well transport for selected cases. The transport during the initial well operation period is several orders of magnitude higher than for the constant climate case, and is summarized for all cases in Table 3.

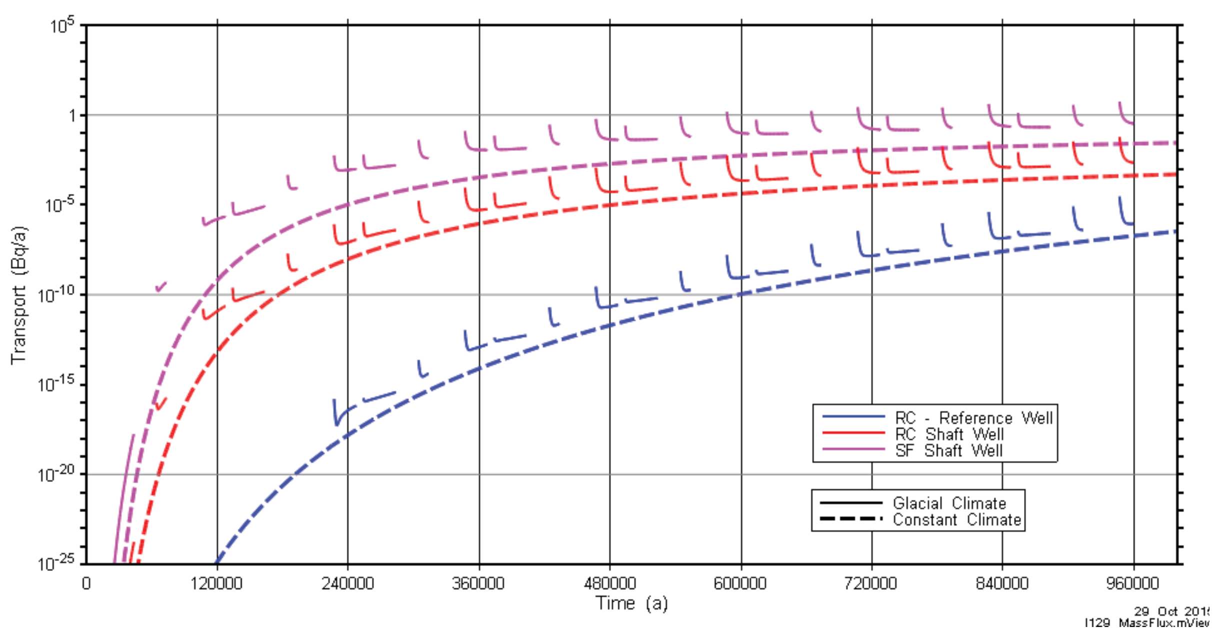

Figure 6-6: Glaciation Site-Scale Transport: Comparison of Constant Climate and Glacial Climate Well Transport Results for Reference and Shaft Fail Cases.

Table 3 - Site Scale Well Transport - Glacial:Constant Climate Ratios

Case	Transport (Bq/a)			Ratio	
	Constant Climate	Glacial Climate		Glacial:Constant	
	Maximum (960 ka)	Peak	Final (960 ka)	Peak	Final
RC Reference Well	1.881E-07	2.933E-05	8.862E-07	155.9	4.7
RC Shaft Well	4.257E-04	5.985E-02	2.201E-03	140.6	5.2
ShaftFail	2.546E-02	5.563E+00	3.320E-01	218.5	13.0
KHigh	2.099E-07	2.023E-04	1.815E-05	963.8	86.5
High Disp	6.661E-07	6.615E-04	3.285E-05	993.1	49.3
High Diff	6.860E-04	5.804E-02	1.430E-03	84.6	2.08

6.3 Glacial Erosion Model: Flow

The Erosion Sub-Regional Flow model simulated the impacts of two cases of glacial erosion on the 5CS sedimentary geosphere. Model construction was similar to the Glaciation Flow model with some differences in grid orientation and discretization (horizontal and vertical). The uniform erosion scenario (UE) removed a constant thickness over the entire model domain, while the valley erosion (VE) case spatially focussed the erosion in the form of a valley centred over the repository. Both cases removed 100 m of material over eight glacial cycles, with an equal amount removed each cycle. Within the cycles, removal was allocated between the two glacial advance/retreat events (A and B) on the basis of peak ice-thickness. The simulated ground surface erosion profile above the repository (Figure 6-7) varies slightly from the specification due to variations in discretization.

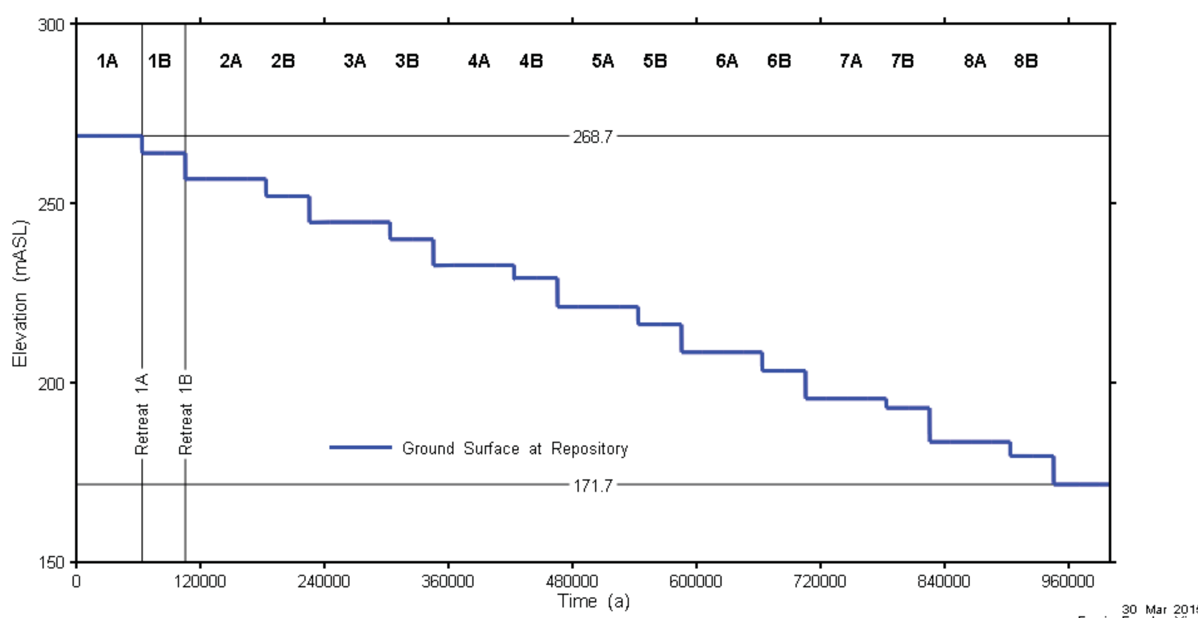

Figure 6-7: Erosion Model Flow: Ground Surface Elevation at the Repository Location

Surface head boundary conditions were adjusted to account for reduced surface elevations after each erosion stage (the end of the glacial retreat). Hydro-mechanical loading rates were also modified to incorporate the removal of overburden and/or weathered bedrock at the end of each retreat.

Groundwater velocities in the Cobourg formation show only minor increases during non ice-cover periods in the final glacial cycles. The simulated erosion has no significant impact on the deep groundwater velocities or on the Repository MLE (Figure 6-8).

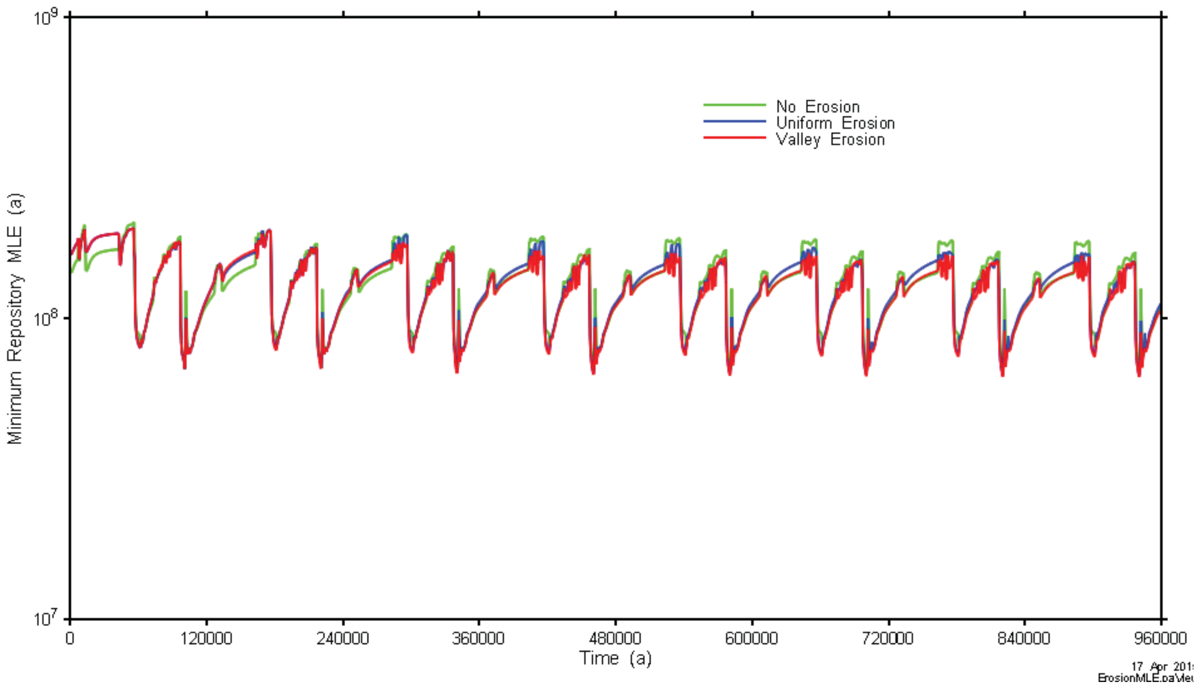

Figure 6-8: Erosion Model Flow: Repository MLE for Uniform and Valley Erosion Cases Compared to Glacial Climate Only Cases.

The head profiles (Figure 6-9) are significantly altered from the no erosion results. Uniform erosion results in significant underpressures at depth, while valley erosion results in an 80 m overpressure at the bottom of the model. The differences between these two illustrate the potential impacts of spatial variation in erosion. Without a detailed (and practically unobtainable) knowledge of past erosion patterns, it is unlikely that anomalous heads, such as those noted at the Bruce DGR, will ever be fully reconstructed.

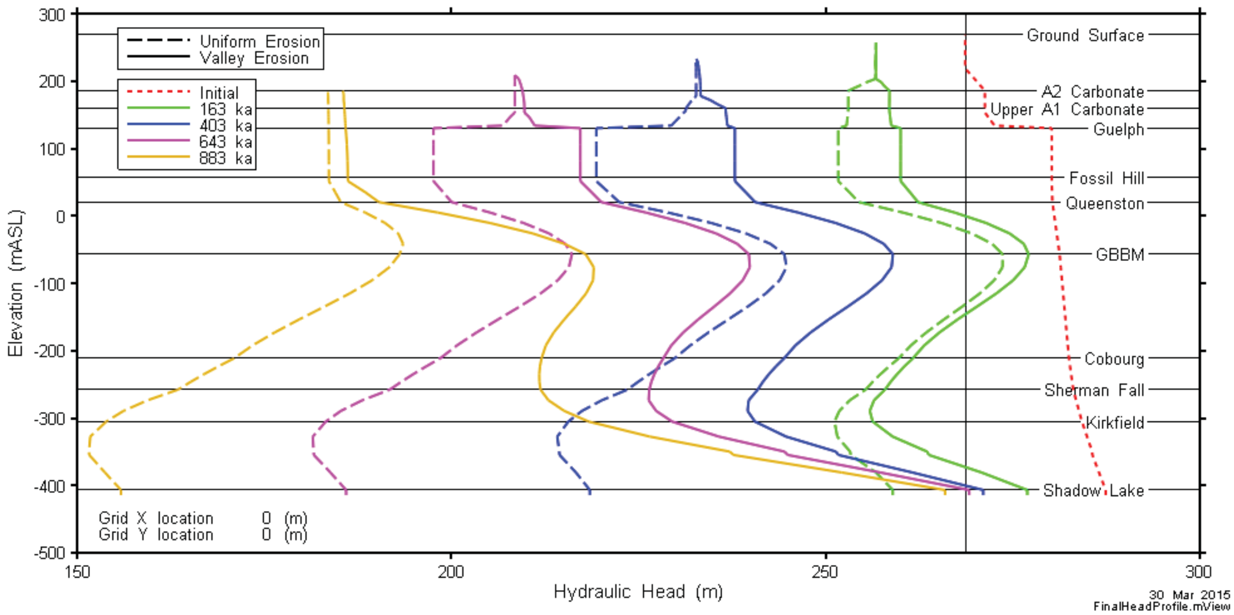

Figure 6-9: Erosion Flow: Head profiles at Time of Maximum Well Operation in Cycles 2, 4, 6, and 8 for Uniform and Valley Erosion.

6.4 Glacial Erosion Model: Transport

Radionuclide transport for the erosion cases was calculated using the same basic Site-Scale Transport model as was used for the glacial climate only I-129 transport model. Modifications to the model were limited to separate property sets for each simulated period, and modified hydro-mechanical loading rates to reflect material removal. Head boundary conditions were extracted from the Erosion Sub-Regional Flow model. Erosion transport results (Figure 6-10) are consistent with the erosion vs. glaciation only MLE comparison (Figure 6-8) and show very similar transport rates to the glacial climate only (no-erosion) case, with slightly reduced transport for the shaft well and release location. Differences between uniform and valley erosion are minimal.

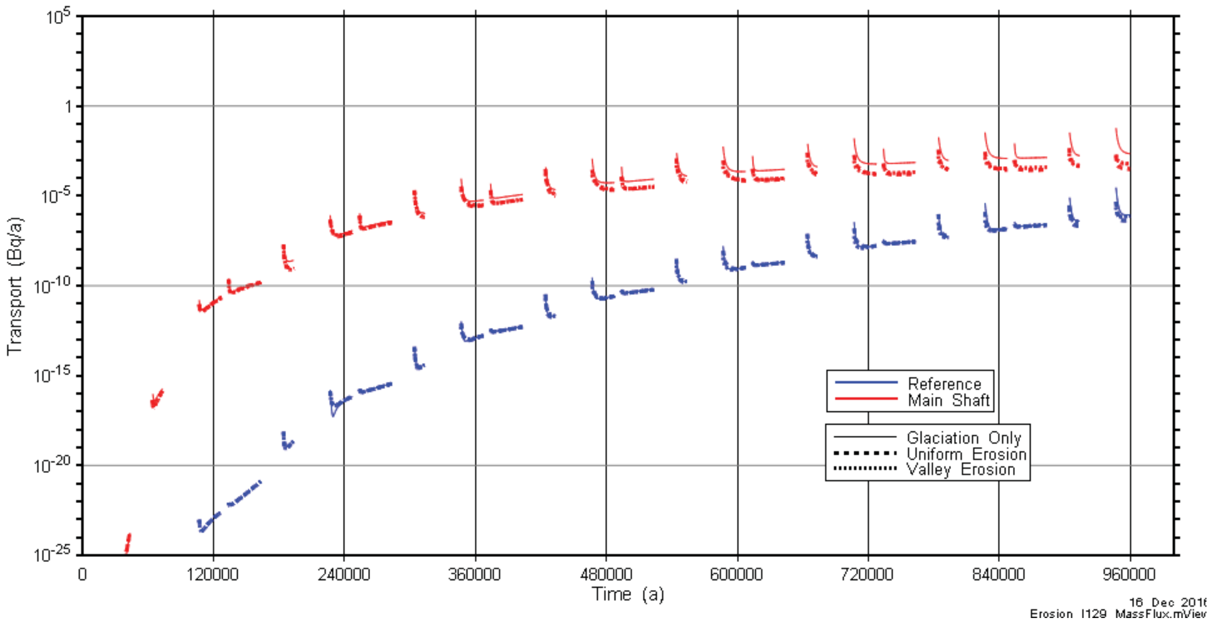

Figure 6-10: Erosion Site-Scale Transport: Comparison of Erosion and Glacial Climate Only Cases.

6.5 Modelling Approach

The overall modelling approach drew upon the experiences gained in previous glaciation modelling (Walsh and Avis, 2010) and transport modelling for the 5CS geosphere and repository (NWMO, 2013). The simulations were extremely data and time intensive, each using hundreds of megabytes to tens of gigabytes of boundary condition and loading files, while generating hundreds of gigabytes of output. Post-processed output files for all reported simulations amounted to over 3TB.

Model execution times varied widely (Table 4). It is obvious that steady-state constant density simulations are much faster than transient simulations incorporating glacial climate. Steady-state (constant density) flow execution time is negligible, while steady-state flow transport execution time is at least a factor of twelve faster than for glacial climate (transient flow) transport, and also requires much less effort to set up and post-process. Glacial climate and erosion site-scale transport results show only minimal differences to constant climate results, supporting the use of constant climate simulations for most Post-Closure Safety Assessment purposes.

The Glacial Sub-Regional Flow model included all eight glacial cycles within a single simulation. This approach exposed inefficiencies in the implementation of variable head boundary conditions, permafrost, and loading rate specifications. The actual degree of inefficiency is difficult to determine strictly from sensitivity results as changes in head response also affect the matrix solution time. Tests were conducted on a synthetic case with minimal transient effects (i.e., constant head, zero loading, well operation only) where the time required to execute the final glacial cycle was a factor of 13 greater than required for the first glacial cycle. In an efficient implementation they should be of similar length. Comparison of the Glaciation and Erosion Sub-Regional flow model timings also illustrates this point. The Erosion models are on average a factor of 3 faster (2.4 versus 7.4 days), in spite of being four times the size. This is due to the smaller time series required for the shorter duration subdivided time periods in the Erosion model.

Variable density flow and transport calculations in FRAC3DVS-OPG are extremely time consuming and result in no significant difference in flow system results for the 5CS geosphere.

A somewhat surprising result was the degree to which the 2D Sub Regional Flow models could reproduce the essential features of the larger 3D model at much reduced execution times. This result opens up the possibility of a full probabilistic assessment of 5CS geosphere performance using 2D models and appropriate performance metrics.

The Repository MLE time series metrics described in Section 4.1.6 provide an easily understood metric for system performance under glacial climate conditions. Currently, creation of the time series requires multiple MLE model executions that can only be accomplished under control of an execution framework. However, it would be a relatively simple enhancement to the FRAC3DVS-OPG code to perform MLE calculations at specified times within a transient flow simulation.

Some constant climate and variable climate transport model results (specifically early time mass flux into the Guelph) were susceptible to early-time oscillations, which could only be ameliorated by selecting very small time step sizes. The effect was of visual concern only as the oscillations were eliminated within several glacial cycles. Transport results beyond the third glacial cycle were virtually identical for 100a and 500a time steps. Adding a capability to modify maximum time step size as a function of simulation time would be helpful in reducing the execution cost associated with removing the oscillations.

All variable climate Site-Scale transport models showed extreme oscillations in well transport calculations when conducted using the default centred-in-time time discretization. Applying fully-implicit time discretization eliminated this error, with no other obvious impacts.

Table 4 - Model Execution Times

Model	Case	Execution Time (days unless noted as sec or min)
Glaciation Sub-Regional Flow - Constant Climate (Constant Density unless noted)		
	RC	30 sec
	RC - Reference Well	32 sec
	RC– Shaft Well	30 sec
	KHigh	28 sec
	KHigh100	30 sec
	KHigh1000	31 sec
	RC Variable Density (to 10 Ma)	118
Glaciation Sub-Regional Flow – Glacial Climate (Constant Density unless noted)		
	RC	7.4
	RC-Reference Well	6.9
	RC-Shaft	7.2
	RC-Centre	6.0
	RC-Reference Well-Variable Density	127.9 (to 650 ka)

Model	Case	Execution Time (days unless noted as sec or min)
	DPF	4.3
	HUnder	7.0
	HOver	9.5
	KHigh	7.7
	KHigh100	7.5
	KHigh1000	10.2
	LEHigh	6.5
	LELow	7.5
	Load Only	6.7
	NoLoad	1.0
	NoPF	3.5
	SHigh	4.8
	SurfaceBC	6.8
2D Glaciation Sub-Regional Flow – Glacial Climate		
	FRAC3DVS-OPG	31 min
	T2GGM - fully water saturated	16 min
	T2GGM -10% Gas	0.41
	T2GGM -5% Gas	0.39
	T2GGM -1% Gas	0.63
Site Scale Transport – Constant Climate (to 1 Ma)		
	RC - Reference Well	0.77
	RC - Shaft Well	0.90
	RC – Centre Well	0.90
Site Scale Transport – Glacial Climate (500 a maximum time step unless noted)		
	RC – Reference Well	12
	RC – Reference Well – 100 a maximum time step	43.2
	RC - Shaft Well	13.1
	RC - Shaft Well – 100 a maximum time step	42.1
	RC - Centre Well – 1000 a maximum time step	5.0
	High Dispersivity	12
	High Dispersivity – 100 a maximum time step	48.4
	High Diffusion	10.3
	KHigh	13.1
	ShaftFail	13.4
Erosion Sub-Regional Flow – Glacial Climate – Constant Density		
	Uniform Erosion – Reference Well	2.4
	Uniform Erosion – Shaft Well	2.6
	Valley Erosion – Reference Well	2.5
	Valley Erosion – Shaft Well	2.6
Erosion Site Scale Transport		
	Uniform Erosion – Reference Well	27.8
	Uniform Erosion – Shaft Well	28.3
	Valley Erosion – Reference Well	25.8
	Valley Erosion – Shaft Well	25.7

7. REFERENCES

AECOM and Itasca Canada. 2011. Regional Geology – Southern Ontario. Nuclear Waste Management Organization (NWMO) DGR-TR-2011-15. Toronto, Canada.

Bear, J. 1979. Hydraulics of Groundwater. McGraw-Hill Inc., New York, USA.

Freeze, R.A and Cherry J.A. 1979. Groundwater, Prentice Hall, New Jersey

INTERA. 2011. Descriptive Geosphere Site Model. Nuclear Waste Management Organization Report NWMO DGR-TR-2011-24 R000. Toronto, Canada.

Huysmans, M. and A Dassargues. 2004. Review of the use of Péclet numbers to determine the relative importance of advection and diffusion in low permeability environments. Hydrogeology Journal, 13, pp 895-904.

McCauley, C.A., D.M. White, M.R. Lilly and D.M. Nyman. 2002. A comparison of hydraulic conductivities, permeabilities and infiltration rates in frozen and unfrozen soils. Cold Regions Science and Technology 34(2), 117–125.

Neuzil, C. 2003. Hydromechanical Coupling in Geological Processes. Hydrogeology Journal, 11, pp 41-83.

NWMO. 2013. Adaptive Phased Management Postclosure Safety Assessment of a Used Fuel Repository in Sedimentary Rock Pre-Project Report. NWMO TR-2013-07. Toronto, Canada.

NWMO. 2012. Used Fuel Repository Conceptual Design and Postclosure Safety Assessment in Crystalline Rock, Pre-Project Report. Nuclear Waste Management Organization (NWMO) TR-2012-16. Toronto, Canada.

Oerlemans, J. 2001. Glaciers and Climate Change. Swets and Zeitlinger BV, Lisse.

Ogata A and Banks RB (1961) A solution of the differential equation of longitudinal dispersion in porous media, U.S. Geological Survey Professional Paper 411-A

Peltier, W.R. 2011. Long-Term Climate Change. Nuclear Waste Management Organization, Technical Report NWMO DGR-TR-2011-14 R000. Toronto, Canada.

Pruess, K., C. Oldenburg and G. Moridis. 1999. TOUGH2 User’s Guide, Version 2.0. Lawrence Berkeley National Laboratory Report LBNL-43134. Berkeley, USA.

Remenda VH, van der Kamp G and Cherry JA (1996) Use of vertical profiles of d18O to constrain estimates of hydraulic conductivity in a thick, unfractured aquitard. Water Resources Research, 32:2979–2987

Rutqvist J. and C.F. Tsang. 2003. Analysis of Thermal-hydrologic-mechanical Behavior near an Emplacement Drift at Yucca Mountain. Journal of Contaminant Hydrology, 62–63, pp 637–652.

Suckling, P., J. Avis, N. Calder, O. Nasir, P. Humphreys, F. King, and R. Walsh. 2015. T2GGM Version 3.2: Gas Generation and Transport Code. Nuclear Waste Management Organization Report NWMO TR-2015-13. Toronto, Canada.

Sykes, J.F., S.D. Normani and Y. Yin. 2011. Hydrogeologic Modelling. Nuclear Waste Management Organization Report NWMO DGR-TR-2011-16. Toronto, Canada.

Therrien, R., R.G. McLaren, E.A. Sudicky, S.M. Panday, and V. Guvanasen. 2010. FRAC3DVS_OPG: a three-dimensional numerical model describing subsurface flow and solute transport. User's Guide. Groundwater Simulations Group, University of Waterloo, Ontario, Canada.

Walsh, R., N. Calder and J. Avis. 2012. A Simple Implementation of 1D Hydro-Mechanical Coupling In TOUGH2. PROCEEDINGS, TOUGH Symposium 2012, Lawrence Berkeley National Laboratory, Berkeley, California, September 17-19, 2012.

Walsh, R. and J. Avis . 2010. Glaciation Scenario: Groundwater and Radionuclide Transport Studies. Nuclear Waste Management Organization (NWMO) TR-2010-09. Toronto, Canada.

Wang, H., 2000. Theory of Linear Poroelasticity with Application to Geomechanics and Hydrology. Princeton University Press. Princeton, USA.

.

APPENDIX A: MODEL PARAMETERS

All model parameters are consistent with those reported in NWMO, 2013, Adaptive Phased Management Postclosure Safety Assessment of a Used Fuel Repository in Sedimentary Rock Pre-Project Report, NWMO TR-2013-07, Toronto, Canada.

Table A-1: Formation Flow Parameters

Formation	K_h (m/s)	K_v (m/s)	Porosity -	Specific Storage (m^{-1})	Loading Efficiency	Bulk Density (kg/m^3)
Drift	1.0E-07	5.0E-08	0.200	1.0E-04	0.99	2000
Detroit R	6.0E-07	2.0E-08	0.077	1.0E-06	0.84	2620
Bois Blanc	1.0E-07	1.0E-08	0.077	1.0E-06	0.84	2620
Bass Islands	5.0E-05	2.0E-06	0.056	2.0E-06	0.92	2710
Unit G	1.0E-11	1.0E-12	0.172	1.0E-06	0.55	2320
Unit F	5.0E-14	5.0E-15	0.100	1.0E-06	0.68	2380
Unit E	2.0E-13	2.0E-14	0.100	7.0E-07	0.51	2490
Unit D	2.0E-13	2.0E-14	0.089	6.0E-07	0.53	2730
Unit B and C	4.0E-13	4.0E-14	0.165	1.0E-06	0.38	2280
B Anhydrite	3.0E-13	3.0E-14	0.089	7.0E-07	0.53	2730
Unit A-2 Carbonate	3.0E-10	3.0E-11	0.120	7.0E-07	0.46	2420
Unit A-2 Evaporite	3.0E-13	3.0E-14	0.089	6.0E-07	0.53	2870
Unit A-1 Upper Carbonate	2.0E-07	2.0E-07	0.070	5.0E-07	0.59	2740
Unit A-1 Carbonate	9.0E-12	9.0E-13	0.019	4.0E-07	0.84	2600
Unit A-1 Evaporite	3.0E-13	3.0E-14	0.007	4.0E-07	0.94	2870
Unit A0	3.0E-13	3.0E-14	0.032	5.0E-07	0.76	2710
Guelph	3.0E-08	3.0E-08	0.057	4.0E-07	0.47	2580
Fossil Hill	5.0E-12	5.0E-13	0.031	3.0E-07	0.62	2720
Cabot Head	9.0E-14	9.0E-15	0.116	1.0E-06	0.60	2520
Manitoulin	9.0E-14	9.0E-15	0.028	8.0E-07	0.86	2650
Queenston	2.0E-14	2.0E-15	0.073	9.0E-07	0.71	2570
Georgian Bay / Blue Mountain	4.0E-14	3.1E-15	0.070	1.0E-06	0.79	2580
Cobourg	2.0E-14	2.0E-15	0.015	3.0E-07	0.80	2660
Sherman Fall	1.0E-14	1.0E-15	0.016	5.0E-07	0.88	2660
Kirkfield	8.0E-15	8.0E-16	0.021	5.0E-07	0.85	2630
Cobokonk	4.0E-12	4.0E-15	0.009	5.0E-07	0.93	2670
GullRiver	7.0E-13	7.0E-16	0.022	5.0E-07	0.85	2670
Shadow Lake	1.0E-09	1.0E-12	0.097	7.0E-07	0.56	2580

Table A-2: Formation Transport Parameters

Formation	Sub-Regional Longitudinal Dispersivity (MLE calculation) (m)	Sub-Regional Transverse Dispersivity (MLE calculation) (m)	Site-Scale Longitudinal Dispersivity (I-129 transport) (m)	Site-Scale Transverse Dispersivity (I-129 Transport) (m)	Dev (NaI) (m^2/s)	Deh:Dev
Drift	250	25	50	5	1.2E-09	1
Detroit R	250	25	50	5	1.0E-11	1
Bois Blanc	250	25	50	5	1.0E-11	1
Bass Islands	250	25	50	5	5.0E-12	1
Unit G	250	25	50	5	8.6E-13	2
Unit F	250	25	50	5	8.2E-12	2
Unit E	250	25	50	5	9.4E-12	2
Unit D	250	25	50	5	9.4E-12	2
Unit B and C	250	25	50	5	2.3E-11	2
B Anhydrite	250	25	50	5	1.5E-13	2
Unit A-2 Carbonate	250	25	50	5	2.4E-12	2
Unit A-2 Evaporite	250	25	50	5	1.5E-13	2
Unit A-1 Upper Carbonate	250	25	50	5	1.4E-11	1
Unit A-1 Carbonate	250	25	50	5	3.6E-13	2
Unit A-1 Evaporite	250	25	50	5	6.0E-14	2
Unit A0	250	25	50	5	6.0E-14	2
Guelph	250	25	50	5	5.8E-11	1
Fossil Hill	250	25	50	5	8.6E-14	2
Cabot Head	250	25	50	5	6.2E-12	2
Manitoulin	250	25	50	5	3.0E-13	2
Queenston	250	25	50	5	2.0E-12	2
Georgian Bay / Blue Mountain	250	25	50	5	1.6E-12	2
Cobourg	250	25	50	5	7.4E-13	2
Sherman Fall	250	25	50	5	4.4E-13	2
Kirkfield	250	25	50	5	8.4E-13	2
Cobokonk	250	25	50	5	5.4E-13	2
GullRiver	250	25	50	5	5.2E-13	2
Shadow Lake	250	25	50	5	2.6E-12	2

Table A-3: Formation Variable Density Initial Conditions

Formation	Fluid Density (kg/m^3)	Initial TDS (g/L)
Drift	1000	0
Detroit R	1001	1.4
Bois Blanc	1002	3.2
Bass Islands	1004	6
Unit G	1010	14.8
Unit F	1040	59.6
Unit E	1083	124
Unit D	1133	200
Unit B and C	1198	296.7
B Anhydrite	1214	321
Unit A-2 Carbonate	1091	136
Unit A-2 Evaporite	1030	45.6
Unit A-1 Upper Carbonate	1019	28.6
Unit A-1 Carbonate	1128	192
Unit A-1 Evaporite	1217	325
Unit A0	1240	360
Guelph	1247	370
Fossil Hill	1200	300
Cabot Head	1204	306
Manitoulin	1233	350
Queenston	1207	310
Georgian Bay / Blue Mountain	1200	299.4
Cobourg	1181	272
Sherman Fall	1180	270
Kirkfield	1156	234
Cobokonk	1170	255
GullRiver	1135	203
Shadow Lake	1133	200

Table A-4: Formation Two-Phase Flow Parameters

Formation	Slr	Sgr	$1/\alpha$ (MPa)	n	m
Drift	0.000	0.100	0.117	3.87	0.818
Detroit R	0.000	0.100	0.115	3.87	0.818
Bois Blanc	0.000	0.100	0.163	3.87	0.818
Bass Islands	0.000	0.100	0.010	3.87	0.818
Unit G	0.000	0.100	24.3	3.87	0.818
Unit F	0.000	0.100	24.3	3.87	0.818
Unit E	0.010	0.150	0.588	4.31	0.046
Unit D	0.010	0.150	0.588	4.31	0.046
Unit B and C	0.550	0.000	0.310	4.22	0.350
B Anhydrite	0.010	0.100	2.06	2.28	0.990
Unit A-2 Carbonate	0.000	0.000	0.758	3.06	0.500
Unit A-2 Evaporite	0.010	0.100	2.06	2.28	0.990
Unit A-1 Upper Carbonate	0.000	0.000	38.9	2.41	0.990
Unit A-1 Carbonate	0.000	0.000	38.9	2.41	0.990
Unit A-1 Evaporite	0.010	0.100	2.06	2.28	0.990
Unit A0	0.010	0.100	2.06	2.28	0.990
Guelph	0.248	0.000	0.037	4.89	0.145
Fossil Hill	0.025	0.000	27.9	6.11	0.684
Cabot Head	0.000	0.050	14.6	6.82	0.243
Manitoulin	0.106	0.050	40.8	3.65	1.305
Queenston	0.086	0.056	35.6	4.45	1.133
Georgian Bay / Blue Mountain	0.166	0.037	30.1	3.82	1.096
Cobourg	0.060	0.025	61.7	3.13	1.689
Sherman Fall	0.170	0.110	28.2	2.33	0.999
Kirkfield	0.000	0.150	173	2.17	7.220
Cobokonk	0.000	0.025	66.2	1.82	1.732
GullRiver	0.210	0.110	40.0	4.06	0.775
Shadow Lake	0.040	0.000	0.227	1.20	0.583

Table A-5: Shaft and EBS Flow Parameters

EDZ/EBS ID	K_h (m/s)	K_v (m/s)	Porosity -	Specific Storage (m^{-1})	Loading Efficiency	Bulk Density (kg/m^3)
BAnhydSI	3.0E-12	3.0E-12	0.178	7.0E-07	0.53	2730
A2CarbSI	3.0E-09	3.0E-09	0.240	7.0E-07	0.46	2420
A2EvapSI	3.0E-12	3.0E-12	0.178	6.0E-07	0.53	2870
A1UCarbSI	2.0E-05	2.0E-05	0.140	5.0E-07	0.59	2740
A1CarbSI	9.0E-11	9.0E-11	0.038	4.0E-07	0.84	2600
A1EvapSI	3.0E-12	3.0E-12	0.014	4.0E-07	0.94	2870
A0SI	3.0E-12	3.0E-12	0.064	5.0E-07	0.76	2710
GuelphSI	3.0E-06	3.0E-06	0.114	4.0E-07	0.47	2580
FossilHillSI	5.0E-11	5.0E-11	0.062	3.0E-07	0.62	2720
CabotHeadSI	9.0E-13	9.0E-13	0.232	1.0E-06	0.60	2520
ManitoulinSI	9.0E-13	9.0E-13	0.056	8.0E-07	0.86	2650
QueenstonSI	2.0E-13	2.0E-13	0.146	9.0E-07	0.71	2570
GBBMSI	3.1E-13	3.1E-13	0.140	1.0E-06	0.79	2580
CobourgSI	2.0E-13	2.0E-13	0.030	3.0E-07	0.80	2660
ShermanFallSI	1.0E-13	1.0E-13	0.032	5.0E-07	0.88	2660
KirkfieldSI	8.0E-14	8.0E-14	0.042	5.0E-07	0.85	2630
CobokonkSI	4.0E-13	4.0E-13	0.018	5.0E-07	0.93	2670
BAnhydSO	3.0E-13	3.0E-13	0.089	7.0E-07	0.53	2730
A2CarbSO	3.0E-10	3.0E-10	0.120	7.0E-07	0.46	2420
A2EvapSO	3.0E-13	3.0E-13	0.089	6.0E-07	0.53	2870
A1UCarbSO	2.0E-06	2.0E-06	0.070	5.0E-07	0.59	2740
A1CarbSO	9.0E-12	9.0E-12	0.019	4.0E-07	0.84	2600
A1EvapSO	3.0E-13	3.0E-13	0.007	4.0E-07	0.94	2870
A0SO	3.0E-13	3.0E-13	0.032	5.0E-07	0.76	2710
GuelphSO	3.0E-07	3.0E-07	0.057	4.0E-07	0.47	2580
FossilHillSO	5.0E-12	5.0E-12	0.031	3.0E-07	0.62	2720
CabotHeadSO	9.0E-14	9.0E-14	0.116	1.0E-06	0.60	2520
ManitoulinSO	9.0E-14	9.0E-14	0.028	8.0E-07	0.86	2650
QueenstonSO	2.0E-14	2.0E-14	0.073	9.0E-07	0.71	2570
GBBMSO	3.1E-14	3.1E-14	0.070	1.0E-06	0.79	2580
CobourgSO	2.0E-14	2.0E-14	0.015	3.0E-07	0.80	2660
ShermanFallSO	1.0E-14	1.0E-14	0.016	5.0E-07	0.88	2660
KirkfieldSO	8.0E-15	8.0E-15	0.021	5.0E-07	0.85	2630
CobokonkSO	4.0E-14	4.0E-14	0.009	5.0E-07	0.93	2670
PlacementEDZ	1.3E-11	1.3E-11	0.030	3.0E-07	0.80	2660
RoomEntryEDZ	2.3E-11	2.3E-11	0.030	3.0E-07	0.80	2660
CrossCutEDZ	1.5E-11	1.5E-11	0.030	3.0E-07	0.80	2660

EDZ/EBS ID	**K_h (m/s)**	**K_v (m/s)**	**Porosity -**	**Specific Storage (m^{-1})**	**Loading Efficiency**	**Bulk Density (kg/m^3)**
PerimiterEDZ	1.7E-11	1.7E-11	0.030	3.0E-07	0.80	2660
MainAccessEDZ	2.1E-11	2.1E-11	0.030	3.0E-07	0.80	2660
RoomEntrySealEDZ	1.7E-11	1.7E-11	0.030	3.0E-07	0.80	2660
CrossCutSealEDZ	1.1E-11	1.1E-11	0.030	3.0E-07	0.80	2660
PerimeterSealEDZ	1.2E-11	1.2E-11	0.030	3.0E-07	0.80	2660
MainAccessSealEDZ	1.4E-11	1.4E-11	0.030	3.0E-07	0.80	2660
Placement Tunnel Seal Material	2.1E-12	2.1E-12	0.481	1.0E-10	0.00	1904
Highly Compacted Bentonite	6.6E-13	6.6E-13	0.413	1.0E-10	0.00	2023
Highly Compacted Bentonite for EDZ seals	8.2E-13	8.2E-13	0.413	1.0E-10	0.00	2002
Gap Fill	6.0E-12	6.0E-12	0.486	1.0E-10	0.00	1896
Shaft Seal	1.6E-11	1.6E-11	0.411	1.0E-11	0.00	2011
Dense Backfill blocks	1.0E-10	1.0E-10	0.194	1.0E-10	0.00	2314
CrossCut DBF	8.0E-11	1.0E-10	0.194	1.0E-10	0.00	2314
Concrete (LHHPC), degraded	1.0E-10	1.0E-10	0.100	1.1E-06	0.00	2491
Asphalt	1.0E-11	1.0E-11	0.020	3.5E-06	0.00	1960

Notes: SI is short for Shaft Inner EDZ, SO is short for Shaft Outer EDZ

Table A-6: Shaft and EBS Transport Parameters

EDZ/EBS ID	Longitudinal Dispersivity (m)	Transverse Dispersivity (m)	De_v (NaI) (m^2/s)	De_h:De_v
BAnhydSI	50	5	1.5E-13	2
A2CarbSI	50	5	2.4E-12	2
A2EvapSI	50	5	1.5E-13	2
A1UCarbSI	50	5	1.4E-11	1
A1CarbSI	50	5	3.6E-13	2
A1EvapSI	50	5	6.0E-14	2
A0SI	50	5	6.0E-14	2
GuelphSI	50	5	5.8E-11	1
FossilHillSI	50	5	8.6E-14	2
CabotHeadSI	50	5	6.2E-12	2
ManitoulinSI	50	5	3.0E-13	2
QueenstonSI	50	5	2.0E-12	2
GBBMSI	50	5	1.6E-12	2
CobourgSI	50	5	7.4E-13	2
ShermanFallSI	50	5	4.4E-13	2
KirkfieldSI	50	5	8.4E-13	2
CobokonkSI	50	5	5.4E-13	2
BAnhydSO	50	5	1.5E-13	2
A2CarbSO	50	5	2.4E-12	2
A2EvapSO	50	5	1.5E-13	2
A1UCarbSO	50	5	1.4E-11	1
A1CarbSO	50	5	3.6E-13	2
A1EvapSO	50	5	6.0E-14	2
A0SO	50	5	6.0E-14	2
GuelphSO	50	5	5.8E-11	1
FossilHillSO	50	5	8.6E-14	2
CabotHeadSO	50	5	6.2E-12	2
ManitoulinSO	50	5	3.0E-13	2
QueenstonSO	50	5	2.0E-12	2
GBBMSO	50	5	1.6E-12	2
CobourgSO	50	5	7.4E-13	2
ShermanFallSO	50	5	4.4E-13	2
KirkfieldSO	50	5	8.4E-13	2
CobokonkSO	50	5	5.4E-13	2
PlacementEDZ	50	5	7.4E-13	2
RoomEntryEDZ	50	5	7.4E-13	2
CrossCutEDZ	50	5	7.4E-13	2

EDZ/EBS ID	Longitudinal Dispersivity (m)	Transverse Dispersivity (m)	De_v (NaI) (m^2/s)	De_h:De_v
PerimiterEDZ	50	5	7.4E-13	2
MainAccessEDZ	50	5	7.4E-13	2
RoomEntrySealEDZ	50	5	7.4E-13	2
CrossCutSealEDZ	50	5	7.4E-13	2
PerimeterSealEDZ	50	5	7.4E-13	2
MainAccessSealEDZ	50	5	7.4E-13	2
Placement Tunnel Seal Material	50	5	4.1E-10	1
Highly Compacted Bentonite	50	5	3.0E-10	1
Highly Compacted Bentonite for EDZ seals	50	5	3.0E-10	1
Gap Fill	50	5	3.0E-10	1
Shaft Seal	50	5	3.0E-10	1
Dense Backfill blocks	50	5	2.0E-09	1
CrossCut DBF	50	5	2.0E-09	1
Concrete (LHHPC), degraded	50	5	1.3E-10	1
Asphalt	50	5	1.0E-13	1

Notes: SI is short for Shaft Inner EDZ, SO is short for Shaft Outer EDZ